πN NEWSLETTER

No. 14, August 1998 ISSN 0942-4148

EDITORS

D. Drechsel G. Höhler W. Kluge H. Leutwyler
B. M. K. Nefkens H.-M. Staudenmaier

Proceedings of the GW/JLab Workshop on N* Physics

Edited by H. Haberzettl, C. Bennhold, and W. J. Briscoe

The George Washington University—Virginia Campus, Ashburn, VA, U. S. A.
October 30 – November 1, 1997

The George Washington University WASHINGTON DC

The Department of Energy's Jefferson Lab Thomas Jefferson National Accelerator Facility

The George Washington University Virginia Campus

102-7194
Ashburn 1997

πN NEWSLETTER

Impressum

Production and distribution:

for Europe, Africa, and Western Asia by
W. Kluge
Institut für Experimentelle Kernphysik
Universität Karlsruhe
Postfach 3640
D-76021 Karlsruhe
Germany

for the Americas, Australia, and Eastern Asia by
B. M. K. Nefkens
Department of Physics
University of California, Los Angeles
Los Angeles, CA 90024-1547
U. S. A.

Editors: D. Drechsel, G. Höhler, W. Kluge, H. Leutwyler,
B. M. K. Nefkens, and H.-M. Staudenmaier

CERN BIBLIOTHEQUE

ISSN 0942-4148

Copyright ©1998 by Institut für Experimentelle Kernphysik (IEKP) der Universität Karlsruhe, Department of Physics of the University of California at Los Angeles (UCLA), Center for Nuclear Studies of The George Washington University, and Thomas Jefferson National Accelerator Facility

Permission is granted to quote from this journal with the customary acknowledgment of the source. To reprint a figure, table, or other excerpt requires, in addition, the consent of one of the original authors and notification of IEKP or UCLA. No copying fee is required when copies of articles are made for educational or research purposes by individuals, libraries, governmental or industrial institutions. Republication or reproduction for sale of articles or abstracts in this journal is permitted only under the license from IEKP. In addition, it is required that permission also be obtained from one of the authors. Address inquiries to W. Kluge, IEKP or B. M. K. Nefkens, UCLA.

πN NEWSLETTER

No. 14 August 1998

Note from the Editors

The purpose of the πN NEWSLETTER is to improve the exchange of information between physicists working in πN scattering and related fields such as nucleon structure, $\pi N \to \pi\pi N$, $\pi^- p \to \eta n$, $\gamma\pi \to \pi N$, $\pi\pi \to \pi\pi$, and electromagnetic form factors of pions and nucleons. The Newsletters will give results of new experiments, plans for experiments in the near future, analyses of experimental data, and related theoretical developments.

Since our first Newsletter appeared, subjects that have come under the limelight are for instance: the 'experimental' value of the πN σ-term and other quantities related to the strange quark content of the nucleon, the origin of the spin of the nucleon, applications of the Skyrme model and the pole structure of πN and $\pi\pi$ resonances in different sheets. There continues to be an interest in various quark and bag models of nucleon resonances, the existence of clusters of nucleon resonances, and so forth.

Copies can be obtained from the editors W. K. and B. M. K. N. at the addresses below.

D. Drechsel
Universität Mainz
Institut für Kernphysik
Postfach 3980
D-55099 Mainz
Germany

Drechsel@kph.uni-mainz.de
FAX: (+49) 6131-395474

G. Höhler
Universität Karlsruhe
Institut für Theoretische Teilchenphysik
Postfach 6980
D-76128 Karlsruhe
Germany

Gerhard.Hoehler@phys.uni-karlsruhe.de
FAX: (+49) 721-370726

W. Kluge
Universität Karlsruhe
Institut für Experimentelle Kernphysik
Postfach 3640
D-76021 Karlsruhe
Germany

Wolfgang.Kluge@phys.uni-karlsruhe.de
FAX: (+49) 7247-823414

H. Leutwyler
Universität Bern
Institut für Theoretische Physik
Sidlerstr. 5
CH-3012 Bern
Switzerland

leutwyle@butp.unibe.ch
FAX: (+41) 31-631-38 21

B. M. K. Nefkens
University of California, Los Angeles
Department of Physics
405 Hilgard Ave.
Los Angeles, CA 90024
U. S. A.

BNefkens@uclapp.physics.ucla.edu
FAX: (+1) 310-206-4397

H.-M. Staudenmaier
Universität Karlsruhe
Institut für Anwendungen der Informatik
Postfach 6980
D-76128 Karlsruhe
Germany

Hans.Staudenmaier@phys.uni-karlsruhe.de
FAX: (+49) 721-370726

MENU99 *First Announcement*

Eighth International Symposium on Meson-Nucleon Physics and the Structure of the Nucleon

Zuoz, Engadine, Switzerland

August 16 – 20, 1999

Conference web site: http://www1.psi.ch/~bader/menu99.html

Conference Secretary:
Christine Kunz
Paul Scherrer Institut
WHGA/138
CH-5232 Villigen PSI
Switzerland

E-mail: Christine.Kunz@psi.ch
Fax: +41 (0)56 310 3294

Organizing Committee:
A. Badertscher, Zurich, Chairman
J.-P. Egger, Neuchatel
Q. Ingram, PSI
M. P. Locher, PSI
U.-G. Meißner, Jülich
M. Sainio, Helsinki

Advisory Committee:
A. M. Bernstein, Cambridge
E. Friedman, Jerusalem
J. Gasser, Bern
C. Guaraldo, Frascati
G. Höhler, Karlsruhe
W. Kluge, Karlsruhe
S. Kruglov, St. Petersburg
B. Nefkens, Los Angeles
R. A. Ristinen, Boulder
G. Smith, TRIUMF
G. Wagner, Tübingen

The eighth symposium in the MENU series will be held at the Lyceum Alpinum in Zuoz in the Engadine. Sunday, August 15 is arrival day and Saturday, August 21 departure day (no lectures). The main topics of the symposium will cover experimental and theoretical developments in pion-nucleon and kaon-nucleon physics, photo- and electroproduction of mesons on the nucleon, eta physics and the structure of the nucleon. There will be invited and contributed talks; no parallel sessions are planned. The proceedings will be published as πN Newsletter(s).

The Lyceum is a private boarding school offering the possibility to host conferences during the summer vacation. Full board is offered for at most 100 people (only August 15–21). Accommodation consists of single rooms (and a few double rooms) with washing basins. Showers and restrooms are shared. If you plan to attend the symposium and want to stay at the Lyceum we strongly recommend to send in a preliminary registration form to be found at the conference web site. Mark the appropriate box if you want to stay in a hotel or a rental apartment. The conference secretary will then mail to you a list of hotels or apartments and it will be your own responsibility to make the reservations.

The Engadine (http://www.engadin.ch) is an alpine valley in the eastern-most part of Switzerland at an altitude ranging from about 1250–1800 m. Zuoz (http://www.zuoz.ch) is a village with beautiful old houses in the traditional Engadine style about 20 km from St. Moritz. Splendid possibilities for hiking and mountaineering exist.

Proceedings
of the
GW/JLab Workshop on N* Physics

The George Washington University—Virginia Campus, Ashburn, VA, U. S. A.
October 30 – November 1, 1997

Editors
H. Haberzettl, C. Bennhold, and W. J. Briscoe

CNS
Center for Nuclear Studies

Sponsors
The George Washington University—Virginia Campus
Center for Nuclear Studies
Thomas Jefferson National Accelerator Facility
National Science Foundation

The George Washington University
WASHINGTON DC

The Department of Energy's
Jefferson Lab
THOMAS JEFFERSON NATIONAL ACCELERATOR FACILITY

The George Washington University
WASHINGTON DC
VIRGINIA CAMPUS

Editors
H. Haberzettl, C. Bennhold, and W. J. Briscoe

Center for Nuclear Studies
Department of Physics
The George Washington University
Washington, D.C. 20052
U. S. A.

Editorial Note: The Workshop originally took place under the title *GW/TJNAF Workshop on N* Physics.* At the request of Jefferson Lab, to conform with present-day usage, the acronym "TJNAF" referring to Thomas Jefferson National Accelerator Faciltity, was replaced in the present Proceedings by the more commonly used abbreviation "JLab" wherever possible.

πN NEWSLETTER
No. 14, August 1998

Preface

Around the turn of the century physicists and chemists observed that when a gas is excited by heat or electricity, it emits light which, when separated into its component wavelengths with a prism or diffraction grating, results in a characteristic pattern of discrete lines called the emission spectrum. This was a puzzling finding since the classical theories of atoms and molecules had no explanation for such discrete wavelengths. The rest is history. The observation of discrete excitation spectra of atoms led to the development of the modern atomic theory, quantum mechanics, and eventually to quantum electrodynamics—the ultimate explanation of how photons and charged particles interact.

It is curious to find the situation seemingly reversed in the realm of nuclear and hadronic physics. While we believe the underlying theory for the strong interaction between quarks and gluons to be given by quantum chromodynamics (QCD), we still have no clean measurements of the excitation spectrum of the nucleon. Obtaining unambiguous information on the excited states of the nucleon is essential for verifying QCD in the realm of nuclear physics. To advance this issue, the *4th International Workshop in N* Physics* sponsored by The George Washington University (GW), the Thomas Jefferson National Accelerator Facility (JLab), and the National Science Foundation took place at the GW Virginia Campus in Ashburn, VA from October 30 to November 1, 1997.

Emphasis during the workshop was placed on:
- The interplay between electromagnetic and hadronic N* excitations and the need for new, precise, hadronic reaction data.
- The possibility and degree of dynamical resonance formation through hadronic rescattering, rather than quark excitation.

Among the highlights of the meeting were:
- On the experimental side, preliminary data from JLab's Hall C on $(e, e'\pi)$, $(e, e'\eta)$ and $(e, e'\mathrm{K}^+)$ were presented, along with new data from the CRYSTAL BALL at BNL.
- On the theoretical side, several dynamical model calculations were presented that include a number of electromagnetic and hadronic meson production reactions in a coupled-channels framework.

It is apparent that with the start of the experiments, JLab is beginning to fulfill its promise of helping unravel the questions of nucleon resonance physics. It is also apparent that the data flow from hadron facilities must continue.

C. Bennhold (GW), W. J. Briscoe (GW), and L. Elouadrhiri (JLab)
Workshop Organizers

Workshop Web Site:
http://www.gwu.edu/~cns/nstar.htm

Postscript files of the talks may be downloaded from this site.
For inquiries, send email to cns@www.gwu.edu

Program of the GW/JLab Workshop on N* Physics

Organizers: C. Bennhold, W. J. Briscoe, and L. Elouadrhiri

Thursday, 30 October, 1997

8:55 am C. Bennhold (GW)
Opening Remarks

9:00 am H. Haberzettl (GW)
Dynamical Resonance Formation

9:40 am P. Siegel (CSPU)
Dynamical Formation of the $S_{11}(1535)$ *and the* $\Lambda(1405)$

10:20 am Coffee

10:40 am T. Feuster (Giessen)
Photon and Meson Scattering on the Nucleon in a Coupled Channels Model

11:20 am S. Dytman (Pittsburgh)
Recent Progress in the Coupled Channels Cutkosky Analysis

Noon Lunch

1:30 pm S. Krewald (Jülich)
The Jülich πN *and* (γ, π) *Models*

2:10 pm R. Workman (VPI)
Review of (γ, π) *and the Delta E2/M1 Ratio*

2:50 pm Coffee

3:10 pm J. Price (RPI)
New $p(e, e'p)\pi$ *Results from JLab*

3:25 pm C. Vellidis (ASU)
New $(e, e'\pi)$ *Results from Bates*

3:40 pm R. Davidson (RPI)
A Relativistic, Unitary Model for $(e, e'\pi)$

4:10 pm Coffee

4:40 pm Working groups meet

Friday, 31 October 1997

9:00 am E. Hourany (GRAAL)
New Results and Future Plans at GRAAL

9:30 am J. Price (RPI)
New $p(e, e'p)\eta$ *Results from JLab*

10:00 am Coffee

10:30 am L. Tiator (Mainz)
Eta Photoproduction

11:00 am M. Benmerrouche (SAL)
Eta Electroproduction

11:30 am B. Tippens (UCLA)
New CRYSTAL BALL Results from BNL

Noon Lunch

2:00 pm W. Plessas (Graz)
Baryon Excitation Spectra from a Semirelativistic Chiral Quark Model

2:40 pm A. Donnachie (JLab)
The Use of Conformal Mapping Methods to Evaluate Dispersion Integrals

3:20 pm D. O. Riska (Helsinki)
Covariant Quark Model for Baryon Spectra and Form Factors

3:50 pm Coffee

4:20 pm Working groups meet

Saturday, 1 November 1997

9:00 am T. Mart (Indonesia)
Overview of (γ, K)

9:40 am R. Mohring (UMD)
New $(e, e'\mathrm{K})$ *Results from JLab*

10:00 am Coffee

10:30 am H. Ströher (Mainz)
Overview of $(\gamma, \pi\pi)$

11:10 am F. J. Klein (JLab)
Overview of Vector Meson Photoproduction

11:50 am Lunch

2:00 pm L. Elouadrhiri (JLab/CNU)
The JLab N Program*

2:45 pm B. Nefkens (UCLA)
The CRYSTAL BALL Baryon Resonance Program

3:30 pm Coffee

4:00 pm M. Manley (Kent)
The Need for New Experiments with both Electromagnetic and Hadronic Probes

4:45 pm Working groups summaries

5:15 pm W. Briscoe (GW)
Closing Remarks

Contents

Papers submitted

Dynamical Formation of the $N^*(1535)$ and $\Lambda(1405)$

Peter B. Siegel
California State Polytechnic University Pomona, Pomona CA 91768

Abstract

The octet-meson octet-baryon interaction is represented by a potential, which is iterated in a Lippman-Schwinger equation to obtain a multi-channel S matrix for two-body final states in the $l = 0$ partial wave. It is shown that a potential which has $SU(3)$ symmetry is able to explain a large amount of hadronic and photoproduction data, including the properties of the $\Lambda(1405)$ and $N^*(1535)$ resonances. In this picture, these resonances are a result of an attractive meson-baryon interaction and coupled-channel dynamics.

INTRODUCTION

In this talk, we discuss the interaction between the pseudo-scalar meson octet and the baryon octet. Our focus will be on the general features of the interaction, and the coupled-channel potential model approach. Although we summarize the results of using the effective chiral Lagrangian to obtain a potential for the interaction, the main points we want to emphasize are: a) the necessity for using a coupled-channel approach, b) the success of using approximate $SU(3)$ symmetry for the potential, and c) the fact that $SU(3)$ symmetric potentials produce at least two dynamically generated $l = 0$ resonances, the $\Lambda(1405)$ and the $N^*(1535)$. We first discuss the coupled-channel potential model approach, then the $SU(3)$ symmetry properties of the interaction, and conclude with an analysis of the experimental data. Our discussion here is restricted to the $l = 0$ partial wave.

COUPLED CHANNEL POTENTIAL MODEL CALCULATIONS

In a coupled channel potential model calculation, a potential is constructed to represent the interaction between the particles. We will be focusing our analysis on two-body initial and final states where the degrees of freedom are the meson-baryon states. The general form for such a potential is $V_{iji'j'}(\sqrt{s}, k, k')$, where i and j correspond to the initial meson and baryon, and i' and j' represent the meson and baryon in the final state. The three momenta k and k' are the center of mass momentum of the initial and final states respectively, and $\sqrt{s}$ is the total center-of-mass energy of the interaction. We abbreviate this potential as $V_{mm'}(\sqrt{s}, k, k')$, where m and m' represent the initial meson-baryon and final meson-baryon states.

The coupled channel potential $V_{mm'}$ which connects all possible initial meson-baryon states to all possible final meson-baryon states is inserted into a Lippman-Schwinger equation to solve for the T matrix for the partial wave $l = 0$:

$$T_{mm'}(\sqrt{s}, k, k') = V_{mm'}(\sqrt{s}, k, k') + \sum_n \int_0^\infty V_{mn}(\sqrt{s}, k, q) G_0(\sqrt{s}, q) T_{nm'}(\sqrt{s}, q, k') q^2 dq \quad (1)$$

Here, n represents an intermediate meson-baryon state, and the sum is over all such possible channels. For the propagator, G_0, we choose $2\mu_n/(k_n^2 - q^2 + i\epsilon)$, where k_n is the on-shell momentum and μ_n is the reduced energy of the intermediate meson-baryon channel n. We find that if the energy range of the analysis is small, the results are not particularly sensitive to the choice of propagator.

One can include photoproduction or radiative capture processes to the calculation by adding a baryon-photon channel, and a potential which connects the baryon-gamma to the

meson-baryon channels. To a very good approximation one can neglect the rescattering of the photon with the baryon. This is the same approximation used in deriving "Watson's Theorem", and amounts to setting the propagator $G_{0(B\gamma)}$ in the baryon-gamma channels to zero. Another consequence of this approximation is that only the off-shell dependence of the hadronic side of $V_{n\to B\gamma}$ enters into the calculation.

It was shown in Ref. [1] that the amplitude for radiative capture is given by the sum over charged hadronic channels of the product of a complex number times the Born amplitude for that channel:

$$F_{K^-p\to\Lambda\gamma(\Sigma\gamma)} = \sum_n A_n(\sqrt{s}) f^{Born}_{n\to\Lambda\gamma(\Sigma\gamma)} \tag{2}$$

The sum n is over all possible intermediate meson-baryon channels. All the initial state interactions are subsummed into the complex numbers $A_n(\sqrt{s})$. In analyzing the radiative capture of K^-p, it was found [1] that the initial state hadronic interactions of the various channels was very important. This result emphasizes the importance of a coupled channels approach to radiative capture and photoproduction processes.

There are some positive (+) and negative (−) aspects in using the coupled channel potential approach described above:

• (+) One obtains a coupled-channel S matrix which is unitary. Since transitions to 3-body final states are small, using only two-body final states is a good approximation. So unitarity is satisfied to a very good degree.

• (−) Complete four-dimensional loop integrals are not done in the iteration process. Only three dimensional iterations over the center of mass momentum are carried out via the Lippman-Schwinger equation. That is, only ladder graphs are included in the multiple scattering. Even though the potential can have crossing symmetry, after iteration, the S-matrix will not.

• (+) However, if the energy range of the coupled channel potential analysis is small, the energy dependence of the S-matrix will be approximated well. Also, if a resonance dominates the interaction, the main energy dependence comes from the pole, and the deficiencies mentioned in b) above are minimal. We note that for the low energy K^-p interaction, potentials which satisfy $SU(3)$ symmetry give very similar results even though different off-shell forms and propagators were used.

WHAT IS DYNAMICAL RESONANCE FORMATION

Dynamical resonance formation means that the resonance is formed as a quasi-bound state due to the attractive nature of the interaction. In other words, there is no pole in the potential $V_{mm'}(\sqrt{s}, k, k')$, but the multiple scattering produces a pole in the T or S matrix of the coupled-channel system. This is to be differentiated from an "s-channel" resonance in which there is a pole in the potential V itself. In this case the pole in the potential V produces a pole, which is shifted in energy, in the S-matrix.

One would like to determine if a resonance is dynamically generated, or is a result of a pole in the potential matrix, directly from the data in a model independent manner. This is not easy, if possible at all, so we look at the physics of the interaction in the next section to help us determine the nature of various s-wave resonances.

THE PHYSICS OF THE POTENTIAL

One of the first coupled-channels calculation involving the pseudo-scalar mesons and baryons dates back to the late 1960's by Dalitz, Wong and Rajasekaran [2]. Here, a vector-meson exchange potential with SU(3) universal coupling is applied to the strangeness -1 sector. Using known coupling strengths, a resonance ($\Lambda(1405)$) is produced just below the K^-p threshold. The potential was taken to be a Yukawa form:

$$V_{mm'} = C_{mm'} \frac{e^{-\mu r}}{r} \tag{3}$$

where the $C_{mm'} = C_{ii' \to jj'} = \sum f_{ijk} f_{ki'j'}$, and f_{ijk} are the $SU(3)$ structure constants.

In a more recent calculation, chiral SU(3)L x SU(3)R symmetry was incorporated in the Lagrangian of the cloudy bag model [3], which was applied to the low energy K^-p system. Excellent fits to the low energy K^-p scattering data and the $\Lambda(1405)$ resonance were obtained. The successes of $SU(3)$ symmetry in the meson-baryon potential led us [4] to investigate to what extent all the low energy K^-p data, including the threshold branching ratios, could be fit. The threshold branching ratios of the K^-p atom decay are precise data and put contraints on any potential model. We found that all the low energy K^-p data could be fit with only a 30 percent variation of the relative coupling strengths from their $SU(3)$ values. It was also shown [5–7] that all the low energy hadronic K^-p data as well as $\pi\eta$ production and some photoproduction data can be fit from a potential derived from an effective chiral Lagrangian, which has approximate SU(3) symmetry. In a recent preprint [8] it was found that all the low energy hadronic K^-p data, including the threshold branching ratios, could be fit without any $SU(3)$ symmetry breaking if one included the $\eta\Lambda$ and $\eta\Sigma^0$ channels.

Good fits were obtained in the above calculations even though different off-shell potential forms and different propagators were used: *the critical ingredient in fitting the low energy K^-p data is to have approximate $SU(3)$ relative coupling strengths in the potentials.* This same result holds in low energy πN scattering, where the leading order, Weinberg-Tomozawa, term in a chiral perturbation expansion has this same symmetry. Therefore, **there is substantial evidence to believe that $SU(3)$ relative coupling strengths hold to a good approximation for the whole meson-baryon octet.**

Let's examine the sectors of the meson-baryon interaction where the $SU(3)$ relative coupling strengths might be sufficiently attractive to form a dynamical resonance:

• **Strangeness $= -1$:** There is a strong attraction for isospin I=0. The constants $C_{mm'}$ are

	$\pi\Sigma$	$\bar{K}N$	$\eta\Lambda$
$\pi\Sigma$	-2	$-\sqrt{6}/4$	$-3\sqrt{2}/4$
$\bar{K}N$	$-\sqrt{6}/4$	$-3/2$	0
$\eta\Lambda$	$-3\sqrt{2}/4$	0	0

The attraction is in both the $\pi\Sigma$ and $\bar{K}N$ channels. Using expected strengths and ranges for the potential a resonance is formed just below the $\bar{K}N$ threshold [5]. This resonance has all the propertics of the $\Lambda(1405)$!

• **Strangeness $= 0$:** For isospin I=1/2 there is an attractive interaction for both $\pi N \to \pi N$ and $K\Sigma \to K\Sigma$ scattering. The $C_{mm'}$ are:

	πN	ηN	$K\Lambda$	$K\Sigma$
πN	-1	0	$3/4$	$-1/4$
ηN	0	0	$3/4$	$3/4$
$K\Lambda$	$3/4$	$3/4$	0	0
$K\Sigma$	$-1/4$	$3/4$	0	-1

There are several important features to note. The interaction between the kaon and the sigma is strongly attractive. This attraction can be enhanced due to the large mass of the kaon. Although there is a no direct interaction between the ηN and the πN channels, there is a strong coupling of both the ηN and the πN channels to the $K\Sigma$ channel. For expected strengths and ranges, *a quasi-bound $K^+\Sigma$ resonance is formed, and it strongly connects the πN and ηN channels via multiple scattering.* The properties of this resonance are very similar to the $N^*(1535)$!

• **Strangeness $= -2$:** In the isospin 1/2 sector, there is attraction between the Ξ and π as well as the $\bar{K}$ and Sigma. The $C_{mm'}$ are given by:

	$\pi\Xi$	$\bar{K}\Lambda$	$\bar{K}\Sigma$	$\eta\Xi$
$\pi\Xi$	-1	$\sqrt{3/8}$	$-5/4$	0
$\bar{K}\Lambda$	$\sqrt{3/8}$	0	0	$3/4$
$\bar{K}\Sigma$	$-5/4$	0	-1	$\sqrt{3}/4$
$\eta\Xi$	0	$3/4$	$\sqrt{3}/4$	0

The attraction between the Ξ and π and the Σ and $\bar{K}$ might be strong enough to form a dynamical resonance. There are two candidates for this resonance, the $\Xi(1609)$ and the $\Xi(1690)$. We are at present examining the properties this system in order to determine whether a resonance is dynamically formed, and if so, which Ξ resonance fits its properties best.

COMPARISON WITH AVAILABLE DATA

The most extensive data to check the baryon-meson coupled channel approach is in the $S = -1$ sector near the K^-p threshold. Here there is a *wealth of data in a small energy range*: the K^-p reaction can scatter into six final states: K^-p, $\overline{K}^0n$, $\pi^+\Sigma^-$, $\pi^0\Sigma^0$, $\pi^-\Sigma^+$, and $\pi^0\Lambda$. Data have been taken for all scattering final states for K^- laboratory momenta from 60 to 200 MeV/c. At threshold, there are very precise branching ratio data of the K^- proton atomic decay to the three hadronic final state as well as the two radiative capture transitions. In addition, there is a resonance, the $\Lambda(1405)$ just below the K^-p threshold for which there are $\Sigma - \pi$ spectrum measurements. These data have two important features: they contain information about the relative coupling to the various channels, and they are in a narrow energy range $1400 < \sqrt{s} < 1460$. The first feature places stringent tests on any model describing the octet meson-baryon interaction. The second feature reduces the model dependence of the analysis.

Effective Chiral Lagrangian Approach

Next, we summarize the results of a coupled channel potential derived from the $SU(3)$ effective chiral Lagrangian. Details of the work are described in Refs. [5–7]. The potential (or pseudo-potential) is constructed such that in the Born approximation it has the same s-wave scattering amplitude as the effective chiral Lagrangian, at order q^2.

The motivation for using this approach are two-fold. First, SU(3)L x SU(3)R chiral symmetry is believed to be approximately valid for meson-baryon interactions. To leading order in

meson momenta "q" the potential has the SU(3) relative coupling strengths, $C_{mm'}$. There is slight breaking however, since the mass of the meson enters in the numerator. Second, $SU(3)$ symmetry breaking can be treated systematically. At next order in the expansion scheme, q^2, there are a finite number of new terms allowed by chiral symmetry [9]. Once these terms are fixed, the relative coupling strengths for the whole octet-meson octet-baryon interaction is determined. This allows one to use "physics" to guide the $SU(3)$ symmetry breaking.

Our initial approach was to use the low energy K^-p data to determine the unknown coefficients in the "q^2" terms of the effective chiral Lagrangian. Once this was done, all the Lagrangian parameters (i.e. potential strengths for all channels) are fixed. We then examined other sectors, where the data was not as precise, to determine if resonances are formed and if so, their properites.

There are no free Lagrangian parameters for the order "q" terms, and six free parameters for the order "q^2" terms. Using data from the πN, K^+N scattering lengths, and the $\sigma_{\pi N}$ term reduces the number of free Lagrangian parameters to 3. In addition to the Lagrangian (potential strengths) parameters, a limited number of off-shell range parameters enter the calculation as well. We found that a satisfactory fit for all the low energy K^-p hadronic data was obtained by using a local potential with one common off-shell range for all the channels. This is not a trivial exercise, since the data have a diverse $SU(3)$ structure and the threshold branching ratios are accurately measured.

There are two interesting results of the analysis. The first is that a fit for the local potential was found using a Yukawa potential with only one common "exchange mass" of 412 MeV for all channels. This value lies between the mass of a vector meson and that of two pions. Since such t-channel exchanges are believed to dominate the interaction, this mass is in line with the physics of the process. The second is that we also found a fit using a separable potential, and the Lagrangian parameters for this fit were very similar to those using the local potential. As mentioned above, this is probably because the energy range of the data is small.

Using the same potential parameters as determined form the K^-p analysis, we examined πN scattering near the ηN threshold [6]. As discussed in Ref. [6], excellent agreement was obtained in describing the $\pi N \to \eta N$ total cross section, and the resonance properties of the $N^*(1535)$.

Recently [7], this analysis was extended to include the photoproduction reactions $\gamma p \to \eta p$, $\gamma n \to \eta n$, $\gamma p \to K^+\Lambda$, $\gamma p \to K^+\Sigma^0$, and $\gamma p \to K^0\Sigma^+$. Also, the analysis was extended up in energy to compare with $\pi^-p \to K^0\Lambda$, $\pi^-p \to K^0\Sigma^0$, $\pi^-p \to K^+\Sigma^-$ and $\pi^+p \to K^+\Sigma^+$ total cross section data. No new potential parameters are needed for the photoproduction channels, since the Born terms, and hence the potential strengths are determined from the effective chiral Lagrangian. *The agreement with the data is remarkable*!!

DETERMINING RESONANCE PARAMETERS FROM THE DATA

There has been some discussion at this workshop regarding the extraction of the mass of a resonance, its width, and the decay branching ratios from the scattering data. Problems arise due to the relatively large width of the resonance compared to its mass. Complications can also occur if the resonace is close to a threshold as in the $N^*(1535)$ case. Often Breit-Wigner forms are used in the parameterization of the data, with the hope that the parameters used in this Breit-Wigner piece correspond to the parameters of the resonance. However, the treatment of the non-resonant background can influence these parameters, and the analysis becomes model dependent.

A possible way to overcome these difficulties is to consider the energy dependence of the full coupled-channel S-matrix on the real axis. The eigenvalues of the S-matrix have modulus 1, and can be expressed in terms of eigenphases δ as $e^{2i\delta}$. Near a resonance, one of the eigenphases, δ_{res}, passes through 90 degrees. For a finite energy range near the resonance, the energy dependence of this eigenphase will follow a Breit-Wigner form:

$$\tan(\delta_{res}) = \frac{\Gamma(\sqrt{s})}{2(M^* - \sqrt{s})}. \tag{4}$$

By fitting the eigenphase to this form, the appropriate resonance parameters can be determined. This is a procedure that can be carried out for any analysis for which a coupled-channel S-matrix can be computed, and is an unambiguous method to compare resonance parameters. In particular, for the $N^*(1535)$ this procedure works well.

Consider the $N^*(1535)$ resonance, where there are two main hadronic channels and consequently two eigenphases. In our analysis the resonant eigenphase has a Breit-Wigner energy dependence $\tan(\delta_{res}) = (k_1\gamma_1 + k_2\gamma_2)/(2(M^* - \sqrt{s}))$ over an energy range of 100 MeV. In Fig. 1 we plot the two eigenphases, resonant and non-resonant, as a function of energy from Ref. [6]. The curve is the best fit Breit-Wigner shape to the resonant eigenphase with parameters $\gamma_1 = 0.26$, $\gamma_2 = 0.25$, and $M^* = 1557$ MeV. We note that even though in our case the resonance was formed dynamically, without an explicit s-channel resonance in the potential, a pole is produced in the S-matrix with the energy dependence of a typical Breit-Wigner resonance.

Fig. 1 shows that the eigenphase passes through 90 degrees at $\sqrt{s} = 1557$ MeV. However, as the energy is increased, the phase shift increases to around 120 degrees at the $K\Lambda$ threshold, and then starts to decrease [7]. For a "clean" resonance, the phase shift should continue through 180 degeees, as is the case for the $\Lambda(1405)$. So, although resonance parameters can be extracted from the eigenphase, the true status of this resonance might need to be re-examined.

Fig. 1 also shows that the background eigenphase makes up a small but significant part of the interaction. The effect of the background can be quantified in a fairly model independent way. Consider the ratio

$$R = \frac{k_1\gamma_1\sigma_{12}}{k_2\gamma_2\sigma_{11}}. \tag{5}$$

For a pure Breit-Wigner resonance this ratio is exactly one, and any deviation from unity is due to the background. The momentum in the center of mass of channel 1 and 2 are k_1 and k_2, and the other parameters are determined from the scattering data. σ_{11} is obtained from a phase-shift analysis of πN scattering, and is the isospin $I = 1/2$, $l = 0$ cross section for $\pi N \to \pi N$. σ_{12} can be obtained directly from the $\pi N \to \eta N$ total cross section, since this cross section is predomanently $l = 0$. The partial widths γ_1 and γ_2 are determined form the resonant eigenphase. In Fig. 2 we plot R, where the triangles are for the phase shift analysis of Ref. [10] and the circles for the phase shift analysis of Ref. [11]. The solid line is R_{BW} from our analysis [6]. These results suggest that there is a significant background for the $N^*(1535)$ resonance.

In conclusion we see that due to the strong interaction of the meson-baryon system, a coupled-channel analysis is necessary in any quantitative analysis. We also discussed different potential models that have been applied to the K^-p interaction at low energy. Although these potential models used different off-shell extensions or cut-off procedures, and used different propagators, the results were similar. The similarity is due to the use of SU(3) symmetry

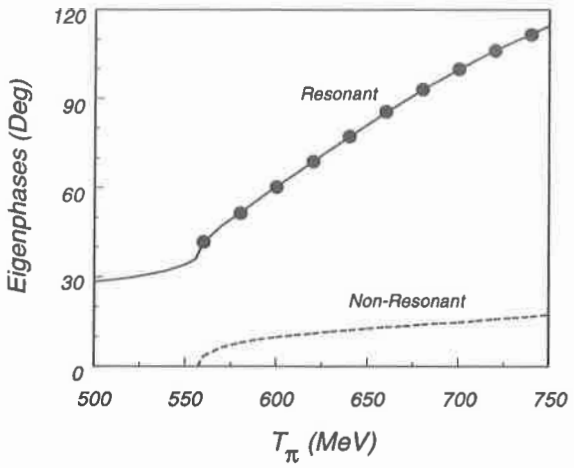

Figure 1. A plot of both the resonant and non-resonant eigenphases for πN, ηN coupled channel system as a function of pion laboratory kinetic energy. There are two other channels included in the calculation, $K\Lambda$ and $K\Sigma$, but they are virtual since the energy is below their threshold. The solid line is a fit to a pure Breit-Wigner form.

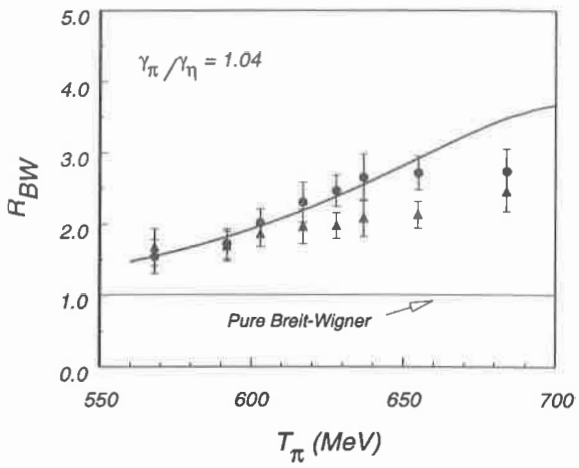

Figure 2. The parameter R_{BW} as defined in Eq. 5 is plotted vs. pion laboratory kinetic energy. The circles (triangles) correspond to using the phase shift analysis of Ref. [11] (Ref. [10]) for the $\pi N \to \pi N$ $l = 0$ cross section.

in the potentials. It was also shown that potentials based on $SU(3)$ symmetry reproduce the hadronic properties of the $\Lambda(1405)$ and $N^*(1535)$ as well as various photoproduction and hadronic data. Thus we conclude that SU(3) symmetry is a good approximation for the potentials representing the interaction between the octet mesons and baryons. These facts strongly suggest that the $\Lambda(1405)$ and the $N^*(1535)$ are dynamically generated resonances.

REFERENCES

[1] P.B. Siegel and B. Saghai, *Phys. Rev.* **C52** 392-400 (1995).

[2] R.H. Dalitz, T.-C. Wong and G. Ragesekaran, *Phys. Rev.* **153** 1617 (1967).

[3] E.A. Veit, B.K. Jennings, A.W. Thomas and R.C. Barrett, *Phys. Rev.* **D31** 1033 (1985).

[4] P.B. Siegel and W. Weise, *Phys. Rev.* **C38** 2221-2229 (1988).

[5] N. Kaiser, P.B. Siegel and W. Weise, *Nucl. Phys.* **A594** 325-345 (1995).

[6] N. Kaiser, P.B. Siegel and W. Weise, *Phys. Lett.* **B362** 23-28 (1995).

[7] N. Kaiser, T. Waas and W. Weise, *Nucl. Phys.* **A612** 297-320 (1997).

[8] E. Oset and A. Ramos, "Non perturbative chiral approach to s-wave $\bar{K}N$ interactions", Los Alamos preprint archives nucl-th/9711022 (1997).

[9] A. Krause, *Helv. Act. Phys.* **63** (1990) 3.

[10] G. Höhler, in Landolt-Börnstein, Vol. 9b2, ed. H. Schopper (Springer, Berlin, 1983).

[11] SAID computer program, R. Arndt *et al.*, Virginia Polytechnic Institute and State University, Blacksburg, VA 24061.

Photon and meson scattering on the nucleon*

T. Feuster and U.Mosel†
Institut für Theoretische Physik, Universität Gießen,
Heinrich-Buff-Ring 16, D-35392 Giessen, Germany

Abstract

In an effective Lagrangian model employing the K-matrix approximation we extract nucleon resonance parameters. To this end we analyze simultaneously all available data for reactions involving the final states γN, πN, $\pi\pi N$, ηN and $K\Lambda$ in the energy range $m_N \leq \sqrt{s} \leq 1.9$ GeV. The background contributions are generated consistently from the relevant Feynman amplitudes, thus significantly reducing the number of free parameters.

INTRODUCTION

In recent years effective Lagrangian models have been widely used to extract information on nucleon resonances from photon-induced reactions [1–4]. The two main reasons for this are:

- the scattering amplitude can be systematically expanded in terms of Feynman diagrams,
- gauge invariance can easily be implemented on the operator level.

The first point allows to reduce the free parameters of the model to masses and couplings of the contributing resonances. Only a few parameters like cutoffs need to be introduced ad hoc. Once the parameters are fixed by some experimental data all other reactions involving the same particles and couplings can in principle be predicted. Furthermore, the invariant amplitude derived from Feynman diagrams contains the spin structure of all intermediate states in a fully relativistic way. The fulfillment of gauge invariance in effective Lagrangian models make them most suitable for the investigation of processes involving real or virtual photons, such as meson photoproduction.

On the other hand, unitarity and analyticity are not guaranteed in this kind of models and are usually only incorporated approximately [2]. Especially the final state interaction in meson photoproduction is normally neglected. Since the number of open channels increases with the photon energies now available at TJNAF and other facilities there is an urgent need for a dynamical treatment of the rescattering in the effective Lagrangian framework.

THE MODEL

To this end we described the purely hadronic reactions in terms of the same Lagrangians and couplings as usually used in photoproduction [5]. Once the hadronic parameters are fixed it is straightforward to extend the calculations to electromagnetic reactions.

Our model employs the K-matrix approximation taking into account only the onshell part of the intermediate propagator G in the Bethe-Salpeter equation $T = V + VGT$ [6]. The resulting equation for T is simple and easy to treat numerically:

$$[K] = [V], \quad [T] = \left[\frac{K}{1 - \mathrm{i}K}\right]. \tag{1}$$

*Work supported by BMBF, GSI Darmstadt and DFG
†E-mail: Thomas.Feuster@theo.physik.uni-giessen.de

The brackets $[\cdots]$ should indicate that V, K and T are $n \times n$-matrices (n being the number of asymptotic channels taken into account) and that (1) is a matrix equation.

In this framework all possible rescattering contributions are included consistently. It has so far been applied successfully to pion photoproduction and Compton scattering in the Δ-region [3] and to eta photoproduction [4].

Our aim is now to extend these calculations to higher energies and to all energetically open mesonproduction channels. As a first step we take into account the final states γN, πN, ζN, ηN and $K\Lambda$, where the coupling to the scalar, isovector ζ meson should simulate the inelasticity coming from $\pi\pi N$-decays of the resonances. The potential V is calculated including contributions from Born terms and s-, u- and t-channel resonances with spin $\leq \frac{3}{2}$. A detailed account of the model can be found in [5]. There also the results of the fits to the purely hadronic reactions are presented.

For some resonances there are indications of additional decay channels like ωN and $K\Sigma$, but these were not included in this first study. From previous works [7,8] it is known that the four final states used here account for most of the width of the nucleon resonances.

Unfortunately the need for additional form factors F introduces a source of systematic error because we a priori do not know their functional form. To investigate the systematic errors in the resonance parameters connected with this uncertainty we have performed three different fits for each of the two πN-partial wave analysis KA84 and SM95 [9,10] using different combinations of the form factors for the nucleon resonances and the t-channels exchanges.

RESULTS OF THE FITS TO HADRONIC DATA

Comparison to the data

From Tab. 1 it can be seen that all combinations of πN-data and form factors lead to fits with equal quality. The χ^2-values for the SM95-PWA are somewhat higher because we use the energy-dependent data in our fits.

πN-PWA	χ^2	χ^2/DF	χ^2_π/DF	$\chi^2_{\pi\pi}$/DF	χ^2_η/DF	χ^2_K/DF
KA84	4130 - 4688	2.80 - 3.17	2.40 - 3.02	5.69 - 6.65	1.54 - 1.64	3.26 - 3.64
SM95	4624 - 4871	3.55 - 3.74	3.70 - 4.04	5.77 - 6.89	1.64 - 1.67	3.23 - 3.34

Table 1. χ^2-values for the different fits to the hadronic data. χ^2/DF gives the χ^2 per datapoint. Also the χ^2/DF-values for the different reaction channels are given separately. The ranges give the results of the fits using different combinations of form factors.

As a general trend, we find that the fits seem to be better in the S_{I1}- and P_{I1}-channels than in P_{I3} and D_{I3}; for example see Fig. 1. This might indicate a shortcoming in the description of spin-$\frac{3}{2}$-resonances. Either the use of a common shape for the form factor for spin-$\frac{1}{2}$ and spin-$\frac{3}{2}$ is too restrictive or we are missing contributions from resonances with spin $\geq \frac{5}{2}$. At this point we cannot distinguish between the two explanations.

Furthermore, the $\pi N \to \pi\pi N$-data (Fig. 2) are not reproduced as well as the other channels. This should come as no surprise keeping in mind our approximate treatment of this channel by an effective ζN-state. Nevertheless it is important to check for unusual discrepancies in specific partial waves, because these might indicate that resonances and/or decay channels are missing in our calculation.

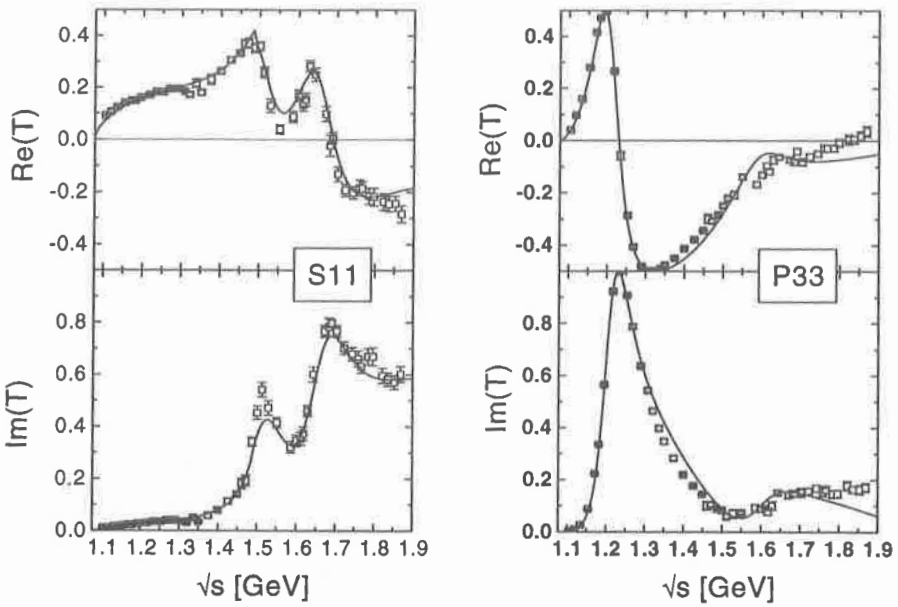

Figure 1. Fits to the S_{11}- and P_{33}-partial waves from SM95 [10].

For the reaction $\pi^- p \to \eta n$ all parameter sets give similar fits to the total and differential cross sections. Starting from about 1.65 GeV on upwards we find that we cannot fully reproduce the falloff in forward direction (Fig. 3). Nefkens et al. [8] are able to describe the differential data over the whole energy range, but require additional S_{11}- and P_{11}-resonances with sizeable ηN-coupling. To investigate this in detail we would need to enlarge the energy range of our fits to be able to reliably extract parameters for resonances with a mass of 1.9 - 2.0 GeV. With 5 - 6 resonances coupling to this channel better differential data and also polarization observables would be needed to safely disentangle their contributions.

As in the case of $\pi^- p \to \eta n$ inconsistencies between different measurements of the cross sections can be observed for $\pi^- p \to K^0 \Lambda$ (e.g. at 1.694 GeV in Fig. 3). Also the errors of the polarization data given in [18] are extremely large. In practice these data do not constrain the couplings at all. So also in this channel better data are needed. The contribution to the total χ^2 is larger for this channel than for the η-production (Table 1). This is mainly due to the fact that we did not enlarge the errors as in the case of $\pi^- p \to \eta n$.

Resonance parameters

We now want to focus our discussion on the S_{11}-and P_{33}-channels because the main features of our calculations can already be seen here and the resonances $S_{11}(1535)$ and $P_{33}(1232)$ are of special interest also for photoproduction reactions. The resonance parameters we have extracted are given in Tab. 2.

For the other parameters we only note that the couplings we extract agree quite well with the values obtained by other groups. The remaining differences can largely be explained by the contribution of the t-channel ρ-exchange that for higher energies is not described very well by the corresponding Feynman diagram. Here a different prescription (eg. in terms of Regge-trajectories) seems to be necessary. Furthermore, we find that the pole parameters

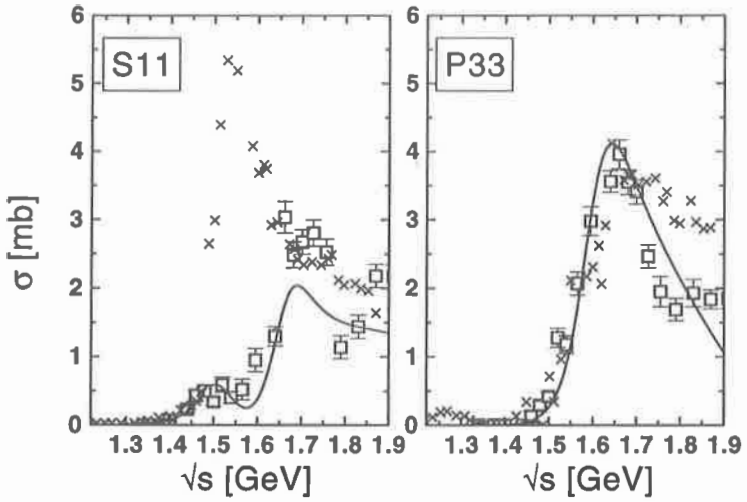

Figure 2. Comparison of the calculated $\pi N \to \pi\pi N$ cross sections for the fits using the SM95-PWA with the data from [7]. In addition the inelastic cross section as determined from the SM95-PWA is shown (×).

extracted from the speed-plots in general exhibit a smaller spreading than the masses and couplings used in the calculation of the amplitudes.

$L_{2I,2S}$	M [GeV]	Γ_{tot} [MeV]	$\Gamma_{\pi N}$ [MeV]	%	$\Gamma_{\zeta N}$ [MeV]	%	$\Gamma_{\eta N}$ [MeV]	%	$\Gamma_{K\Lambda}$ [MeV]	%
$S_{11}(1535)$	1.541	185	70(+)	39	14(+)	8	101(+)	56	0(+)	0
	1.544	171	66(+)	39	10(+)	6	94(+)	55	0(+)	0
$S_{11}(1650)$	1.697	250	195(+)	75	40(+)	16	1(-)	1	14(+)	5
	1.689	207	151(+)	73	42(+)	20	1(-)	1	13(+)	6
$P_{33}(1232)$	1.229	113	113(+)	100	–	–	–	–	–	–
	1.230	110	110(+)	100	–	–	–	–	–	–
$P_{33}(1600)$	1.672	385	50(+)	13	335(+)	87	–	–	–	–
	1.684	393	59(+)	15	334(+)	85	–	–	–	–

Table 2. Extracted resonance parameters for the S_{11}-and P_{33}-resonances from fits to the hadronic data only. Given are the averages of the fits performed in [5]. The first line shows the values using the KA84-PWA, the second line is for the SM95-data. The signs of the couplings are given in brackets.

S_{11}: This resonance is of special interest because of its large ηN-branching. The deeper reason for this is not well understood and the ηN-decay width cannot be reproduced in most quark-models [19–22]. A reliable value for this parameter would therefore put strong restrictions on all models for this resonance. Since we have at least two resonances in this channel close to each other, a satisfactory fit is only possible if both are included [4]. Furthermore, the s-waves S_{11} and S_{31} at threshold are dominated by the Born terms and the ρ-meson that determine the scattering lengths. In addition, at least the two channels $\pi N \to \pi N$ and $\pi N \to \eta N$ have to be taken into account because of the large branching of the $S_{11}(1535)$

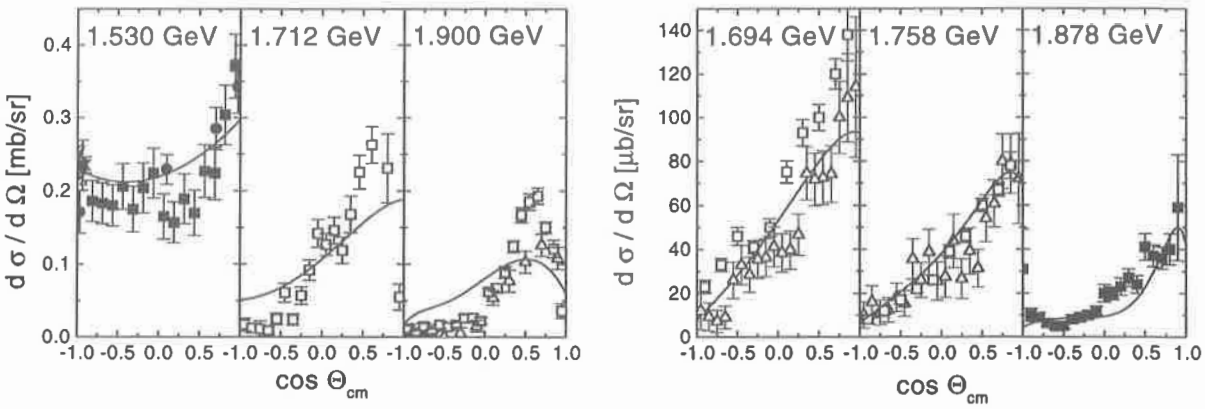

Figure 3. Comparison with data for the calculated differential cross sections. **Left:** $\pi^- p \to \eta n$, the datapoints are taken from: [11] (●), [12] (×), [13] (△), [14] (□), [15] (■). **Right:** $\pi^- p \to K^0 \Lambda$, the datapoints are taken from: [16] (□), [17] (△), [18] (■).

($\approx$ 50% πN, $\approx$ 45% ηN) into both of these. This has two consequences: i) only within a model accounting for all these points a reliable determination of the $S_{11}(1535)$-parameters is possible and ii) all extractions are limited by the quality of the $\pi N \to \eta N$ data.

Unfortunately, the spreading of the parameters is larger for the fits to the SM95-PWA. This is because we were not able to fully reproduce the data for energies $\approx$ 1.50 GeV (Fig. 1). This is also the region of the largest differences between both the KA84-PWA and the energy-dependent solution of SM95 to the energy-independent data. Maybe the assignment of larger error bars for these energies would lead to more consistent values for the $S_{11}(1535)$ parameters.

***P*$_{33}$**: As expected, all fits lead to the same parameters for the $P_{33}(1232)$. The numbers are slightly lower than in other works. This can be explained by the t-channel ρNN-form factor used in our calculation, that forces a smaller ρNN-coupling than usual. The fits try to compensate for this by lowering the mass and the width of the $P_{33}(1232)$.

The second resonance, $P_{33}(1600)$, can be clearly seen in the $\pi N \to \pi\pi N$-channel, whereas the contribution to the πN-phase shift is negligible. Despite the discrepancy between the inelasticities from KA84/SM95 and the $\pi N \to \pi\pi N$-cross section, the couplings of the $P_{33}(1600)$ are well determined and are comparable to the values of Manley et al. (M = 1.706 GeV, Γ_{tot} = 430 MeV).

PHOTON-INDUCED REACTIONS

Ideally, pion photoproduction could now be used to fix the electromagnetic couplings of the resonances and all other reactions could then be predicted from our model. This does not work in practice because the quality of the data is not good enough to determine the couplings uniquely. This can already be seen in the hadronic channels (eg. $\pi^- p \to \eta n$). Furthermore, there might be inconsistencies between the data for different reactions that can best be studied in global fits to all channels.

As a compromise between the two approaches "prediction of channels" and "global fit to all data" we have adopted the following strategy:

- Start with the electromagnetic couplings set to the average values given in the PDG-

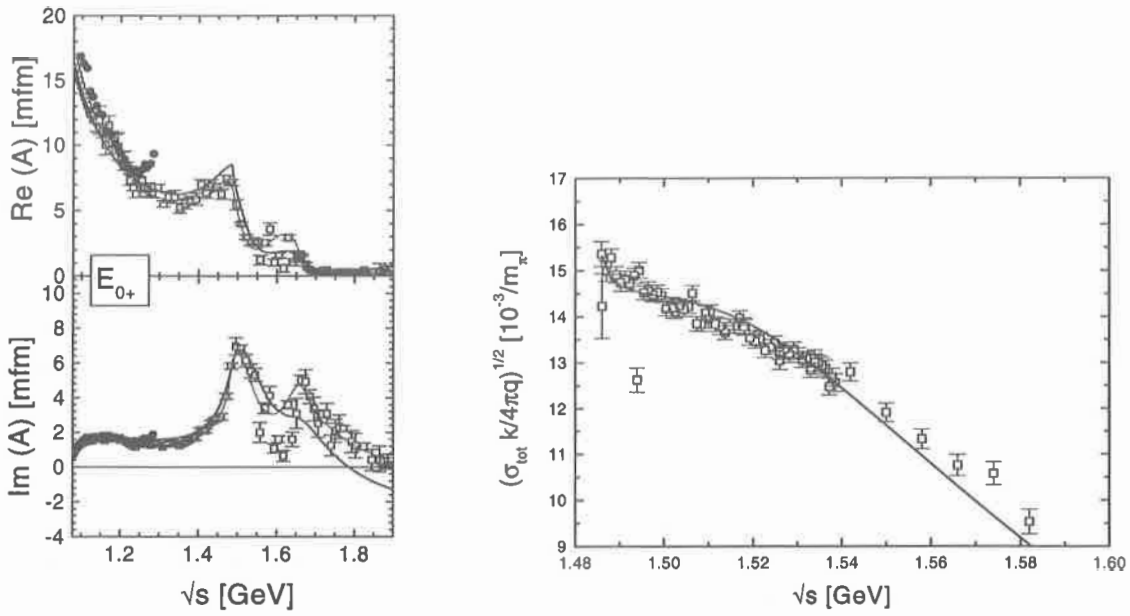

Figure 4. Left: Calculated E^p_{0+}-multipole as compared to data. Shown are the SP97-PWA [10] (□: single-energy values, thin line: energy-dependent solution) and the single-energy solution of Hanstein et al. [24] (●). **Right**: Reduced $\gamma p \to \eta p$ cross section. The data are from Krusche et al. [25] and Wilhelm [26].

booklet [23]. Allow these values to vary in fits to $\gamma N \to \gamma N$ and $\gamma N \to \pi N$.

- Check for deviations in the other mesonproduction reactions. If there are any, try global fits to all photon-induced data.
- If no satisfactory fits can be found allow also the hadronic parameters of single resonances to vary.

Since these fits are still underway, we can only present preliminary results here:

- Due to the larger scattering of the photoproduction data the χ^2/DF increases to ≈ 10.
- For the $P_{33}(1232)$ the helicity couplings extracted from $\gamma N \to \gamma N$ and $\gamma N \to \pi N$ are in good agreement. In the case of the $D_{13}(1520)$ the inclusion of the Compton data leads to a reduction of the helicity couplings of about 25%.
- A fit to the very accurate data on eta photoproduction [25] is only possible, if we allow all $S_{11}(1535)$ parameters to vary. Accordingly, the $S_{11}(1650)$ mass and couplings also need to be readjusted.
- Even upon inclusion of a hadronic form factor in the $KN\Lambda$-vertex the coupling $g_{KN\Lambda}$ is found to be only 1/3 of the predicted SU(3)-value.

Again we want to focus on the results for the S_{11} and P_{33}. Shown in Fig. 4 are the E^p_{0+}-multipole and the reduced $\gamma p \to \eta p$ cross section. In Tab. 3 we list the resonance parameters deduced from the global fit. We also quote the helicity amplitudes given by the Particle Data Group [23]. These values have been extracted using pion photoproduction.

$L_{2I,2S}$	M [GeV]	Γ_{tot} [MeV]	$\Gamma_{\pi N}$ [MeV]	$\Gamma_{\zeta N}$ [MeV]	$\Gamma_{\eta N}$ [MeV]	$\Gamma_{K\Lambda}$ [MeV]	A_{OWN} $[10^{-3}\ \mathrm{GeV}^{-1/2}]$	A_{PDG}
$S_{11}(1535)$	1.541	195	70(+)	15(+)	110(+)	0(+)	105, -43	70, -46
$S_{11}(1650)$	1.700	315	220(+)	74(+)	5(-)	16(+)	33, -15	53, -15
$P_{33}(1232)$	1.230	113	113(+)	–	–	–	-129, -250	-140, -258
$P_{33}(1600)$	1.698	492	92(+)	400(+)	–	–	-16, -27	-23, -9

Table 3. Extracted resonance parameters for the S_{11}-and P_{33}-resonances from a combined fit to all data using the KA84-PWA. For the S_{11}-resonances the two values for A are the proton- and neutron-helicity couplings, for the P_{33}-resonances we list the $\frac{1}{2}$- and $\frac{3}{2}$-couplings.

The helicity amplitudes of the $S_{11}(1535)$ are in good agreement with other extractions using $\gamma p \to \eta p$ ($A^p_{1/2} = 120 \pm 26$ [27]) but are higher than the values usually found in $\gamma N \to \pi N$ ($A^p_{1/2} = 70 \pm 12$ [23]). The coupled channel approach therefore allows to solve this puzzle by a dynamical treatment of all relevant contributions.

In the case of the $P_{33}(1232)$ a combined fit to the $\gamma N \to \gamma N$ and $\gamma N \to \pi N$ data yields $\approx$ 5% smaller couplings (comp. Tab. 3) than a fit to the pion photoproduction alone. From this we conclude that there is no disagreement between the data of the two reactions. Especially the LEGS data on the photon asymmetries (Fig. 5) [28] can be reproduced fairly well in our calculation. Older predictions of isobar models [29] are not able to describe these data.

CONCLUSIONS

We have developed a coupled channel model taking into account the final states γN, πN, $\pi\pi N$, ηN and $K\Lambda$. The K-matrix approximation is used and the potential is derived from effective Lagrangians. Within this framework we were able to extract resonances masses and couplings from fits to the purely hadronic data. Unfortunately, some of the parameters are not very well determined, mainly because of the poor quality of the data for $\pi^- p \to \eta n$ and $\pi^- p \to K^0\Lambda$. Using also the data on photon-induced reactions we found that a global fit is possible and that the helicity couplings extracted are in good agreement with the results of other calculations.

Especially for the $S_{11}(1535)$ the $\gamma p \to \eta p$ data impose strict constraints on the resonance masses and widths and we conclude that a reliable extraction of these parameters is only possible if the data from both hadronic and electromagnetic reactions are taken into account.

Acknowledgements

One of the authors (T.F) would like to thank the organizers of this workshop for their invitation and kind hospitality. Furthermore, we would like to thank C. Bennhold, H. Haberzettl, T. Mart and I.I. Strakovsky for many stimulating and fruitful discussions.

REFERENCES

[1] S. Nozawa, B. Blankleider und T. - S.H. Lee, *Nucl. Phys.* **A513**, 459 (1990); S. Nozawa und T.-S.H. Lee, *Nucl. Phys.* **A513**, 511 (1990);

[2] M. Benmerrouche, N. C. Mukhopadhyay und J.-F. Zhang, *Phys. Rev.* **D51**, 3237 (1995)

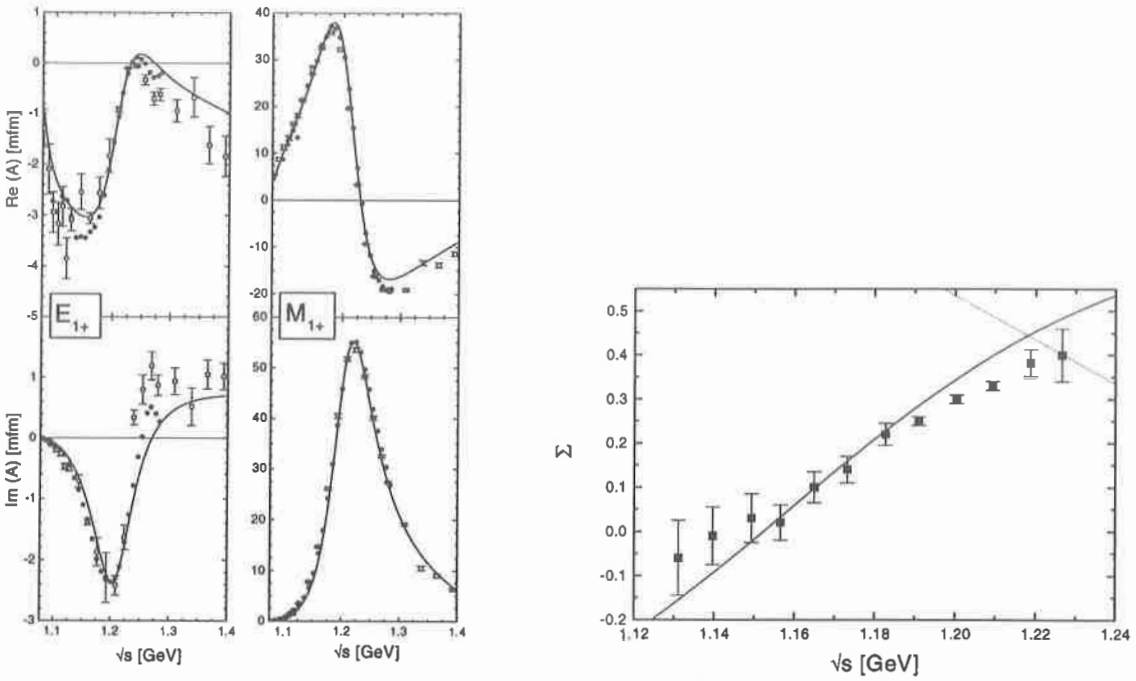

Figure 5. Left: Calculated $E_{1+}^{3/2}$- and $M_{1+}^{3/2}$-multipoles as compared to data. Shown are the SP97-PWA [10] (□: single-energy values, thin line: energy-dependent solution) and the single-energy solution of Hanstein et al. [24] (•). **Right**: Polarization asymmetries in Compton scattering. Shown are the results of this calculation (——) and the predictions of the isobar model of Ishii et al. (· · ·) [29]. The data are from Blanpied et al. [28].

[3] V. Pascalutsa and O. Scholten, *Nucl. Phys.* **A591**, 658 (1995); O. Scholten, A.Yu. Korchin, V.Pascalutsa and D. Van Neck, *Phys. Lett.* **B384**, 13 (1996)

[4] C. Sauermann, PhD-thesis, Darmstadt 1996; C. Deutsch-Sauermann, B. Friman and W. Noerenberg, *Phys. Lett.* **B409**, 51 (1997)

[5] T. Feuster and U. Mosel, *nucl-th@xxx.lanl.gov* preprint #9708051

[6] B. C. Pearce und B. K. Jennings, *Nucl. Phys.* **A528**, 655 (1991)

[7] D.M. Manley, R.A. Arndt, Y. Goradia and V.L. Teplitz, *Phys. Rev.* **D30**, 904 (1984) D.M. Manley and E.M. Saleski, *Phys. Rev.* **D45**, 4002 (1992)

[8] M. Batinić, I. Dadić, I. Šlaus, A. Švarc, B.M.K. Nefkens and T.-S.H. Lee, *nucl-th@xxx.lanl.gov* preprint #9703023; M. Batinić, I. Dadić, I. Šlaus, A. Švarc and B.M.K. Nefkens *Phys. Rev.* **C51**, 2310 (1995)

[9] E. Pietarinen, *Nucl. Phys.* **B107**, 21 (1976); R. Koch, *Nucl. Phys.* **A448**, 707 (1986) and *Z. Phys.* **C29**, 597 (1985); G. Höhler, F. Kaiser, R. Koch and E. Pietarinen, *Handbook of pion-nucleon scattering*, Physics Data 12-1, Karlsruhe, 1979

[10] SM95 and SP97 solutions of the VIRGINIA TECH PARTIAL-WAVE ANALYSIS, available via WWW from http://clsaid.phys.vt.edu/~CAPS. For further reference see, for example, R.A. Arndt, I.I. Strakovsky, R.L. Workman and M.M. Pavan, *Phys. Rev.* **C52**, 2120 (1995); R.A. Arndt, R.L. Workman, Z. Li and L.D. Roper, *Phys. Rev.* **C42**, 1853 (1990)

[11] F. Bulos et al., *Phys. Rev.* **187**, 1827 (1969)

[12] N.C. Debenham et al., *Phys. Rev.* **D12**, 2545 (1975)
[13] B.W. Richards et al., *Phys. Rev.* **D1**, 10 (1970)
[14] R.M. Brown et al., *Nucl. Phys.* **B153**, 89 (1979)
[15] J. Feltesse et al., *Nucl. Phys.* **B93**, 242 (1975)
[16] R.D. Baker et al., *Nucl. Phys.* **B141**, 29 (1978)
[17] T.M. Knasel et al., *Phys. Rev.* **D11**, 1 (1975)
[18] D.H. Saxon et al., *Nucl. Phys.* **B162**, 522 (1980)
[19] S. Capstick and W. Roberts, *Phys. Rev.* **D49**, 4570 (1994)
[20] L.Ya. Glozman and D.O. Riska, *Phys. Lett.* **B366**, 305 (1996)
[21] R. Bijker, F. Iachello and A. Leviatan, *Phys. Rev.* **D55**, 2862 (1997)
[22] N. Kaiser, T. Waas and W. Weise, *Nucl. Phys.* **A612**, 297 (1997)
[23] Particle Data Group, *Phys. Rev.* **D54**, 1 (1996)
[24] O. Hanstein, D. Drechsel and L. Tiator, *nucl-th@xxx.lanl.gov* preprint #9709067; O. Hanstein, *private comunications*
[25] B. Krusche et al., *Phys. Rev. Lett.* **74**, 3736 (1995); *Phys. Rev. Lett.* **75**, 3023 (1995); *Phys. Lett.* **B358**, 40 (1995)
[26] M. Wilhelm, Phd-thesis, Bonn, Germany 1993
[27] B. Krusche, N. C. Mukhopadhyay, J.-F. Zhang und M. Benmerrouche, *Phys. Lett.* **B397**, 171 (1997)
[28] G. Blanpied et al., *Phys. Rev. Lett.* **76**, 1023 (1996)
[29] T. Ishii et al., *Nucl. Phys.* **B165**, 189 (1980)

Baryon Resonance Extraction from πN and γN Data using a Unitary Multichannel Model

S.A. Dytman and T.P. Vrana
Dept. of Physics and Astronomy, University of Pittsburgh, Pittsburgh, PA 15260
T.-S. H. Lee
Physics Division, Argonne National Laboratory, Argonne, IL 60439

Abstract

We present almost final solutions for a combined analysis of all πN elastic and the major inelastic channels and photoproduction data for πN and ηN final states to extract detailed characteristics of the contributing baryon resonances. This work is based on the work of R. Cutkosky and collaborators at CMU about 20 years ago extended to include photoproduction. The model features analyticity at the amplitude level and multichannel unitarity. Results are similar to previous analyses for strongly excited states, but can vary considerably from previous analyses when the states are weak, the data is poor, or there is a strong model dependence. We emphasize the $S_{11}(1535)$ resonance which has particularly strong model dependence.

INTRODUCTION

A primary goal in analyzing pion-nucleon scattering and photoproduction data is to ascertain the underlying resonant structure. The properties of the N* resonances are an important window into the behavior of strongly interacting systems at large distance ($\sim$ 1 fm). For example, the photocouplings of nucleons to resonances can be calculated from theoretical wave function models of baryons.

The data must be decomposed into partial waves and separated into the various resonance contributions and their asymptotic channel excitation widths (e.g. the partial decay width into γN, πN, ηN, γN, ωN, ρN, $\pi\Delta$, $\pi N^*(1440)$, and others) before the model calculations can be compared to data. Many inelastic channels contribute roughly equally to the total πN total cross section. A correct analysis should account for all of them in satisfying unitarity, matching all available data, and including the proper threshold characteristics. In the resonance region, the threshold effects of asymptotic channels must be handled correctly to ensure a proper identification of resonances. This is particularly important for the $S_{11}(1535)$ where the ηN threshold comes just below the resonance pole position.

Resonance extraction requires a significant calculational effort and many articles have presented various ways to determine resonance parameters (masses, pole positions, and decay widths) from data. The PDG mostly bases its recommendations on older work by Cutkosky et al. (the Carnegie-Mellon Berkeley or CMB group)[1] and Höhler et al. (the Karlsrühe-Helsinki or KH group) [2], and more recent work by Manley and Saleski (KSU) [3] and the VPI group.[4] All these efforts use reaction data with πN initial states. All maintain unitarity, though the methods employed are quite different. These models handle also the multichannel character of the reactions in quite different ways. For most strongly excited states, the four analyses tend to agree within expected errors on resonance masses and widths. A notable exception is $S_{11}(1535)$ where extracted full widths are 66 MeV[4], 120$\pm$20 MeV[2], 151$\pm$27 MeV[3], and 270$\pm$50 MeV[1]. This large variation is due to the close proximity of the resonance pole to the ηN threshold.

Fewer unified analyses of photoproduction data have been published, with the VPI group [8] presenting the most recent results. The published values for the photocoupling amplitudes for $S_{11}(1535)$ also show a large variation.

This work presented here applies the CMB model[1] to πN and γN data with a large variety of final states. This model emphasizes the proper treatment of all analytic features

that might be found in the complex energy plane. The main publication where the CMB model was used was published in 1979. Although they used both elastic and inelastic πN data, the elastic data was emphasized. We extend the model to include photoproduction consistently.

We present a minimal account of the model and show the model dependence for the analysis of the data discussed above. In this paper, we discuss some representative results. We will provide a more complete list of baryon resonances and description of the model in a forthcoming paper[5].

FEATURES OF THE MODEL

The CMB model [1] seeks a representation of the scattering T matrices for many channels combining desirable properties of analyticity and unitarity. The phase space factors (called the channel propagators in the original paper) are calculated with a dispersion relation which guarantees analyticity in the solutions and provides a description of the off-shell propagation of states. Analyticity makes the search for the actual pole of the T matrix in complex s space possible. Self energies are calculated for the coupling of each resonance to asymptotic states as it propagates and are included via a Dyson equation. Since there are multiple open channels, we use the matrix form of the Dyson equation to calculate the full resonance propagator G. The self energies provide the required dressing of the bare states to produce the physical states seen in experiments. Final states of two pions and a nucleon are included in the phase space factors as quasi-two-body states with an appropriate width.

A separable form for the T matrix is assumed. Although this form most easily allows reproduction of s-channel processes, additional nonresonant processes are included in background terms.

We have reproduced the CMB model. The same form factors and dispersion relations are used as in the original work [1]. Up to eight asymptotic channels of the meson-nucleon type and up to four photon-nucleon multipoles are allowed to couple to each resonance in each partial wave. Three nonresonant terms are included in each partial wave. These are represented as resonances at energies well below or well above the resonance region. Lacking a specific model for these processes, they have the same bare energy dependence (except the width is much larger) used for resonances, but the inelastic thresholds produce the appropriate analytic behavior for each nonresonant term.

Pion and eta photoproduction processes have been added to the T-matrix to allow coupling to each resonance with the same threshold dependence as is used for the purely hadronic states. The Born terms for pion and eta photoproduction are added to the resonant and other nonresonant amplitudes as K-matrices. The summed amplitude is then converted back to a T-matrix for resonance extraction.

RESULTS AND DISCUSSION

The analysis presented here is unique because the πN and photoproduction data is fit simultaneously. We have applied the CMB model to the πN elastic T matrices of VPI [4], the inelastic T matrices of Manley et al. [6], and our own partial wave analysis of the $\pi N \to \eta N$ data. We simultaneously fit the pion photoproduction amplitudes of VPI [8] and the total cross section data for eta photoproduction [7].

A partial list of resonances found in this analysis is given in Tables 1 and 2 and compared to the results of KSU, and the latest recommended values given by PDG. The number of states sought in each partial wave was the same as used by KSU[3]. Table 3 lists the photocouplings for representative isospin 1/2 states.

For a complicated multi-parameter fit, errors are difficult to determine because correlations can be significant. The partial wave data we use as input quotes only diagonal errors. We include error estimates in all extracted quantities due to propagation of errors quoted in the

partial wave data. In addition, we add contributions determined from additional fits where the background parameterization and the Born photoproduction amplitude form factor range are varied. No systematic sources (e.g. due to the assumption of a Breit-Wigner shape for the bare resonance) are included.

Strong isolated resonances that have a strong elastic coupling are fit well with all models. The resonance parameters for these states, e.g. the $D_{15}(1675)$ and $F_{15}(1680)$ masses and widths, tend to have close agreement between previous results and the new results.

At the other extreme, the extracted characteristics of the $S_{11}(1535)$ and $S_{11}(1650)$ resonances vary considerably in the literature. This is in part due to model dependence and in part due to use of incomplete data sets. We find that by relaxing the constraints of our model (e.g. disabling the dispersion relation) or by leaving out data sets (especially data with ηN final states), considerable variation in the results occurs. For example, the $S_{11}(1535)$ width we determine can vary between 80 and 160 MeV when we make assumptions similar to those in published models.

For S_{11} states, $A_{1/2}$ is the only contributing photocoupling amplitude; it has separate values for proton and neutron targets. The extracted values are traditionally obtained by fitting the resonance parameters other than the photocoupling to $\pi N \to \pi N$ data. These parameters are then held fixed during the fit to $\gamma N \to \pi N$ data for the photocoupling amplitudes. We first do the fit this way, then fit all the data simultaneously. The total width increases by 10% and the proton photocoupling amplitude changes commensurately.

Figures 1-3 show the πN elastic and πN proton photoproduction T-matrix amplitudes and the $\pi^- p \to \eta n$ and $\gamma p \to \eta p$ total cross section data together with the fit amplitudes. The final fit that uses the full data set is shown as a solid line and the fit ignoring the Mainz $\gamma p \to \eta p$ data [7] data is dashed. We find the Mainz data to be of great importance in the fit. This is because η production data (either from πN or γN) provides the basic information needed to characterize the cusp seen in πN elastic scattering and πN photoproduction observables about 25 MeV from the resonance pole.

When the Mainz data is not included in the fit, the 'predicted' total cross section is about half the size of the data (see Fig. 3b). However, about half of the discrepancy is due to the poor quality of the other data. In Fig. 2, the two fits to πN elastic T-matrices are indistinguishable. In Fig. 3a, the fit to the $\pi^- p \to \eta n$ total cross section changes very little. The $\gamma N \to \pi N$ (Fig. 1) fit moves from just above the data at $W \sim 1535$ MeV to somewhat below the data. (We show the proton amplitude which shows more sensitivity than the neutron amplitude.)

While the $S_{11}(1535)$ parameters change noticeably between the two fits, the $S_{11}(1650)$ parameters change very little. Adding the (γ, η) data, the extracted mass of the 1535 MeV state increases by 2 MeV, the total width increases by 11 MeV, and the division of the total amplitude between πN and ηN is essentially unchanged. However, the proton photocoupling amplitude increases by 40% and the neutron amplitude increases by 13%. The final fit results are found in Tables 1-3.

Fits using only pion photoproduction data [8] get somewhat lower values than our result and fits using only eta photoproduction data [9] get somewhat larger values. We find that both data sets are needed to simultaneously fit the cusp and the resonance characteristics.

CONCLUSIONS

We present results for a new analysis of the *best available* πN and γN "partial wave decomposed" data. We apply a model [1] that contains all the correct analytic properties and correctly handles the multichannel nature of resonance excitation. The results can differ significantly from previous analyses, due to either the new data sets used in this work or due to model dependence. A more complete discussion can be found in forthcoming papers [5].

The most significant new result is for $S_{11}(1535)$ where there has been a wide range of values published for its width and photocoupling amplitude. With the formalism available in

the CMB model, we are able to simultaneously fit all available data for the first time. The new value for the mass is unchanged from the PDG value, the width is at the low end of their range and the photocoupling amplitude is significantly larger. The photocoupling amplitude is not as large as that obtained in recent analyses of the η photoproduction data [9] because they do not handle the coupled channel effects correctly.

Acknowledgments
We are grateful to Mark Manley and Dick Arndt for providing the "partial wave decomposed" data used in this study. We also wish to thank Jeremy Greenwald, Matt Mihalcin, Jay deMartino, and David Kokales for their significant programming contributions to this work.

Table 1. Comparison of Resonance Masses and Widths for Selected Resonances

Resonance	Mass (MeV)	Width (MeV)	Elasticity %	Reference
$S_{11}(1535)$ ****	1542(15)	127(30)	35(5)	Pitt-ANL
	1534(7)	151(27)	51(5)	KSU
	1520-1555	100-250	35-55	PDG
$P_{11}(1440)$ ****	1479(9)	489(18)	72(3)	Pitt-ANL
	1462(10)	391(34)	69(3)	KSU
	1430-1470	250-450	60-70	PDG
$D_{13}(1520)$ ****	1520(13)	118(25)	61(4)	Pitt-ANL
	1524(4)	124(8)	59(3)	KSU
	1515-1530	110-135	50-60	PDG
$D_{15}(1675)$ ****	1687(13)	126(26)	32(4)	Pitt-ANL
	1676(2)	159(7)	47(2)	KSU
	1670-1685	140-180	40-50	PDG
$F_{15}(1680)$ ****	1679(11)	125(23)	69(4)	Pitt-ANL
	1684(4)	139(8)	70(3)	KSU
	1675-1690	120-140	60-70	PDG

REFERENCES

[1] R.E. Cutkosky, C.P. Forsyth, R.E. Hendrick, and R.L. Kelly, Phys. Rev. D**20**, 2839 (1979).
[2] G. Höhler, F. Kaiser, R. Koch, and E. Pietarinen, *Handbook of Pion-Nucleon scattering*, [Physics Data No. 12-1 (1979)]
[3] D.M. Manley and E.M. Saleski, Phys. Rev. D**45**, 4002 (1992).
[4] Richard A. Arndt, Igor I. Strakovsky, Ron L. Workman, and Marcello M. Pavan, Phys. Rev. C**52**, 2120 (1995).
[5] T.P. Vrana, S.A. Dytman, and T.-S.H. Lee, to be published.
[6] D.M. Manley, R.A. Arndt, Y. Goradia, and V.L. Teplitz, Phys. Rev. D**30**, 904 (1984).
[7] B. Krusche, et al., Phys. Rev. Lett. **74**, 3736 (1995).
[8] R.A. Arndt, I.I. Strakovsky, and R.L. Workman, Phys. Rev. C**53**, 440 (1996).
[9] B. Krusche, N. Mukhopadhyay, J.F. Zhang, and M. Benmerrouche, Phys. Lett. **B397**, 171 (1997).

Table 2. Branching Ratios for Selected Resonances

Resonance	Channel	Pitt-ANL	KSU	PDG
$S_{11}(1535)$	πN	35(5)	51(5)	35-55
	ηN	51(6)	43(6)	30-55
	$\rho_1 N$	2(6)	2(1)	0-4
	$(\rho_3 N)_D$	0(0)	1(1)	
	$(\pi\Delta)_D$	1(1)	0(0)	0-1
	$(\sigma N)_P$	2(6)	1(1)	0-3
	$\pi N^*(1440)$	10(10)	2(2)	0-7
$S_{11}(1650)$	πN	74(3)	89(7)	55-90
	ηN	6(6)	3(5)	3-10
	$\rho_1 N$	1(3)	0(0)	4-14
	$(\rho_3 N)_D$	13(4)	3(2)	
	$(\pi\Delta)_D$	2(5)	2(1)	3-7
	$(\sigma N)_P$	1(4)	2(2)	0-4
	$\pi N^*(1440)$	3(5)	1(1)	0-5

Table 3. Photocouplings for Selected I=1/2 Resonances

Resonance	$A^p_{\frac{1}{2}}$	$A^p_{\frac{3}{2}}$	$A^n_{\frac{1}{2}}$	$A^n_{\frac{3}{2}}$	Group
	$[\mathrm{GeV}]^{-1/2} * 10^{-3}$				
$S_{11}(1535)$	87 ± 3		-52 ± 7		PITT-ANL
	70 ± 12		-46 ± 27		PDG
	76		-63		CAP92
$S_{11}(1650)$	48 ± 9		-19 ± 5		PITT-ANL
	53 ± 16		-15 ± 21		PDG
	54		-35		CAP92
$P_{11}(1440)$	-65 ± 7		16 ± 7		PITT-ANL
	-65 ± 4		40 ± 10		PDG
	4		-6		CAP92
$D_{13}(1520)$	-25 ± 6	171 ± 7	-37 ± 9	-124 ± 15	PITT-ANL
	-24 ± 9	166 ± 5	-59 ± 9	-139 ± 11	PDG
	-15	134	-38	-114	CAP92
$D_{15}(1675)$	12 ± 6	11 ± 4	-34 ± 4	-48 ± 6	PITT-ANL
	19 ± 8	15 ± 9	-43 ± 12	-58 ± 13	PDG
	2	3	-35	-51	CAP92
$F_{15}(1680)$	-13 ± 3	143 ± 3	31 ± 8	-22 ± 5	PITT-ANL
	-15 ± 6	133 ± 12	29 ± 10	-33 ± 9	PDG
	-38	56	19	-23	CAP92

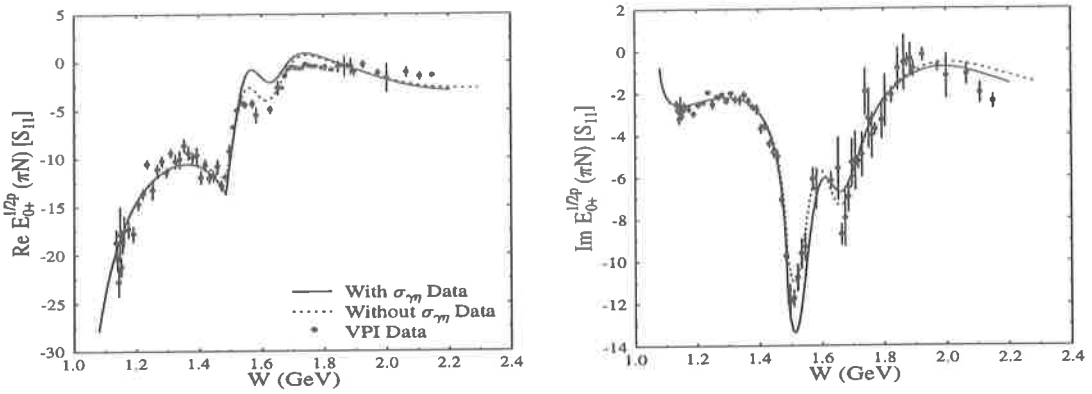

Figure 1. S_{11} E_{0+} proton Multipole

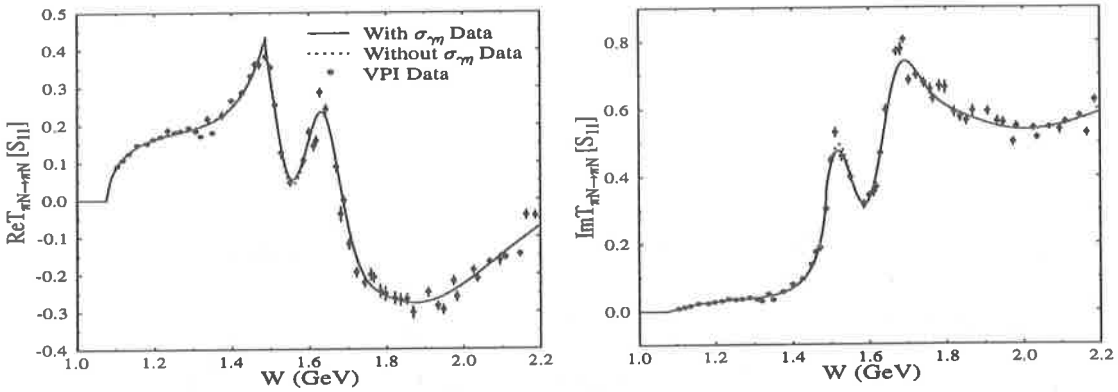

Figure 2. S_{11} $\pi N \to \pi N$ T-matrix Element

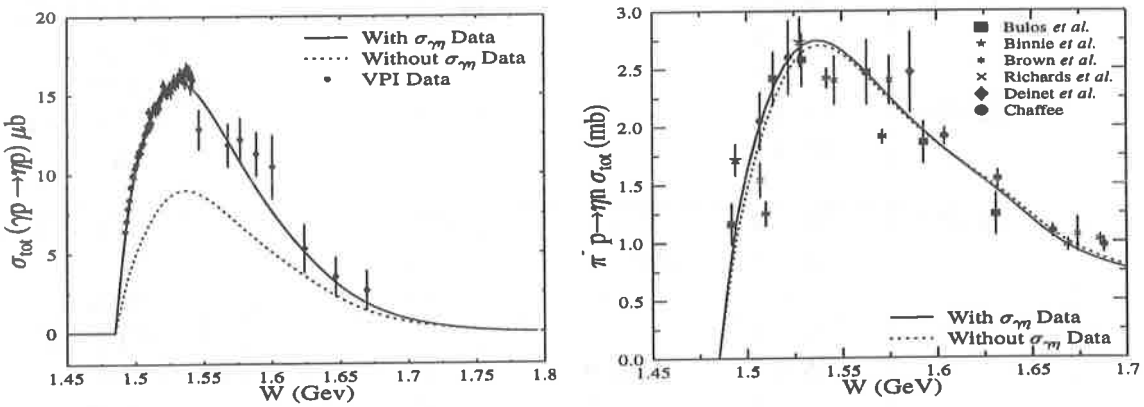

Figure 3. $\gamma p \to \eta p$ (a) and $\pi^- p \to \eta n$ (b) Total Cross Section

A Meson-Exchange Model for Pion-Nucleon Scattering and Pion Photoproduction

J.W.Durso, J.Haidenbauer, O.Krehl, K.Nakayama, C.Schütz, J.Speth, and S. Krewald*
Institute für Kernphysik,
Forschungszentrum Jülich, D-52425 Jülich, Germany

Abstract

Pion-nucleon scattering is described in a model which couples the pion-nucleon, eta-nucleon, sigma-nucleon, and pion-Delta reaction channels. Both phase shifts and inelasticities are reproduced up to $s = 1.6GeV$. The model has been used to calculate pion photoproduction. The form factors required in photoproduction are softer than the ones determined from purely hadronic reactions.

INTRODUCTION

One of the challenges of intermediate energy physics is to understand the structure of the many resonances seen in hadronic reactions. Can we describe a given resonance entirely by the dynamics of the three valence quarks? Are seaquarks or meson clouds a relevant degree of freedom? Do final state interactions modify or even build up resonances? In order to address these questions, a detailed theory of the reaction mechanisms is called for.

We therefore have started to develop a model which takes baryons and mesons as the relevant degrees of freedom for center-of-mass energies less than 2GeV. The interactions between the mesons and baryons are modelled by effective Lagrangians which respect chiral symmetry. In our approach, the quark degrees of freedom appear implicitly in the form of bare resonances, bare coupling constants and form factors. These quantities are not derived from an underlying quark model, but are adjusted to the experimental data. The aim of the model is to describe a large set of different hadronic and electromagnetic reactions with a limited number of effective coupling constants and cut-off masses. So far, we concentrate on the interaction of two particles only. Then, one has to solve a relativistic scattering equation which guarantees unitarity, at the cost of losing crossing symmetry.

COUPLED CHANNEL MODELS

A first step is to model the interaction between a pion and a nucleon. Several models of pion-nucleon dynamics have been developped recently [1–5]. The pion and the nucleon can interact by the exchange of a nucleon or a Δ_{33} in the s- and in the u-channel. In the t-channel, mesons may be exchanged, such as the sigma or the rho. Our model differs from other approaches by replacing both the unphysical sigma-meson and the rho-meson by the exchange of a two interacting pions. In the scalar pion-nucleon channel, our interaction is repulsive in the S-waves, but attractive in the P-waves. This is in contrast to [2], where a sharp mass approximation has been used.

Recently, the model has been extended to couple the $\pi N, \eta N, \sigma N$, and $\pi\Delta$ channels [6]. The phase shifts are shown in Fig. 1. The inclusion of the ηN channel allows to discuss the structure of the $N^*_{S11}(1535)$ resonance which is the only known resonance that couples strongly to the ηN channel. The contribution of the ηN channel to the total decay width of the resonance is $30 - 55$ percent. In the speed plot of the S11 πN partial wave, Höhler finds a sharp maximum at an energy which is indistinguishable from the ηN threshold, but

*E-mail: S.Krewald@fz-juelich.de

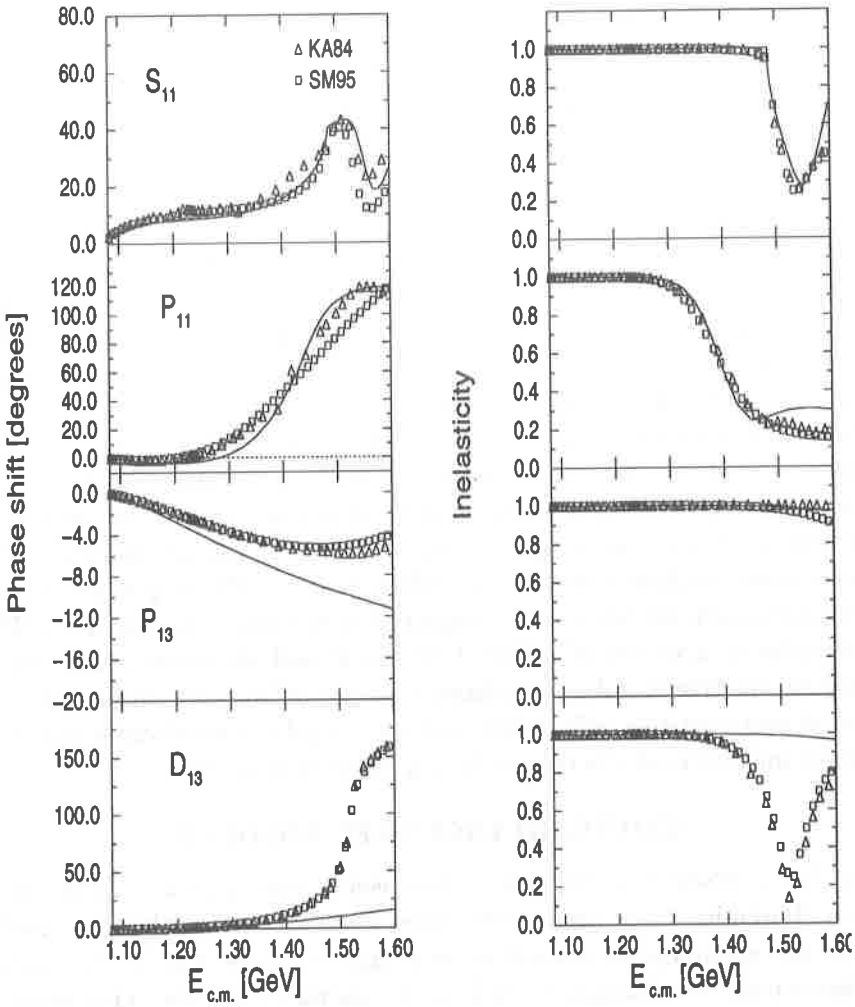

Figure 1. Phase shifts and inelasticities in the πN channel evaluated in a model which couples the reaction channels $\pi N/\eta N/\pi\Delta/\sigma N$. The model needs an explicit $N^*_{S11}(1535)$ pole diagram, but does not require a pole diagram to generate the Roper resonance.

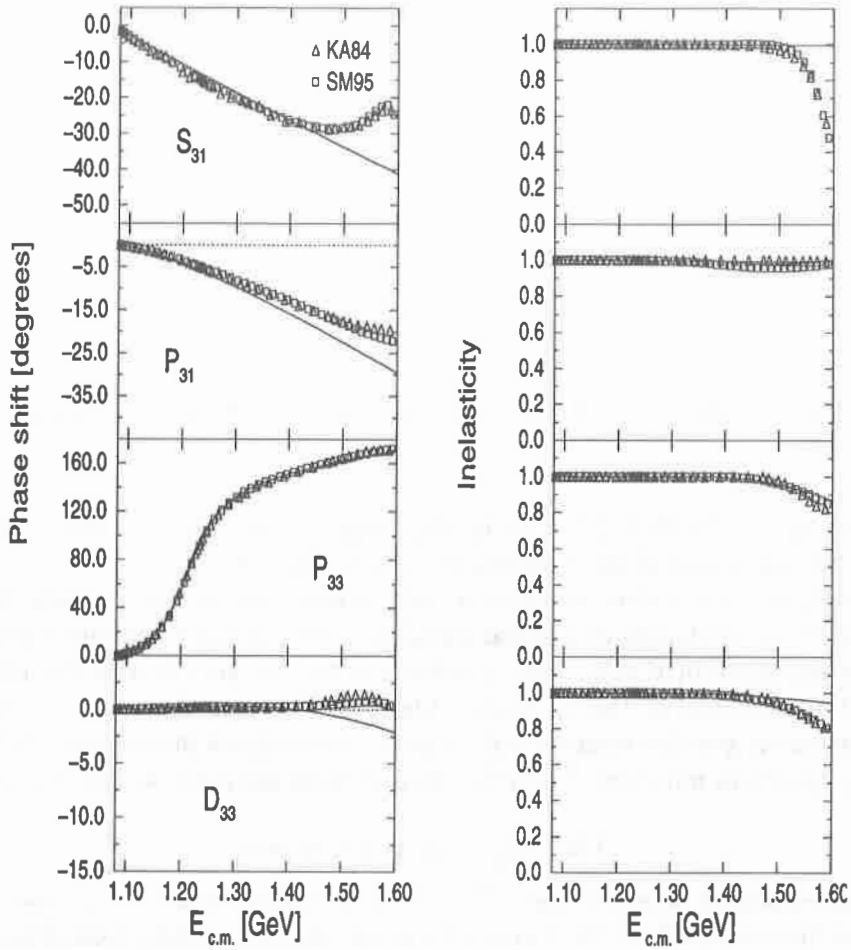

Figure 2. Phase shifts and inelasticities in the πN channel evaluated in a model which couples the reaction channels $\pi N/\eta N/\pi\Delta/\sigma N$.

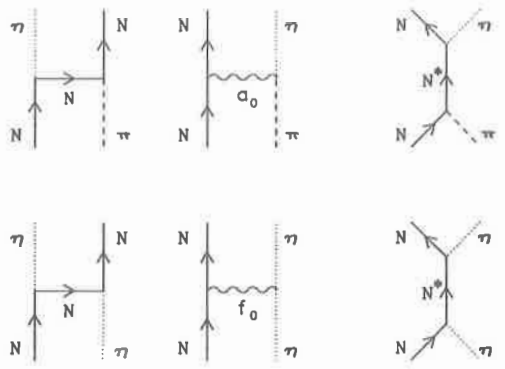

Figure 3. Feynman diagrams defining the πN toηN transition potential (upper part) and the diagonal ηN potential (lower part).

no structure around 1535 MeV [7]. This finding suggests that the S11 resonance is strongly influenced by the dynamics of the opening of the ηN channel.

In our model, the interaction between η and nucleon can be due to three processes: exchange of a N, N^* or exchange of a scalar-isocalar meson in the t-channel which we parameterize by the exchange of the f_0. The transition between the πN and the ηN channels is modelled by the exchange of the a_0 meson. One has to stress that both a_0 and f_0 should not be interpreted as genuine mesons, but as parameterizations of mesonic systems with the corresponding quantum numbers. The relevant diagrams are displayed in Fig. 3.

The $N^*_{S11}(1535)$ resonance

We have investigated whether the $N^*_{S11}(1535)$ resonance can be described as a purely dynamical and threshold effect. To do so, we left out the $N^*_{S11}(1535)$ pole diagram and only included the exchange of the f_0 meson in the t-channel. Then the maximum of the phase shift is exactly at the ηN threshold (1487 MeV) and has to be interpreted as a cusp effect. No reasonable variation of the coupling strength could shift the position of the maximum and the description of the $S11$ phase shifts is not very good. Therefore one has to conclude that the description of the $N^*_{S11}(1535)$ as a threshold phenomenon is incomplete. If one adds a pole diagram, one may neglect the coupling to the f_0 meson and yet get a quatitative description of the S11 phase in the vicinity of the $N^*_{S11}(1535)$ resonance.

The $N^*_{P11}(1440)$ resonance

In πN scattering, the Roper resonance $N^*_{P11}(1440)$ contributes only to the background of other resonances and can be recognized only after a partial wave analysis. In inelastic α-

scattering, it can be excited directly [8]. It is difficult to understand the relatively low mass of the $N^*_{P11}(1440)$ resonance in quark models. Isgur and Karl introduce an anharmonicity in the confining potential [9], while Glozman and Riska produce it through flavor symmetry breaking in the exchange of the pseudoscalar mesons in the residual quark-quark interaction. The width of the resonance remains an open issue in these approaches, however. The behaviour of the P11 phase shifts may be understood qualitatively considering the πN reaction channel by itself. For small energies, the exchange of a nucleon which is repulsive dominates. This results in a small negative phase shift. The exchange of a rho-meson in the t-channel is attractive and grows with energy. At the CM-energy of 1240 MeV, the rho-exchange starts to dominate and changes the sign of the phase shift. In a one-channel model, the inelasticity is unity, of course. The P11 partial wave begins to show significant inelasticities at energies as low as $E_{cm} = 1.3GeV$. We find that the σN channel contributes significantly to the inelasticity, whereas the contribution of the $\pi\Delta_{33}$ channel to the inelasticity is quite small. This is in apparent disagreement with the results of the Particle Data Group[11].

The present model produces too much repulsion in the P13 partial wave. In this partial wave, there is a resonance, $N^*_{P13}(1720)$, which predominantly couples to the ρN channel. Work on coupling the ρN channel is in progress. In the D13 and in the S31 partial waves, the model yields only a background for the $N^*_{D13}(1520)$ and $\Delta S31(1620)$ resonances, respectively.

PION PHOTOPRODUCTION

Pion photoproduction is an important tool to study the structure of the excited baryons. A lot of progress has been achieved in the theoretical description of pion photoprodution during the last few years. The elementary production mechanisms are well-established. Pions are produced via nucleon and Δ intermediate states in the s- and u-channels; gauge invariance requires a contact diagram. Furthermore, there is pion production via the exchange of π, ρ, ω, and a_1 in the t-channel. Final state interactions are included by a pion-nucleon scattering matrix, see Fig. 4. The various theoretical groups mainly differ by the various approximations used for the pion-nucleon interaction. Nozawa et al. developped a model which treats the pion-nucleon final state interaction by a phenomenological separable ansatz that fits the πN phase shifts up to 500 MeV [1]. Their model is unitary and gauge invariant. Surya and Gross employ a final state interaction based on a meson-theoretic model. They include the Δ_{33}, the Roper and the D_{13} as explicit resonances and approximate t-channel contributions by contact terms [4]. Sato and Lee have developped an effective Hamiltonian method [5]. In our calculation, we employ the pion-nucleon scattering model discussed above as a final state interaction [12]. For the present application, we left out the coupling to reaction channels other than πN. Gauge invariance is achieved as in Ref.[1] by attaching a common form factor of monopole type to all diagrams defining the photon-nucleon to pion-nucleon transition potential. The results of our model for pion photoproduction are shown in Fig. 5.

The fit quality is comparable to the one of Ref.[1]. In the present calculation, the electromagnetic form factors of the Δ_{33} are $G_M = 1.45$ and $G_E = 0.08$. This gives an E2/M1 ratio of -5.3 percent. The cut-off parameter Λ of the monopole form factor has been adjusted to 450 MeV. For values much larger than 450 Mev, one cannot obtain a reasonable fit to the data. Close to the pion production threshold, the cut-off has to be reduced to $\Lambda = 200$ MeV in order to get agreement with the experimental data. Pion photoproduction in general appears to require soft form factors. The pion-nucleon form factor employed by Surya and Gross has a complicated form including a Θ-function. It roughly corresponds to a monopole form factor with a cut off of $\Lambda = 300MeV$. Sata and Lee use a dipole form factor for the pion-nucleon

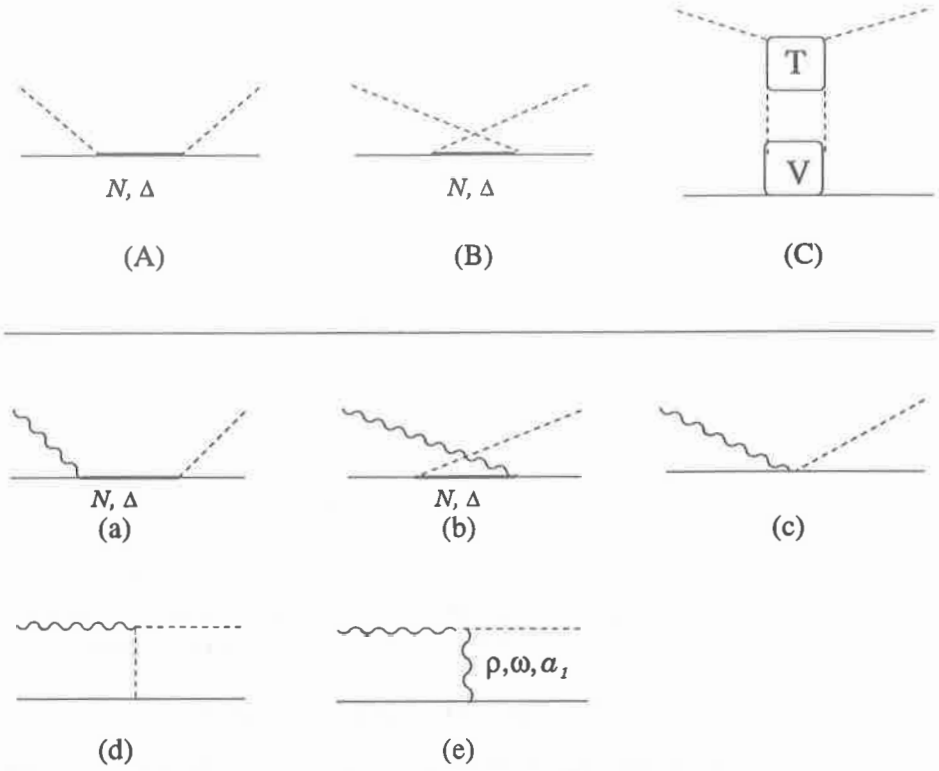

Figure 4. Diagrams taken into account for the πN scattering (upper part) and for the photo-production transition potential (lower part).

vertex which would correspond to a monopole form factor of $\Lambda = 400MeV$. If transformed into monopole form, the pion-nucleon formfactors employed by the various groups cluster in the range of $\Lambda = 300...500MeV$. One should note that such soft form factors are not consistent with the pion-nucleon form factor employed in our microscopic model of pion-nucleon scattering. If transformed to a monopole form, our cut-off corresponds to $\Lambda = 800MeV$. This value is consistent with the form factors derived e.g. by lattice QCD studies [13]. A QCD sum-rule calculation produces a cut off of $\Lambda = 800 \pm 140MeV$ [14].

In nucleon-nucleon scattering, one-boson exchange models require much larger form factors. For cut offs less than $\Lambda = 1300MeV$, the quadrupole moment of the deuteron cannot be reproduced because a too soft form factor would cut down the tensor force too much. One has to recall, however, that the pion in a one-boson exchange model is not the physical free pion, but an effective meson which partly simulates the exchange of an interacting $\pi - \rho$ pair between two nucleons. If one incorporates the exchange of a correlated $\pi - \rho$ pair explicitly, one generates additional strength with pionic quantum numbers at larger momentum transfers and therefore can reduce the cut-off employed in the actual one-pion exchange potential. The relatively soft pion-nucleon formfactor can be understood as an effect of correlated $\pi - \rho$ pairs as well. The form factor of the pion consists of several microscopic processes. One process is the direct coupling of the pion to the nucleon. On the other hand, the pion may first couple to a $\pi - \rho$ pair, the $\pi - \rho$ may interact and finally couple to the nucleon. In this way, the coupling of the pion to the nucleon effectively is spread out in co-ordinate space and in this way, a soft form factor is produced. Actual calculations find that the dressed form factor may be parameterized by a monopole with a cut-off of $\Lambda = 1000MeV$[15]. It seems unlikely that

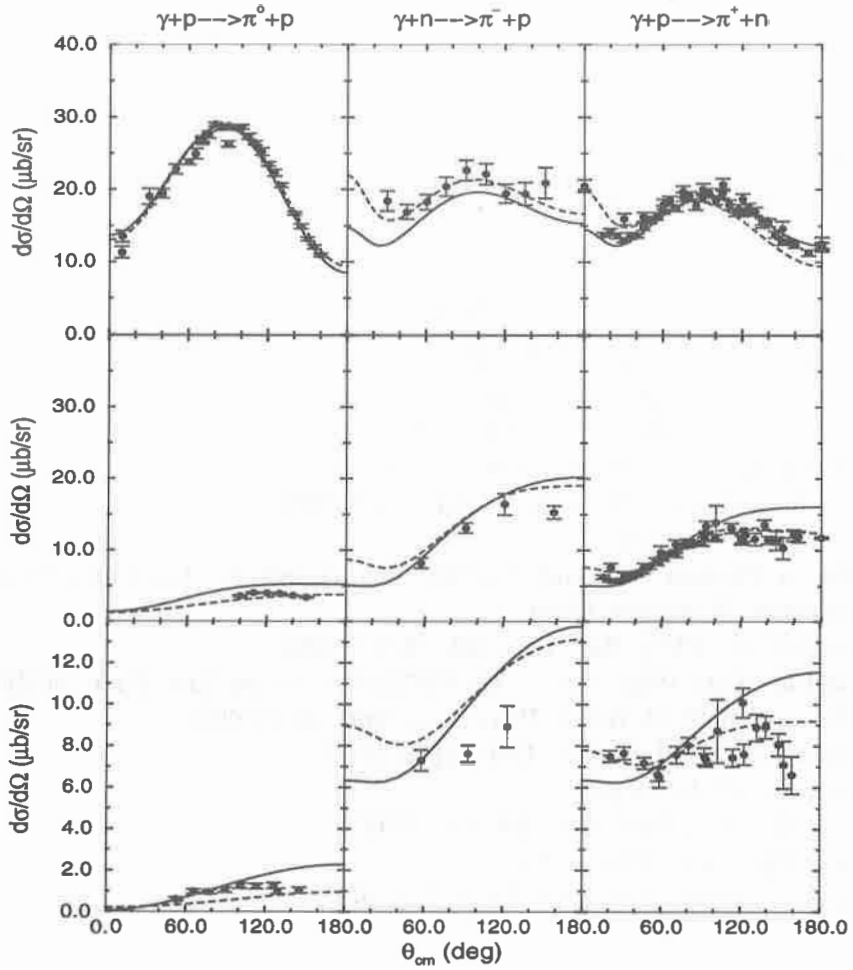

Figure 5. Differential cross sections at photon energies of $T_{lab} = 340MeV$ (upper part), $T_{lab} = 220MeV$ (middle part), and $T_{lab} = 180MeV$ (lower part). The first,second and third columns refer to π^0, π^-,and π^+ production, respectively. The results obtained from the present model are shown by the solid line, those of Ref. [1] by the dashed line.

a more elaborate calculations would lower the cut-off parameter far below $\Lambda = 800MeV$.

A possible explanation for the disagreement of the form factors needed in pion photoproduction and in microscopic models of hadronic reactions might be that a model of photoproduction which only includes final state interactions in the $\pi - N$ channel is incomplete. In order to search for other processes which might produce some cancellation of the strong final state interaction in the $\pi - N$ channel, we have analysed the photoproduction amplitude E_{0+} in a simple model, where the full pion-nucleon scattering amplitude was replaced by the lowest order diagrams. For the case of π^0 photoproduction, we found that the coupling to charged pions in the intermediate states gives by far the largest contribution to the final state interaction. If one allows an uncorrelated $\rho - N$ system as an intermediate state, one finds a 40 percent cancellation of the contributions of the pionic final state interactions, using a cut-off parameter of $\Lambda = 800MeV$. We conclude that the photoproduction of pions requires a model which includes final state interactions other than mere rescatterings in the pion-nucleon channel. The rho-nucleon channel should be treated simultaneously with the pion-nucleon channel.

REFERENCES

[1] S. Nozawa et al., Nucl. Phys. A**513**, 459(1990).
[2] B. C. Pearce and B. K. Jennings, Nucl. Phys. A**528**, 655 (1991).
[3] C. Schütz et al., Phys. Rev. C**49**, 2671(1994).
[4] Y.Surya and F. Gross, Phys. Rev. C**47**, 703(1993).
[5] T. Sato and T.S. H. Lee, Phys. Rev. C**54**, 2660(1996).
[6] C. Schütz et al., to be publ.
[7] G. Hoehler, in Physics with GeV-Particle Beams, eds. H. Machner and K. Sistemich (World Scientific, Singapore,1995).
[8] H. P. Morsch et al., Phys. Rev. Lett. **69**, 1336 (1992).
[9] N. Isgur and G. Karl, Phys. Rev. D**18**, 4187(1978); Phys. Rev. D**19**, 2653(1979).
[10] L. Y. Glozman and D. O. Riska, Phys. Rep. **268**, 263(1996).
[11] Particle Data Group, Phys. Rev. D**50**, 1173(1994).
[12] K. Nakayama et al., to be publ.
[13] K. F. Liu et al., Phys. Rev. Lett. **74**, 2172(1995).
[14] T. Meissner, Phys. Rev. C**52**, 3386(1995).
[15] G. Janßen et al., Phys. Rev. Lett. **73**, 1332(1994).

Review of (γ, π) and the Delta E2/M1 Ratio

Ron Workman and Richard Arndt
Department of Physics, Virginia Tech, Blacksburg, VA 24061, U.S.A.

Abstract

A number of recent multipole analyses from Mainz, RPI, BNL, and Virginia Tech have focused on the first resonance region. One goal common to these studies was an improved set of $\Delta(1232)$ photo-decay amplitudes. In the following, we will attempt to review the issues surrounding the extraction of these amplitudes, with an emphasis on the E2/M1 ratio.

INTRODUCTION

Although the above title implies a broader review of the (γ, π) analyses, there has been sufficient work over the first resonance region to justify a more focused discussion. We can expect to transfer some of this methodology to the higher resonances. However, the $S_{11}(1535)$ and $P_{11}(1440)$ have shown that unique problems emerge when more precise results are desired. The recent flurry of papers on the E2/M1 ratio has similarly exposed difficulties associated with the extraction of a small amplitude from pion photoproduction data. Even the interpretation of this ratio, in terms of model-based calculations, is unclear.

In the following, we will try to give a balanced review of recent work on the $\Delta(1232)$ parameters. We will first summarize the results of the various groups in order to make apparent the discrepancies in both measurements and multipole analyses. Having done this, we will give our present understanding of the problems.

RECENT EXPERIMENTS

A number of groups have been producing data over the delta region. New total cross sections[1] from Mainz have been used to argue for a reduced M1 amplitude, below that given in the PDG 96 estimate[2]. Mainz has also produced both differential cross section $[\sigma(\theta)]$ and polarized-photon asymmetries $[\Sigma(\theta)]$ in 10 MeV increments from 270 to 420 MeV[3].

The LEGS group at BNL has carried out a similar program to obtain precise values of $\sigma(\theta)$ and $\Sigma(\theta)$ ranging from 213 to 333 MeV[4]. The LEGS and Mainz Σ data are in reasonable agreement, though the LEGS values span a larger angular range. Unfortunately, the cross sections are quite different, the BNL $\pi^0 p$ points lying on the order of 10% above the Mainz points.

In trying to understand the different cross sections, one generally compares with the older and quite precise Bonn data[5]. While the Bonn data covers a much larger angular range, they agree with the Mainz data over the angular range where they can be compared. (A slight systematic shift between the Mainz and Bonn $\pi^0 p$ points is noticeable at 340 MeV.) It should be mentioned that the BNL $\pi^0 p$ cross sections do not disagree with *all* previous measurements. Near the delta, there is reasonable agreement with a Lund measurement[6]. However, this agreement is degraded at lower energies.

Target-polarization $[T]$ data have also been measured recently at Bonn[7]. Before these and the above mentioned Σ data were available, fits were mainly constrained by the P, Σ and T measurements from Kharkov[8]. As the polarization observable Σ is most sensitive to the E2/M1 ratio, and the Kharkov data had much larger errors, all previous determinations of this ratio are certainly obsolete.

RECENT ANALYSES

In this section, we will concentrate on those analyses which have attempted to determine the E2 and M1 amplitudes from the recent Mainz and LEGS data. Analyses have been performed at Mainz (by both the theory and experimental groups)[3,9], VPI[10], RPI[11], BNL[4], and ANL[12]. The ANL analysis was based on a dynamical model and analyzed $\Sigma(\theta)$ data from LEGS along with an older set of observables, mainly from the Bonn compilation. The VPI analyses were based on a K-matrix formalism and utilized the full database, including the preliminary LEGS $\Sigma(\theta)$ data and the Mainz $\Sigma(\theta)$ and $\sigma(\theta)$ data. The BNL analysis was similar in its parameterization of the pion photoproduction data, but also included Compton scattering data via the dispersion relation code of L'vov[13]. This analysis was based mainly on data measured at BNL. The Bonn and Mainz data were only included in tests. The Mainz (theory group) analysis also used dispersion relations. However, in this case they were applied to the pion photoproduction data. As expected, this work emphasized the influence of the Mainz dataset. In contrast to the above methods, the RPI analysis was based on an effective Lagrangian approach, and therefore had very few (5) free parameters. The results reported in Ref.[11] were based on a fit to the Mainz data near the delta resonance peak. Finally, the Mainz (experimental) group[3] extracted the E2/M1 ratio directly from a polynomial fit to their polarized-photon asymmetry data. This method was subsequently criticized by the RPI, VPI, and BNL groups. As this debate may have seemed confusing to those viewing it from the 'outside', in the next section we will attempt to simplify the arguments.

Before discussing the E2/M1 problem, we should first note that the values for $A_{1/2}$ and $A_{3/2}$ are in reasonable agreement. The PDG 96 averages[2] were: $A_{1/2} = -140 \pm 5$ and $A_{3/2} = -258 \pm 6$ (in 10^{-3} GeV$^{-1/2}$). (The VPI values ($A_{1/2} = -141 \pm 5$ and $A_{3/2} = -261 \pm 5$) were heavily weighted in this determination.) A noticeable shift is seen in the new values from Mainz ($A_{1/2} = -129 \pm 2$ and $A_{3/2} = -247 \pm 4$) and RPI ($A_{1/2} = -127.8 \pm 1.2$ and $A_{3/2} = -252.4 \pm 1.3$) which are in reasonable agreement with the latest VPI results. The BNL value for $A_{3/2} = -269 \pm 3 \pm 5$ is the most significant deviation. The ANL results are also quite different. However, this approach appears to be more model dependent. Values for both $A_{1/2}$ and $A_{3/2}$ (dressed) are much lower in magnitude, mainly due to a smaller M1 amplitude. (This would seem to imply a different resonance-background separation.)

The reasonable agreement between values for $A_{1/2}$ and $A_{3/2}$ mainly reflects an overall agreement on the M1 amplitude, but does not reveal the differences in E2. (The large BNL value for $A_{3/2}$ is a reflection of their larger magnitudes for both E2 and M1. These two effects cancel in $A_{1/2}$.) Our result for the E2/M1 ratio (from the full database) is $-1.5 \pm 0.5\%$. This is in marked disagreement with values from RPI (-3.2%), Mainz(-2.5%), and BNL(-3%).

MODEL VS DATABASE EFFECTS

This disagreement between E2/M1 determinations has persisted for several years. In 1992, we summed up our understanding in a paper[14] entitled, 'How well do we know the E2/M1 ratio for the Δ?'. At that time, we found (again from a fit to the entire database) an E2/M1 ratio of about -1.5%. However, in this paper we also 'forced' a fit to the preliminary LEGS $\Sigma(\theta)$ data. This resulted in an E2/M1 ratio of about -2.9%. (We also fitted data using Harry Lee's 'background', finding values for $A_{1/2}$ and $A_{3/2}$ which were consistent with quark model predictions.) At the time, we didn't take our forced fit too seriously, as it resulted in a much higher χ^2 for the non-LEGS data. Given that so many groups have now found values consistent with this forced-fit result, we have reexamined the database, hoping to isolate those

datasets most sensitive to this ratio.

By removing individual datasets and refitting the remainder, we found that our E2/M1 ratio jumped from -1.5% to about -2.5% with the removal of some older (but quite precise) Bonn $\pi^0 p$ differential cross sections[5]. This sensitivity has been verified by the BNL, RPI, and Mainz groups. Having found this sensitivity, the VPI and RPI groups constructed a reduced dataset (σ, Σ, P, and T) including the Mainz and Bonn data. This set was then fitted, with and without the Bonn $\pi^0 p$ cross sections, using the very different VPI and RPI parameterization schemes. This eliminated any possibility of database-dependence which might have influenced previous comparisons. Preliminary results are in good agreement. The Mainz group has also attempted to reproduce the BNL analysis (ignoring the effect of Compton scattering data). Here too, the results are in good agreement[15]. This test by the Mainz group also indicates the extent to which Compton scattering influenced the BNL fit to the pion photoproduction database.

The $R_{\pi^0 p}$ determination of the E2/M1 ratio

Here we briefly consider a much simpler way[3] to estimate the E2/M1 ratio by fitting a polynomial, in $\cos(\theta)$, to the polarized-photon cross sections. The cross section is parameterized as

$$\frac{d\sigma}{d\Omega} = \frac{q}{k}\left(A + B\cos(\theta) + C\cos^2(\theta)\right). \tag{1}$$

For parallel-polarization, the coefficients are

$$\begin{aligned} A_{||} &= |E_{0+}|^2 + |3E_{1+} - M_{1+} + M_{1-}|^2, \\ B_{||} &= 2\mathrm{Re}\left[E_{0+}\left(3E_{1+} + M_{1+} - M_{1-}\right)^*\right], \\ C_{||} &= 12\mathrm{Re}\left[E_{1+}\left(M_{1+} - M_{1-}\right)^*\right]. \end{aligned} \tag{2}$$

Having determined these coefficients, the E2/M1 ratio is given by the correspondence

$$R_{\pi^0 p} = \frac{1}{12}\frac{C_{||}}{A_{||}} \approx R_{EM} \tag{3}$$

where R_{EM} is the usual E2/M1 ratio (to be evaluated at resonance)

$$R_{EM} = \frac{\mathrm{Re}\left(E_{1+}M_{1+}^*\right)}{|M_{1+}|^2}. \tag{4}$$

In judging whether this is a good approximation, several points should be noted. First, the method uses a truncated expansion in $\cos(\theta)$. Second, the superscripts labeling these as charge or isospin multipoles have been dropped. (In Eq.(4), the definition of R_{EM} requires isospin 3/2 multipoles, whereas the $\pi^0 p$ multipoles are actually used.) Finally, the method relies on the cancellation of specific multipole combinations in $A_{||}$ and $C_{||}$.

The simplest way to see if this is a good approximation is to just calculate $R_{\pi^0 p}$ and compare it to the exact result, as found from the various multipole solutions. We have done this using the RPI, Mainz, BNL, and several VPI analyses. In some cases (for example, using the Mainz or SM95 solutions), the difference is quite small (0.2% or less). However, in other cases (for example, using the RPI or BNL solutions), the difference can be significant (about 0.3% for BNL and about 0.5% for RPI). As a result, it is difficult to assign an uncertainty to $R_{\pi^0 p}$ in advance of a full multipole analysis.

CHALLENGES TO THE METHODOLOGY

In the above, we have mainly concentrated on sensitivities associated with the database. Here we briefly pause to check the assumptions underlying our analyses. The most widely used 'assumption' is the validity of Watson's theorem[16]. This result is based upon unitarity, isospin symmetry, and the neglect of Compton scattering relative to $\pi N \to \pi N$ and $\gamma N \to \pi N$. At MENU 97, there was some discussion of isospin breaking over the resonance, given the claim of significant effects near threshold in pion-nucleon elastic scattering[17]. The influence of Compton scattering in the extraction of a small E2 amplitude has also been discussed recently[18]. Given that fits with and without Watson's theorem yield similar results[19,20], the same being true of fits including or excluding Compton scattering data, we have (as yet) no reason to abandon Watson's theorem (except possibly to determine the Δ^+ mass more precisely).

SUMMARY AND FUTURE PROSPECTS

Where are we now?

We can now say why the VPI result for the E2/M1 ratio has been so stable in the face of the new Mainz data. The two factors most influential in our perennial value of -1.5% were the Bonn neutral-pion cross sections and the preliminary LEGS data (which we have used in our fits since they were first released more than 5 years ago). While the following is a database-dependent statement, we can give an E2/M1 ratio of about -2% to -3%, if the Bonn cross sections are removed. Looking at the quality of fits to both the Mainz and LEGS Σ data, a value nearer to the upper limit of this range appears to be favored.

Clearly, it is important to check the Bonn results, particularly at more forward and backward angles. Experiments of this type have been performed at Mainz[21] and so we can hope for an answer in the near future. The disagreement between the Mainz and BNL results is more troubling. For this, an independent check based on the expected TJNAF data will be helpful.

Aside: The $\Delta^+(1232)$ parameters

Here we want to add a few comments on the Δ^+ mass, width, and pole position/residue as given in the last PDG review[2]. These have been based on an older multipole analysis[22] which used πN phases giving an 'average mass' close to 1236 MeV (as opposed to the 1232 MeV found in more recent πN analyses). As a result, an inconsistent picture of the splitting of Δ charge states results if this value is used in conjunction with the Δ^0 and Δ^{++} masses listed in the PDG review. This has been discussed in Ref.[23]. (It is interesting to note that this value was usually ignored in fits to the baryon octet and decuplet masses[24].)

The only comment on the E2 and M1 pole residues, listed in PDG 96, was also based on the analysis of Ref.[22]. There it was stated that the phase of the M1 residue was consistent with the phase of the residue found in elastic πN scattering. Actually, the phase of the M1 pole residue, found in Refs.[9,10], is reasonably consistent with this claim. However, we now have information on the E2 residue as well.

Projects for the coming year

Given the apparent sensitivity of the E2/M1 ratio to the employed database, it will be useful to have a 'benchmark' set. In this way data-dependence can be separated from model-

dependence. Together with the RPI group, tests of this type have been initiated. We hope efforts of this kind can be continued as the new Mainz data become available. So far, it seems that any model-dependence is greatly reduced when a common dataset is analyzed and the *same* quantity is compared.

Given that both pole and resonance values of the E2/M1 ratio are now being extracted, we should try to clarify the relation between these two quantities. Differing points of view have been presented in Refs.[9,25]. At this point, it is not clear whether the Mainz, VPI and RPI groups are evaluating identical quantities at the T-matrix pole. This can probably be clarified before the next N* meeting.

The reader can decide whether it is worthwhile studying the recent result of Aznauryan[26], wherein she extracts values of $A_{1/2}$ and $A_{3/2}$ consistent with quark model predictions. The similarity between this result and the result presented in Ref.[27] is intriguing, considering that very different methods were used. However, reading these two works, it is not clear whether the authors have interpreted their results in the same way.

Acknowledgments

We would like to thank the RPI, Mainz, and BNL groups for their data, analyses, and comments. Without this input, such a comprehensive report would not have been possible. This work was supported in part by the U.S. Department of Energy Grant No. DE-FG02-97ER41038.

REFERENCES

[1] M. MacCormick et al., Phys. Rev. C **53**, 41 (1996).
[2] R.M. Barnett et al., Phys. Rev. D **54**, 1 (1996).
[3] R. Beck et al., Phys. Rev. Lett. **78**, 606 (1997).
[4] G. Blanpied et al., Phys. Rev. Lett. **79**, (Nov.17) (1997).
[5] H. Genzel et al., Z. Phys. **268**, 43 (74); G. Fischer et al., Z. Phys. **245**, 225 (71).
[6] P. Dougan et al., Z. Phys. A **276**, 155 (1976).
[7] G. Anton, private communications.
[8] A.A. Belyaev et al., Nucl. Phys. **B188**, 397 (1981); V.A. Getman et al., Nucl. Phys. **B213**, 201 (1983); some G, H data have also been reported in: A.A. Belyaev et al., Sov. J. Nucl. Phys. **40**, 83 (1984); **43**, 947 (1986).
[9] O. Hanstein, D. Drechsel, and L. Tiator, Phys. Lett. **399B**, 13 (1997); 'Multipole analysis of pion photoproduction based on fixed t dispersion relations and unitarity', nucl-th/9709067; L. Tiator, private communications.
[10] R.A. Arndt, I.I. Strakovsky, and R.L. Workman, Phys. Rev. C **56**, 577 (1997); contribution to MENU 97, Vancouver (1997).
[11] N.C. Mukhopadhyay and R.M. Davidson, contribution to MAX-lab Workshop on the Nuclear Physics Program with Real Photons below 200 MeV, Lund, Sweden (1997); R.M. Davidson and N.C. Mukhopadhyay, private communications.
[12] T. Sato and T.-S. H. Lee, Phys. Rev. C **54**, 2660 (1996).
[13] See, for example, A.I. L'vov, V.A. Petrun'kin, and M. Schumacher, Phys. Rev. C **55**, 359 (1997).
[14] R.L. Workman, R.A. Arndt, and Z. Li, Phys. Rev. C **46**, 146 (1992).
[15] L. Tiator, private communication.
[16] K.M. Watson, Phys. Rev. **95**, 228 (1954).

[17] E. Matsinos, ETHZ-IPP PR-97-02; W.R. Gibbs, Li Ai, and W.B. Kaufmann, Phys. Rev. Lett. **74**, 3740 (1995).
[18] P. Christillin and G. Dillon, J. Phys. G **22**, 1773 (1996); see also M. Benmerrouche and N.C. Mukhopadhyay, Phys. Rev. D **46**, 101 (1992).
[19] R.M. Davidson, private communications.
[20] V.F. Grushin, A.A. Shikanyan, E.M. Leikin, and A. Ya Rotvain, Sov. J. Nucl. Phys. **38**, 881 (1983).
[21] R. Beck, private communications.
[22] I.I. Miroshnichenko et al., Sov. J. Nucl. Phys. **29**, 94 (79); **26**, 99 (1977).
[23] R. Workman, Phys. Rev. C **56**, 1645 (1997); see also R.M. Davidson and N.C. Mukhopadhyay, Phys. Rev. D **42**, 20 (1990).
[24] R.E. Cutkosky, Phys. Rev. C **47**, 367 (1993).
[25] P. Wilhelm, Th. Wilbois, and H. Arenhövel, Phys. Rev. C **54**, 1423 (1996); Th. Wilbois, P. Wilhelm, and H. Arenhövel, 'On the extraction of electromagnetic properties of the $\Delta(1232)$ excitation from pion photoproduction', nucl-th/9708005.
[26] I.G. Aznauryan, 'How to extract the $P_{33}(1232)$ resonance contributions from the amplitudes $M_{1+}^{3/2}$, $E_{1+}^{3/2}$, $S_{1+}^{3/2}$ of pion electroproduction on nucleons', hep-ph/9708238.
[27] T.-S. H. Lee, in *Baryons '92* (World Scientific, Singapore, 1993), p.99.

$\Delta(1232)$ Electroproduction at High Momentum Transfer

J.W. Price[1], V. Frolov[1], G. Adams[1], A. Ahmidouch[5], C. Armstrong[3], K. Assamagan[4], S. Avery[4], K. Baker[4], P. Bosted[2], V. Burkert[7], J. Dunne[7], T. Eden[4], R. Ent[7], D. Gaskell[4], P. Guèye[4], W. Hinton[4], C. Keppel[4], W. Kim[6], M. Klusman[1], D. Koltenuk[8], D. Mack[7], R. Madey[4,5], D. Meekins[3], R. Minehart[9], J. Mitchell[7], H. Mkrtchyan[10], J. Napolitano[1], G. Niculescu[4], I. Niculescu[4], M. Nozar[1], P. Stoler[1], V. Tadevosyan[10], L. Tang[4], M. Witkowski[1], S. Wood[7]

[1] *Rensselaer Polytechnic Institute, Troy, NY 12180*
[2] *American University, Washington, D.C. 20016*
[3] *College of William and Mary, Williamsburg, VA 23187*
[4] *Hampton University, Hampton, VA 23668*
[5] *Kent State University, Kent, OH 44242*
[6] *Kyungpook National University, Taegu, Korea*
[7] *Thomas Jefferson National Accelerator Facility, Newport News, VA 23606*
[8] *University of Pennsylvania, Philadelphia, PA 19104*
[9] *University of Virginia, Charlottesville, VA 22903*
[10] *Yerevan Physics Institute, Yerevan, Armenia*

Abstract

The differential cross section for the exclusive process $p(e,e'p)\pi^0$ has been measured in Hall C at the Thomas Jefferson National Accelerator Facility at momentum transfers of 2.8 and 4.0 $(\mathrm{GeV}/c)^2$. The cross section measurements were used to extract the M_{1+} and E_{1+} amplitudes, the ratio of which is compared with theoretical predictions.

INTRODUCTION

Constituent quark models have been used to predict the properties of the hadrons with moderate success. These models, being largely nonrelativistic in nature, work best in the photoproduction sector, where the relativistic effects are minimized. In electroproduction, as Q^2 increases, they are expected to fail. Where this failure occurs, and how it is manifested, is a topic of much debate. At large enough Q^2, one expects perturbative QCD (pQCD) to be the correct theory.

The photoexcitation of the $\Delta(1232)$ resonance may be used to study the nature of this transition. The transition from the nucleon state ($J^P = 1/2^+$) to the Δ ($J^P = 3/2^+$) may take place via either the M1 or the E2 photon multipole. In the nonrelativistic quark model, this transition is seen as a single quark spin-flip. Since both the nucleon and the $\Delta(1232)$ are $l = 0$ nuclear states, they cannot be connected by an $l = 2$ operator; thus, the E2 multipole is expected to be small. The most recent experimental results suggest that the ratio is actually about -2-3%, which is reasonable agreement when the limitations of the constituent quark model are considered. At high Q^2, helicity conservation requires E2$\approx$M1, or E2/M1$\approx$1.

The existing exclusive data on this process consists of several points below $Q^2 \simeq 1.2(\mathrm{GeV}/c)^2$, and a single point at $Q^2 \simeq 3(\mathrm{GeV}/c)^2$. The low Q^2 points are consistent with an E2/M1 ratio of 0; the high Q^2 point is at $E2/M1 = 0.06 \pm 0.05$ in one analysis, and very close to zero in another. There is no current theoretical consensus on where pQCD effects should become apparent, and the E2/M1 ratio should deviate from 0. Consequently, it is of great interest to study the evolution of this ratio at higher Q^2.

To this end, experiment E94-014 at the Thomas Jefferson National Accelerator Facility was conceived. The details of this experiment are discussed elsewhere in these proceedings[1];

this report will concern itself only with the analysis and preliminary results of the process $p(e,e'p)\pi^0$ near the $\Delta(1232)$.

EXPERIMENTAL DETAILS

Two beam energies were used in this experiment: 3.2 and 4.0 GeV. This corresponds to two values of Q^2 in the region of the $\Delta(1232)$: 2.8 and 4.0 $(\mathrm{GeV}/c)^2$. Q^2 was determined by the SOS spectrometer, which was left fixed for each Q^2 point. The HMS was used to detect the outgoing proton; the π^0 was not detected directly, but was inferred via missing mass. During the run, the HMS was placed at several settings to cover the angular and momentum range of the resonance decay proton; by overlapping the settings, essentially every point in the experiment was measured by at least two separate parts of the spectrometer acceptance. This will be used to suppress the systematic uncertainties in the measurement.

Data reduction included a requirement that the proton and electron had a good coincidence time between the two spectrometers, and that they had tracks within a fiducial region in their respective spectrometers. The π^0 is then identified by missing mass, which is calculated for each event. The data is then binned in $\cos\theta_\pi$, ϕ, Q^2, W, and $\phi_{e'}$, and corrected for acceptance and radiative effects, and normalized to the beam current. The virtual photon flux is divided out to determine the c.m. differential cross section, $d^2\sigma/d\Omega_\pi$. This cross section may then be fit using a model to include the properties of the Δ. Such a model was presented at this workshop, and is described elsewhere in these proceedings[7].

Davidson's fits to the data are shown in Figures 1 and 2. As can be seen from the data, the preliminary E2/M1 ratio is small but nonzero, and negative, in contrast to either of the analyses of the previous data at $3.2\,(\mathrm{GeV}/c)^2$.

CONCLUSIONS AND FUTURE PLANS

Bolstered by the quality of the data obtained for this experiment, we have proposed an extension of this experiment to higher Q^2, shown in the figures. This experiment will use the same experimental apparatus as this experiment, and will make use of higher-energy beams of 5 and 6 GeV, when they become available. It is clear that such experiments will be necessary if we are ever to understand the transition from the low-energy regime, in which the constituent quark model provides a good description of the physics of the baryon sector, to the high-energy regime, where perturbative QCD must prevail.

REFERENCES

[1] J.W. Price, these proceedings.
[2] R. Davidson, these proceedings.
[3] R. Beck et al., Phys. Rev. Lett. **78**, 606 (1997).
[4] G.S. Blanpied et al., Phys. Rev. Lett. **69**, 1880 (1992).
[5] V. Burkert and L. Elouadrhiri, Phys. Rev. Lett. **75**, 3614 (1995).
[6] R. Haiden, DESY Report No. F21-79-03, unpublished (1979).
[7] R. Davidson and N. Mukhopadhyay, Phys. Rev. Lett. **79**, 4509 (1997).
[8] V.M. Belyaev and A.V. Radyushkin, Phys. Rev. D **53**, 6509 (1996).
[9] S. Capstick, Phys. Rev. D **46**, 2864 (1992).

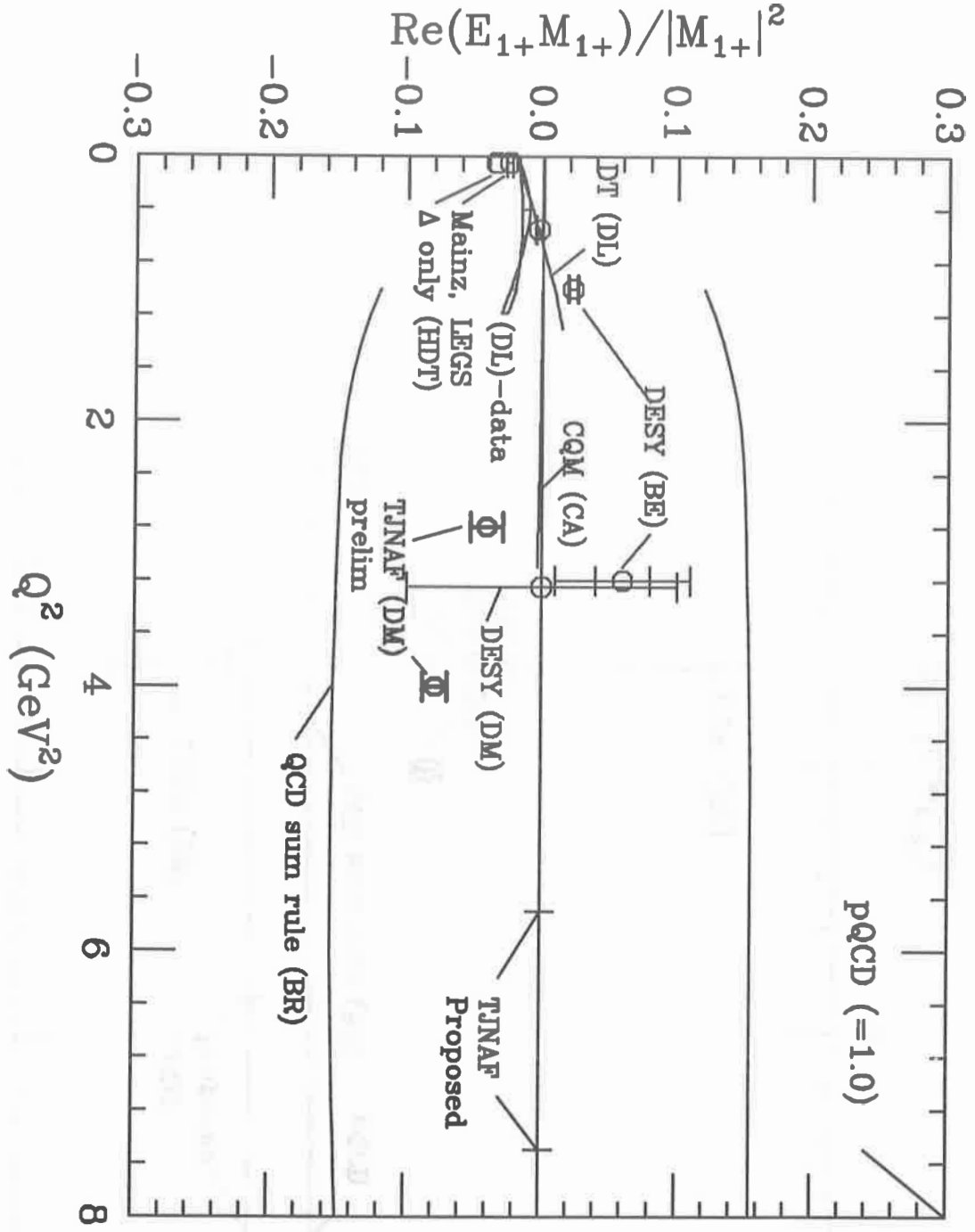

Figure 1. The preliminary results of this experiment for the E2/M1 ratio, fit by R. Davidson[2]. Only statistical error bars are shown. The points marked "TJNAF (DM)" are the preliminary results from this experiment; the points at $Q^2 = 0$ labelled "Mainz" and "LEGS" are from Refs. [3,4] respectively; the points labelled "DESY (BE)" near $Q^2 = 0.5$, 1.0, and 3.2$(\mathrm{GeV}/c)^2$ are due to an analysis[5] of earlier data from DESY[6]; the point labelled "DESY(DM)" at $Q^2 = 3.2\,(\mathrm{GeV}/c)^2$ is a recent analysis of the same DESY data from Ref. [7]; the curve labelled "QCD sum rule (BR)" is from Ref. [8]; the curve labelled "CQM (CA)" is due to a quark model calculation from Ref. [9]. The pQCD prediction for E2/M1 of 1 is off the scale of this plot. Also shown in this plot are the two Q^2 points of our upcoming proposal in Hall C at Jefferson Lab, at $Q^2 = 5.7$ and 7.5 $(\mathrm{GeV}/c)^2$.

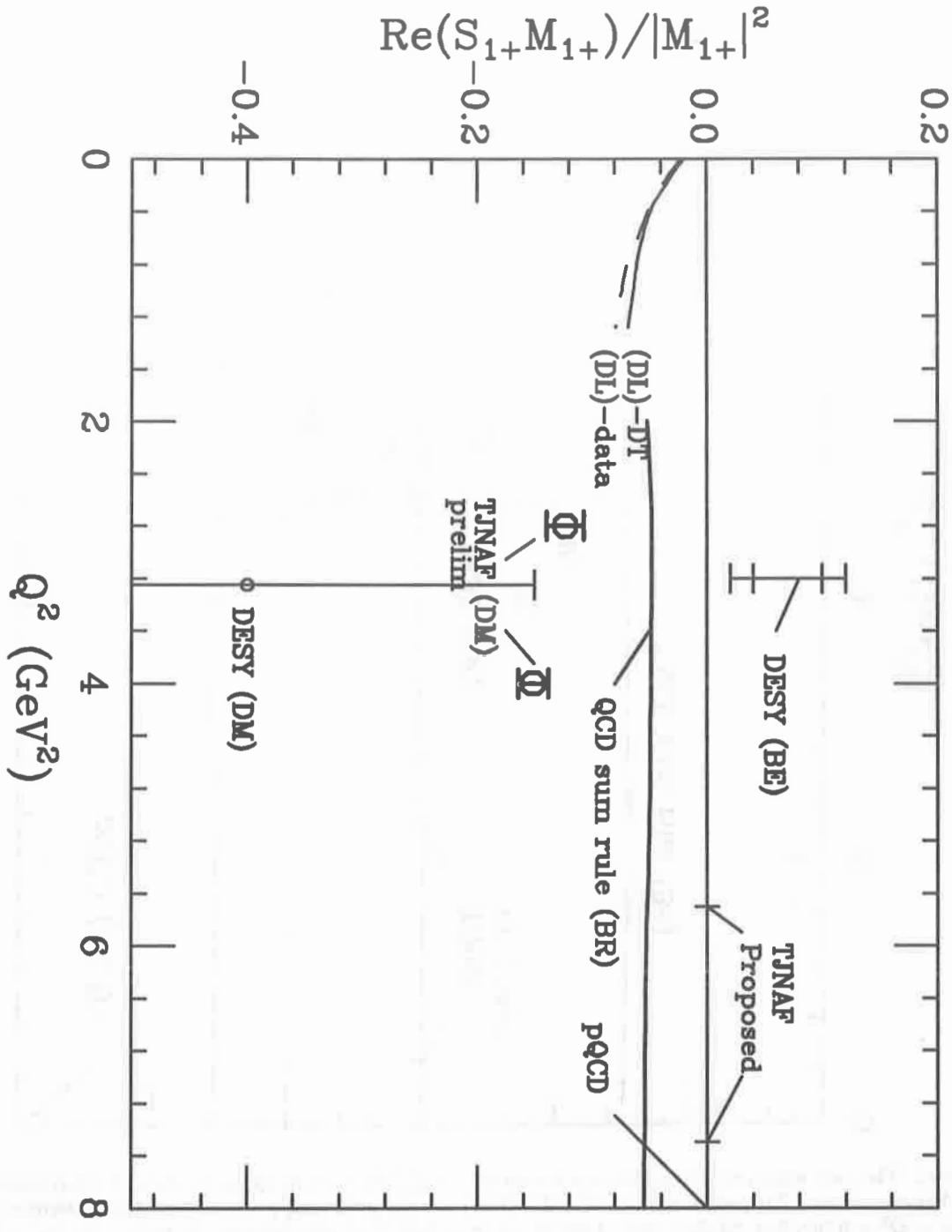

Figure 2. The preliminary results of this experiment for the S2/M1 ratio, fit by R. Davidson[7]. Only statistical error bars are shown. The labelling of the data points and curves is the same as in the previous figure.

$H(e,e'p)\pi^0$ and $H(e,e'\vec{p})\pi^0$ results from Bates at $Q^2 = 0.126$ (GeV/c)^2 around the $\Delta(1232)$ resonance

Costas E. Vellidis
Department of Physics, University of Athens, Greece
and the OOPS and FPP Collaborations*

Abstract

The preliminary cross section, LT−asymmetry and polarization results of a $H(e,e'p)\pi^0$ and $H(e,e'\vec{p})\pi^0$ experiment, conducted at the MIT/Bates Accelerator Facility at central $Q^2 = 0.126$ (GeV/c)^2, are presented and compared with model calculations. The data can constrain the magnetic dipole and Coulomb quadrupole $\gamma N \rightarrow \Delta$ amplitudes and, to some degree, the non−resonant background.

1. Motivation

Three amplitudes are related to the $\gamma N \rightarrow \Delta$ transition: a magnetic dipole, an electric quadrupole and a Coulomb quadrupole. The determination of the quadrupole amplitudes is of particular importance for our understanding of the nucleon and Δ structure. Within most existing microscopic baryon pictures, they imply tensor effective interactions, either in the form of color hyperfine interactions in quark models or in the form of non−uniform pressure exerted from the pion cloud in meson field theoretical approaches. A sensitive reaction for their determination is the electromagnetic pion production on the free nucleon in the mass region of the $\Delta(1232)$ resonance. Existing data show that these amplitudes are much smaller than the magnetic dipole amplitude, of the order of 10% or less. Their extraction is therefore complicated due to their small magnitude, but also due to the existence of a relatively strong non−resonant background. This background comes from various other couplings of the photon to the nucleon and the pion as well as to heavier meson and baryon states, not involving a $\Delta(1232)$ excitation. The subtraction of the background contributions from the observables of interest is difficult because the reaction mechanism is poorly understood.

Older experiments in this field involved measurements of angular distributions of pion production yields with unpolarized electrons and photons at the Δ resonance [1]. Such measurements can access components of only the real part of the electromagnetic response tensor which contain mixed resonant and background contributions. Separation of the background from the resonant terms can be best achieved through measurements over a wide range of the invariant hadron mass, where interference effects between different reaction mechanisms are varying, and especially through measurements of polarization observables. These are related to the imaginary part of the response tensor, which would vanish in the absence of background. The determination of the quadrupole amplitudes requires also a precise knowledge of the dominant magnetic dipole amplitude. Recently, photoproduction experiments with polarized photon beams yielded high precision results which constrain the transverse electric amplitude [2]. Polarization measurements at finite Q^2 are still entirely missing. Consequently, the older extractions of the "Coulomb−to−Magnetic amplitude Ratio" (CMR) have significant systematic errors due to background contamination. The experiment reported here was designed to determine the magnetic and Coulomb $\gamma N \rightarrow \Delta$ amplitudes, addressing at the same time the issue of the background.

*C.N. Papanicolas and R.W. Lourie, spokesmen

2. Methodology

The $H(e,e'p)\pi^0$ cross section in the One Photon Exchange Approximation (OPEA) takes the form:

$$\sigma = J\Gamma \left(v_L R_L + v_T R_T + v_{LT} R_{LT} \cos\phi + v_{TT} R_{TT} \cos 2\phi\right) \quad (1)$$

The factors v_K, with $K = L, T, LT, TT$, are related to the elements of the electron tensor on a basis attached to the momentum transfer direction. Γ is interpreted as the flux of virtual photons absorbed by the target protons and J is the Jacobian transforming the proton solid angle from the hadron Center–of–Momentum (CM) frame to the laboratory frame. The information on the hadron dynamics is contained in the response functions R_K, which are elements of the hadron electromagnetic tensor. These are evaluated in the CM frame and are functions of the invariant hadron mass W, of the (opposite) 4–momentum transfer squared Q^2, and of the polar angle θ of proton emission about the momentum transfer vector $\vec{q}$. The angle ϕ is the proton azimuth about $\vec{q}$. At $\theta = 0$ ("parallel kinematics"), only the combination $\sigma_{||} = v_L R_L + v_T R_T$ survives.

With an unpolarized electron beam and target, the final state proton polarization in parallel kinematics has only a component normal to the scattering plane:

$$P_n = \frac{v_{LT} R^n_{LT}}{\sigma_{||}} \quad (2)$$

The response functions in Eqs.(1–2) are expanded in terms of pion partial–wave multipole amplitudes which are functions of W and Q^2. Truncated to S and P waves only, these expansions can be written as follows [3]:

$$R_L(\theta = 0°) = |S_{0+} - 4S_{1+} - S_{1-}|^2 \quad (3)$$

$$R_T(\theta = 0°) = |E_{0+} - 3E_{1+} - M_{1+} + M_{1-}|^2 \quad (4)$$

$$R_{LT} = \Re e\left[(S_{0+} + 6S_{1+}\cos\theta)^* M_{1+}\right] \sin\theta \quad (5)$$

$$R_{TT} = -\frac{3}{2}\left(|M_{1+}|^2 + 2\Re e\left[(E_{1+} + M_{1-})^* M_{1+}\right]\right)\sin^2\theta \quad (6)$$

$$R^n_{LT} = \Im m\left[(S_{0+} - 4S_{1+} - S_{1-})^* M_{1+}\right] \quad (7)$$

where, in the interference response functions R_{LT}, R_{TT}, R^n_{LT}, terms not containing M_{1+} are also neglected. In the absence of background, M_{1+}, E_{1+} and S_{1+} correspond to the magnetic dipole, electric quadrupole and Coulomb quadrupole (photon) amplitudes, respectively, and all other multipoles vanish. The parallel kinematics cross section $\sigma_{||}$ is dominated by R_T, which contains $|M_{1+}|^2$. The most sensitive response functions to the multipole S_{1+} are R_L and R_{LT}, but R_{LT} can be extracted more easily from the asymmetry

$$A_{LT} = \frac{\sigma(\phi = 0°) - \sigma(\phi = 180°)}{\sigma(\phi = 0°) + \sigma(\phi = 180°)} = \frac{v_{LT} R_{LT}}{v_L R_L + v_T R_T + v_{TT} R_{TT}} \quad (8)$$

Finally, R^n_{LT} is sensitive to the background contributions, since without such contributions S_{1+} and M_{1+} would have the same phase and this response function would vanish. In this experiment, P_n, $\sigma_{||}$ and A_{LT} were measured.

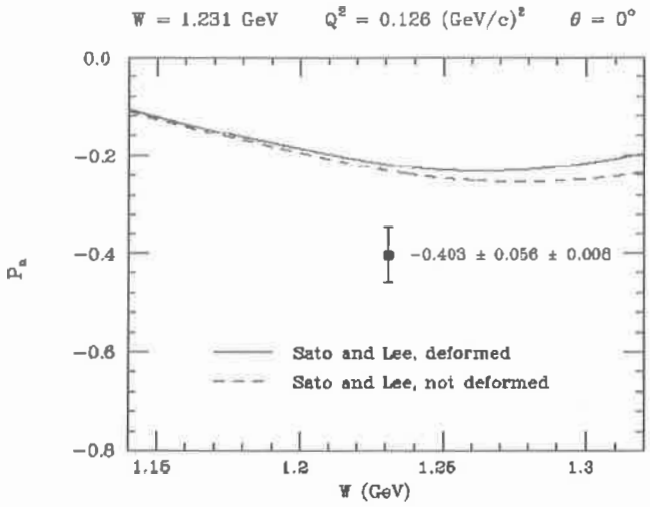

Figure 1. Induced proton polarization.

3. Experimental Setup

The experiment was conducted with an unpolarized electron beam of a 0.85% duty factor. A cryogenic liquid H_2 target was used in a cylindrical cell of 3 cm diameter with a 10 μm thick Havar wall. The liquid H_2 was provided by the MIT "Basel Loop" system. The scattered electrons were detected in the Bates Medium Energy Pion Spectrometer (MEPS), which has a QQSP configuration, and the coincident protons in the Bates One Hundred Inch Proton Spectrometer (OHIPS), which has a QQD configuration. The focal plane instrumentation of each spectrometer consisted of one crossed vertical drift chamber for track reconstruction and scintillators for triggering.

For the polarization measurement, OHIPS was additionally equipped with a Focal Plane Polarimeter (FPP) containing a 9.5 cm thick ^{12}C block where the protons were undergoing second scattering. The spin–dependent azimuthal asymmetry in the inclusive $\vec{p}$–^{12}C cross section was determined using two pairs of proportional drift chambers, one before and one after the ^{12}C block, for track reconstruction of the protons in the secondary reaction. The analyzing power of the ^{12}C block was measured with a polarized proton beam at the Indiana University Cyclotron Facility [4]. The proton polarization in the primary reaction is determined from the focal plane asymmetry by a transformation accounting for the precession of the proton spin in the fields of the OHIPS magnets [6]. The first pair of proportional chambers was also used in the cross section measurements, to improve the proton angle resolution.

Detailed optics studies were done for each spectrometer and the detection efficiencies were measured as functions of all independent reaction coordinates. The overall efficiency of the system was calibrated using elastic electron scattering data on the liquid H_2 target. Boiling effects in the target were studied by varying the beam current. The polarimeter was calibrated by the H_2 elastic measurement, in which P_n vanishes in OPEA. Finally, a detailed Monte Carlo model was developed which provides the phase space normalization of the cross section

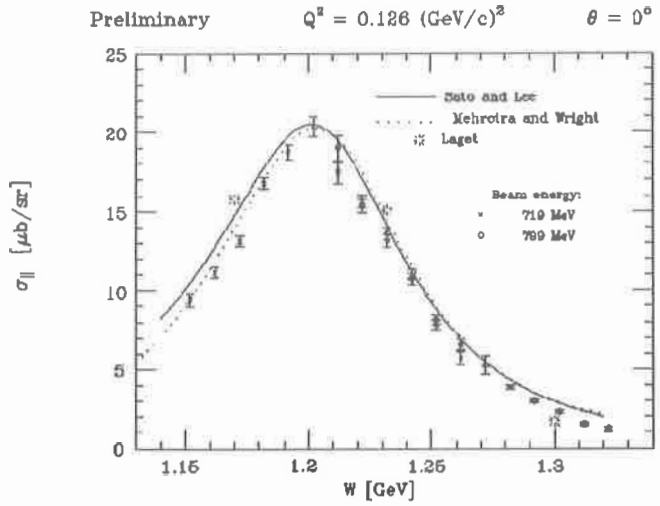

Figure 2. CM cross section in parallel kinematics. The errors are statistical only.

and various corrections applied to the data.

4. Results and discussion

In Fig. 1 the measured P_n is compared with preliminary π^0 electroproduction calculations according to the model of Sato and Lee [7]. Two calculations are shown, one for which the $\gamma N \rightarrow \Delta$ dressed–vertex form factors G_E (electric) and G_C (Coulomb) are set equal to zero and one for which their ratios to the magnetic form factor G_M are $G_E/G_M = 1.8\%$ and $G_C/G_M = -9.3\%$ at $Q^2 = 0$.

Fig. 2 shows the preliminary $\sigma_{||}$ data compared with the model predictions of Sato and Lee, of Mehrotra and Wright ("Fit A", simultaneous to π^0 and π^+ production data) [8] and of Laget [9]. There are two sets of points in the range of W between 1.21 and 1.27 GeV which were measured with two different beam energies of 719 MeV and 799 MeV. In these measurements, the spectrometer central angles and the scattered electron central momentum were different in order to keep W and Q^2 the same. The change in the central v_L value between the two measurements is 14%, so that there is no sensible change in the cross section. The two data sets agree within statistical errors, which shows that systematic effects in the experiment are well under control.

Fig. 3 shows the preliminary asymmetry data below and at the resonance, compared with predictions from the same models as those shown in Fig. 2. For each model, the lower curve corresponds to finite quadrupole $\gamma N \rightarrow \Delta$ form factors ($G_E/G_M = G_C/G_M = -4\%$ in the model of Laget) and the upper curve corresponds to zero quadrupole form factors, except for the model of Mehrotra and Wright which does not consider such form factors. It should be noted that A_{LT} at this point is about a factor of two weaker than A_{LT} at the resonance, while it is expected to be equal in the absence of background. This result and the strong P_n result show important background contributions to both the real and the imaginary part of

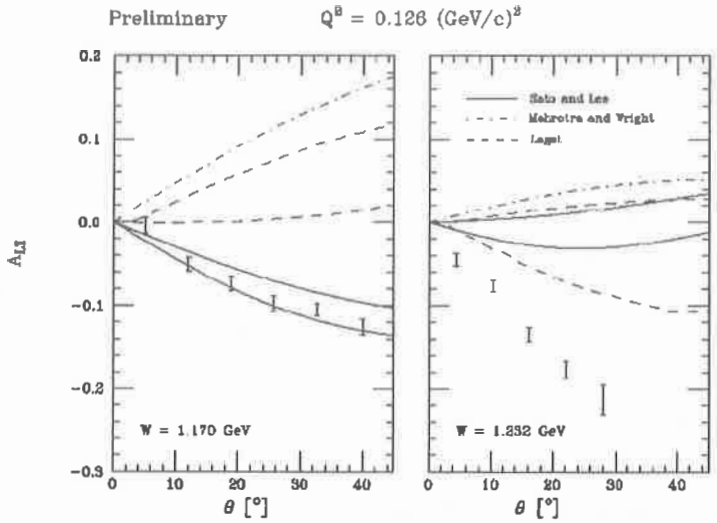

Figure 3. Cross section asymmetry in the scattering plane. The errors are statistical only.

the response tensor.

The failure of the models examined here to predict the measured observables related to the LT−interference is not primarily due to the transverse part, since the parallel kinematics cross section is fairly well predicted by all these models. Therefore, it is the longitudinal electromagnetic couplings, either the resonant quadrupole coupling or other background−related ones or both, which are not well understood. Also, the phases of non−resonant terms arising from the final state interaction of the π−N system can play an important role, particularly in the induced proton polarization. The data presented here have sufficient sensitivity to constrain considerably the longitudinal couplings, since the measured observables are much stronger than the statistical errors. A final analysis for the determination of the magnetic dipole and Coulomb quadrupole $\gamma N \rightarrow \Delta$ amplitudes is currently underway.

REFERENCES

[1] R. Siddle et al., Nucl. Phys. **B35**, 93 (1971); J. C. Alder et al., Nucl. Phys. **B46**, 573 (1972); W. Albrecht et al., Nucl. Phys. **B27**, 615 (1971); F. Kalleicher et al., Z. Phys. **A359**, 201 (1997).

[2] R. Beck et al., Phys. Rev. Lett. **78**, 606 (1997); G. Blanpied et al., Phys. Rev. Lett. **79**, 4337 (1997).

[3] D. Drechsel et al., J. Phys. G: Nucl. Part. Phys. **18**, 449 (1992).

[4] R. W. Lourie et al., I.U.C.F. Scientific and Technical Report **135** (1993).

[5] R. W. Lourie et al., Nucl. Inst. Meth. **A306**, 83 (1991).

[6] M. Berz, Nucl. Inst. Meth. **A298**, 473 (1990).

[7] T. Sato et al., Phys. Rev. **C54**, 2660 (1996).

[8] S. Mehrotra et al., Nucl. Phys. Abf 362, 461 (1981).

[9] J. M. Laget, Nucl. Phys. **A481**, 765 (1988).

A Relativistic, Unitary Model for Pion Electroproduction

R.M. Davidson*
Department of Physics, Applied Physics and Astronomy
Rensselaer Polytechnic Institute, Troy, NY, 12180, U.S.A.

Abstract

The effective Lagrangian model of Davidson, Mukhopadhyay and Wittman (DMW) [1] for pion photoproduction in the $\Delta(1232)$ region is extended to electroproduction. The model is fully relativistic, and is made unitary via a K-matrix approach. The model is used to analyze the preliminary JLab data [2] for neutral pion electroproduction off protons at Q^2 values of 2.8 and 4.0 GeV^2. The resulting values of E2/M1 are found to be small and negative, indicating that the perturbative region of QCD has not yet been reached in this reaction.

INTRODUCTION

One goal, if not the primary goal, of the N* program at JLab is to "measure" the nucleon-resonance electromagnetic transition form factors as a function of the four-momentum squared, Q^2, of the virtual photon. The behavior of these form factors will provide invaluable information on the structure of the nucleon and its resonances. Two classic examples of the use of the photon as a probe of hadronic structure are the nucleon electromagnetic form factors and nucleon-Delta(1232) electromagnetic transition amplitudes. The nucleon form factors clearly indicate that the nucleon is not point-like and from the behavior of the form factor near the real photon point one can determine the size of the nucleon. In addition, for the neutron one can infer that the negative charge distribution has a slightly larger spatial extent than the positive charge distribution. For the N-$\Delta(1232)$ electromagnetic transition at the real photon point, the dominance of the magnetic dipole transition, M1, over the electric quadrupole transition, E2, lends support to the SU(6) classification of these particles and at the same time indicates that the nucleon and Delta wave functions are, to a large extent, spherically symmetric.

Although the extraction of the nucleon form factors from the elastic scattering data is straight forward, extraction of the transition form factors from, for example, electromeson production is much more difficult. There are often overlapping resonances that decay into many strong channels and significant backgrounds may also be present. In this regard, the Delta(1232) is a special case since it is a well isolated resonance with only one strong decay channel. The problem of separating the background and resonance contributions still remains, but in this case we have a very good theoretical understanding of the background mechanism [1]. The main point here is that theory is first needed to extract the electromagnetic transition form factors from the data and then again needed to interpret what they mean in the context of QCD.

The N-Δ transition form factors are expected to have a dramatic Q^2 dependence. At the real photon point, the ratio of E2/M1 is about -3% [3,4] in *qualitative* agreement with quark model predictions that this ratio is small and negative. On the other hand, at some unknown large Q^2, this ratio should approach the pQCD value of +100%, that is, E2 and M1 become equal. At what Q^2 one starts entering the pQCD domain is unknown, and it is also unknown if it is E2 or M1 that ultimately changes sign. The general prejudice seems to be that it is the E2 that changes sign, but this needs to be determined experimentally.

*E-mail: davidr@rpi.edu

To extract E2, M1 and C2 from the data, one would ideally like to have lots of $p\pi^0$ and $n\pi^+$ differential cross section data in order to perform the isospin decomposition, and polarization observables to help pin down the background contribution. In reality, there are very little $n\pi^+$ data and practically no explicit polarization data* [5]. It is clear that to determine E2, M1 and C2 from just the $p\pi^0$ differential cross sections one either needs a model or needs to make some assumptions. Based on what happens at the real photon point, many authors in the past have made the assumption of M_{1+} dominance. In short, one first assumes that only s and p waves are important such that the differential cross section takes on the form

$$\begin{aligned} \frac{\mathrm{d}\sigma}{\mathrm{d}\Omega} &= \frac{q}{K_C}\Gamma\Big[A_0 + A_1\cos\theta + A_2\cos^2\theta \\ &+ \epsilon C_0\cos 2\phi\sin^2\theta + \sqrt{2\epsilon(1+\epsilon)}\,(D_0 + D_1)\cos\phi\sin\theta\Big]\,, \end{aligned} \tag{1}$$

where θ is the cm photon-pion angle and ϕ is the angle between the scattering plane and the reaction plane. In addition, q is the pion cm three-momentum, K_C is the cm equivalent real photon energy, and Γ is the virtual photon flux factor.

The six angular coefficients in (1), A_i, C_i, and D_i, can be determined from the θ and ϕ dependence of the differential cross section. Evidently, these angular coefficients are bi-linears of the s and p wave multipoles. In particular, assuming M_{1+} dominance, that is, keeping only terms involving M_{1+}, one may extract $|M_{1+}|^2$ and the interference terms $\mathrm{Re}(E_{1+}M_{1+}^*)$, $\mathrm{Re}(S_{1+}M_{1+}^*)$, $\mathrm{Re}(E_{0+}M_{1+}^*)$, $\mathrm{Re}(M_{1-}M_{1+}^*)$, and $\mathrm{Re}(S_{0+}M_{1+}^*)$, from the angular coefficients. While one can certainly produce numbers with this approach, there are several potential problems. First, the above interference terms refer to the $p\pi^0$ multipoles whereas one is really interested in the isospin 3/2 multipoles. Second, is the amplitude really M_{1+} dominated at these Q^2 values? As pointed out by Warren and Carlson [6], as $Q^2 \to \infty$, $E_{1+}/M_{1+} \to 1$, and therefore A_{1+} dominance is more appropriate. Third, what if the amplitude is not Δ dominated? Although the matter is far from settled, there are indications from the inclusive data that the Δ is, at least initially, falling faster than its background [7,8]. Finally, what happens when the extracted interference terms are large compared to $|M_{1+}|^2$? This is an indication that the assumption of M_{1+} dominance is breaking down and the results are not trust worthy. Indeed, as shown below, at the Q^2 values of the recent TJNAF experiment the interference terms are large and one is forced to use a model to analyze these data.

THE MODEL

Having discussed the need for a model, there are some obvious properties the model should have. It should be Lorentz invariant, gauge invariant, and crossing symmetric. It should contain the nearby poles, which for neutral pion production are the nucleon and Delta poles, and for charged pion production additionally the pion pole. No *a priori* assumptions about M1, E2, and C2 should be made. The model should be unitary, and because only $p\pi^0$ data are available, the isospin structure of the model must in some way be constrained.

At the real photon point, all of these properties are satisfied in the effective Lagrangian model of Davidson, Mukhopadhyay, and Wittman (DMW) [1], and the extension of this model to electropion production is straight forward. The nucleon Born terms for neutral pion production pick up the Dirac and Pauli form factors, F_1 and F_2. For charged pion production,

*Since the virual photons are polarized, one can effectively determine the polarized photon asymmetry by measuring the ϕ dependence of the differential cross section.

one also needs the pion electromagnetic form factor, F_π, and, if pseudovector coupling (PV) is used, one also needs the form factor $F_A(Q^2) = g_A(Q^2)/g_A(0)$, g_A being the axial-vector form factor. Based on current-algebra and PCAC, this latter form factor multiplies the so-called "seagull" diagram.

The PV nucleon Born amplitude is consistent with the leading order low-energy theorems for these reactions, and thus PV coupling is preferred over the pseudoscalar (PS) coupling near the real photon point. On the other hand, for Q^2 larger than a few μ^2, μ the pion mass, it is not clear that chiral arguments apply and therefore not clear if PV is preferred over PS. However, for neutral pion production in the vicinity of the Δ, the difference between PS and PV is not too significant. At low Q^2, the E_{0+} and M_{1-} multipoles obtained from either PV or PS are small compared to the dominant M_{1+} multipole. As Q^2 increases, the background multipoles seem to be growing in their relative importance, but the difference between PV and PS is decreasing. To understand this, recall at the real photon point the "equivalence" breaking term between PV and PS contributes only to the E_{0+} and M_{1-} multipoles and is proportional to the anomalous magnetic moment, κ. Thus, it is not suprising that for electroproduction the equivalence breaking term is proportional to F_2, which falls like Q^{-6}. On the other hand, the s-channel "electric" contribution is proportional to F_1, which falls like Q^{-4}, and therefore the equivalence breaking term is suppressed at large Q^2. For example, at 2.8 GeV^2 the total cross sections obtained from PS and PV agree to within a few percent.

For charged pion electroproduction, part of the equivalence breaking term does survive at large Q^2. In this case, there is an additional breaking term between PS and PV proportional to F_A-F_1. This term evidently vanishes at the real photon point and falls like Q^{-4} at large Q^2, i.e. at the same rate as the s-channel electric contribution. One other interesting feature of charge pion electroproduction is that it has a rather rapid multipole convergence even at a modest Q^2, in sharp contrast to what occurs at the real photon point. At the real photon point, one can get fairly close to the pion pole which causes the slow multipole convergence. However, as Q^2 increases one moves away from this pole. To leading order in Q^2, one finds,

$$\frac{1}{t-\mu^2} \approx -\frac{W}{Q^2 q}\frac{1}{(E_f/q - x)}\,, \tag{2}$$

where W is the total cm energy, E_f is the final nucleon energy in the cm frame, and x is the cosine of the angle between the photon and pion in the cm frame. Since E_f/q is rather large and the multipole expansion is essentially an expansion in x, one finds rapid convergence even at modest Q^2. At large Q^2, one does approach the u-channel pole at backward angles and this term could potentially cause a slow multipole convergence. However, at large Q^2 one finds that $u \sim Q^2$, and thus the u-channel contribution is suppressed compared to the s-channel. At 2.8 GeV^2, one finds that the total cross section for charged pion production is essentially saturated by s and p waves.

Another possible "background" contribution is t-channel vector meson exchange. The relevant couplings and electromagnetic form factors are not well-known, but for any reasonable choice of form factor this contribution is suppressed at large Q^2 due to both the form factors and the propagator since $t \sim Q^2$. At a Q^2 around 2 GeV^2, the t-channel vector meson exchange becomes negligible.

The remaining important contribution is the s-channel Δ exchange, which is associated with a pole in the complex W plane, and by crossing symmetry, the u-channel Δ exchange. Although no free parameters appear in the nucleon Born sector, there are unknown parameters describing the Δ contribution. Obviously, there are three parameters describing the

transition amplitudes M1, E2 and C2. Since we treat the Delta as a relativistic spin 3/2 particle, there is an "off-shell" parameter associated with each of the electromagnetic three-point vertices [9]. In addition, there is an off-shell parameter coming from the $\pi N\Delta$ vertex. As the mass and width of the Delta are taken from analyses of elastic πN scattering, the model contains a total of seven parameters that are determined by fits to the data. Note that no *a priori* assumptions are made about the values of these parameters, e.g. M_{1+} dominance is not assumed. The s-channel Delta contribution is pure isospin 3/2 while the u-channel contribution is both isospin 3/2 and 1/2. However, the parameters that describe the isospin 3/2 sector also describe the isospin 1/2 sector, and thus the isospin structure of the amplitude is constrained.

To satify unitarity, the s and p wave multipoles are projected out and unitarized via a K-matrix approach,

$$\mathcal{M} = \mathcal{M}_T \cos\delta e^{i\delta} \ , \tag{3}$$

where $\mathcal{M}$ denotes a generic s or p wave multipole, $\mathcal{M}_T$ is its tree-level projection and δ is the appropriate πN elastic scattering phase shift. The importance of unitarizing the multipoles, particularly the resonant multipoles, cannot be underestimated. Whatever the values of E2, M1, and C2 are, Watson's theorem, i.e. unitarity, demands that the real parts of isospin 3/2 multipoles E^3_{1+}, M^3_{1+}, and S^3_{1+} must vanish at resonance. If a Breit-Wigner resonance is added to a real, smooth background, the extracted values of E2, M1, and C2 can be extremely biased since they may adjust themselves to enforce the zero.

After the s and p waves are unitarized (the d and higher l waves have very small phases in this energy region), the CGLN $\mathcal{F}$'s are reconstructed by adding in the unitarized multipoles and subtracting off the tree level s and p wave multipoles (to avoid double counting). In this manner, all multipoles are kept in the model and the pole structure of the amplitude is maintained.

RESULTS

The model described in the previous section has been used to analyze the preliminary JLab data [2] for neutral pion electroproduction off protons at Q^2 values of 2.8 and 4.0 GeV^2. Despite the fact that the isospin structure of the amplitude is rather tightly constrained, a natural worry is whether it is tightly enough constrained to accurately determine M1, E2 and C2 from just the $p\pi^0$ data. While this can only be answered once the $n\pi^+$ data become available at this Q^2, there is a test at the real photon point. Fitting just the recent Mainz π^0 data [10] results in almost identical values for E2 and M1 as when both the π^0 and π^+ data are fitted together.

The preliminary JLab data were fitted in the W range from 1.115 to 1.295 GeV. At each Q^2, each data set contained well over 500 points. Results of the fit (solid line) around resonance are shown in Fig. 1 for $Q^2 = 2.8$ GeV^2 and in Fig. 2 for $Q^2 = 4.0$ GeV^2. At 2.8 GeV^2, the results are

$$\begin{aligned} \mathrm{M1} &= 40.2 \pm 0.6 \ \times 10^{-3}\ \mathrm{GeV}^{-1/2} \ , \\ \frac{\mathrm{E2}}{\mathrm{M1}} &= -(4.1 \pm 1.2)\% \ , \\ \frac{\mathrm{C2}}{\mathrm{M1}} &= -(12.3 \pm 1.6)\% \ , \end{aligned}$$

with a χ^2 per degree of freedom of 1.85. At 4 GeV^2 the results are

$$\begin{aligned} \mathrm{M1} &= 23.3 \pm 0.8 \ \times 10^{-3}\ \mathrm{GeV}^{-1/2}\,, \\ \frac{\mathrm{E2}}{\mathrm{M1}} &= -(7.9 \pm 0.8)\%\,, \\ \frac{\mathrm{C2}}{\mathrm{M1}} &= -(15.1 \pm 1.3)\%\,, \end{aligned}$$

with a χ^2 per degree of freedom of 1.59. The errors here are statistical only.

The values for M1, E2 and C2 given here are obtained from the K-matrix residues [11]. In particular, in terms of the isospin 3/2 multipoles M^3_{1+}, E^3_{1+}, and S^3_{1+}, one finds

$$\begin{aligned} M1 &= \mathrm{Im}M^3_{1+}A_\Delta \\ E2 &= \mathrm{Im}E^3_{1+}A_\Delta \\ C2 &= \mathrm{Im}S^3_{1+}A_\Delta\,, \end{aligned} \tag{4}$$

with

$$A_\Delta = \sqrt{\frac{8\pi M_\Delta q \Gamma_\Delta}{3MK_C}}\,. \tag{5}$$

In (4,5), all kinematical quantities should be evaluated at the resonance energy, i.e. the energy where the 3,3 pion-nucleon elastic scattering phase shift passes through 90^0. In addition, in (5), M is the nucleon mass, M_Δ is the Delta mass, and Γ_Δ is the width of the Delta.

The often quoted helicity amplitudes $A_{1/2}$ and $A_{3/2}$ are related to E2 and M1 by

$$\begin{aligned} A_{1/2} &= -(M1 + 3E2)/2 \\ A_{3/2} &= -\sqrt{3}(M1 - E2)/2\,. \end{aligned} \tag{6}$$

Thus, at 2.8 GeV^2 one obtains

$$A_{1/2} = -(17.6 \pm 0.8) \qquad A_{3/2} = -(36.2 \pm 0.7)\,,$$

in units of 10^{-3} GeV$^{-1/2}$, while at 4.0 GeV^2, one obtains

$$A_{1/2} = -(8.9 \pm 0.3) \qquad A_{3/2} = -(21.8 \pm 0.4)\,,$$

in the same units. The relations amongst M1, E2, and C2 and the form factors G^*_M, G^*_E, and G^*_C given by Jones and Scadron [12] are

$$\begin{aligned} G^*_M &= \frac{M1}{C_\Delta 6M_\Delta(M_\Delta + M)} \\ G^*_E &= -\frac{E2}{C_\Delta 6M_\Delta(M_\Delta + M)} \\ G^*_C &= -\frac{C2}{C_\Delta 3k(M_\Delta + M)}\,, \end{aligned} \tag{7}$$

where

$$C_\Delta = \frac{ek}{12MM_\Delta S_1\sqrt{2MK_C}}\,. \tag{8}$$

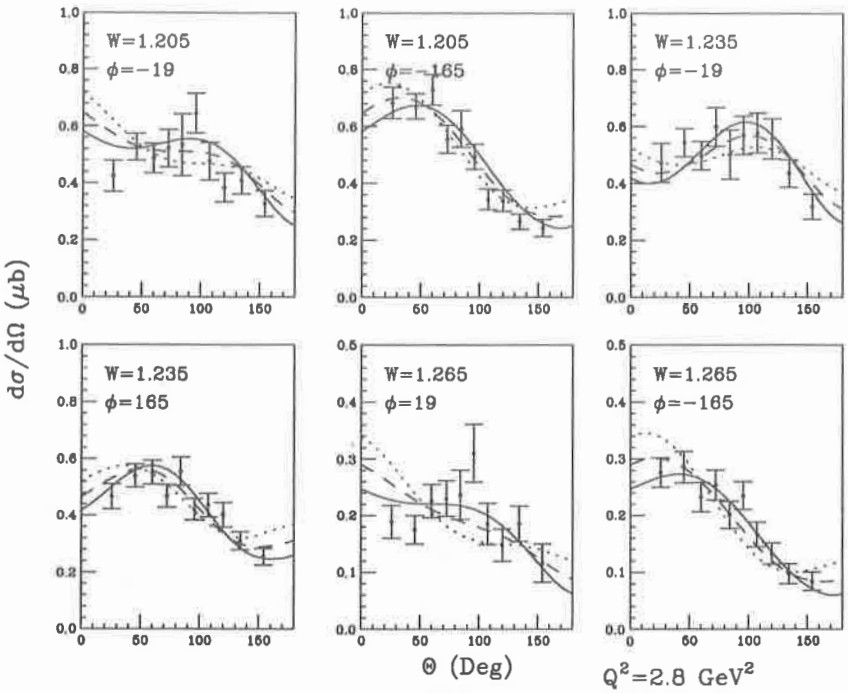

Figure 1. A comparison of the best fit (solid line) with a subset of the preliminary JLab data [2] around resonance at $Q^2 = 2.8$ GeV^2. The dashed line is obtained from the solid line by setting E2 = 0, while the dotted line is obtained by changing the sign of E2.

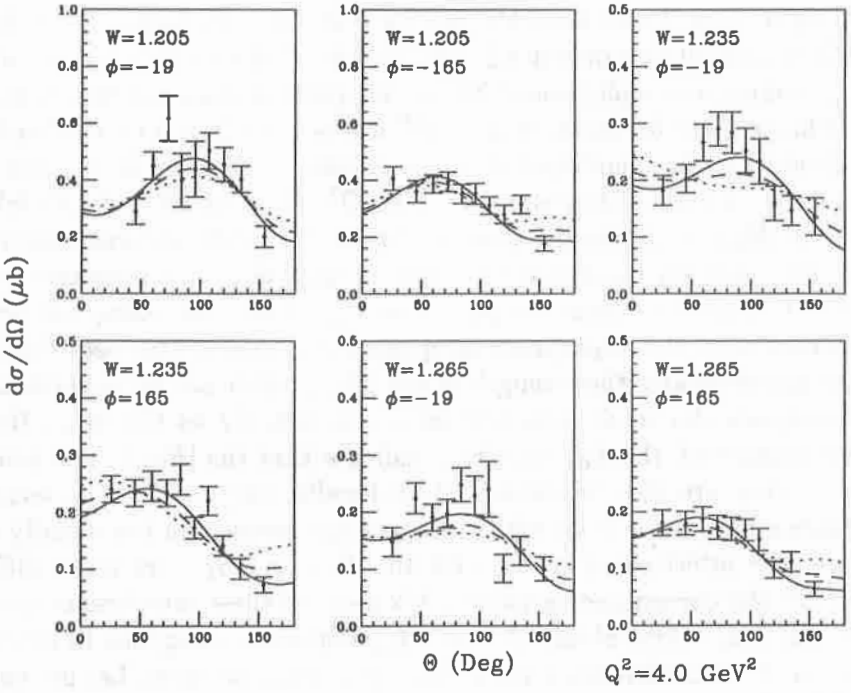

Figure 2. Caption as in Fig. 1, but at $Q^2 = 4.0$ GeV^2.

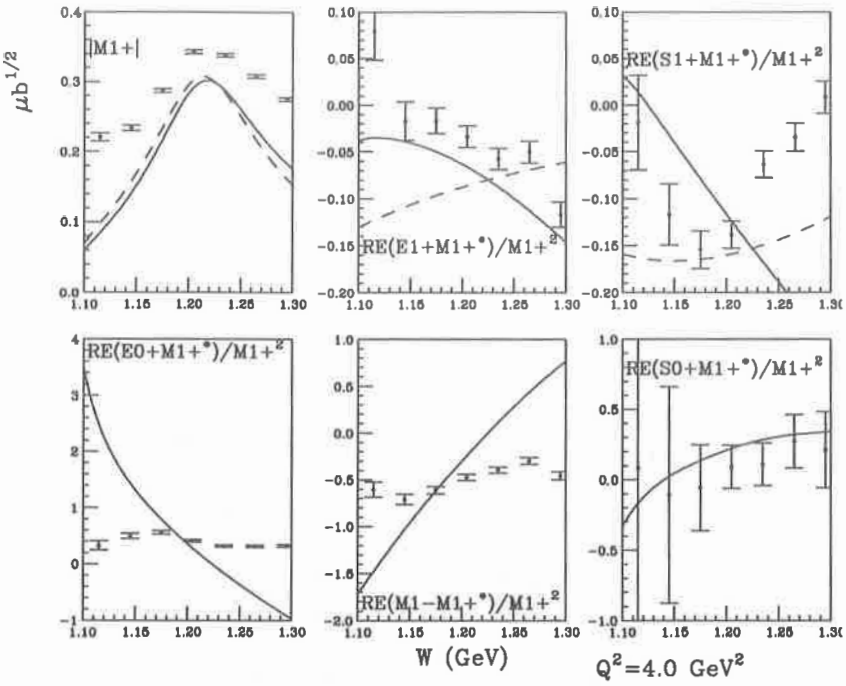

Figure 3. Results obtained from the assumption of M_{1+} dominance (points) at $Q^2 = 4.0$ GeV^2 compared with the actual results from the fit (solid line). For M_{1+}, E_{1+}, and S_{1+}, the isospin 3/2 components are also shown (dashed line).

In (7,8), k is the photon cm three-momentum, $e = \sqrt{4\pi\alpha}$, and $S_1 = \sqrt{E_i + M}$, E_i being the initial proton energy in the cm frame.

Also shown in Figs. 1 and 2 are the results with E2 = 0 (dashed line). By just eyeballing the figures it is difficult to rule out E2 = 0, but the χ^2 does rule it out in this model. On the other hand, making the replacement E2 → -E2 (dotted line) one sees that a positive E2 is ruled out. This is most dramatic at $\phi = 19^0$ where the E2 > 0 curve clearly has the wrong shape. It should also be mentioned that the off-shell paramters X, Y, and Z lie within the ranges found at the real photon point for both Q^2 values of 2.8 and 4.0 GeV^2.

As a test of M_{1+} dominance, I show in Fig. 3 the results obtained from this assumption at 4 GeV^2 (the points) compared with the actual M_{1+} and interference terms obtained from the fit. I emphasize that the points in Fig. 3 are not data, but are obtained from M_{1+} dominance with the appropriate propagation of errors. One sees that M_{1+} dominance significantly overestimates the strength of the M_{1+}, which can be understood by noting that in M_{1+} dominance the total cross section is due entirely to the M_{1+}. However, the large interference terms with the E_{0+} and M_{1-} indicate that the $|E_{0+}|^2$, etc. contributions to the total cross section are also important. Additionally, the interference terms obtained from M_{1+} dominance have little to do with reality except perhaps in the vicinity of the resonance. Furthermore, the interference terms with the E_{1+} and S_{1+} are quite different away from resonance from the corresponding isospin 3/2 parts of these interference terms (dashed line). The E_{1+} interference term obtained from M_{1+} dominance happens to be close to the model result, but the S_{1+} interference term differs by a factor of three. Let me emphasize that the failure of M_{1+} dominance is not due to the E_{1+} such that A_{1+} dominance would be better. Rather, it fails because the background multipoles have risen in their relative importance.

CONCLUSIONS

Based on the preliminary JLab data and this model, E2/M1 remains small and negative at Q^2 values of 2.8 and 4.0 GeV^2, indicating that the pQCD domain has not yet been reached for this reaction. Amusingly, the nucleon form factors and other transition form factors seem to be consistent with pQCD counting rules starting at about 4 GeV^2. Whether pQCD for these reactions is valid at 4 GeV^2 is open to debate, but in either case it is difficult to understand why these form factors are behaving "normally" while the Delta is not. In particular, at 4 GeV^2, the E2/M1 ratio is qualitatively unchanged from its real photon point value. This means that the helicity amplitudes $A_{1/2}$ and $A_{3/2}$ are falling at roughly the same Q^2 rate and helicity conservation is still grossly violated at these Q^2 values.

Needless to say, since the data are not yet final, the results presented here are not final. Once the data are final, one must naturally redo the fit in the event some of the points or error bars change. More importantly, the effect of the systematic errors on E2, M1 and C2 must be estimated. In addition, the chi-squared as a function of E2/M1 should be mapped out in order to look for additional minima. In particular, one would like to see if there is a solution with a relatively large, positive E2/M1 ratio. From the shape of the data, this seems unlikely to me, but it needs to be checked. Finally, other, *unitary* models should be used to assess the model dependence in extracting the E2, M1 and C2 from just the $p\pi^0$ differential cross section data, and it should be agreed upon exactly what quantity one reports for these transition amplitudes. Here, I have quoted the values at the K-matrix pole, but the values at the T-matrix pole may also be easily found.

Acknowledgements

I would like to thank the organizers of this workshop for their invitation and for their efforts in making it a successful workshop. I am indebted to V. Frolov and P. Stoler for making the E94-014 data available to me, and to N.C. Mukhopadhyay for his many stimulating discussions. This work was supported by the US Dept. of Energy grant number DE-FG02-88ER40448.

REFERENCES

[1] R. M. Davidson, N. C. Mukhopadhyay and R. S. Wittman, Phys. Rev. D**43**, 71 (1991).
[2] V. Frolov and P. Stoler for the E94-014 collaboration, private communications, (1997). The preliminary JLab data from this experiment were presented at this workshop by J. Price.
[3] R. M. Davidson and N. C. Mukhopadhyay, Phys. Rev. Lett. **79**, 4509 (1997).
[4] For a review of the current status of E2 and M1 at the real photon point, see Ron Workman's contribution to this workshop.
[5] Preliminary polarization data from Bates were presented at this workshop by C. Vellidis.
[6] G. A. Warren and C. E. Carlson, Phys. Rev. D **42**, 3020 (1990).
[7] R. M. Davidson and N. C. Mukhopadhyay, Phys. Lett. **B353**, 131 (1995).
[8] P. Stoler, Phys. Rev. Lett. **66**, 1003 (1991); Phys. Rep. **226**, 103 (1993).
[9] M. Benmerrouche, R. M. Davidson and N. C. Mukhopadhyay, Phys. Rev. C **39**, 2339 (1989).
[10] R. Beck *et al.*, Phys. Rev. Lett. **78**, 606 (1997).
[11] R. M. Davidson and N. C. Mukhopadhyay, Phys. Rev. D **42**, 1546 (1990).
[12] H. F. Jones and M. D. Scadron, Ann. Phys. **81**, 1 (1973).

The GRAAL experiment: plans and first results

J. Ajaka,[1] M. Anghinolfi,[2] V. Bellini,[3] G. Berrier,[1] J.P. Bocquet,[4] M. Breuer,[5] P.M. Calvat,[4] M. Capogni,[5] C. Cassano,[5] M. Castoldi,[2] L. Ciciani,[5] P. Corvisiero,[2] A. D'Angelo,[5] J.-P. Didelez,[1] R. Di Salvo,[1] Ch. Djalali,[1] M.A. Duval,[1] R. Frascaria,[1] G. Gervino,[6] F. Ghio,[7] P. Girard,[1] B. Girolami,[7] E. Guinault,[1] P. Hoffmann-Rothe,[1] E. Hourany,[1] J. Kilvington,[11] V. Kuznetsov,[8] A. Lapik,[8] P. Levi Sandri,[9] D. Moricciani,[4] M. Morlet,[1] V. Nedorezov,[8] L. Nicoletti,[5] C. Perrin,[4] D. Rebreyend,[4] F. Renard,[4] M. Ripani,[2] L. Rosier,[1] P. Rossi,[9] F. Roudot,[5] T. Russew,[4] M. Sanzone,[2] C. Schaerf,[5] M. L. Sperduto,[5] A. Sudov,[8] M. Taiuti,[2] A. Turinge,[10] J. Van de Wiele,[1] A. Zucchiatti,[2]

[1]IN2P3, Institut de Physique Nucléaire, 91406 Orsay, France

[2]INFN Genova and Dipartimento di Fisica, 16146 Genova, Italy

[3] INFN Laboratori Nazionali del Sud and Università di Catania, Italy

[4]IN2P3, Institut des Sciences Nucléaires, 38026 Grenoble, France

[5]INFN sezione di Roma II and Università di Tor Vergata, Italy

[6]INFN sezione di Torino and Università di Torino, Italy

[7]INFN sezione Sanità and Instituto Superiore di Sanità, Roma, Italy

[8]Institute for Nuclear Research, Moscow, Russia

[9]Laboratori Nazionali di Frascati, Italy

[10]I. Kurchacov Institute of Atomic Energy, Moscow, Russia

[11]European Synchrotron Radiation Facility, 38026 Grenoble, France

Abstract

The GRAAL experiment is presented. A tagged and polarized photon beam is produced by backscattering an argon laser beam on the 6 GeV electron beam of the ring of the ESRF. A detection system of $\approx 4\pi$ solid angle was constructed. The photoproduction of η, K and other mesons is performed with an incident energy, first in the range of 500 MeV to 1100 MeV, then up to 1500 MeV. The present experiments of GRAAL and the future plans are described. Samples from first results of beam asymmetry Σ are shown.

INTRODUCTION

GRAAL (GRenoble Anneau Accélérateur Laser) is an experimental program running at the line D7 (Fig.1) of the ring of the ESRF (European Synchrotron Radiation Facility). The goal is the study of the photoproduction of mesons, in a first stage with a polarized photon beam of an energy range up to 1.5 GeV and in a second stage with polarized target and beam, the latter having an energy range up to 1.8 GeV. The present report on GRAAL comes after the installation of all the parts of the experimental setup and after the data taking of a few months started in the fall of 1996. The good running of the different important parts of the setup and the successful analysis of the first results together with the scientific program previously drawn allow now to outline the future plans and to give some preliminary results. This text will describe the setup, mainly the polarized and tagged photon beam and the $\approx 4\pi$ detection system. The main performances of the GRAAL system will be given. A detailed description of typical experiments of the program will be presented. Then, some preliminary results will be shown.

THE GRAAL SETUP

The GRAAL system produces a high quality tagged and polarized photon beam obtained by backscattering a laser photon beam on the electron beam of the ESRF. The laser beam

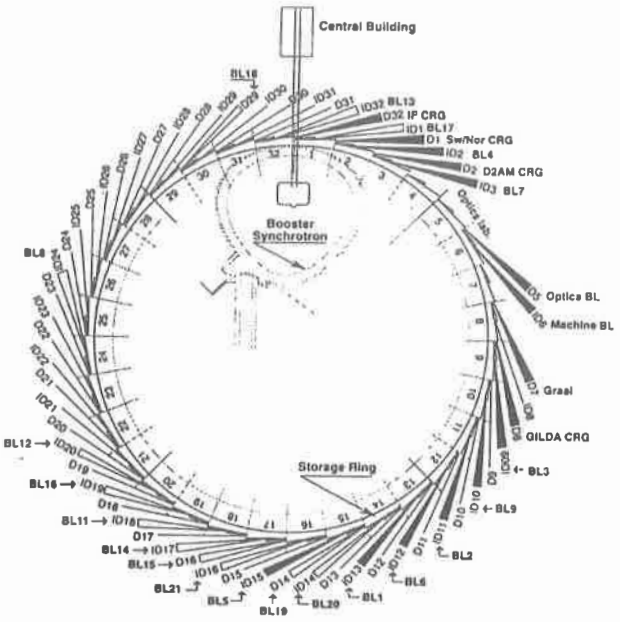

Figure 1. The ESRF with its beam lines

delivered by an argon laser generator (Coherent type Innova 200-25/7) is deflected by a Be mirror toward the ring of the ESRF where it collides with the electron beam characterized by an intensity of 200 mA and an energy of 6 GeV (Fig.2). The collision between a photon and an electron mainly gives a Compton backscattering. After the scattering, the electron and the photon share the initial energy of 6 GeV. The scattered electron of degraded energy is separated from the main beam by a magnetic dipole of the ring and hits a position sensitive detector, called tagging detector, which provides the energy of the electron and allows to deduce the energy of the scattered photon. Such scattered photons constitute the high energy photon beam which then hits the target and is monitored downstream by two successive monitors, a thin monitor and a total absorption detector. This is shown in figure 2 together with the detection system which will be described later.

The energy spectrum of the photon beam shown in figure 3 (left side) is flat having the characteristic shape of a Compton spectrum. The polarization of the initial laser beam is transmitted to the final photon beam through Compton scattering. When the polarization of the laser beam is linear or circular, curve (L) or curve (C) are obtained respectively (right side in figure 3). The energy spectrum and the rate of the polarization have maximum values at the maximum energy which is the most interesting part of the energy spectrum. In addition the polarization is close to 100% at maximum energy and has a value better then 70% for the upper third of the energy range.

Also, the energy and polarization figures shown correspond to one line of wavelength of the laser beam. Since there are several lines produced by the argon laser generator, one can obtain similar spectra but with different maximum energies (Compton edge). So, by selecting optically a given line, one can choose the right beam energy which optimizes a given nuclear reaction channel. As to the type or the direction of the polarization, it is easily obtained by acting on the linear natural polarization of the laser beam, using a $\lambda/2$ plate to rotate a linear polarization by 90° or a $\lambda/4$ plate to transform a linear polarization into a circular one. All

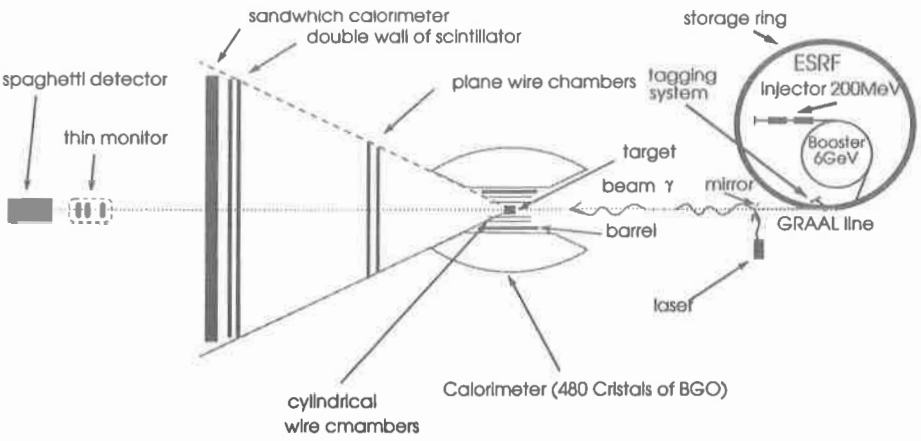

Figure 2. Layout of the GRAAL experiment at the ESRF in Grenoble. On the right side, the ESRF composed of a linear injector, a synchrotron and a storage ring (844 m of circumference). The laser beam is deflected by a mirror toward the ring and collides with the electron beam. The scattered photons form the γ beam which then hits the target (liquid hydrogen) and continues until the stopper (spaghetti detector). The central part of the figure represents the detection system which consists of three layers of detectors (see text). The different parts of the figure are not in scale

these properties of the GRAAL beam are much superior to the traditional Bremsstrahlung beam characterized by an exponentially decreasing intensity versus the energy and low polarization values with hard handling.

As to the tagging system, it consists of two successive arrays of detectors encountered by the Compton scattered electrons: a microstrip (128 strips) Si detector with a step of 300 μm to measure the energy and an array of 10 plastic scintillators with partial overlapping to measure the time. The total width of both arrays is $\approx$40 mm. The system is located at 10 mm from the 200 mA electron beam. It is protected by a sheet of 2mm of heavy material against the huge X radiation flux. The GRAAL tagging system is called internal tagging, because it uses a common magnet with the ring. This is an alternative to the external tagging existing in other facilities, where a special external magnet is matching a larger size (1 or 2 m) of tagging detectors. In figure 4, the tagging setup is drawn and an energy spectrum of the beam measured by the microstrips is shown.

The path of the beam since its production until its stopping is shown in figure 2. At the right, there are the laser beam, the electron beam in the ring and the tagging system. At the left, one can see the high energy γ beam hitting the target after being cleaned from electrons by a magnet (not shown) then collimated and continuing until the monitors which consist of a thin monitor and a total energy detector. The thin monitor is composed of a telescope of 3 scintillators, 5 mm thick. The first scintillator facing the beam vetoes the two others which are in coincidence. An Al plate of 2 mm is inserted between the first and the second scintillator creating electron pairs with an efficiency of 3%. The total energy monitor stops the beam. The thin monitor with a counting rate less then 10^5 accepts the flux without an important pileup, whereas the total energy monitor is affected by the pileup at high flux but calibrates the thin monitor at low flux. The monitors are in coincidence with the scintillators of the tagging. Monitor events are generated and mixed to physics events.

Also, in figure 2 a detailed drawing of the detection system surrounding the target is given. The detection system is composed of two parts, lateral ($25° \leq \theta \leq 155°$) and frontal($1° \leq \theta \leq 25°$), each one comprising three layers of similar detectors.

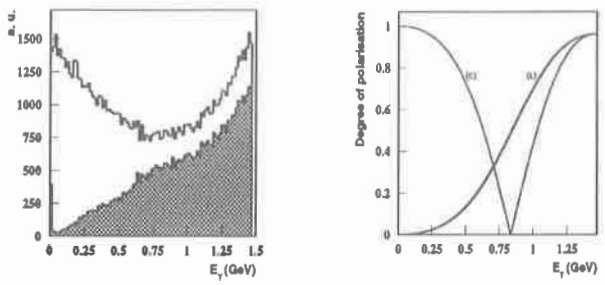

Figure 3. On the left, the energy spectrum of backscattered photon beam (the hatched spectrum is after collimation). On the right, the degree of polarization of the photon beam versus the energy, as transmitted by Compton scattering from linear (L) or circular (C) polarization of the laser beam. These curves are given by a simulation

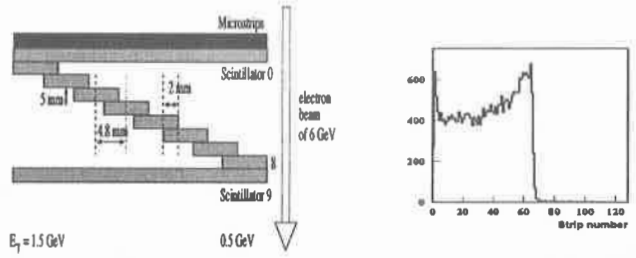

Figure 4. On the left, the tagging detection setup with Si microstrips backed by an array of 10 scintillators. On the right, a flux spectrum measured by the microstrips, where the unit is the strip number

The lateral part is constituted by a layer of two cylindrical wire chambers to measure the directions of charged particles emitted from the target, then by a layer of scintillator bars forming a barrel and finally by a BGO ball of 480 crystals arranged in sectors and crowns, the sectors being matched by the barrel scintillator bars. The BGO ball with the barrel can measure the energy of the charged or neutral particles and in particular of the electromagnetic showers. In the forward direction, there are a layer of two planar wire chambers, followed by a double wall of vertical and horizontal scintillator bars (26 horizontal and 26 vertical) then by a lead plus scintillator sandwhich wall. The third layer is completed in the backward directions ($155° \leq \theta \leq 180°$) by a lead plus scintillator sandwhich disc.

PRESENT EXPERIMENTS AT GRAAL

Let us summarize the global features of the GRAAL setup. The beam has a unique high quality polarization (circular or linear with a polarization of $\approx$100% at maximum energy) in the domain of energy of 500 to 1500 MeV. The flat shape of the energy spectrum which is characteristic of a Compton spectrum is very advantageous for physics in comparison with Bremsstrahlung spectrum which favours low energy part. The tagging has a precision of 16 MeV which is allowed by the emittance of the beam. The monitoring is good with a precision of 1%. With the far UV line of the argon laser, an energy of 1.6 GeV is obtained. An energy of 1.8 GeV is possible using a frequency doubled laser with a wavelength of 256 nm.

As to the detector, it has a good performance to detect high energy γ, charged particles

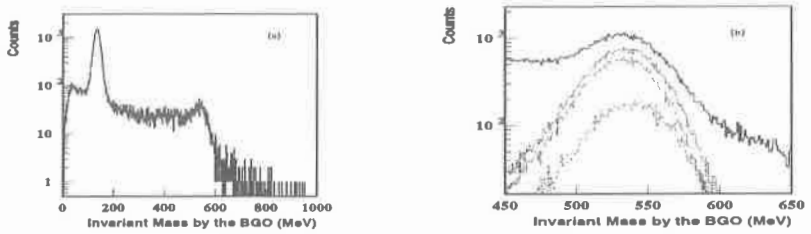

Figure 5. In (a), the invariant mass spectrum for two gammas detected in the BGO ball. Two peaks corresponding to π° and η mesons are seen. In (b), the part of the spectrum of (a) at the η location is selected: the upper curve is as in (a); the three lower curves are with the condition of a charged particle detected in coincidence: the first higher one in any direction of the charged particle, the second one when the direction is in the forward walls and the third one in the lateral scintillators. The coincidence condition strongly rejects the background.

and neutrons. The γ are detected in an almost complete 4π and in particular with a high resolution of $\Delta E/E=3\%$ by the BGO ball in the range ($25^\circ \leq \theta \leq 155^\circ$). The charged particles are detected in the range ($1^\circ \leq \theta \leq 155^\circ$) by wire chambers and for $\theta \leq 25^\circ$ by the double wall which gives ΔE and the time of flight, and in the range ($25^\circ \leq \theta \leq 155^\circ$) by the barrel of scintillators which gives the ΔE. The neutrons are detected by the sandwhich wall for $\theta \leq 25^\circ$.

Identification of particles and reactions

The first experiment started in the fall of 1996 is the η meson photoproduction with the laser green line giving γ beam in the energy range of 500 - 1088 MeV, the lower edge being imposed by the geometrical limit of the tagging detector and the upper one by the Compton edge. A linear polarization of the beam was used with sequencing: a period of about 10 mn with a vertical polarisation of the laser beam, followed by a similar period with a horizontal polarization and terminated by a period where the laser is off. This sequencing allows to correct the asymmetry measurement from the detection efficiency and to monitor the Bremsstrahlung component in the beam. A liquid hydrogen target of 3 cm was used allowing to obtain a good angular resolution in the BGO ball whose crystals are pointing to the center of the target. The trigger corresponds to a threshold of 200 MeV on the total energy detected in the BGO ball. This trigger cuts enough the electromagnetic showers in order to get a total rate of electromagnetic and hadronic events of about 100 events per second.

The trigger described above favours the detection of η mesons, but allows to study several other channels. For all channels which will be described in this section, the beam asymmetry Σ and the differential cross section $d\sigma/d\Omega$ could be carried out.

The trigger is not very selective. Only, it strongly reduces electromagnetic reactions. There are all possible channels detected. It is the role of the off-line analysis to select a specific channel and an ambitious goal would be to identify all sizeable channels. For the identification of a given channel, there are two stages in the identification, i.e., the identifications of the particles produced in the final state and the identification of the channel from others. It is worth to comment the various identification possibilities.

a) Identification of neutral mesons: the system constituted by the BGO and the scintillator barrel identifies the neutral mesons by their decay modes into γs: first it identifies each γ as a

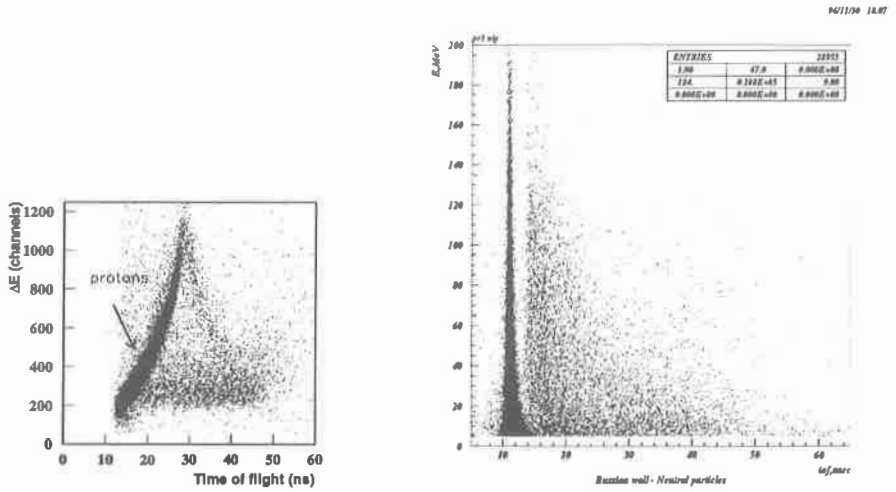

Figure 6. On the left, the loss of energy against the time of flight for charged particles measured with the first and second walls, as obtained in the η photoproduction experiment. One can see the characteristic pattern of the protons. On the right, A similar plot, but for the third wall vetoed by the two others. One can see the sharp line in time of flight from gamma radiation and the other events corresponding to neutrons.

"neutral" cluster of BGO crystals which are hit (neutral refers to the fact that geometrically corresponding barrel scintillator is not hit) then it associates two or more γs using their energies and angles to identify the meson which could have decayed into them. For instance, for two neutral clusters detected in the BGO, the invariant mass spectrum clearly shows the presence of two sharp peaks corresponding to the π° and the η (Fig.5a).

b) Identification of charged particles: the double wall of scintillators measures the loss of energy and the time of flight of charged particles. This allows in particular to identify the protons by their characteristic pattern in the bidimensional plot of ΔE against the time of flight (Fig. 6, left side). The good granularity of the wall ($\Delta\phi \leq 2^\circ$ and $\Delta\theta \leq 2^\circ$) gives the angles ϕ and θ of the detected paricle.

c) Identification of the neutron: the sandwhich wall in the forward direction with the veto of the scintillator double wall can recognize the neutral particles. Its time of flight capability identifies the electromagnetic showers (travelling at light velocity) from neutrons which have longer time of flight depending on their kinetic energy (Fig.6, right side).

d) Identification of two-body reactions: this will be illustrated by the case of π° or η photoproduction. The neutral meson M is identified in the BGO and its energy and angles measured. Using these and the incident energy given by the tagging detector together with two-body kinematics will allow to calculate the missing mass, i.e. the mass of the particle X in the reaction $\gamma p \rightarrow MX$. The spectrum of the missing mass will display a sharp peak at the location of the mass of the proton corresponding to the two-body reaction $\gamma p \rightarrow Mp$, lying on a background originating from three or four body reactions.

A similar two-body reaction identification is performed using the time of flight and the angles of the proton measured by the double wall. In this case, the spectrum of the missing mass Y in the reaction $\gamma p \rightarrow pY$ is established. There will be a sharp peak at the location of the meson M corresponding to the two-body reaction $\gamma p \rightarrow pM$ lying on a background from three or four body reactions.

The plot of the missing mass Y against the missing mass X allows to separate among

different two-body channels and three or four body reaction channels.

e) Identification of $2\pi^\circ$ photoproduction: here events of four neutral clusters in the BGO giving $\pi^\circ\pi^\circ$ are selected and the invariant mass M_{inv} of the $2\pi^\circ$ system is calculated together with the associated energy and angles. This allows again as in the preceding case to calculate the missing mass X which should be a proton. On the other hand, the identification of a proton detected in the wall and the measurement of its time of flight and angles will allow to calculate the missing mass Y which, in case of $\gamma \rightarrow p\pi^\circ\pi^\circ$ reaction, should be equal to the invariant mass M_{inv} of the $2\pi^\circ$ system. The appropriate plot could be the difference Y- M_{inv} against X. The location of the reaction is: X equal the mass of the proton and Y=0.

f) Identification of other reactions: in the preceding examples there was an overdetermination in the experimental measurements of the kinematical variables. When other charged particles are created, the sign of the electric charge could not be identified but the angles could be measured and in some cases the energy loss ΔE could be determined in the wall or in the barrel. These quantities depending of the reaction could be sufficient to identify a reaction as complex as $\gamma p \rightarrow K^+\Lambda$, when the Λ is detected through its decay into $p\pi^-$.

Reactions under study

Several channels are accessible in the experiment performed with incident photon energy in the range of 500-1100 MeV, someones will be commented here.

1. $\gamma p \rightarrow p\ \eta$: this reaction is detected for two decay modes of η, (2γ and $3\pi^\circ$) with an overdetermination in its identification. The polarization rate of the beam is very convenient, varying from 0.98 at the maximum photon energy to 0.69 at the η threshold. It has appeared that this reaction is a selective tool to study the S11 (1535) resonance of the nucleon. Only recently, precise measurements of the cross section, from threshold to 790 MeV, have been obtained (Ref.1). Here, the range of energy will be extended to higher values and the measurement of the beam asymmetry Σ will evidence the contribution of other resonances.

2. $\gamma p \rightarrow p\ \pi^\circ\pi^\circ$: the identification of this reaction requires the detection of 4γ. The best identification is obtained when the 4γ falls into the BGO ball while the proton falls into the double scintillator wall. An increasing interest in this reaction has motived two successive experiments with DAPHNE and TAPS at MAMI, whose results indicated that the reaction proceeds rather via the excitation of D13(1520) and its subsequent decay into $\Delta\pi^\circ$ than by the excitation of the P11(1440) Roper-resonance and its decay into two correlated neutral pions, as proposed in some models (Ref. 2 and 3). The GRAAL results will clarify the mecanism by extending the energy and measuring the observable Σ.

3. $\gamma p \rightarrow p\ \pi^\circ$ and $\gamma p \rightarrow n\ \pi^+$: the reaction $\gamma p \rightarrow p\ \pi^\circ$ is identified by detecting the π° in the BGO ball, through its decay mode into 2γ, and the associated proton by different detectors. The reaction $\gamma p \rightarrow n\ \pi^+$ is identified by detecting the neutron in the forward direction ($\theta \leq 25^\circ$) and the charged pion in the other detectors. It is expected not only to extend the cross section and Σ observable measurements but also to cover the very forward or backward angles in the center of mass system, taking advantage from the large angular acceptance of the GRAAL setup. This will strongly improve the single-pion photoproduction database used to provide photodecay amplitudes for resonances coupled to the pion-nucleon channel (Ref.4).

4. $\gamma p \rightarrow \gamma p$: this reaction has a low cross section. Its identification is difficult mainly because it can be confused with the reaction $\gamma p \rightarrow p\pi^\circ$ of much higher cross section when one of the 2γ moves in the forward direction and the other is not detected. It is nevertheless possible to identify it as a two-body reaction of well defined location in kinematical plots.

The rejection of the events containing more than one gamma or one charged particle could strongly help, since the detection system is very close to a 4π detector.

5. Other decays of the η: the branching ratios of the decay of η into 2γ, $3\pi^\circ$, $\pi^+\pi^-\pi^\circ$, $\pi^+\pi^-\gamma$ and probably $\pi^\circ 2\gamma$ can be measured and Dalitz plots could be drawn for the decay into 3 pions. For instance, for the decay into $3\pi^\circ$ the coefficient α entering in the matrix element could be extracted to improve the known measured values whose precision is not sufficient to test the predictions of chiral perturbation theory.

FUTURE PLANS

1. Photoproduction of kaons:

The reaction $\gamma p \rightarrow K^+\Lambda$ has a cross section one order of magnitude lower than that of η meson photoproduction. In addition its identification will not be as overdetermined as in η photoproduction. However, because of its high interest in studying hyperons and their resonances (Ref.5), the design of several parts of the setup was optimized for this measurement. With a threshold at 911 MeV, the reaction $\gamma p \rightarrow K^+\Lambda$ requires higher energy photons. Using the UV laser line, the energy ranges up to 1.47 GeV. The K^+ decays with $c\tau$=3.7 m and the Λ with $c\tau$=7.9 cm. The Λ decays into either $p\pi^-$ or $n\pi^\circ$. This gives two possible three particle final state $K^+p\pi^-$ and $K^+n\pi^\circ$. In case of $K^+p\pi^-$ in the final state, a trigger of 3 charged particles will be used, and the identification will be performed with the full 3-body kinematics, using all quantities measured by the wire chambers and the scintillation counters. In the other case ($K^+n\pi^\circ$), the neutron will be identified by its time of flight in the forward direction and the π° by the BGO.

Also the reaction $\gamma p \rightarrow K^+\Sigma^\circ$ could be measured. The Σ° decays instantaneously into $\Lambda\gamma$ in the target and the γ has a 90% probability chance to be detected by the BGO ball and measured. The rest of the reaction products behave as $\gamma p \rightarrow K^+\Lambda$ reaction and will be identified in the same way.

2. Other reactions: The reaction $\gamma p \rightarrow p\ \eta'$ has a threshold of 1447 MeV and hence can be produced with the UV line. Several decay channels could be identified.

The reaction $\gamma p \rightarrow p\ \omega$ has a threshold of 1108 MeV . The mass of the ω is well defined with a width of 8.4 MeV. The main decay of the ω is into $\pi^+\pi^-\pi^\circ$, so, it will be possible to identify the reaction $\gamma p \rightarrow p\ \omega$ as the $\gamma p \rightarrow p\ \eta$ by a reconstruction of the ω invariant mass and the two body kinematics.

In addition the study of the reactions $\gamma p \rightarrow \eta p$, ... could be extended to higher energies. Moreover, it will be interesting to extend the study of several of these reactions on a deuterium target discriminating between coherent and incoherent production.

3. Double polarization measurements: this type of measurements will start with the installation of a pure HD polarized target. The target could be considered as a polarized proton or a polarized deuteron or a polarized neutron target. The different meson photoproduction reactions already considered can be studied for the whole range of energy of 500-1500 MeV with a polarized target and with both polarized beam and target. The linear or circular polarization of the beam and the perpendicular or parallel target polarization with respect to the beam will be used in order to extract the various double polarization observables. In particular, when the recoil baryon polarization, e.g. as for the Λ, can be deduced from the decay products, triple polarization measurements could be obtained. These multiple polarization observable measurements will allow to carry out a full determination of the transition amplitudes in pseudoscalar meson photoproduction, where the measurement of seven polarization observables is required.

A particular case of a double polarization experiment is the test of the Drell-Hearn-Gerasimov sum rule. For this experiment, a circular beam polarization is needed together with a polarization of the proton or the neutron parallel and antiparallel to the beam direction. Here, the HD target makes possible the direct measurement of the difference between proton and neutron target in the same experimental conditions. This difference is expected to give the most significant positive or negative answer of the test. It is worth noting that the DHG sum rule test requires the control of all the hadronic production channels and in consequence the electromagnetic background. The extension of this energy range is already considered, toward lower energies with the installation of a low-energy tagging system (down to the pion threshold) and toward higher energies by using a frequency doubled laser.

PRELIMINARY RESULTS

The beam asymmetry Σ is extracted for various channels. In this section, there are given the method and samples from two channels.

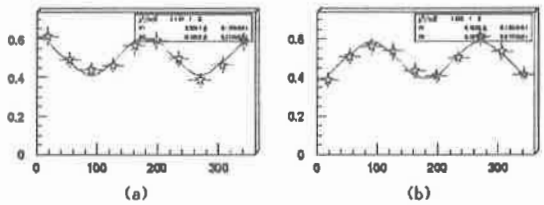

Figure 7. In $\gamma p \rightarrow \eta p$ experiment, the distribution in ϕ of η mesons plotted after their identification and their selection. In (a), the distribution correspond to a vertical polarisation of the photon beam and in (b) for an horizontal polarization, for one couple of values of E_γ and $\theta_{\eta CM}$.

After identification of the events of the reaction $\gamma p \rightarrow p\eta$, these were classified into a three dimensional table according to the variables: incident photon energy E_γ, $\theta_{\eta CM}$ and ϕ_η. For each couple of values E_γ and $\theta_{\eta CM}$, the distribution of ϕ is plotted. Actually, there are two distinct tables and two corresponding plots $N_1(\phi)$ and $N_2(\phi)$ which are obtained from each measurement, $N_1(\phi)$ for the sequencies where the polarization of the photon beam is vertical and $N_2(\phi)$ where it is horizontal. In figure 7, are shown typical $N_1(\phi)$ and $N_2(\phi)$ distributions. The ϕ distributions could be fitted by the following expressions:

$N_1(\phi) = k.\ \epsilon(\phi)\ (1 - P\ \Sigma \cos(2\phi))$

$N_2(\phi) = k.\ \epsilon(\phi)\ (1 + P\ \Sigma \cos(2\phi))$

where $\epsilon(\phi)$ is the detection efficieny, P is the value of the polarization of the beam and Σ is the beam asymmetry to be deduced.

Usually, if $\epsilon(\phi)$ is known either of the two fits give the product $P\Sigma$ from which Σ is deduced. Here, it was found more straightforward to fit the ratio $N_1(\phi)/(N_1(\phi) + N_2(\phi))$ by an expression $\alpha.(1\text{-}\beta.\cos(2\phi))$. The deduced β value together with the computed value of P will allow to obtain the value of the beam asymmetry Σ.

For $\gamma p \rightarrow p\eta$ reaction, positive assymetries were found with large values at high energy and forward angle. They constitute a strong constraint to theoretical models. The results corresponding to lower energies are explained by a dominant excitation of S11 (1535 MeV) baryonic resonance, with a small contribution from D13, while the results at high energy are not explained at all by the existing predictions and therefore require new calculations

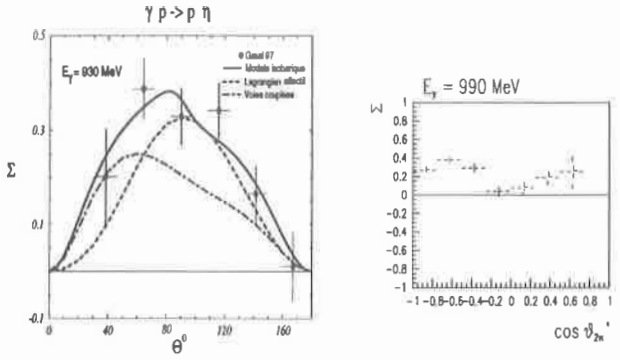

Figure 8.
These are samples from the first results of GRAAL experiment performed with photon energy from 500 to 1100 MeV. On the left, for $\gamma p \rightarrow \eta p$, the beam asymmetry Σ versus the angle θ of η in the centre of mass system, for a photon energy of 930 MeV. The theoretical curves are predictions or fit of the experimental results. On the right, for the reaction $\gamma p \rightarrow p\pi^\circ\pi^\circ$, the beam asymmetry Σ versus cos (θ) in the CM frame of the system $\pi^\circ\pi^\circ$, for photon energy of 990 MeV and $200 \leq M_{inv}(\pi^\circ\pi^\circ) \leq 500$ MeV.

involving probably higher angular momentum resonances. In figure 8 (left side) an example of Σ against θ is given.

For the reaction $\gamma p \rightarrow p\pi^\circ\pi^\circ$, the asymmetry was calculated in two different kinematics. On one hand, in the final state, the proton and one pion were considered as a subsystem characterized by an invariant mass M($p\pi^\circ$) and then the asymmetry Σ was extracted for the second pion for different ranges of M($p\pi^\circ$). On the other hand, the 2 π° were considered as a subsystem characterized by an invariant mass M($\pi^\circ\pi^\circ$) and also the asymmetry was extracted in function of the angle of the subsystem for different ranges of M($\pi^\circ\pi^\circ$). Asymmetry values as high as 0.5 were obtained in some points of either kinematics, a fact which indicates both the complexity and the interest of the asymmetry results. In figure 8 (right side) an example of Σ against cos (θ) is given.

Finally, the asymmetry Σ results for the photoproduction of η, π° and $2\pi^\circ$ and the reaction $\gamma p \rightarrow n\pi^+$ will be soon published and followed by the publication of the corresponding cross sections.

REFERENCES

[1] B. Krusche et al., Phys. Rev. Lett. **78**, 606 (1997).
[2] A. Braghieri et al., Phys. Lett. **B363**, 46 (1995)
[3] F. Harter et al., Phys. Lett. **B401**, 229 (1997).
[4] R. A. Arndt et al., Phys. Rev. **C56**, 577 (1997) and Phys. Rev. **C53**, 430 (1996).
[5] R. A. Adelseck and B. Saghai, Phys. Rev. **C42**, 108 (1990).

$S_{11}(1535)$ Electroproduction at High Momentum Transfer

J.W. Price[1], C. Armstrong[3], G. Adams[1], A. Ahmidouch[5], K. Assamagan[4], S. Avery[4], K. Baker[4], P. Bosted[2], V. Burkert[7], J. Dunne[7], T. Eden[4], R. Ent[7], V. Frolov[1], D. Gaskell[4], P. Guèye[4], W. Hinton[4], C. Keppel[4], W. Kim[6], M. Klusman[1], D. Koltenuk[8], D. Mack[7], R. Madey[4,5], D. Meekins[3], R. Minehart[9], J. Mitchell[7], H. Mkrtchyan[10], J. Napolitano[1], G. Niculescu[4], I. Niculescu[4], M. Nozar[1], P. Stoler[1], V. Tadevosyan[10], L. Tang[4], M. Witkowski[1], S. Wood[7]

[1] *Rensselaer Polytechnic Institute, Troy, NY 12180*
[2] *American University, Washington, D.C. 20016*
[3] *College of William and Mary, Williamsburg, VA 23187*
[4] *Hampton University, Hampton, VA 23668*
[5] *Kent State University, Kent, OH 44242*
[6] *Kyungpook National University, Taegu, Korea*
[7] *Thomas Jefferson National Accelerator Facility, Newport News, VA 23606*
[8] *University of Pennsylvania, Philadelphia, PA 19104*
[9] *University of Virginia, Charlottesville, VA 22903*
[10] *Yerevan Physics Institute, Yerevan, Armenia*

Abstract

The differential cross section for the exclusive process $p(e,e'p)\eta$ has been measured in Hall C at the Thomas Jefferson National Accelerator Facility at momentum transfers of 2.4 and 3.6 $(\mathrm{GeV}/c)^2$. The cross section measurements were used to extract the total cross section, which is compared with the world data sample.

INTRODUCTION

Among the various baryon states, the $S_{11}(1535)$ has a number of properties which make it an excellent topic of study. Several recent experiments in Bonn, Mainz, and Bates have attempted to discern its nature via photoproduction of the η meson on hydrogen. Theoretical efforts at RPI and Mainz have sought to explain its behavior in this same regime. Among the properties that make it so interesting a subject are the slow falloff of its form factor with increasing Q^2, the precise determination of its width, and the strength of its decay to the $|\eta\mathrm{N}\rangle$ state.

Unlike those of the bulk of the baryon spectrum, the form factors of the $S_{11}(1535)$ are notably stiff. This is shown in Fig. 1. While the proton form factors follow the dipole form factor, the $\Delta(1232)$ falls off faster, and the $S_{11}(1535)$ falls off more slowly than the dipole form factor. The reason for this slow falloff is not understood. As Q^2 increases, the form factor appears to approach the dipole behavior, which is predicted by duality and valence pQCD. This conclusion is based on the assumption that the second resonance region is entirely due to the $S_{11}(1535)$, using inclusive data. Exclusive measurements are needed to confirm this conclusion.

The total width of the $S_{11}(1535)$ is also poorly understood. The current situation is shown in Table 1. Previous analyses [2] that studied the process $p(e,e'p)\eta$ at the photoproduction point quoted a large value ($\approx 200\,\mathrm{MeV}$) for the width, while those at high Q^2[1,3] quoted a low value ($\approx 100\,\mathrm{MeV}$). Clearly, the actual width of the $S_{11}(1535)$ should not depend on the momentum transfer one uses to study it; a reliable value is thus needed.

The $S_{11}(1535)$ has a property unique within the baryon spectrum in that it has a very strong decay to the $|\eta\mathrm{N}\rangle$ final state. This allows one to study the nature of this resonance

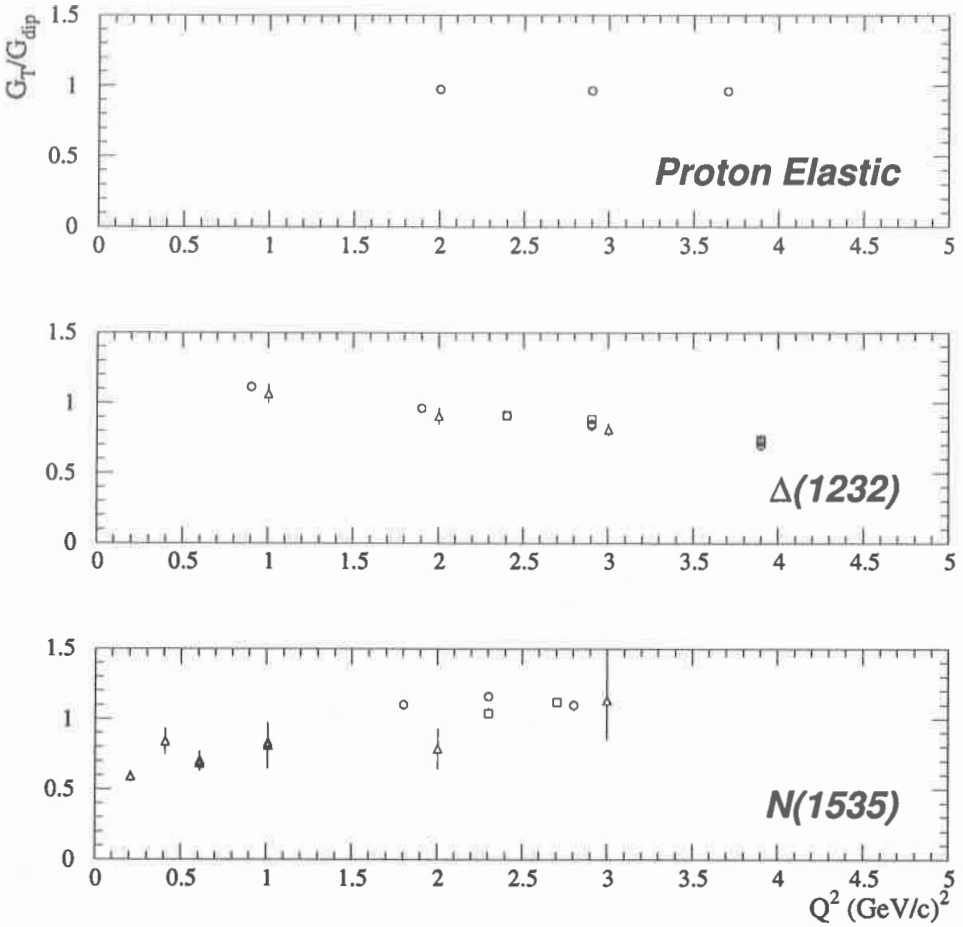

Figure 1. (a) The Q^2 behavior of the proton elastic magnetic form factor divided by the dipole shape, G_M/G_{dipole}, for $0 < Q^2 < 5(\mathrm{GeV}/c)^2$; (b)-(c) the Q^2 behavior of the quantity G_T/G_{dipole} for (b) the $\Delta(1232)$; (c) the second resonance region, consisting of mostly the $D_{13}(1520)$ at low Q^2, and mostly the $S_{11}(1535)$ at high Q^2. This data in this figure was compiled in Ref. [1].

Table 1. Results used in the Particle Data Group determination of the width of the $S_{11}(1535)$.

Measurement	Value
Hoehler (1979)	120 ± 20 MeV
Cutkosky (1980)	240 ± 80
Manley (1992)	151 ± 27
PDG Average	**100 to 250 (≈ 150) MeV**

Table 2. Physical properties of the HMS and SOS spectrometers.

HMS		
	Acceptance	Resolution
Horizontal angle	$\pm 25\, mrad$	$\pm 1\, mrad$
Vertical angle	$\pm 70\, mrad$	$\pm 1\, mrad$
Momentum	$\pm 10\%$	$\pm 0.1\%$
SOS		
	Acceptance	Resolution
Horizontal angle	$\pm 60\, mrad$	$\pm 3\, mrad$
Vertical angle	$\pm 40\, mrad$	$\pm 1\, mrad$
Momentum	$\pm 20\%$	$\pm 0.1\%$

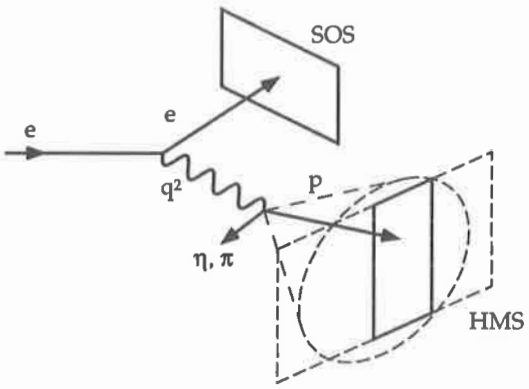

Figure 2. A schematic of the experimental setup. The outgoing meson is either a π^0 or an η.

with the use of η production on the nucleon. Several groups have used this technique in recent years, as theorists and experimentalists alike have shown renewed interest in the $S_{11}(1535)$.

EXPERIMENT

An experimental effort to study the properties of the $S_{11}(1535)$ and the $\Delta(1232)$ was made at the Thomas Jefferson National Accelerator Facility (Jefferson Lab). The processes under study were $p(e,e'p)\eta$ near the $S_{11}(1535)$ and $p(e,e'p)\pi^0$ near the $\Delta(1232)$. The analysis and results of $p(e,e'p)\pi^0$ are presented elsewhere in these Proceedings[4]. This experiment utilized the Hall C spectrometer combination of the Short Orbit Spectrometer (SOS), which was used to detect the outgoing electrons from these processes, and the High Momentum Spectrometer (HMS), which was used to detect the outgoing protons from the decay of the intermediate resonant state. The properties of the two spectrometers are listed in Table 2, and the experimental setup is shown schematically in Fig. 2.

The very large momentum acceptance of the SOS, shown in the table, allowed the study of both resonances simultaneously with a single setting of the SOS. As seen in Fig. 3, missing mass peaks for both the pion from the decay of the $\Delta(1232)$ and the η from the decay of the $S_{11}(1535)$ were visible. The HMS does not have sufficient acceptance to detect all of the

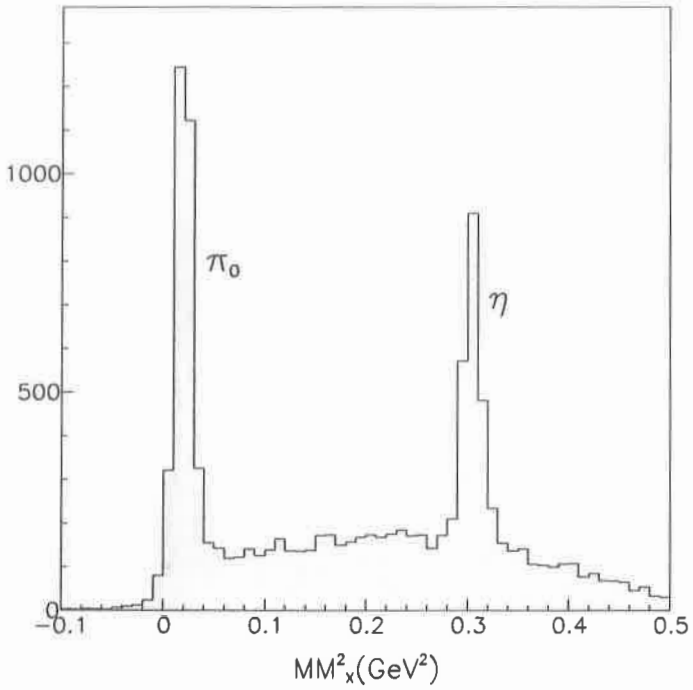

Figure 3. Missing mass spectrum for a single setting of the HMS spectrometer. Both the pion from $\Delta(1232)$ production and the η from $S_{11}(1535)$ production are clearly seen.

protons produced in $p(e,e'p)\pi^0$ or $p(e,e'p)\pi^0$. However, by taking several settings of the HMS spectrometer, almost the entire phase space for the outgoing protons may be obtained. At high Q^2, the outgoing protons from both $p(e,e'p)\eta$ and $p(e,e'p)\pi^0$ are boosted forward in the lab frame. This results in a very good acceptance for this process, with a relatively small number of spectrometer settings. By overlapping the HMS settings, each point was effectively measured by at least two different parts of the spectrometer acceptance, which will allow for greater control of our systematic uncertainties.

The data for this experiment was taken in November-December 1996, using beam energies of 3.2 and 4.0 GeV. This translates to Q^2 values of 2.4 and 3.6 $(\mathrm{GeV}/c)^2$ for the process $p(e,e'p)\eta$. Previously, the largest value of Q^2 obtained for this process was 3.0 $(\mathrm{GeV}/c)^2$[3]. Approximately 50,000 $p(e,e'p)\eta$ events were collected at each value of Q^2.

The data reduction included cuts on the coincidence time between the two spectrometers, and the requirement that the tracks from both particles fell within a fiducial region of their respective spectrometer. The data was then binned in the variables $\cos\theta_\eta$, ϕ, and W. For each event, the missing mass was calculated. For the process $p(e,e'p)\eta$, the main physics background is multipion production, of which two pion production dominates. This background was fit to and subtracted from the data with a functional form inspired by a monte carlo simulation. The data was then corrected for acceptance and radiative effects, and normalized to the beam current. The virtual photon flux was divided out to get the c.m. differential cross section, which was fit by an equation of the form

$$\frac{d^2\sigma}{d\Omega_\eta} = A + B\cos\theta_\eta + C\sqrt{2\epsilon(\epsilon+1)}\sin\theta_\eta\cos\phi. \qquad (1)$$

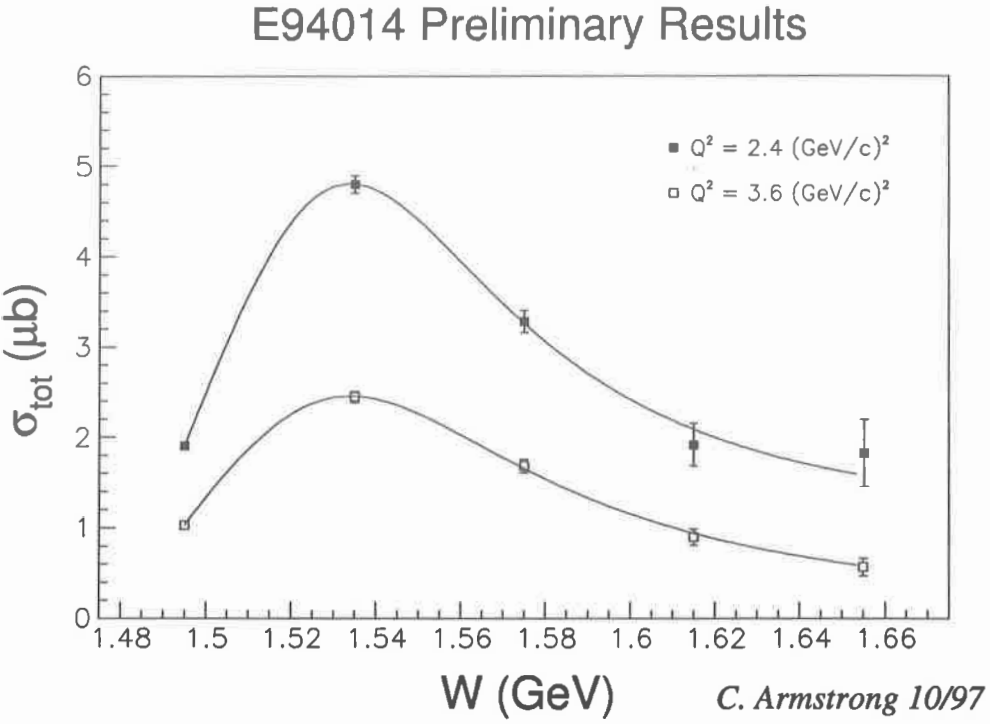

Figure 4. The preliminary total cross section results from this experiment for $Q^2 = 2.4$ and $3.6(\mathrm{GeV}/c)^2$. Only statistical error bars are shown.

The leading term in this fit, A, is related to the total cross section by the equation

$$4\pi A = \sigma_{tot}(\gamma_v p \to p\eta). \tag{2}$$

The W dependence of the total cross section is fit to the equation

$$\sigma_{tot}(\gamma_v p \to p\eta) = \frac{|p^*_\eta| W}{m_p K} \frac{A}{(W - W_{res})^2 + \frac{\Gamma(W)^2}{4}}, \tag{3}$$

where $K = (W^2 - m_p^2)/(2m_p)$. The width Γ is written as

$$\Gamma(W) = \left(b_\eta \cdot \frac{|p^*_\eta|}{|p^*_\eta|_{Res}} + b_\pi \cdot \frac{|p^*_\pi|}{|p^*_\pi|_{Res}} + 0.05 \right), \tag{4}$$

where the branching ratios are taken to be $b_\eta = 0.65$ and $b_\pi = 0.3$. Figure 4 shows the results for the two Q^2 points taken during this experiment. The point at $Q^2 = 2.4\,(\mathrm{GeV}/c)^2$ has a small non-resonant background added to it, which is assumed to be of the form

$$B = k\sqrt{W - W_{thr}}; \tag{5}$$

the background term for the point at $Q^2 = 3.6\,(\mathrm{GeV}/c)^2$ fits to a value consistent with zero.

The results may be compared with previous data by looking at the value of the cross section at the resonance position; this is shown in Fig. 5. Only the statistical uncertainties are shown in this figure.

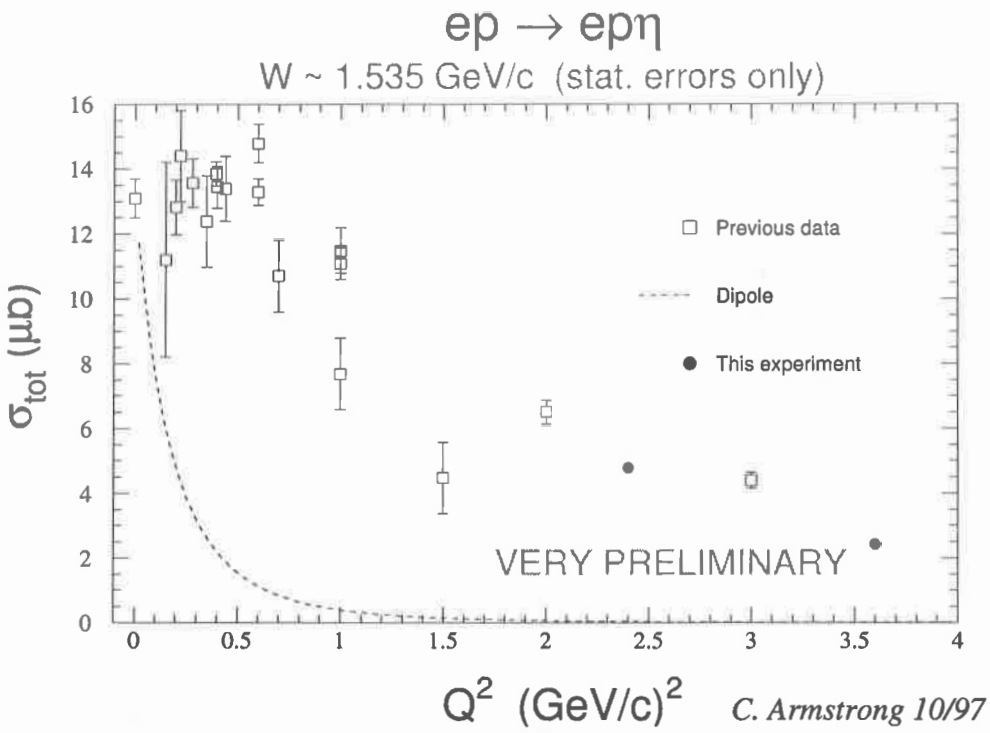

Figure 5. The preliminary cross section results from this experiment in comparison with the world data. Only statistical error bars are shown.

CONCLUSIONS

The preliminary nature of these results precludes making a strong conclusion at this time. Work remains to be done to completely understand the systematic uncertainties, and to extract the helicity transition amplitudes or the electrostrong amplitudes of Mukhopadhyay[5]. However, the quality of the data is clear, and we are confident that our results will provide strong constraints on the models being used to describe the nature of the baryon spectrum.

REFERENCES

[1] P. Stoler, Physics Reports **226**, 103 (1993).
[2] B. Krusche et al., Phys. Lett. B **397**, 171 (1997).
[3] F.W. Brasse et al., Zeit. Phys. C **22**, 33 (1984).
[4] J.W. Price, these proceedings.
[5] N. Mukhopadhyay et al., nucl-th/9611032.

Eta Photoproduction

Lothar Tiator* and Germar Knöchlein†
Institut für Kernphysik, Johannes Gutenberg-Universität, D-55099 Mainz, Germany

Cornelius Bennhold‡
Center for Nuclear Studies, Department of Physics, The George Washington University, Washington, D.C., 20052

Abstract

We present a combined analysis of the new eta photoproduction data for total and differential cross sections, target asymmetry and photon asymmetry. Using basic assumptions, this allows a model-independent extraction of the E_{2-} and M_{2-} multipoles as well as resonance parameters of the $D_{13}(1520)$ state. At higher energy, we show that the photon asymmetry is extremely sensitive to small multipoles that are excited by photons in the helicity 3/2 state. These could be, e.g., the $F_{15}(1680)$, the $F_{17}(1990)$, or the $G_{17}(2190)$ resonances.

INTRODUCTION

Over the last several years, eta photoproduction has demonstrated its potential as a new, powerful tool to selectively probe certain resonances that are difficult to explore with pions. It is well known that the low energy behavior of the eta production process is governed by the $S_{11}(1535)$ resonance[1–3]. The recent, precise measurements of total and differential cross sections for eta photoproduction at low energies[4,5] have allowed determining the $S_{11}(1535)$ resonance parameters with unprecedented precision. However, it is because of the overwhelming dominance of the S_{11} that the influence of other resonances in the same energy regime, such as the $D_{13}(1520)$, is difficult to discern. It has been pointed out[2] that polarization observables provide a new doorway to access these non-dominant resonances which relies on using the dominant E_{0+} multipole to interfere with a smaller multipole. Especially the polarized photon asymmetry was shown to be sensitive to the $D_{13}(1520)$. Recently, polarization data for the target and photon asymmetries in eta photoproduction were measured at ELSA[6] and GRAAL[7], respectively, for the first time. Taken together with the data for the unpolarized cross section from MAMI, they allow a determination of the $D_{13}(1520)$ contribution in eta photoproduction.

MULTIPOLE ANALYSIS

In the following all considerations refer to the c.m. frame. The three measured observables have the following representation in terms of the response functions defined in [8]:

$$\frac{d\sigma}{d\Omega} = \frac{|\vec{k}_\eta|}{|\vec{q}|} R_T^{00}, \tag{1}$$

$$T = \frac{R_T^{0y}}{R_T^{00}}, \tag{2}$$

$$\Sigma = -\frac{{}^c R_{TT}^{00}}{R_T^{00}}. \tag{3}$$

*E-mail: tiator@kph.uni-mainz.de
†E-mail: knoechle@kph.uni-mainz.de
‡E-mail: bennhold@gwis2.circ.gwu.edu

Because of the overwhelming dominance of the S_{11} channel in eta photoproduction, the observables can be expressed in terms of s–wave multipoles and interferences of the s wave with other multipoles. In the CGLN basis this leads to an F_1 dominance and the observables can simply be expressed as

$$R_T^{00} = |F_1|^2 - \mathrm{Re}\left\{2\cos\theta F_1^* F_2 - \sin^2\theta F_1^* F_4\right\}, \quad (4)$$

$$R_T^{0y} = 3\sin\theta\,\mathrm{Im}\left\{F_1^* F_3 + \cos\theta F_1^* F_4\right\}, \quad (5)$$

$${}^cR_{TT}^{00} = \mathrm{Re}\left\{F_1^* F_4\right\}. \quad (6)$$

If we retain only interferences with p– and d–waves (an approximation that is valid at least up to 1 GeV photon lab energy) we obtain

$$\begin{aligned} R_T^{00} &= |E_{0+}|^2 - \mathrm{Re}\left[E_{0+}^*\left(E_{2-} - 3M_{2-}\right)\right] \\ &\quad +2\cos\theta\mathrm{Re}\left[E_{0+}^*\left(3E_{1+} + M_{1+} - M_{1-}\right)\right] \\ &\quad +3\cos^2\theta\mathrm{Re}\left[E_{0+}^*\left(E_{2-} - 3M_{2-}\right)\right], \end{aligned} \quad (7)$$

$$\begin{aligned} R_T^{0y} &= 3\sin\theta\mathrm{Im}\left[E_{0+}^*\left(E_{1+} - M_{1+}\right)\right] \\ &\quad -3\sin\theta\cos\theta\mathrm{Im}\left[E_{0+}^*\left(E_{2-} + M_{2-}\right)\right], \end{aligned} \quad (8)$$

$${}^cR_{TT}^{00} = -3\sin^2\theta\mathrm{Re}\left[E_{0+}^*\left(E_{2-} + M_{2-}\right)\right]. \quad (9)$$

With the following angle-independent quantities

$$a = |E_{0+}|^2 - \mathrm{Re}\left[E_{0+}^*\left(E_{2-} - 3M_{2-}\right)\right], \quad (10)$$

$$b = 2\mathrm{Re}\left[E_{0+}^*\left(3E_{1+} + M_{1+} - M_{1-}\right)\right], \quad (11)$$

$$c = 3\mathrm{Re}\left[E_{0+}^*\left(E_{2-} - 3M_{2-}\right)\right], \quad (12)$$

$$d = \frac{1}{a + \frac{1}{3}c}3\mathrm{Im}\left[E_{0+}^*\left(E_{1+} - M_{1+}\right)\right], \quad (13)$$

$$e = -3\frac{1}{a + \frac{1}{3}c}\mathrm{Im}\left[E_{0+}^*\left(E_{2-} + M_{2-}\right)\right], \quad (14)$$

$$f = 3\frac{1}{a + \frac{1}{3}c}\mathrm{Re}\left[E_{0+}^*\left(E_{2-} + M_{2-}\right)\right], \quad (15)$$

we can express the observables in a series of $\cos\theta$ terms that can be fitted to the experimental data at various energies $E_{\gamma,lab}$

$$\frac{d\sigma}{d\Omega} = \frac{|\vec{k}_\eta|}{|\vec{q}|}\left(a + b\cos\theta + c\cos^2\theta\right), \quad (16)$$

$$T = \sin\theta\left(d + e\cos\theta\right), \quad (17)$$

$$\Sigma = f\sin^2\theta. \quad (18)$$

It is remarkable that a combined analysis of the three above observables allows a determination of the d–wave contributions to eta photoproduction once the quantities a, c, e and f have been determined from experiment. Already with the knowledge of e and f the helicity 3/2 multipole B_{2-}, defined below, and the phase relative to the S_{11} channel can be determined:

$$|B_{2-}| \equiv |E_{2-} + M_{2-}| = \frac{\sqrt{e^2 + f^2}}{3\sqrt{a + c/3}}, \quad (19)$$

$$\tan(\phi_{E_{0+}} - \phi_{B_{2-}}) = \frac{e}{f}. \quad (20)$$

If one neglects electromagnetic effects from the background of eta photoproduction affecting the phase of the electric and magnetic multipoles differently ($\phi_{E_{l\pm}} = \phi_{M_{l\pm}} = \phi_{l\pm}$), one can write

$$E_{l\pm} = |E_{l\pm}|e^{i\phi_{l\pm}}\,, \tag{21}$$

$$M_{l\pm} = |M_{l\pm}|e^{i\phi_{l\pm}}\,, \tag{22}$$

and one finds the following representation for the real and imaginary parts of the d–wave multipoles:

$$\mathrm{Re}E_{2-} = \frac{1}{4}\sqrt{a+\frac{1}{3}c}\,(f\cos\phi_{0+} + e\sin\phi_{0+})\left(1+\frac{c}{3f}\right)\,, \tag{23}$$

$$\mathrm{Im}E_{2-} = \frac{1}{4}\sqrt{a+\frac{1}{3}c}\,(f\sin\phi_{0+} - e\cos\phi_{0+})\left(1+\frac{c}{3f}\right)\,, \tag{24}$$

$$\mathrm{Re}M_{2-} = \frac{1}{12}\sqrt{a+\frac{1}{3}c}\,(f\cos\phi_{0+} + e\sin\phi_{0+})\left(1-\frac{c}{f}\right)\,, \tag{25}$$

$$\mathrm{Im}M_{2-} = \frac{1}{12}\sqrt{a+\frac{1}{3}c}\,(f\sin\phi_{0+} - e\cos\phi_{0+})\left(1-\frac{c}{f}\right)\,. \tag{26}$$

We note that this determination of the E_{2-} and M_{2-} multipoles is rather model independent. To be more explicit we list the assumptions used to arrive at the above formulae:

- Phase difference between electric and magnetic multipoles neglected, $\phi_{E_{l\pm}} = \phi_{M_{l\pm}} = \phi_{l\pm}$
- Restriction to the truncated multipole representation of Eqs. (7), (8), (9)
- Knowledge of the phase of the E_{0+} multipole.

The last point deserves further discussion: From total cross section data [4] it is obvious that in the region of the $S_{11}(1535)$ resonance the cross section can be perfectly fitted by a Breit–Wigner resonance resulting in s–wave dominated differential cross sections. An investigation of the background from the Born terms [2] yielded a very small eta–nucleon coupling constant. As a consequence, the E_{0+} multipole can be treated as being completely dominated by the $S_{11}(1535)$ contribution, which, as shown in ref.[4], allows parametrizing it through a Breit–Wigner form. In principle, an arbitrary phase for the complex E_{0+} multipole could be added which is set equal to 0 by convention. For the complex E_{0+} multipole we use the Breit–Wigner parametrization

$$E_{0+} = -\sqrt{\frac{a}{4\pi}}\frac{\Gamma^* M^*}{M^{*2} - W^2 - iM^*\Gamma(W)}\,, \tag{27}$$

where W is the c.m. energy. The energy dependence of the resonance width is given by

$$\Gamma(W) = \Gamma^*\left(b_\eta\frac{|\vec{k}|}{|\vec{k}^*|} + b_\pi\frac{|\vec{k}_\pi|}{|\vec{k}_\pi^*|} + b_{\pi\pi}\right)\,. \tag{28}$$

The analysis of the E_{0+} interference with the E_{2-} and M_{2-} multipoles determines the d wave multipoles and therefore the difference $\phi_{2-} - \phi_{0+}$. It does not yield direct information on ϕ_{2-}. However, making the above assumptions for the E_{0+} multipole and thus the phase ϕ_{0+} permits the determination of ϕ_{2-}.

To perform a similar analysis of the p–wave multipoles more information from additional polarization observables is required; in particular, a measurement of the recoil polarization would be very helpful. As before we obtain

$$P = \frac{R_T^{y0}}{R_T^{00}}, \tag{29}$$

$$= \sin\theta\,(g + h\cos\theta) \tag{30}$$

$$\tag{31}$$

with

$$g = -\frac{1}{a+\frac{1}{3}c}\mathrm{Im}\left[E_{0+}^{*}\,(2M_{1-}+3E_{1+}+M_{1+})\right], \tag{32}$$

$$h = 3\frac{1}{a+\frac{1}{3}c}\mathrm{Im}\left[E_{0+}^{*}\,(E_{2-}-3M_{2-})\right]. \tag{33}$$

After performing single-energy fits we used a polynomial fit to the energy dependence of the coefficients a, b, c, d, e and f in order to arrive at a global (energy dependent) solution for the multipoles. This has several advantages: First the experimental data have been obtained in different set–ups at different labs, thus their energy bins do not match each other. Second, except for quantity a that is in principle determined already by the total cross section, all other quantities contain considerable error bars, therefore, a combined fit can reduce the uncertainty of individual measurements considerably. In a simple Taylor expansion in terms of the eta momentum with only 1-3 parameters in each coefficient we obtain good results for an energy region from threshold up to about 900 MeV.

RESULTS

Fig. 1 shows 4 out of 10 angular distributions measured by the TAPS collaboration at Mainz [4] in the energy range between 716 and 790 MeV. While our isobar model falls a bit low close to threshold, a perfect fit is possible using the Ansatz in Eq. (16). Our results for the coefficients a, b and c agree perfectly with the results ontained in Ref. [4]. As mentioned before, the a coefficient can be fitted to a Breit-Wigner form with an energy-dependent width leading, e.g., to parameters of $M^* = (1549 \pm 8)MeV$, $\Gamma_R = (202 \pm 35)MeV$ and an absolute value of the s-wave multipole at threshold, $|E_{0+}| = 16.14 \cdot 10^{-3}/m_\pi^+$ (Fit 1, Ref. [4]). For our purpose here it is more convenient to use a general polynomial expansion as mentioned above.

Fig. 2 shows the target polarization with the preliminary data from Bonn[6]. Here our isobar model fails to reproduce the angular shape of the data. In particular there is no node in our calculation and the role of the D_{13} resonance plays a very small and insignificant role. In our previous coupled channel analysis the D_{13} resonance came out much stronger and a node developed, however, with a minus sign at forward and a positive sign at backward angles. This is opposite to the experimental observation and, as we will see later, indicates a drastically different relative phase between s- and d–waves. With the ansatz of Eq. (17) we can fit the data and obtain a node at low energies that disappears around 800 MeV.

In Fig. 3 we show our isobar calculations for the photon asymmetry. This observable has been measured recently at GRAAL [7], however, the data are still in the analysis. A preliminary comparison, however, shows general agreement for energies below 1 GeV. From our

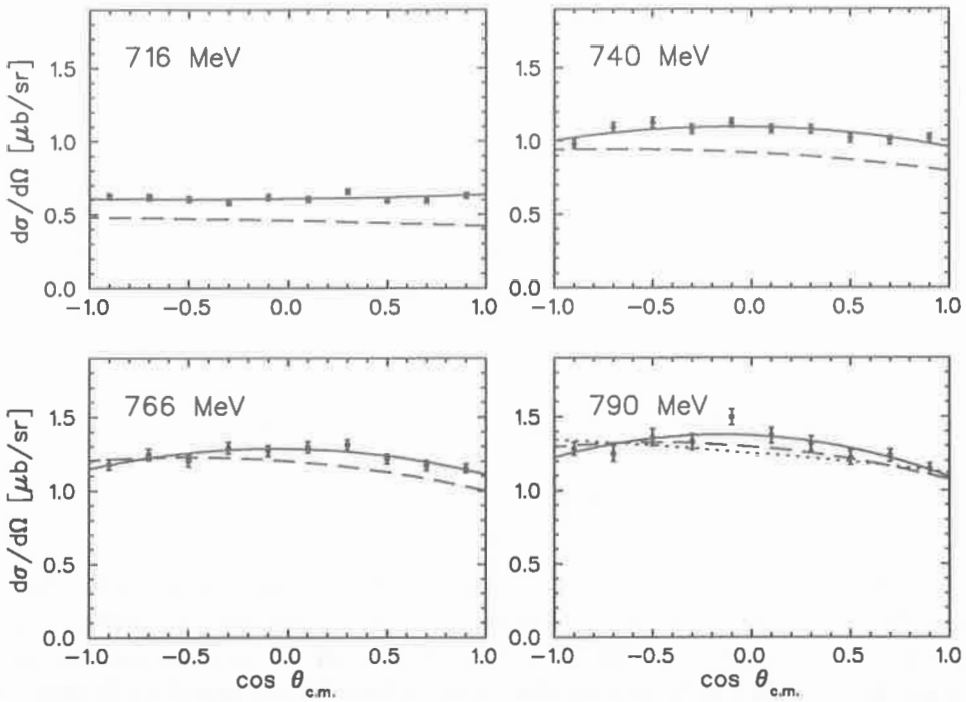

Figure 1. Differential cross section for $p(\gamma,\eta)p$. The solid lines show the fit to the experimental data of Krusche et al. [4]. The dashed lines show our calculations in the isobar model [8]. The dotted line at the highest photon lab energy of $790MeV$ are obtained from our calculations when the D_{13} resonance is turned off.

calculations the importance of the D_{13} channel for the photon asymmetry becomes obvious. Without this nucleon resonance, the asymmetry would be almost zero up to about 900 MeV. Even as the experimental data for the photon asymmetry are not yet available we can already perform a preliminary analysis of the D_{13} multipoles under the constraint of the photon asymmetries determined by our isobar model. In this case, all coefficients of Eqs. (10-15) are available and we can evaluate the d–wave multipoles using Eqs. (21-24). As mentioned before, the solution for the individual multipoles E_{2-} and M_{2-} requires the additional assumption for the phase of the s–wave amplitude. This is taken from the Breit-Wigner Ansatz Eqs. (27-28) with the parameters of fit 1 in Ref. [4]. Of course, this form is rather ad hoc, however, comparing with coupled channels calculations [9,10] we find that the results of these very different approaches agree very well not only for the absolute magnitude of the s–wave but also for the phase.

Fig. 4 shows the result of our multipole analysis and compares it with our isobar model calculation. The biggest difference occurs in the relative phase between the s- and d–waves. As shown in Eq. (20) this phase difference is model independent. If we consider two Breit-Wigner type resonances for both, $S_{11}(1535)$ and $D_{13}(1520)$ this phase difference would be rather constant as both resonances are very close in their energy position and, furthermore, have a similar resonance width. From the fact that the S_{11} is a bit higher in energy, the phase difference $\Phi_0 - \Phi_2$ should be negative as is shown in the figure as the dotted line.

From the above analysis we conclude that this completely unexpected discrepancy is directly connected to the node structure of the target asymmetry. Without a node or with a node but an e–coefficient of opposite sign, the phase difference would be much smaller and

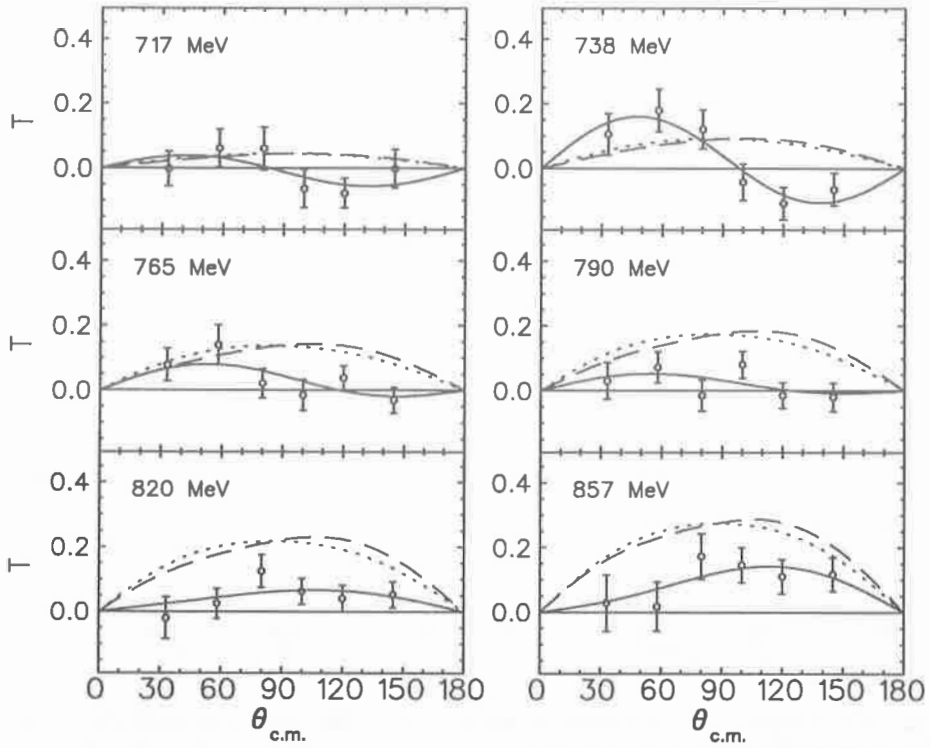

Figure 2. Target asymmetry for $p(\gamma,\eta)p$. The dashed and dotted lines show our calculations in the isobar model [8] with and without the $D_{13}(1520)$ resonance. The solid line is the result of our fit to the experimental data of [6].

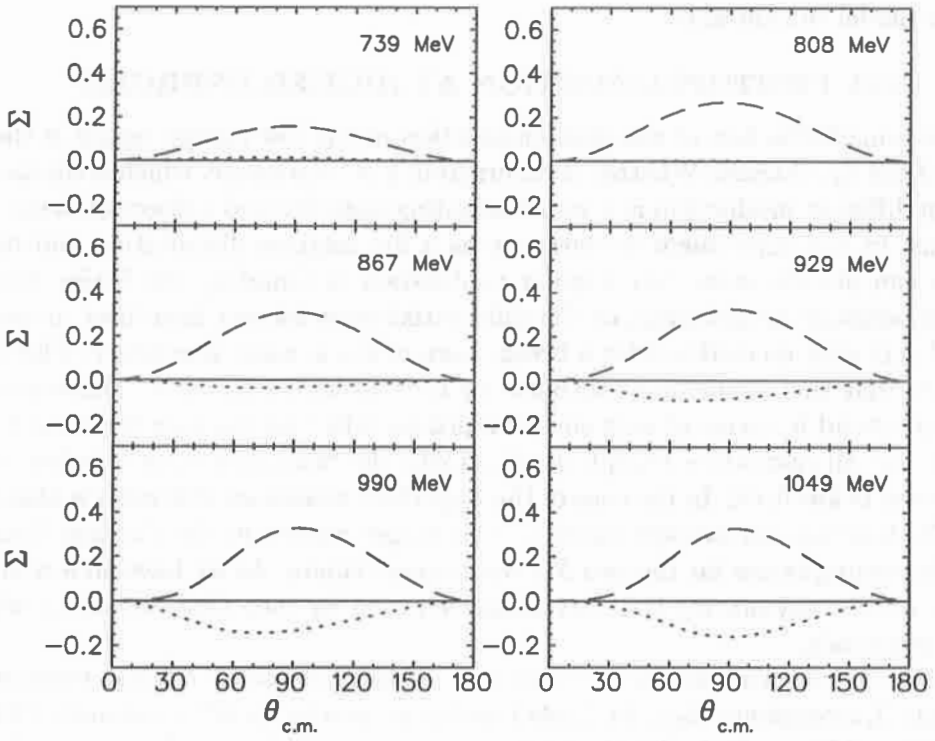

Figure 3. Photon asymmetry for $p(\gamma,\eta)p$. The dashed and dotted lines show our calculations in the isobar model [8] with and without the $D_{13}(1520)$ resonance.

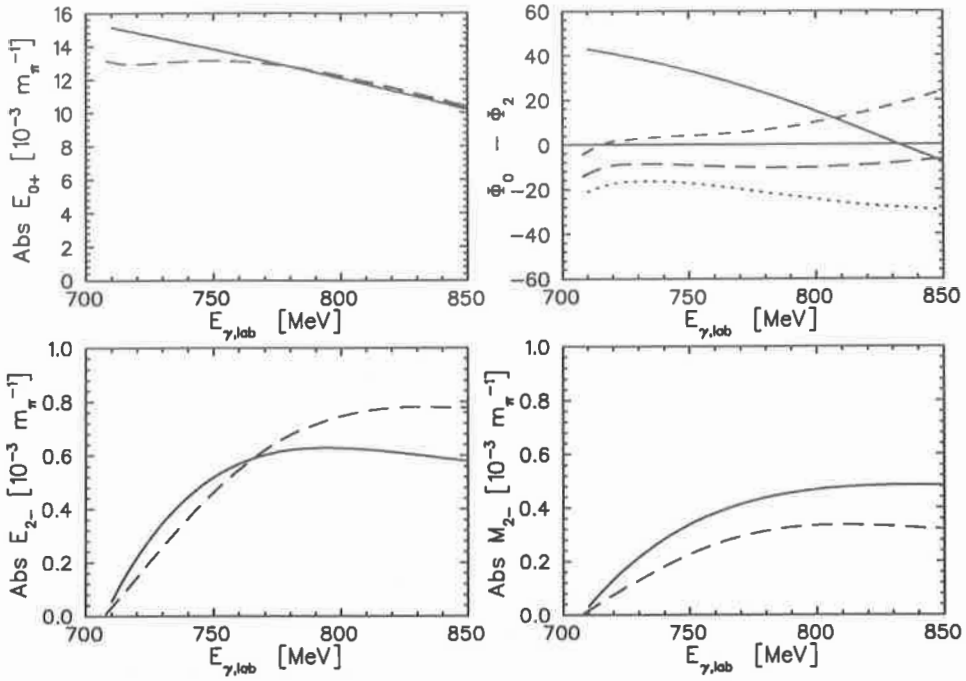

Figure 4. Result of the multipole analysis for s- and d- waves. The solid lines show the result of the fit. The short and long dashed lines are obtained from the isobar model. In the upper right figure we compare the phase difference of our fit with the isobar model. The short and long dashed curves show the difference obtained with the E_{2-} and M_{2-}, respectively. The dotted line is the difference of two Breit-Wigner forms.

closer to our model calculations.

ETA PHOTOPRODUCTION AT HIGHER ENERGIES

The most remarkable fact of eta photoproduction in the low energy region is the strong dominance of the S_{11} channel. Whether it occurs from a N^* resonance, which is the most likely case, or from different mechanism is a very interesting question and subject of many ongoing investigations. In the experiment it shows up as a flat angular distribution and only very precise data can observe some tiny angular modulation as found by the Mainz experiment [4]. At Bonn, angular distributions of the differential cross section have been measured up to 1.15 GeV [11] with no evidence for a break-down of the s–wave dominance. Therefore, we can speculate that this dominance continues up to even higher energies. Theoretically, this could be understood in terms of very small branching ratios for nucleon resonances into the ηN channel. For all resonances except the $S_{11}(1535)$ the branching ratio is below 1%, or in most cases even below 0.1%. In the case of the $D_{13}(1520)$ resonance this ratio is also assumed around 0.1%, however, an average number is no longer quoted in the Particle Data Tables [12]. Only branching ratios for the two S_{11} resonances remain. As we have shown in the last Section, the photon asymmetry is a very sensitive probe for even tiny branching ratios such as the D_{13} resonance.

In the following, we demonstrate that this is especially the case for nucleon resonances with strong helicity 3/2 couplings $A_{3/2}$. In Table 1 we list all entries for N^* resonances with isospin 1/2. From this table one finds the D_{13} as the strongest candidate to show up in the photon asymmetry. However, other resonances include the $F_{15}(1680)$ which plays an important role

in pion photoproduction and, furthermore, the $F_{17}(1990)$ and the $G_{17}(2190)$ that are less established in photoproduction reactions. Furthermore, since these numbers are determined from data in the pion photoproduction channel, surprises in the eta photoproduction channel are not only possible but indeed very likely.

Table 1. Photon couplings and multipolarities for N^* Resonances with helicity 3/2 excitation. The numbers are taken from PDG96[12], average numbers above and single quoted numbers (less certain) below the horizontal line.

N^* Resonance	$A_{3/2}[10^{-3}GeV^{-1/2}]$	Multipoles
$D_{13}(1520)$	$+166 \pm 5$	$B_{2-} = E_{2-} + M_{2-}$
$D_{15}(1675)$	$+15 \pm 9$	$B_{2+} = E_{2+} - M_{2+}$
$F_{15}(1680)$	$+133 \pm 12$	$B_{3-} = E_{3-} + M_{3-}$
$D_{13}(1700)$	-2 ± 24	$B_{2-} = E_{2-} + M_{2-}$
$P_{13}(1720)$	-19 ± 20	$B_{1+} = E_{1+} - M_{1+}$
$F_{17}(1990)$	$+86 \pm 60$	$B_{3+} = E_{3+} - M_{3+}$
$D_{13}(2080)$	$+17 \pm 11$	$B_{2-} = E_{2-} + M_{2-}$
$G_{17}(2190)$	$81 - 180$	$B_{4-} = E_{4-} + M_{4-}$

Assuming S–wave dominance and therefore F_1–dominance in the amplitude we can derive a general expression for the photon asymmetry,

$$\Sigma(\theta) = -\sin^2\theta \, \mathrm{Re}[F_1^* F_4]/R_T^{00}\,, \tag{34}$$

$$= \sin^2\theta \, \mathrm{Re}\Big[E_{0+}^* \sum_{\ell\geq 2}(B_{\ell-} + B_{\ell+}) P_\ell''(\cos\theta)\Big]/R_T^{00} \tag{35}$$

$$\tag{36}$$

with $B_{\ell-} = E_{\ell-} + M_{\ell-}$ and $B_{\ell+} = E_{\ell+} - M_{\ell+}$. Both multipole combinations are helicity 3/2 multipoles and for resonance excitation they are proportional to the photon couplings $A_{3/2}$. The helicity 1/2 couplings $A_{1/2}$ do not enter here, they appear in the differential cross section and in the recoil polarization, e.g. as $A_{2-} = (3M_{2-} - E_{2-})/2$. Explicitly, we obtain up to $\ell_{max} = 4$

$$\Sigma(\theta) = \frac{\sin^2\theta}{|E_{0+}|^2} \mathrm{Re}\Big\{E_{0+}^* \Big[3(B_{2-} + B_{2+}) - \frac{15}{2}(B_{4-} + B_{4+}) + 15(B_{3-} + B_{3+})\cos\theta + \frac{105}{2}(B_{4-} + B_{4+})\cos^2\theta\Big]\Big\}\,. \tag{37}$$

In Fig. 5 we demonstrate how such interferences of higher resonances with the S_{11} channel could show up in the photon asymmetry. Even if two small resonances of different multipolarity are excited in the same energy region they will produce a clear signal that will eventually allow determining η branching ratios down to values well below 0.1%.

SUMMARY

We have demonstrated that polarization observables are a powerful tool in analyzing individual resonances in the eta photoproduction channel. The strong dominance of the S_{11} channel allows a much easier analysis compared to pion photoproduction. Furthermore, the

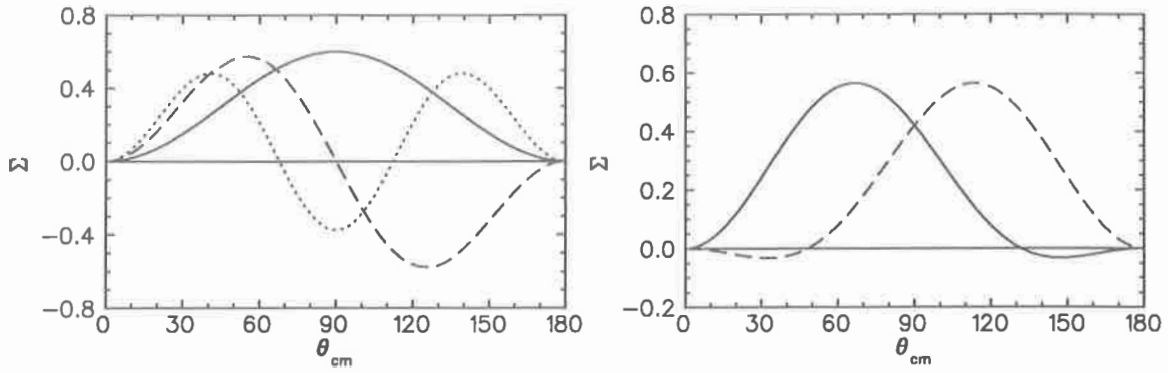

Figure 5. Possible signatures of N^* resonances in the photon asymmetry of eta photoproduction. The solid, dashed and dotted lines in the left figure show the angular distributions for the interference of the dominant S_{11} channel with an isolated D–, F, or G–wave, respectively. On the right, the situation of two resonances in the same energy region is demonstrated for a (D_{13}, F_{15}) pair (solid curve) and a (D_{13}, F_{17}) pair (dashed curve). Opposite signs are also possible if the photon or eta couplings of the resonances obtain a negative sign, see Table 1.

nonresonant background in eta physics appears to be small due to a very weak coupling of the eta to the nucleon. A combined analysis of differential cross section, photon asymmetry and target polarization allows a determination of s– and d–wave multipoles. The target polarization measured at Bonn reveals an unexpected phase shift between the S_{11} and D_{13} resonances that could lead to the conclusion that either of these resonances, perhaps the S_{11}, is heavily distorted or is even a completely different phenomenon, as frequently speculated. The new experiments therefore add another piece to the eta puzzle that makes the field of eta physics so exciting.

REFERENCES

[1] C. Bennhold and H. Tanabe, Nucl. Phys. **A530**, 625 (1991).
[2] L. Tiator, C. Bennhold and S.S. Kamalov, Nucl. Phys. **A580**, 455 (1994).
[3] M. Benmerrouche, N.C. Mukhopadhyay and J.-F. Zhang, Phys. Rev. **D51**, 3237 (1995).
[4] B. Krusche et al., Phys Rev. Lett. **74**, 3736 (1995).
[5] M. Wilhelm, Thesis (Bonn University, 1993).
[6] A. Bock et al., submitted for publication in Phys. Rev. Lett. (1998).
[7] J. Ajaka et al., contribution to this workshop.
[8] G. Knöchlein, D. Drechsel and L. Tiator, Z. Phys. **A 352**, 327 (1995).
[9] N. Kaiser, T. Waas and W. Weise, Nucl. Phys. **A 25** (1997) 297 and N. Kaiser, private communication.
[10] T. Feuster and U. Mosel, nucl-th/9708051 and T. Feuster, private communication.
[11] A. Bock, Thesis (Erlangen, 1997).
[12] Review of Particle Physics, Particle Data Group, Phys. Rev. D 54 (1996) 1.

Eta Electroproduction

M. Benmerrouche*
Saskatchewan Accelerator Laboratory
University of Saskatchewan
107 North Road
Saskatoon, SK, S7N 5C6 Canada

Abstract

We study the process $ep \to ep\eta$ as a probe of the $S_{11}(1535) \leftrightarrow \gamma N$ transition form factor. Our consideration are based on the effective lagrangian approach wherein contributions from nucleon Born terms, vector meson exchange diagrams and the $S_{11}(1535)$ resonance are included. The calculated total cross sections are in good agreement with the available data for $Q^2 = 0.0, 0.22, 0.6, 1.0, 2.0, 3.0\, GeV^2$. We show that the $S_{11}(1535)$ transition form factors can be parametrized by a simple 3-parameters function based on perturbative QCD scaling law. This then allow us to give predictions for the total cross section recently measured at two Q^2 settings of 2.4 and $3.6\, GeV^2$ in hall C at JLab.

INTRODUCTION

Extensive calculations of eta photoproduction on the nucleon[1–4] and nuclei[5–7] have been carried out within the effective Lagrangian approach. Such a model has been proven to be quite successful in describing existing data[8] in particular the very recent precise data from Mainz on proton and deuteron[9]. A topic of special interest is the resonance region encompassing the $S_{11}(1535)$ often referred to as the "second resonance region". In this energy range only the $S_{11}(1535)$ has a significant coupling to the ηN channel, roughly 50%, in contrast to a small couplings by other resonances to this channel, typically less than 20%[10]. Hence, eta photo- and electro-production offers a powerful tool to study the $S_{11}(1535)$ resonance and its properties.

With the advent of high-duty-cycle electron accelerators around the world such as those at the Jefferson Lab, Mainz and Bates, meson production by real and virtual photons has become a valuable tool in the field of baryon resonance excitation. In electroproduction, it is possible to extract the electroweak excitation amplitude of resonances and their evolution as a function of the four-momentum transfer squared Q^2. Because the virtual photons that are exchanged between the electrons and target particles can assume transverse as well as longitudinal (or scalar) polarization states, one can explore both these responses of the target hadron with meson electroproduction. In particular, electroproduction of etas allows us to study the Q^2 dependence of the $S_{11}(1535)$ electromagnetic transition form factors. These offer the opportunity to test the underlying dynamics responsible for the internal structure of the baryons. A remarkable feature of the $S_{11}(1535)$ is its relatively slow falling transverse transition form factor which could not be explained by quark models based on the $SU(6)$ symmetry[11,12]. For example, in the constituent quark model[12] one should expect that the $S_{11}(1535)$ and $D_{13}(1520)$ resonances, belonging to the same $[70, 1^-]$ multiplet, might have similar form factors, contrary to the experimental observations[13]. The $S_{11}(1535)$ electromagnetic transition form factor has also been calculated using the light-cone formalism[14], which attempts to provide a consistent relativistic theory for composite system. In this model, the slow falloff for the $S_{11}(1535)$ form factor can be predicted and is seen as a relativistic effect.

*E-mail: benmer@skatter.usask.ca

However, the proton and neutron charge form factor in this model are not well-reproduced. Recent calculations in a light-front framework[15] have indicated that transverse helicity amplitude is less sensitive to relativistic corrections while the longitudinal helicity amplitude show considerable sensitivity to relativistic effects. In general, QCD inspired models have not been able to describe the properties of the $S_{11}(1535)$ very well. Calculations in the lattice QCD framework[16] could be the way to go but they are numerically yet to reach sufficient accuracy to challenge the quality of the available measurements.

There were some suggestions by Kummer et al.[17] that the flat Q^2 dependence of the cross section could be due to a significant contribution of σ_S which vanishes at $Q^2 = 0$. Measurements of σ_S/σ_T[17] have demonstrated that the effect is unlikely to be due to scalar (or alternatively longitudinal) photon excitation. The ratio of scalar to transverse cross section was determined to be as follows[17]

$$\begin{array}{ccc} Q^2(GeV^2) & \sigma_S/\sigma_T & Experiment \\ 0.4 & 0.23 \pm 0.14 & Bonn \\ 0.6 & 0.25 \pm 0.23 & DESY \\ 1.0 & -0.13 \pm 0.16 & DESY. \end{array} \quad (1)$$

Thus, the cross section is dominated by the transverse part. While we await more precise data from experiments already approved at CEBAF[18], the older data set can already give us some valuable insights in S_{11} electromagnetic excitation.

In this paper, the effective Lagrangian model, developed in our previous extensive work on photoproduction of eta[1], will be extended to the electroproduction process. The primary difference, apart from the form factors at the nucleon and vector mesons vertices, is the appearence of an additional interaction Lagrangian (Dirac type interaction) for the excitation of the resonances[19]. The main goal here is to extract the $N^*(1535)$ electromagnetic form factor as a function of Q^2. An important result from our photoproduction studies is the relative insensitivity of the $S_{11}(1535)$ electrostrong transition amplitude to a variation of the parameters of the model inputs, such as the resonance parameters, the ηNN coupling, other resonances parameters, and so on. Therefore to simplify the model only the contribution from the nucleon Born terms and the vector mesons along with the $S_{11}(1535)$ will be considered. Also, it turned out that reasonably good fit to the eta electroproduction data *could* be achieved with this simplified model (see below). We assume the *PDG*[10] nominal mass and strong decay parameters for the $S_{11}(1535)$ parameters.

1 $S_{11}(1535) \leftrightarrow \gamma N$ TRANSITION FORM FACTORS

The most general electromagnetic $S_{11}N\gamma$ vertex may be written as[22]

$$\mathcal{L}^1_{\gamma NR} = \frac{e}{2(M_R+M)}\bar{R}(G_1^s(k^2)+G_1^v(k^2)\tau_3)\gamma_5\sigma_{\mu\nu}NF^{\mu\nu} + H.c., \quad (2)$$

$$\mathcal{L}^2_{\gamma NR} = \frac{e}{(M_R+M)^2}\bar{R}(G_2^s(k^2)+G_2^v(k^2)\tau_3)\gamma_5\gamma_\mu N\partial_\nu F^{\mu\nu} + H.c., \quad (3)$$

using the PS coupling at the ηNS_{11} strong vertex and M_R and M are the relevant baryon masses. $F^{\mu\nu}$ is the electromagnetic field tensor, s and v are superscripts indicating isoscalar and isovector transition form factors, which are unknown, to be determined from a fit to the existing data[17] on differential cross-section. Here the kinematics for the virtual photon four momentum $k^\mu = (k_0,\vec{k})$ is the usual one: $k^2 \equiv -Q^2 = (k_1 - k_2)^2 \approx -4E_1E_2\sin^2\psi/2$, ψ is

the electron scattering angle, E_1, E_2, $\vec{k}_1$, $\vec{k}_2$ are energies and momenta of the incident and scattered electrons.

By convention[10], the resonances electromagnetic couplings are expressed in terms of the helicity amplitudes $A_{1/2}$ and $S_{1/2}$ (or $C_{1/2}$). Using[15]

$$A_{1/2} = \sqrt{\frac{2\pi\alpha}{k_\gamma^\star}} < S_{11}, J_z = 1/2| - \mathcal{L}_{em}|N, J_z = -1/2 > \tag{4}$$

$$S_{1/2} = \sqrt{\frac{2\pi\alpha}{k_\gamma^\star}} < S_{11}, J_z = 1/2| - \mathcal{L}_{em}|N, J_z = 1/2 > \frac{k_R}{\sqrt{-k^2}} \tag{5}$$

and

$$< S_{11}, \lambda_S|J \cdot \epsilon|N, \lambda_N >= \frac{e}{(M+M_R)}\bar{U}_S\gamma_5\left[G_1^p i\sigma_{\mu\nu}k^\nu\epsilon^\mu + \frac{G_2^p}{(M+M_R)}\gamma\cdot\epsilon\, k^2\right]U_N, \tag{6}$$

derived from our interaction Lagrangians (2) and (3), we obtain the desired relations:

$$A_{1/2}(Q^2) = -\frac{M_R}{2}\left[\frac{Q_R^+}{2M(M_R^2-M^2)}\right]^{1/2} h_3(Q^2), \tag{7}$$

$$S_{1/2}(Q^2) = -\frac{k_R}{2}\left[\frac{Q_R^+}{4M(M_R^2-M^2)}\right]^{1/2} h_1(Q^2). \tag{8}$$

Here, $k_\gamma^\star = (M_R^2-M^2)/2/M_R, Q_R^\pm = (M_R \pm M)^2+Q^2$ and $k_R^2 = Q_R^+Q_R^-/(4M_R^2)$. The relations between G_i^p and h_i are

$$h_1 = \frac{2e}{M+M_R}\left\{\frac{M_R-M}{M_R+M}G_2^p - G_1^p\right\}, \tag{9}$$

$$h_3 = -\frac{2e}{(M+M_R)M_R}\left\{\frac{Q^2}{M_R+M}G_2^p + (M_R-M)G_1^p\right\}. \tag{10}$$

The form factors h_1 and h_3 which denote the longitudinal and transverse transition form factors respectively are related to those defined by eq. (2.33) in Devenish et al paper[23].

The S-matrix for the s-channel excitation of the $S_{11}(1535)$, using the above lagrangians is simply:

$$i\mathcal{M}_{fi}^1 = \frac{eg_\eta G_1^p(k^2)}{(M+M_R)}\bar{U}_f\frac{\gamma\cdot(p_i+k)+M_R}{s-M_R^2}\gamma_5\gamma\cdot k\gamma\cdot\epsilon U_i, \tag{11}$$

$$i\mathcal{M}_{fi}^2 = \frac{eg_\eta G_2^p(k^2)k^2}{(M+M_R)^2}\bar{U}_f\frac{\gamma\cdot(p_i+k)+M_R}{s-M_R^2}\gamma_5\gamma\cdot\epsilon U_i. \tag{12}$$

Here g_η, the $\eta NS_{11}(1535)$ coupling, U_i and U_f, the spinors for incoming and outgoing nucleons, $s = W^2$ the standard invariant mass and p_i the target nucleon four momentum. Note that the second term vanishes for the real photon. For the u-channel, the amplitude can be constructed by crossing symmetry. For the lack of space, we omit the Born terms for the non-resonant meson production but can be found along with a detailed formalism on meson electroproduction in Ref. [19].

2 RESULTS

The standard procedure for calculating cross sections for the process and polarization observables, is to write $\mathcal{M}_{fi}$ in terms of the CGLN amplitudes $\mathcal{F}$[20,19,21]: $\mathcal{M}_{fi} = (4\pi W/M)\chi_f^\dagger \mathcal{F} \chi_i$, where the χ_i and χ_f are the nucleon Pauli spinors, taking into account the transitions $\gamma N \to N^* \to \eta N$, where γ is the virtual photon. The amplitude $\mathcal{F}$ is given by $\mathcal{F} = i\vec{\sigma}\cdot\vec{b}\mathcal{F}_1 + \vec{\sigma}\cdot\hat{q}\vec{\sigma}\cdot(\hat{k}\times\vec{b})\mathcal{F}_2 + i\vec{\sigma}\cdot\hat{k}\hat{q}\cdot\vec{b}\mathcal{F}_3 + i\vec{\sigma}\cdot\hat{q}\hat{q}\cdot\vec{b}\mathcal{F}_4 - i\vec{\sigma}\cdot\hat{q}b_0\mathcal{F}_5 - i\vec{\sigma}\cdot\hat{k}b_0\mathcal{F}_6$, with $b_\mu = \epsilon_\mu - (\vec{\epsilon}\cdot\hat{k}/|\vec{k}|)k_\mu$ (Note that $\mathcal{F}_5, \mathcal{F}_6$ are usually labelled $\mathcal{F}_7, \mathcal{F}_8$ in the litterature[20]). The $\mathcal{F}_i$'s can be converted into helicity amplitudes H_i (i = 1, ... 6), in terms of which all observables can be expressed appropriately[19].

In an earlier work[19,22] we analysed the existing differential cross-section data[17] at $Q^2 = 0.2, 0.28, 0.4, 1.0, 2.0, 3.0\,GeV^2$ as follows *. We fixed the Born terms for nucleon and vector meson exchanges as in the real photon case[1], except for the form factors. The nucleon form factors have the usual dipole form, while the $\rho\eta\gamma$ and $\omega\eta\gamma$ electromagnetic form factors are parametrized in terms of the prescription of the vector dominance i-e, $G_{V\gamma\eta}(k^2) = (1 - k^2/m_V^2)^{-1}$, where $m_V \approx \frac{1}{2}(m_\rho + m_\omega)$, the average vector meson mass. It is a reasonable approximation to neglect relatively small contributions from nucleonic resonances, such as D13(1520), to the angular distributions at the crude level of precision of the old data. However, high precision of data expected in new facilities and polarization observables would require their inclusion. With the existing data base on electroproduction of etas, it is not possible to extract any meaningful information on other resonances. Given the relative importance of the nucleon Born terms, vector meson exchanges and the excitation of N*(1535) in the ascending order, the model was used to determine the $A_{1/2}(Q^2)$, given some Ansätze for the small scalar (longitudinal) amplitude $S_{1/2}(Q^2)$. In the present work, we have found that a reasonable description of the very precise TAPS data for the total cross-section at the photon point $Q^2 = 0$ is obtained with $A_{1/2} \equiv 100\,10^{-3} GeV^{-1/2}$. In Fig. 1, we show the total cross section as function of the c.m. energy W. The values of the helicity amplitudes used for the non-zero Q^2 calculation are taken from the second column of Table 1 in Ref. [22]. Similarly, we show in Fig. 2 our calculation for the high Q^2 electroproduction data. Clearly, the experimental data are well reproduced in particular the data at the real photon point $Q^2 = 0$[9]. It is important to emphasize that the $S_{11}(1535)$ mass and strong decay parameters, including the total width, are Q^2 independent and are fixed to $M_R = 1.535 GeV$ and $\Gamma_T = 0.150 GeV$ in the current analysis. This is in contrast to previous investigations where the total width was found to change as a function of Q^2. For example, the total width dropped from $\Gamma = 150 MeV$ at $Q^2 = .2, 0.6, 1.0\,GeV^2$ (see Alder et al. in ref. [17]) to $\Gamma = 69 MeV$ at $Q^2 = 2, 3 GeV^2$ (see Brasse et al. in Ref. [17]). We have assumed that the helicity amplitude $S_{1/2}$ is zero since the current experimental data are not accurate enough to pin down the longitudinal strength of $S_{11} \leftrightarrow \gamma N$. To get an idea how big of a cross section associated with the longitudinal stength of S_{11}, we compare in Fig. 3 the transverse and scalar total cross section at $Q^2 = 0.6\,GeV^2$ for two values for the scalar helicity amplitude $S_{1/2} = 0$ and $25\,10^{-3}\,GeV^{-1/2}$. The latter value is consistent with the calculation within the light-front framework of Capstick and Keister[15]. As one can see the scalar total cross section σ_S is no more that 15% of the transverse σ_T at the resonance peak.

*The new differential cross section measured in Hall C at Jlab at $Q^2 = 2.4, 3.6\,GeV^2$[24] are not yet available to us

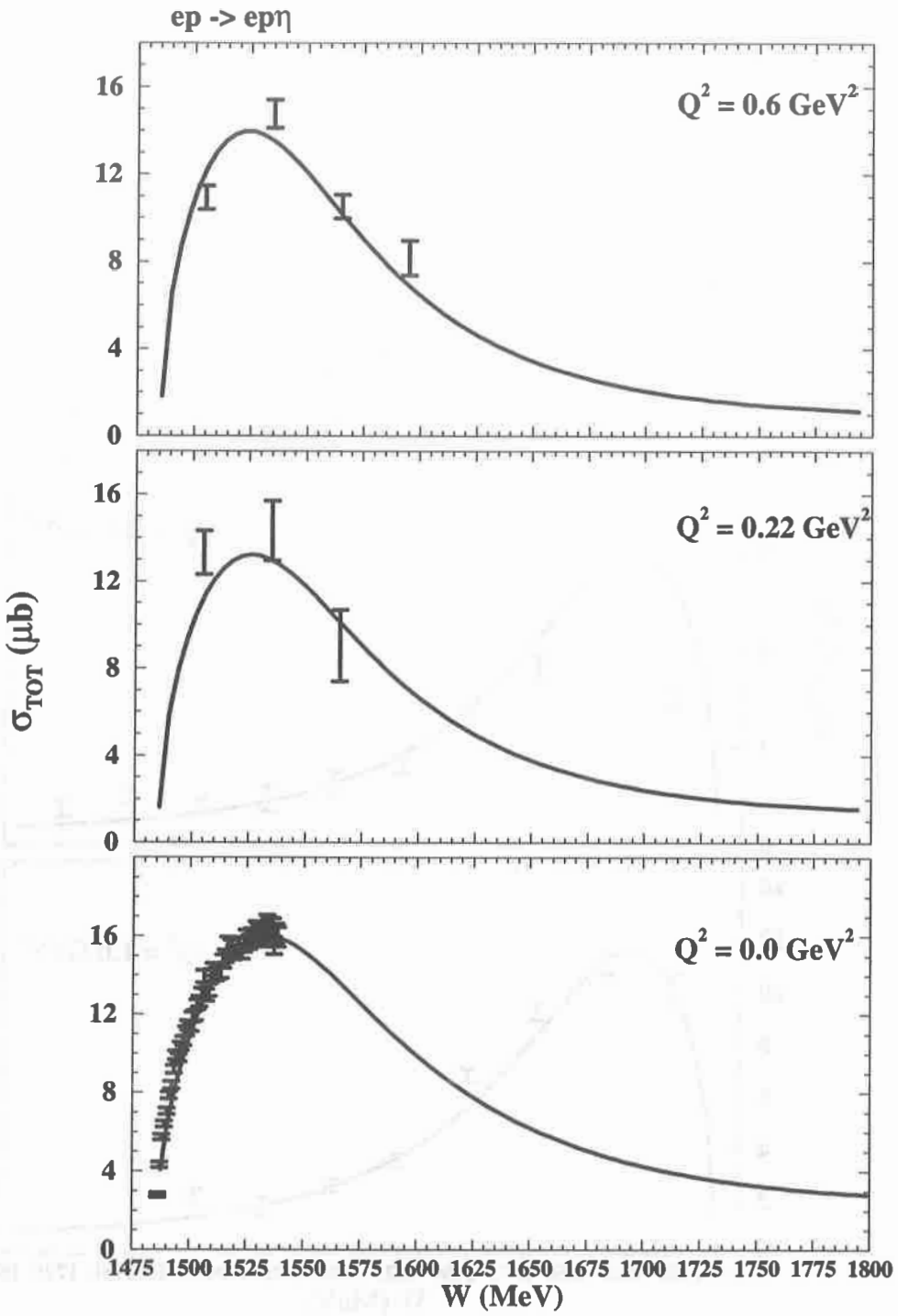

Figure 1. Total cross section vs. c.m. energy for the process $ep \to ep\eta$. The data at the photon point is the recent TAPS data[9]. The other Q^2 data are taken from Ref. [17].

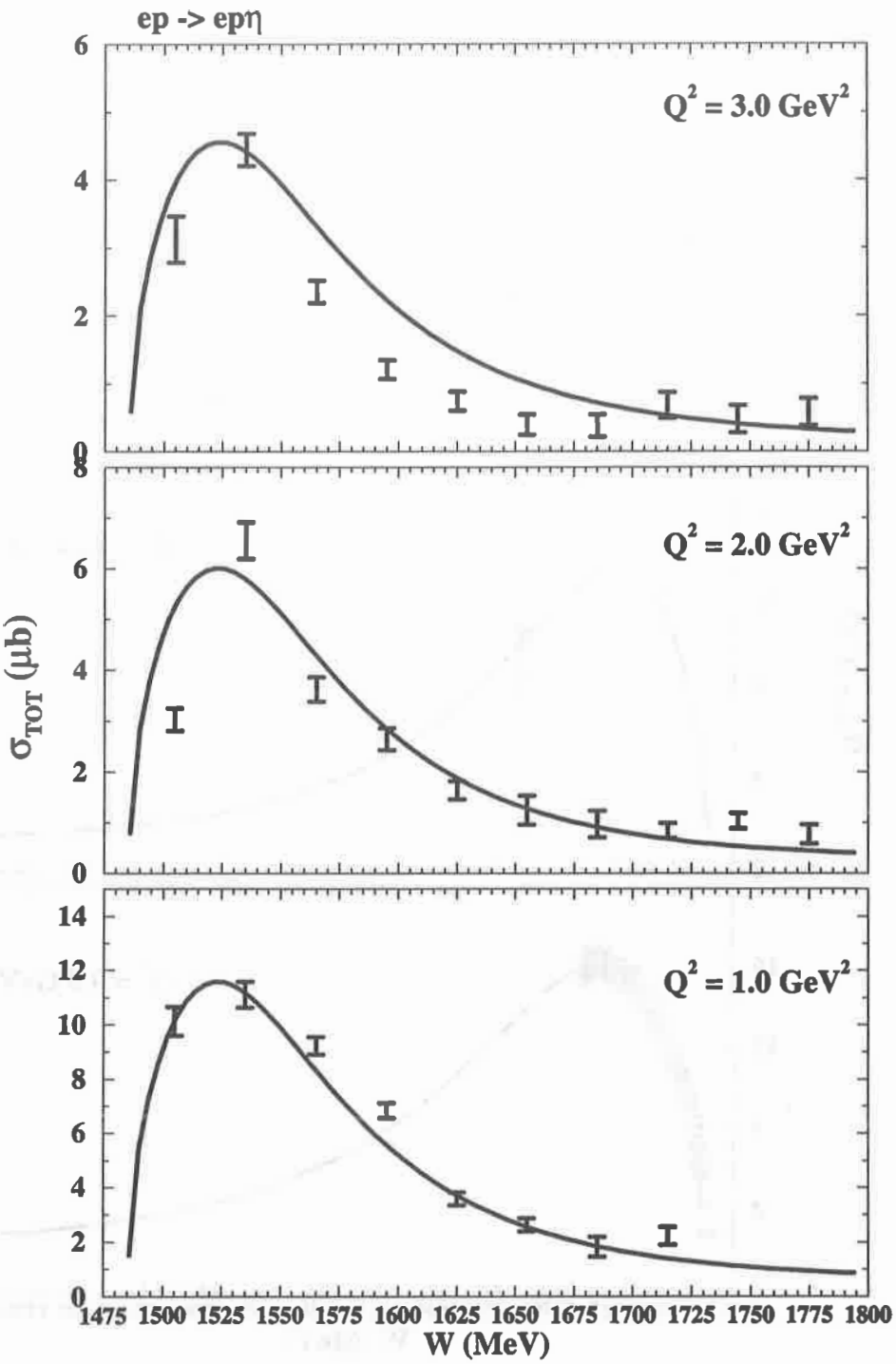

Figure 2. Total cross section vs. c.m. energy for the process $ep \to ep\eta$. Data are taken from Ref. [17].

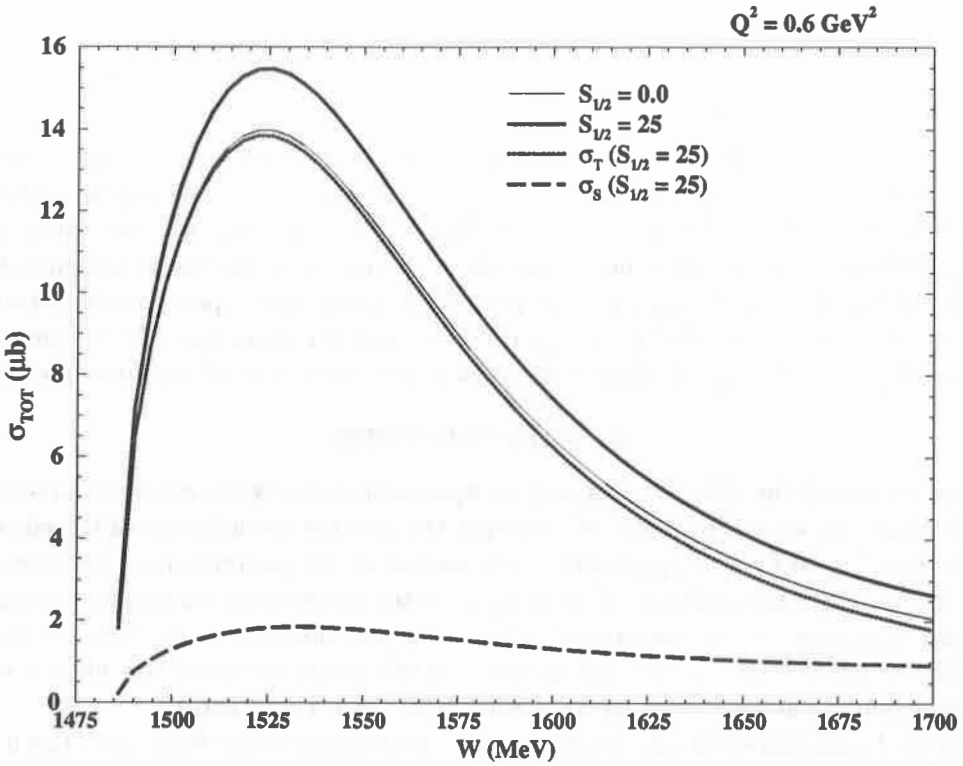

Figure 3. Transverse (dotted line) and scalar (dashed line) total cross section at $Q^2 = 0.6\,GeV^2$ for two values of helicity amplitude $S_{1/2} = 0$ and $25\,10^{-3}\,GeV^{-1/2}$. $\sigma_T + \epsilon\sigma_S$ is shown in a solid line with $\epsilon = 0.9$.

3 SIMPLE PARAMETRIZATION OF $S_{11}(1535)$ FORM FACTORS

Here we propose a parameterization of the $N^*(1535)$ electromagnetic form factors based on the assumption that the constraint-free transition form factor $G_1^p(Q^2)$ and $G_2^p(Q^2)$ have a common k^2 dependence[23], i-e $G_i^p(Q^2) = g_i F(Q^2)$ with F(0) = 1). Now using perturbative QCD scaling law for the transverse helicity amplitude $A_{1/2}$ which translates into[13]

$$Q^4 A_{1/2}/\sqrt{Q^+} \to Constant \tag{13}$$

$F(Q^2)$ assumes the following form:

$$F(Q^2) = \frac{1}{1+\tau}\frac{1}{(1+Q^2/\Lambda^2)^2}, \quad \tau = \frac{Q^2}{(M_R^2 - M^2)} \tag{14}$$

where Λ is fitted to the extracted helicity amplitudes[22]. To a good accuracy, the following Q^2 dependence is achieved:

$$A_{1/2}(Q^2) = (g_1 + g_2\tau)G(Q^2), \quad G(Q^2) = \sqrt{1 + \frac{Q^2}{(M_R+M)^2}}F(Q^2) \tag{15}$$

with $\Lambda = 1.8GeV, g_1 = 100 \times 10^{-3}GeV^{-1/2}, g_2 = 182 \times 10^{-3}GeV^{-1/2}$. In Fig. 4 we indicate the result of the fit by a thick solid line. The thin line is the result of setting $g_1 = 88.83$ which was obtained in our earlier[22] using the old data at the real photon point rather than the latest TAPS data. Once we have made the above assumptions on the constraints-free form factors, the scalar form factor can now be predicted and its Q^2 dependence is shown in Fig. 4 by the dashed line. Notice that $g_1 = A_{1/2}(Q^2 = 0)$ and therefore sensitive to the amplitude at the photon point while g_2, Λ control the asymptotic behaviour of the form factor.

4 CONCLUSIONS

We have extended the effective Lagrangian approach to study eta electroproduction in the $S_{11}(1535)$ region. In an earlier work[22] we noted the relative insensitivity of the electrostrong transverse form factor for the $S_{11}(1535)$ to a variation of the parameters of the model inputs, such as the resonance parameters, value of $g_{\eta pp}$, vector meson form factor, and so on. Within the existing database on eta electroproduction, it is not possible to extract any meaningful information on other resonances. Current versions of the quark model are unable to explain the Q^2 evolution of the extracted electrostrong transverse form factor.

A combined analysis of of the η photo- and electroproduction data has shown that the $S_{11}(1535)N\gamma$ transverse form factor falls off relatively slowly, in agreement with previous studies[17]. We have shown that the form factor can be described by a three-parameter function which is based on two assumptions: (i) the constriant-free form factor have a common Q^2 and (ii) the helicity amplitude must have the proper perturbative QCD scaling law.

Based on the above parametrization, we were able to make predictions for the total cross-section at two Q^2 settings of the very recent JLab experiment[24]. Our results are displayed in Fig.5.

5 ACKNOWLEDGEMENT

I wish to thank the organizers of this N^* workshop for the happy and stimulating atmosphere. I am grateful to Cornelius Bennhold for the invitation and Nimai Mukhopadhyay for many stimulating discussions. The research is supported by the National Sciences and Engineering Research of Canada.

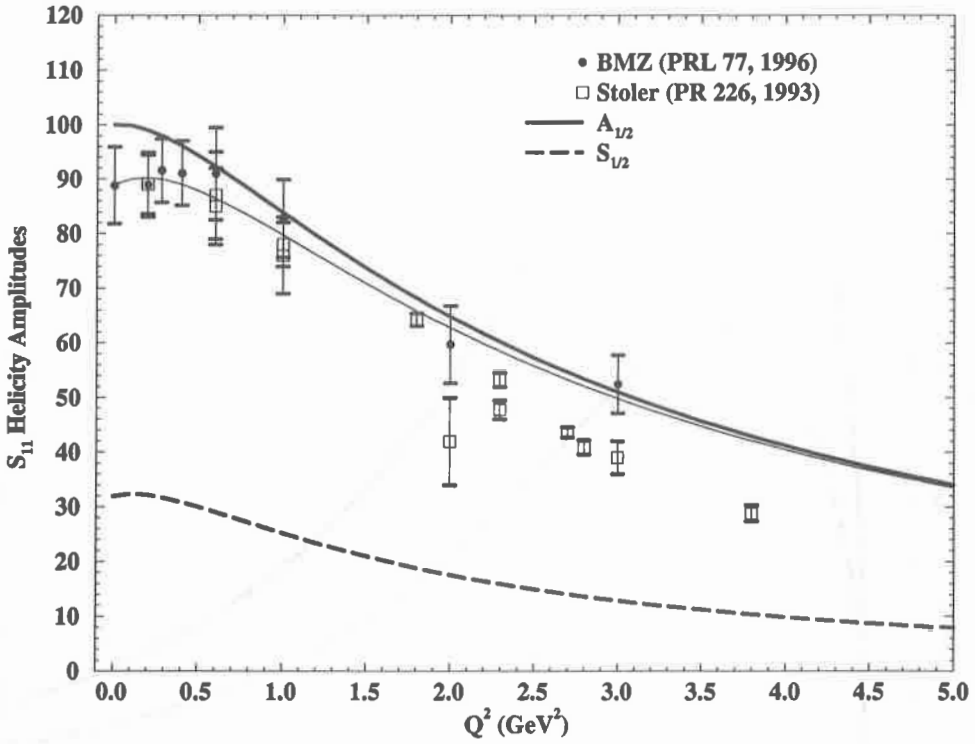

Figure 4. Transverse and scalar helicity amplitudes as a function of the four momentum transfer Q^2 for the transition $S_{11}(1535) \leftrightarrow \gamma p$. The circles and squares are due to an analysis of data by [22] and [13] respectively.

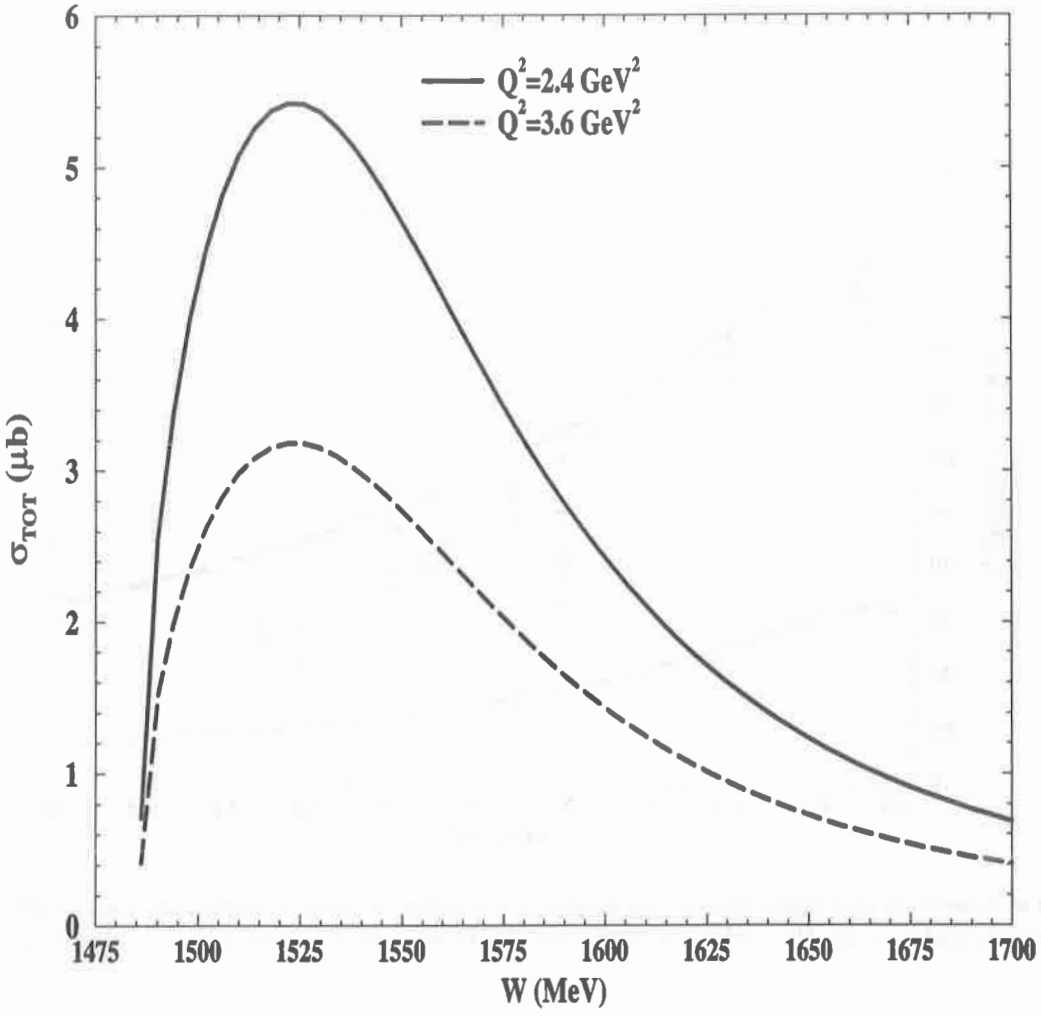

Figure 5. Predicted total cross section vs. c.m. energy at the two Q^2 settings of the recent Jlab experiment in Hall C[24].

REFERENCES

[1] M. Benmerrouche and N. C. Mukhopadhyay, Phys. Rev. Lett. **67**, 1070 (1991); M. Benmerrouche, N. C. Mukhopadhyay and J. -F. Zhang, Phys. Rev. **D51**, 3237 (1995). N. C. Mukhopadhyay, J. -F. Zhang and M. Benmerrouche, Phys. Rev. Lett. **75**, 3022 (1995); Phys. Lett. **B364**, 1 (1995). B. Krusche, N. C. Mukhopadhyay, J. -F. Zhang and M. Benmerrouche, Phys. Lett. **B397**, 171 (1997).

[2] C. Sauermann *et al.*, Phys. Lett. **B341**, 261 (1995).

[3] T. Feuster and U. Mosel, these proceedings.

[4] L. Tiator, C. Bennhold and S.S. Kamalov, Nucl. Phys. **A580**, 455 (1994).

[5] J. Piekarewicz, A.J. Sarty and M. Benmerrouche, Phys. Rev. **C55**, 2571 (1997); L.J. Abu-Raddad, J. Piekarewicz, A. J. Adam and M. Benmerrouche, nucl-th/9710005.

[6] M. Hedayati-Poor and H.S. Sherif, Phys. Rev. **C56**,1557 (1997).

[7] E. Breitmoser and H. Arenhövel, Nucl. Phys. **A612**, 321 (1997); A. Fix and H. Arenhövel, Nucl. Phys. **A620**, 457 (1997).

[8] H. Genzel et al., in Landolt-Börnstein, New series I/8, Springer (New York, 1973) p. 361; S. Homma et al., J. Phys. Soc. Japan **57**, 828 (1988); S. Dytman et al., Phys. Rev. **C51**, 2170 (1995); J. Price et al., Phys. Rev. **C51**, R2383 (1995).

[9] B. Krusche et al., Phys. Rev. Lett **74**, 3736 (1995); Phys. Lett **B358**, 40 (1995).

[10] Review of Particle Physics, Phys. Rev. **D54**, 1 (1996).

[11] M. Warns, H. Schröder, W. Pfeil and H. Rollnick, Z. Phys. **C45**, 613 (1990); 627 (1990), M. Warns, W. Pfeil and H. Rollnick, Phys. Rev. **D42**, 2215 (1990).

[12] R. Koniuk and N. Isgur, Phys. Rev. **D21**, 1868 (1980).

[13] P. Stoler, Phys. Rep. **226**, 103 (1993) and references therein.

[14] W. Konen and H.J. Weber, Phys. Rev. **D41**, 2201 (1990).

[15] S. Capstick and B.D. Keister, Phys. Rev. **D51**, 3598 (1995).

[16] D. Leinweber, T. Draper and R. M. Woloshyn, Phys. Rev. **D46**, 3067 (1992).

[17] P.S. Kummer et al., Phys. Rev. Lett. **30**, 873 (1973); H. Breuker et al., Phys. Lett. **B74**, 409 (1978); F.W. Brasse et al., Nucl. Phys. **B139**, 37 (1978); U. Beck et al., Phys. lett. **B51**, 103 (1974); F. W. Brasse et al., Z. Phys. **C22**, 33 (1984); J.C. Alder et al., Nucl. Phys. **B91**, 386 (1975).

[18] S.A. Dytman et al., CEBAF proposal PR-89-039; J.J. Kelly et al., CEBAF proposal PR-96-001.

[19] M. Benmerrouche, Ph.D. Thesis, Rensselaer Polytechnic Institute, 1992, unpublished.

[20] A. Donnachie, *Photo- and Electroproduction Processes*, in high energy Physics, E.H.S. Burhop ed., Academic, New York (1972) p. 1.

[21] G. Knöchlein, D. Drechsel and L. Tiator, Z. Phys. **A352**, 327 (1995).

[22] M. Benmerrouche, N. C. Mukhopadhyay and J. -F. Zhang, Phys. Rev. Lett. **77**, 4716 (1996).

[23] R.C.E. Devenish, T.S. Eisenschitz and J.G. Körner, Phys. Rev. **D14**, 3063 (1976).

[24] J.W. Price, these proceedings.

New Crystal Ball Results from BNL

B. Tippens* for the Crystal Ball Collaboration
University of California, Los Angeles

Abstract

The SLAC Crystal Ball (CB) detector was recently installed on the C6 beamline at the AGS. A two week engineering run and a two week data run looking at all neutral final states from $\pi^- p$ interactions were completed in the spring of 1997. This marks the beginning of a new diverse program in baryon spectroscopy at BNL. Some of its goals are to improve the determination of the masses, widths and decay modes of baryon resonances in the region $E_{cm} < 2150$ MeV/c, to search for possible exotic states such as pentaquarks and hybrids, to determine meson-nucleon scattering lengths such as η-n, η-Λ, and η-Σ, for example, and to measure inverse photoproduction of K^- mesons from the unstable Λ and Σ hyperons. A description of the experimental setup and performance of the detector is given along with some preliminary results from the data run.

Introduction

Experiments 913 and 914 at the AGS are concerned with the systematic precision measurement of neutral final states in $\pi^- p$ and $K^- p$ interactions in the baryonic resonance region of $1100 < E_{cm} < 2150$ MeV/c. This energy regime covers most of the known N^*, Δ^*, Λ^*, Σ^* resonances; many which have poorly determined masses and widths. More importantly, many have neutral decay channels which are unknown. Some of the channels we intend to measure are: $\pi^\circ n, 2\pi^\circ n, 3\pi^\circ n, \eta n, \eta\pi^\circ n, \omega\pi^\circ n$, and $\omega\eta n$. The capability of detecting sequential decays will make it possible for us to study such rarely observed resonances as the $\Lambda(1405)$. Measurement of the fundamental properties of the elementary πN and KN systems tests the theoretical models that predict the spectra and characteristics of the baryon resonances. In addition, the measurement of hadronic resonance production is necessary to successfully extract the coupling constants for radiative decays as Mark Manley has pointed out in his talk at this conference.

We can also search for possible new resonances. Only about half of the resonances below 2 GeV expected from different quark models have been discovered. Either many of these resonances have not been identified or there is some underlying symmetry or symmetries which suppress their formation. In either case, the full understanding of the resonances in this regime is needed to answer this question. Related to this search for missing resonances is the search and identification of possible hybrid or exotic baryonic states. An advantage of exploring the neutral channels is that many of them have a uniquely defined isospin state which can be exploited to select resonances with specific isospin, for instance, $\Lambda\pi^\circ\pi^\circ$ and $\Sigma\pi^\circ$ are exclusively $I = 0$ states. Isospin selection makes it possible to sort out which resonances are contributing to a particular channel in a regime where several resonances overlap. A more detailed discussion of the hadron program for the Crystal Ball is described in the presentation by Ben Nefkens.

In addition to the spectroscopy program, approved experiment E927 will make a precision measurement of the Ke3 decay using the CB detector in order to determine the element V_{us} with an absolute precision of 0.7%. This would improve the determination of other parameters of the CKM matrix in the Wolfenstein parameterization.[1] It would also test the unitarity of the CKM matrix; a violation would suggest an opening for new physics such as

*E-mail: tippens@bnldag.phy.bnl.gov

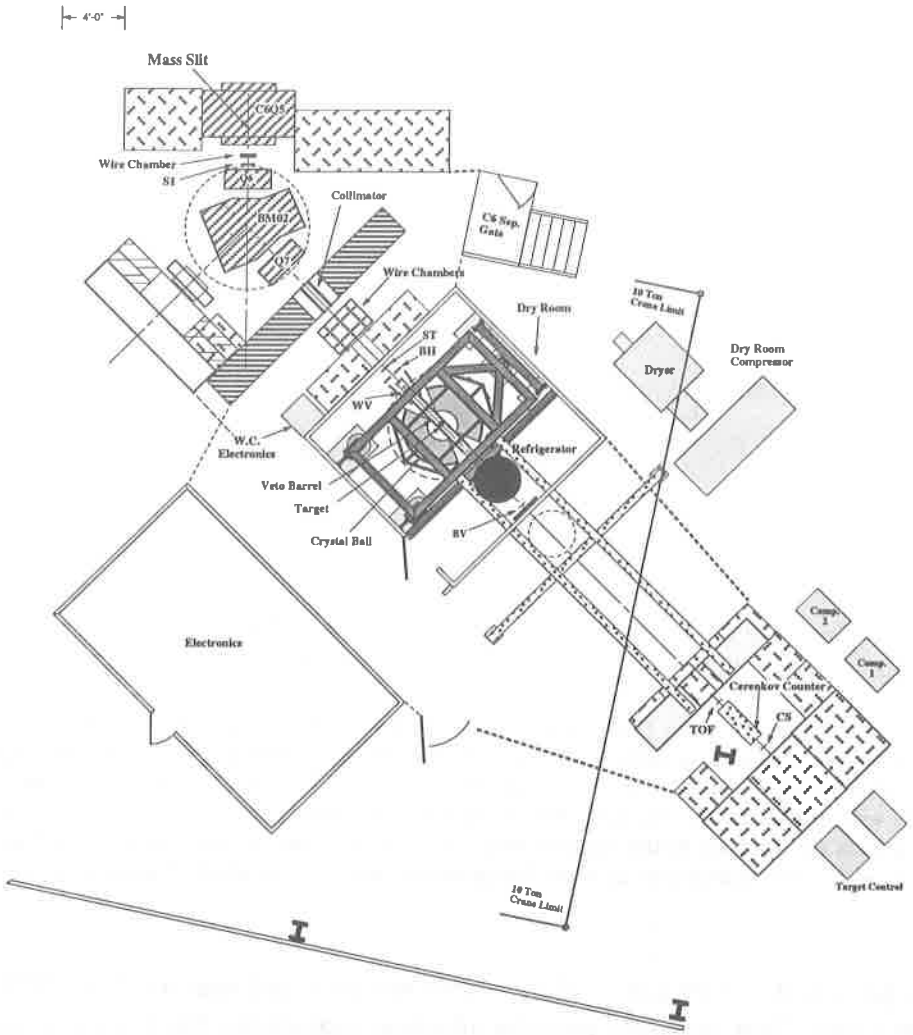

Figure 1. Floor layout of E913/914 on the C6 beamline at the AGS.

Supersymmetry. Concomitant with this, we will collect data on other interesting K decays such as K_{e4} which provides an important test of the $\Delta I = 1/2$ rule.

The Experimental Setup

Many of the neutral final states of interest involve a high number of photons in the final state and thus require a 4π photon spectrometer to reconstruct the reaction. The SLAC Crystal Ball detector (CB) is ideally suited for this work. The detector consists of 672 NaI crystals which are each shaped like a truncated triangular pyramid 16 radiation lengths thick. The inner active radius of the CB is 25.4 cm. The CB is based on the icosahedron geometry of 20 triangles each made up of 36 crystals, requiring 720 crystals to completely fill the 4π solid angle. The omitted crystals provide upstream and downstream access tunnels to the center active region.

We have inserted a liquid hydrogen target through the downstream tunnel using a 15.2 cm diameter by 2 mm thick aluminum beam pipe to provide a vacuum jacket for the target.

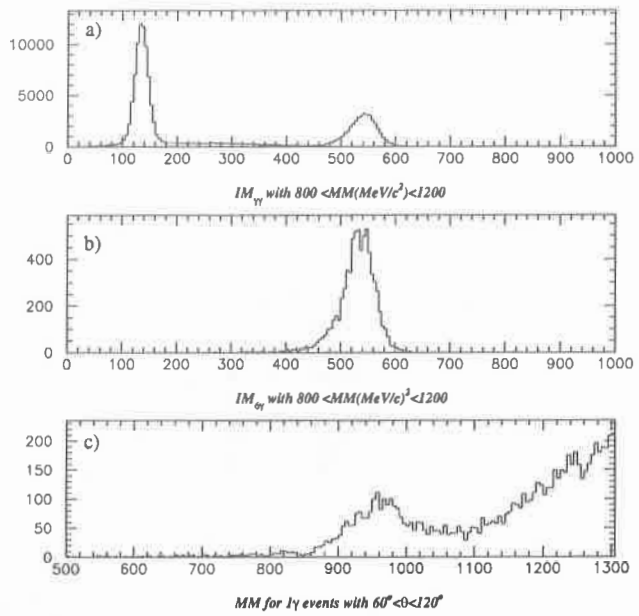

Figure 2. (a) Invariant mass (IM) spectrum for 2γ events. The only cut applied to this spectrum is the requirement that the missing mass (MM) be between 800 and 1200 MeV/c^2. The two peaks, one at the π° and the other at the η mass, indicate the reactions $\pi^- p \to \pi^\circ n$ and $\pi^- p \to \eta n$. (b) The invariant mass for 6γ events with the same missing mass cut showing the dominant decay $\eta \to 3\pi^\circ$. (c) A missing mass plot of single γ events for photons in the angular range $60^\circ - 120^\circ$. The peak at the neutron mass indicates events from $\pi^- p \to n\gamma$. The background is from charge exchange events in which 1 photon escapes detection.

The target is a 10 cm diameter cylinder with spherical endcaps which is 10.56 cm long at the cylinder's axis. This pipe also provides physical support for the 4 Veto Barrel (VB) plastic scintillators which are 120 cm long and 5 mm thick. These counters provide a charged particle veto for determining the neutral final state in the trigger.

The CB detector was installed on the C6 beamline at the AGS facility, see fig. 1. This is a doubly separated beamline originally designed to provide kaon beams with a maximum momentum of 760 MeV/c. During this year's running we concentrated on pion beams from 200-760 MeV/c. Typical flux rates were 100k pions per 1.6 second spill every 3.6 seconds. The C6 beamline was designed to provide high flux and large divergence kaon beams. This is incompatible with the constraint of the CB detector which requires us to pass the beam through a 15 cm diameter beam pipe which is 3.2 m long. Fortunately, with a nearly 4π detector, we do not need the high flux capability and so we strongly collimated the beam to provide a low divergence beam. The second bending magnet (BM02) on the beamline is used as a magnetic spectrometer to momentum analyze the individual beam particles triggering the system. Wire chambers are placed upstream and downstream of the magnet for this purpose. Time-of-flight information allows us to tag each π and K beam particle.

The trigger for a neutral event consisted of a beam trigger in coincidence with an energy trigger greater than 75 MeV in the CB detector and no veto signal from any of the veto counters. These counters included the four veto barrel (VB) counters which surround the

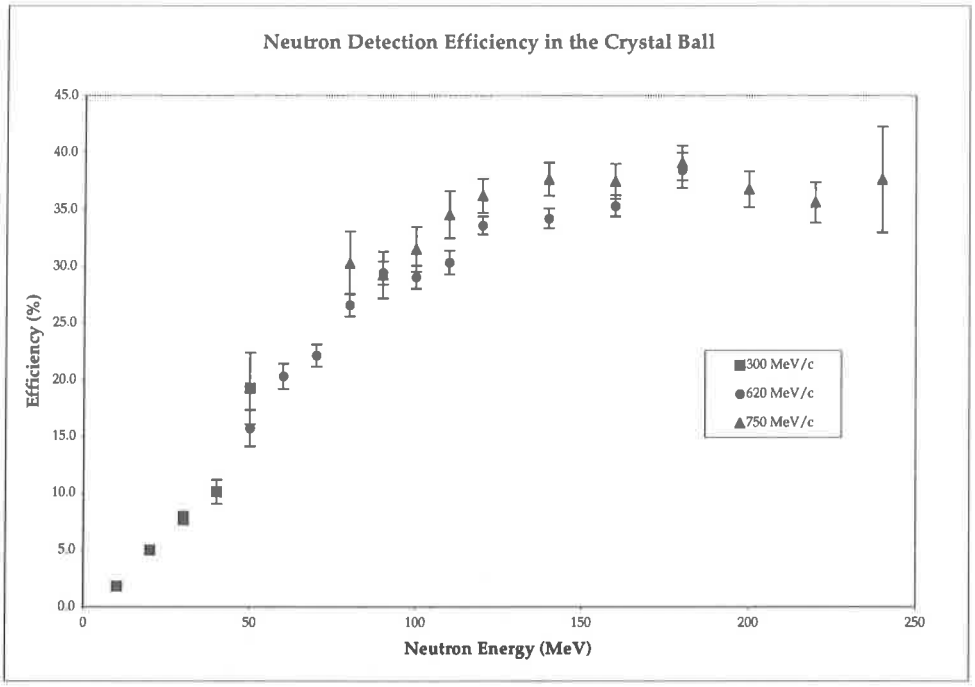

Figure 3. Measured neutron detection efficiency for the CB as a function of the neutron energy. Events from the reaction $\pi^- p \rightarrow \pi^\circ n$ were used for this study in which the π° information is used to identify the CEX reaction. The efficiency is determined by the percentage of events in which the neutron is also picked up in the CB as an additional cluster.

beam pipe passing through the CB, four wave shifter vetoes (WV) which cover the beam just upstream of the VB counters, four beam halo counters (BH) located just downstream of ST, and two beam veto counters located 2m downstream of the CB detector. The beam trigger was determined by a coincidence of two scintillators (S2, ST) placed in the beam upstream of the CB detector. The two BV counters are designed to veto the beam particles which pass through the target and charged particles which emerge at small angles to the beam. The BH counters restricted the beam to the size of the LH_2 target and vetoed the beam halo.

There was a time-of-flight (TOF) counter 963 cm downstream of the ST counter which was used to determine the velocity of kaons, low momentum pions, and protons for calibrating the absolute momentum of the beam. There was also a gas Čerenkov counter located just before the beam stop to monitor the electron contamination of the beam. Muon contamination of the beam at momenta above 600 MeV/c has been measured in a previous experiment to be less than 2%.

Preliminary Results

E913 performed a two week test run from April 3, 1997 through April 15, 1997. The test run was used to make a high energy calibration of the Crystal Ball detector using monoenergetic photons from the reaction $\pi^-_{stop} p \rightarrow n\gamma$, to verify the proper operation of the detector by measuring the two photon spectrum below and above the η threshold, and to study possible background sources in the experimental setup. A H_2 high pressure gas target was used for the calibration and a CH_2 target was used to study the detector performance. We were able

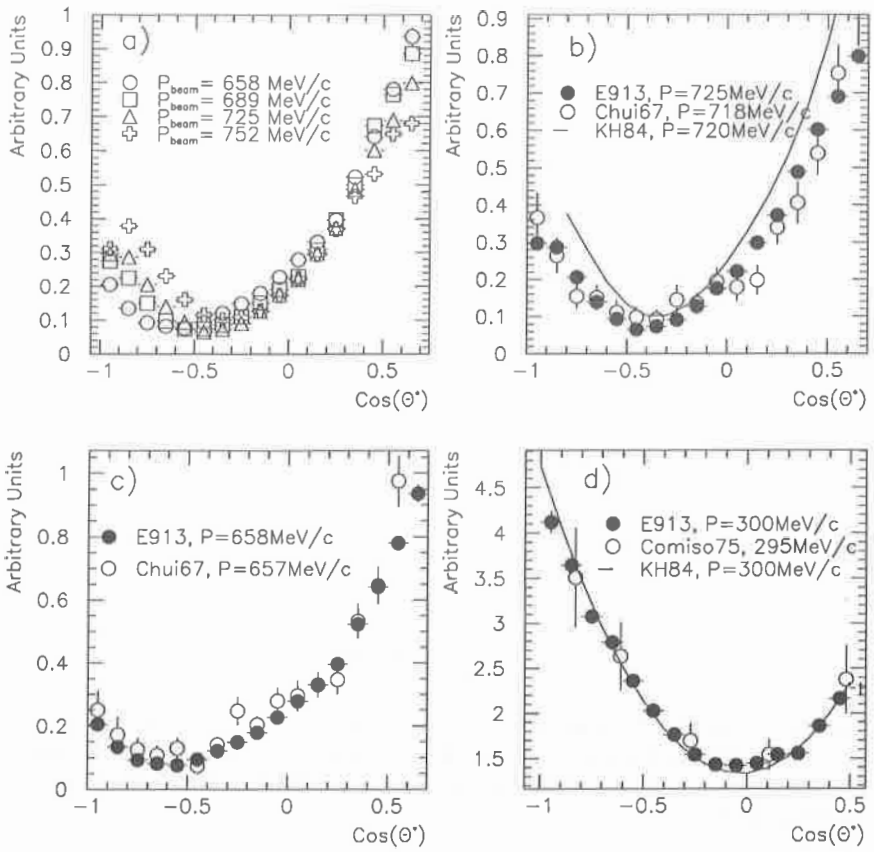

Figure 4. a) Relative differential cross sections for the $\pi^- p$ CEX reaction at four beam momenta. b) Comparison of our results at 725 MeV/c with the data of Chiu, *et al.*[2] and with the phase shift analysis KH84.[3] Our data were normalized to the Chiu data at $cos\theta = 0$ for this comparison. c) Comparison of our data and Chiu, *et al.* at a beam momentum of 658 MeV/c. d) Comparison of our data with Comiso, *et al.*[4] and KH84 at 300 MeV/c.

to cleanly identify the following $\pi^- p$ reactions: $\pi^\circ n, \eta n, \gamma n,$ and $2\pi^\circ n$ with the π° decaying to 2γ and the η decaying to the 2γ, and $3\pi^\circ$ channels. Figures 2(a-c) show typical spectra from the LH_2 target for some of these reactions. The 2γ invariant mass spectrum, fig. 2 (a), demonstrates exceptionally clean π° and η peaks with preliminary energy resolutions of 9.2% and 4.3%, respectively. These resolutions are limited by the large size of the present target. Background to peak ratios are of the order of a few percent using only a missing mass selection.

As part of the analysis of our data, we wish to understand the interaction of neutrons in the CB. Shirvel Stanislaus, from Valparaiso University, has performed an analysis of the interaction of neutrons from the reaction $\pi^- p \rightarrow \pi^\circ n$ (CEX). Additional efforts are also underway at the University of Regina, Canada and Petersburg Nuclear Physics Institute in St. Petersburg, Russia. The neutrons are tagged by the detection of the π° from three cluster events and calculating the expected neutron direction. He then tested whether the third detected cluster corresponds to the neutron. A crystal energy threshold of 0.3 MeV and a cluster detection threshold of 10 MeV was used for the analysis. The π° was identified

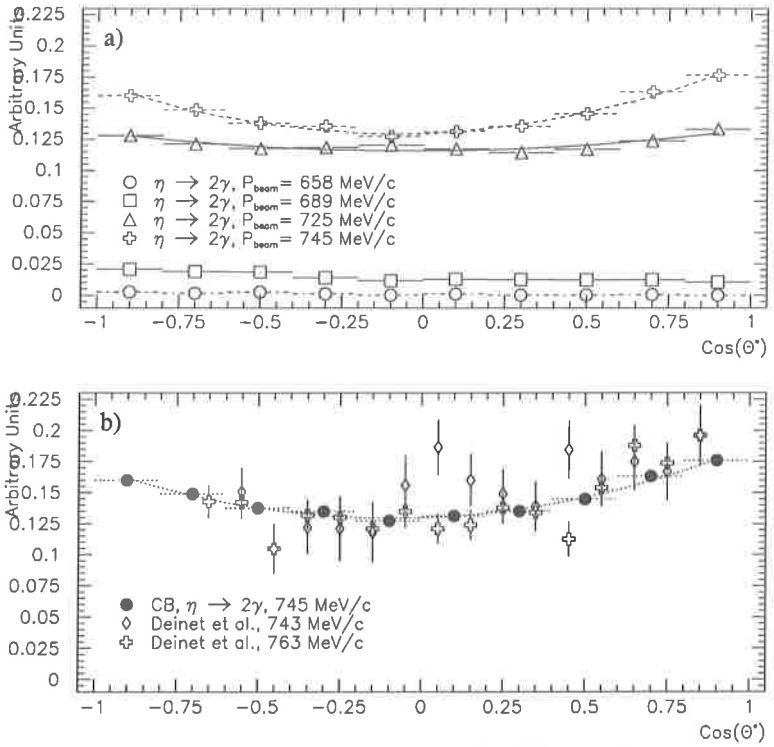

Figure 5. (a) Relative differential cross sections for $\pi^- p \rightarrow \eta n$ at four different beam momenta. (b) The relative differential cross sections for η production compared to the data of Deinet, *et al.*[5] Our data have been normalized to Deinet, *et al.*

with selection cuts on the π° invariant mass and neutron missing mass set at $\pm 1.25\sigma$ which corresponds to about 15 MeV for the π° and ± 50 MeV for the neutron and requiring an opening angle on the photons from the π° to be greater than 30°. From these events, the neutron detection efficiency for the CB was determined. Fig. 3 shows we have detection efficiencies as high as 30-40%. This gives us a unique, highly efficient, neutron detector with nearly 4π acceptance in which the angle of the neutron is determined to about 2°, but with effectively no energy resolution. These events in which the neutron is also detected will allow us to study backgrounds from misidentified channels. An added bonus is that we can experimentally study the interaction of neutrons with energies up to 250 MeV in the CB to verify our simulation of neutrons in the experiment.

A short data run was conducted from May 15, 1997 through June 3, 1997. The liquid hydrogen target was installed for this running period. This run measured the reactions $\pi^- p \rightarrow$ *neutrals* at 12 beam momenta between 300 MeV/c and 760 MeV/c. Alexander Starostin from St. Petersburg Nuclear Physics Institute has performed a preliminary determination of the angular distributions of the CEX reaction as a function of 4 momenta which is shown in fig. 4. The high statistics combined with the fact that nearly complete angular distributions are taken simultaneously means that we will be able to significantly improve these distributions

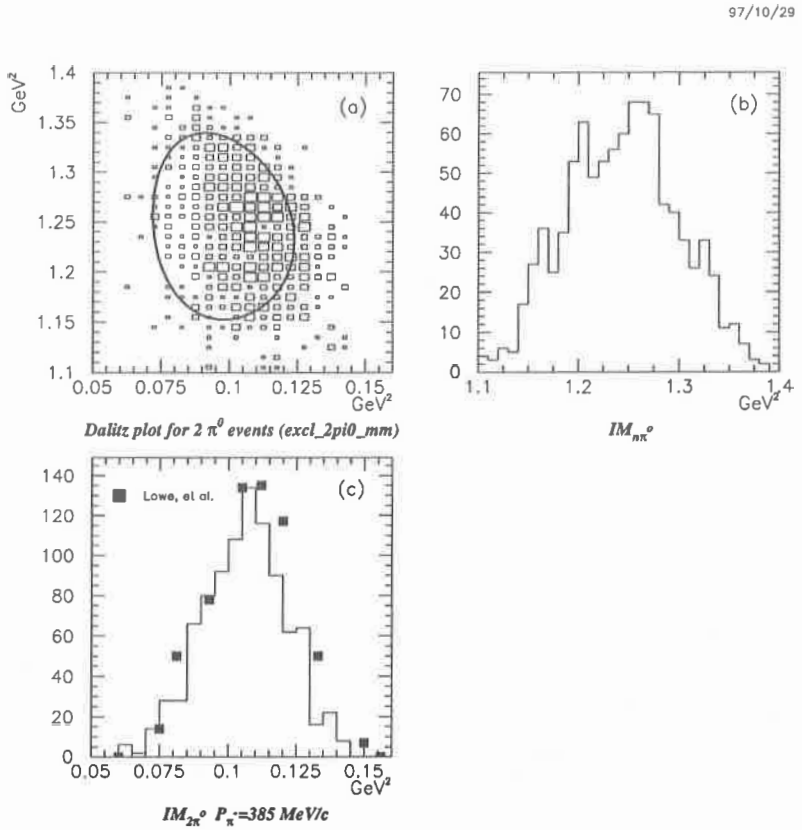

Figure 6. a) Dalitz plot for the reaction $\pi - p \rightarrow \pi^\circ\pi^\circ n$ at 385 MeV/c. This plot has not been corrected for the acceptance of the CB detector or the efficiency of the analysis. The line marks the phase space limits of the reaction. b) The n-π° invariant mass squared projection of (a). c) The $2\pi^\circ$ invariant mass squared projection of (a). The points are the data of Lowe,*et al.*[6] which were taken at 400 MeV/c.

for the partial wave analyses. One point to note is that these preliminary data already indicate a turn over in the cross section at a value of $cos\theta = -0.85$ for beam momenta above 725 MeV/c. The high rates for CEX combined with the very small background for this reaction makes it ideal for studying systematic errors. It also provides us with a means for determining the beam momentum for every data set.

Dr. Starostin also has done a preliminary analysis of η production from hydrogen. Figure 5 show angular distributions from η production for four different beam momenta. As in the CEX reacton, the cross sections are relative only. The shape of the distributions is consistent with S wave production below 720 MeV/c; however, D wave production is evident above that momentum.

Finally, we show preliminary results from thesis work by Kelly Craig of Arizona State University on the $\pi - p \rightarrow \pi^\circ\pi^\circ n$ reaction at two beam momenta, 400 MeV/c and 720 MeV/c. Figure 6 shows a Dalitz plot uncorrected for the CB acceptance at 400 MeV/c. The solid line maps the phase space limit. The X and Y projections are also shown. The $2\pi^\circ$ invariant mass is compared with that of Lowe, *et al.*[6] to show that we have good agreement with them in the general shape of the distribution. Figure 7 shows the same plots for 720

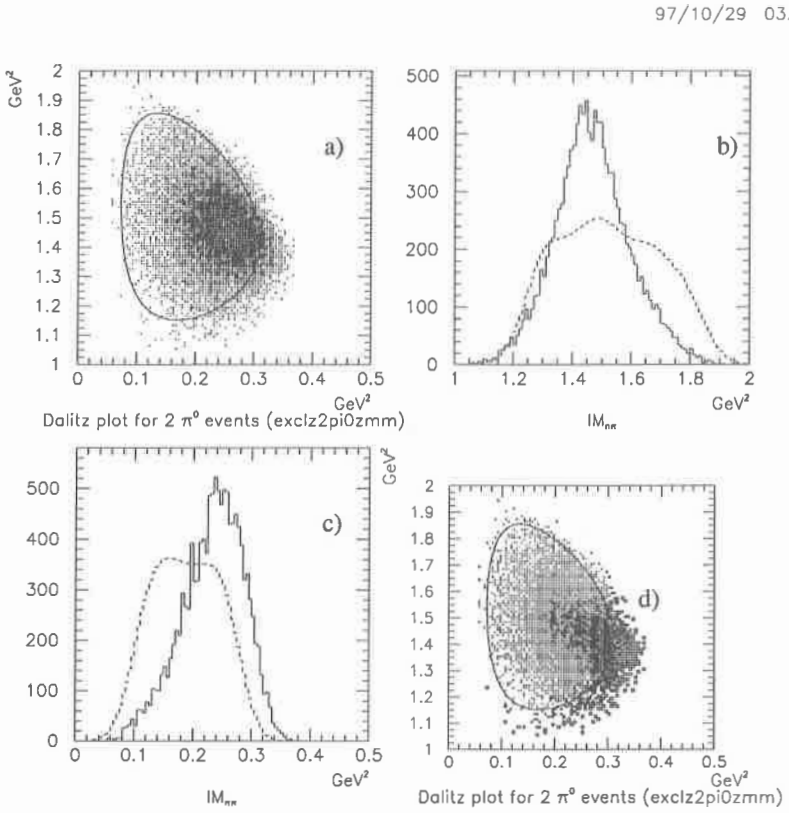

Figure 7. Similar plots as fig. 6 for 700 MeV/c beam momentum. The dashed curves in (b) and (c) are the response line shapes of the CB for phase space. d) The Dalitz plot in (a) corrected for acceptance of the CB and analysis efficiency.

MeV/c. An additional Dalitz plot which has been corrected for the CB acceptance is also shown. The extension of events outside of the phase space limits is due to resolution effects of the CB combined with the shift of the density of the Dalitz plot to the very edge of the phase space limit. At present, the data are consistent with that of Lowe, *et al.* in that the density is skewed to the high limit of the $2\pi^\circ$ invariant mass indicating $2\pi^\circ$ production is probably due to a resonance whose mass is higher than the present limit of 1500 MeV/c. The highest energy we can obtain on this line is 1530 MeV, which will allow us to investigate the D_{13} and the S_{11} resonances.

Conclusion

The successful running this year of the CB detector makes us extremely optimistic about the future of E913 and E914 to study neutral final states of baryon resonances below 2.2 GeV. The excellent resolution of the detector combined with very low backgrounds indicate that a wealth of high quality precision data will emerge from these experiments and make a significant impact on our knowledge of baryon spectroscopy. We expect to run for 12 weeks in 1998. We will focus on K^-p interactions as well as finishing our running with π^- beam. In addition, we will measure the rare decay $\eta \rightarrow \pi^\circ\gamma\gamma$, place new limits on several C and CP

violating η decays, and study the $\eta \to 3\pi^\circ$ decay.

Acknowledgment

I wish to thank the organizers of this workshop for their invitation and hospitality. This work was supported, in part, by USDOE, NSF, NSERC, Russian Ministry of Sciences, and Volkswagen Stiftung.

REFERENCES

[1] L.Wolfenstein, Phys. Rev. Lett. **51**, 1945 (1983).
[2] C.B. Chiu, *et al.*, Phys. Rev. **156**, 1415 (1967).
[3] G. Höhler, *et al.*, Handbook of Pion-Nucleon Scattering, Physics Data 12-1 (1979).
[4] J.C. Comiso *et al.*, Phys. Rev. **D12**, 738 (1975).
[5] W. Deinet, "Die Messung differentieller und totaler Wirkungsquerschnitte der Reaktion $\pi^- + p \to \eta + n$ im Bereich von 718-1050 MeV/c," Dissertation, Univ. of Karlsruhe (1968).
[6] J. Lowe,*et al.*, Phys. Rev. C **44**, 956 (1991).

Baryon Excitation Spectra and Hadronic Decays of Resonances in a Semirelativistic Chiral Quark Model

L. Ya. Glozman[1], W. Plessas[2,*], L. Theußl[2], K. Varga[3], and R. F. Wagenbrunn[2]
[1]*Department of Physics, University of Helsinki, Siltavuorenpenger 20D, FIN-00014 Helsinki*
[2]*Institute for Theoretical Physics, University of Graz, Universitätsplatz 5, A-8010 Graz, Austria*
[3]*RIKEN, Hirosawa 2-1, Wako, Saitama 35101, Japan*

Abstract

We discuss the properties of light and strange baryons in a semirelativistic constituent quark model whose hyperfine interaction relies on Goldstone-boson-exchange dynamics. It is shown that a unified description of all light- and strange-baryon spectra can be achieved in close agreement with phenomenology. The behavior of three-quark wave functions obtained from a precise variational solution of the constituent quark model is exemplified. These wave functions are then applied to calculate strong decays of N and Δ resonances within the elementary emission model.

INTRODUCTION

An intricate question of low-energy QCD is the one after the effective degrees of freedom that govern the properties of light and strange baryons. Beyond the limit of spontaneous breaking of chiral symmetry (SBχS) the original QCD degrees of freedom — *current* quarks q and gluons g — are no longer adequate. Rather, as a consequence of the SBχS, *constituent* quarks Q and Goldstone Bosons G appear and furnish the effective degrees of freedom in this energy domain [1,2]. The constituent quarks bear dynamical masses related to the $<\bar{q}q>$ condensate and couple directly to the Goldstone bosons. Thus, light and strange baryons are to be considered as systems of three constituent quarks that interact by Goldstone-boson exchange (GBE) and are subject to confinement [3,4].

CONSTITUENT QUARK MODEL BASED ON GOLDSTONE-BOSON EXCHANGE

From the simplest ansatz for an effective interaction Lagrangian coupling constituent quark fields ψ and Goldstone-boson fields $\vec{\phi}$ (the latter manifesting themselves in the pseudoscalar mesons),

$$\mathcal{L} \sim i g_{PS} \bar{\psi} \gamma_5 \vec{\lambda}^F \cdot \vec{\phi} \psi + g_S \bar{\psi} \sigma \psi, \tag{1}$$

where g_{PS} and g_S are the pseudoscalar resp. scalar coupling constants and $\vec{\lambda}^F$ are the Gell-Mann flavor matrices, one may deduce a spin- and flavor-dependent Q-Q interaction [3,4]. Its most dominant contribution to the hyperfine interaction in baryons is provided by the spin-spin component of the octet and singlet pseudoscalar meson-exchange potentials

$$\begin{aligned} V_\chi(\vec{r}_{ij}) \;=\; & \left[\sum_{F=1}^{3} V_\pi(\vec{r}_{ij}) \lambda_i^F \lambda_j^F + \sum_{F=4}^{7} V_K(\vec{r}_{ij}) \lambda_i^F \lambda_j^F \right. \\ & \left. + V_\eta(\vec{r}_{ij}) \lambda_i^8 \lambda_j^8 + \frac{2}{3} V_{\eta'}(\vec{r}_{ij}) \right] \vec{\sigma}_i \cdot \vec{\sigma}_j, \end{aligned} \tag{2}$$

*E-mail: plessas@kfunigraz.ac.at

where $\vec{\sigma_i}$ are the quark spin matrices. Note, that the σ meson exchange in (1) produces no spin-spin (and tensor) interactions and can thus effectively be included into the confinement potential. In the simplest derivation, when pseudoscalar or pseudovector couplings are employed at point-like meson-quark vertices and the boson fields satisfy the linear Klein-Gordon equation, one obtains, in static approximation, the well-known meson-exchange potentials

$$V_\gamma(\vec{r}_{ij}) = \frac{g_\gamma^2}{4\pi}\frac{1}{12 m_i m_j}\left\{\mu_\gamma^2 \frac{e^{-\mu_\gamma r_{ij}}}{r_{ij}} - 4\pi\delta(\vec{r}_{ij})\right\}, \tag{3}$$

with constituent-quark masses m_i, meson masses μ_γ ($\gamma = \pi, K, \eta, \eta'$), and the meson-quark coupling constant $\frac{g_\gamma^2}{4\pi}$. Taking into account the extended structure of the quasiparticles a suitable parametrization of these potentials turns out to be [5,6]

$$V_\gamma(\vec{r}_{ij}) = \frac{g_\gamma^2}{4\pi}\frac{1}{12 m_i m_j}\left\{\mu_\gamma^2 \frac{e^{-\mu_\gamma r_{ij}}}{r_{ij}} - \Lambda_\gamma^2 \frac{e^{-\Lambda_\gamma r_{ij}}}{r_{ij}}\right\}, \tag{4}$$

involving the cut-off parameters Λ_γ; the latter are assumed to scale with the meson masses like

$$\Lambda_\gamma = \Lambda_0 + \kappa\mu_\gamma, \tag{5}$$

where Λ_0 and κ are free parameters.

Due to the explicit chiral symmetry breaking in QCD the various quark-meson coupling constants could naturally be different. In trying to keep the number of free parameters as small as possible, a single octet coupling constant $\frac{g_8^2}{4\pi}$ is assumed for all octet mesons (π, K, η). Its value can be extracted from the phenomenological pion-nucleon coupling constant [3]. Because of the particular character of the η' meson, the singlet coupling constant may well be different from the octet one. Therefore the ratio $(g_0/g_8)^2$ is treated as a free parameter.

The chiral interaction (2) must be supplemented by the confinement potential, which is chosen in the linear form

$$V_{conf}(r_{ij}) = V_0 + C r_{ij}, \tag{6}$$

to build up the Hamiltonian of the constituent quark model:

$$H = \sum_{i=1}^{3}\sqrt{\vec{p}_i^{\,2} + m_i^2} + \sum_{i<j=1}^{3}(V_{conf} + V_\chi)_{ij}. \tag{7}$$

Here, the relativistic form of the kinetic-energy operator is employed, with $\vec{p}_i$ the 3-momentum of the constituent quarks. It provides for the inclusion of kinematical relativistic effects which turn out very important in three-quark systems. In any nonrelativistic approach these effects get compensated into the parametrization of the dynamical part, what not only leads to unrealistic parameter values of the Q-Q potential but also causes such disturbing shortcomings as $v/c > 1$ (where v is the mean velocity of the constituent quark and c is the velocity of light).

We refer to the parametrization of the GBE constituent quark model as given in Refs. [5,6]; the parameter values are summarized in Table 1. The three-quark system with the semirelativistic Hamiltonian (7) is treated by solving the Schrödinger equation with the stochastic variational method [7]. This technique has been tested in a number of benchmark cases before, e.g., opposite Faddeev calculations [7–9]. The corresponding results prove reliable to an accuracy of better than 1%.

Table 1. Parameters of the semirelativistic constituent quark model based on GBE.

Fixed parameters						
Quark masses [MeV]		Meson masses [MeV]				
m_u, m_d	m_s	μ_π	μ_K	μ_η	$\mu_{\eta'}$	$\frac{g_8^2}{4\pi}$
340	500	139	494	547	958	0.67

Free parameters				
$(g_0/g_8)^2$	Λ_0 [fm^{-1}]	κ	V_0 [MeV]	C [fm^{-2}]
1.34	2.87	0.81	-416	2.33

LIGHT AND STRANGE BARYON SPECTRA

In Fig. 1 we show the predictions of the GBE constituent quark model for all light- and strange-baryon excitation levels up to $M \lesssim 1850$ MeV; the nucleon is "normalized" to its mass of 939 MeV (by adjusting the parameter V_0 in the confinement potential). All masses corresponding to three- and four-star resonances in the most recent compilation of the PDG [10] are included.

From the results it is immediately evident that quite a satisfactory description of the spectra of all low-lying light and strange baryons is achieved in a unified framework. In particular, the level orderings of the lowest positive- and negative-parity states in the nucleon spectrum are reproduced correctly, with the $\frac{1}{2}^+$ Roper resonance $N(1440)$ falling well below the negative-parity $\frac{1}{2}^-$ and $\frac{3}{2}^-$ states $N(1535)$ and $N(1520)$, respectively.

Likewise, in the Λ and Σ spectra the positive-parity $\frac{1}{2}^+$ excitations $\Lambda(1600)$ and $\Sigma(1660)$ fall below the negative-parity $\frac{1}{2}^-$-$\frac{3}{2}^-$ states $\Lambda(1670)$-$\Lambda(1690)$ and the $\frac{1}{2}^-$ state $\Sigma(1750)$, respectively. In the Λ spectrum, at the same time, the negative-parity $\frac{1}{2}^-$-$\frac{3}{2}^-$ states $\Lambda(1405)$-$\Lambda(1520)$ remain the lowest excitations above the Λ ground state. By the correct level orderings of the positive- and negative-parity states a long-standing problem of baryon spectroscopy is resolved. At this stage, only one state is not reproduced in agreement or close to experiment, the flavor singlet $\Lambda(1405)$.

The remarkable successes of the GBE quark-quark interaction of Eqs. (2) and (4) are, of course, brought about by the particular symmetry introduced through the spin-flavor operators $\vec{\sigma}_i \cdot \vec{\sigma}_j \vec{\lambda}_i^F \cdot \vec{\lambda}_j^F$ and by the short-range part of the interaction with a proper sign [3,4]. This makes the GBE potential just adequate for the level structures found in experiment, and thus a unified description of all light- and strange-baryon spectra is possible, even though our model in the present simplest version involves only a handful of free parameters.

At the present stage, tensor forces are not yet included in our model. However, we have already made estimates and numerical tests of their influences. They turn out to be much less important for baryon masses, as compared to the spin-spin part, at least for the states considered in Fig. 1. It is clear also from phenomenology that tensor forces can play only a subordinate role as the splittings of corresponding LS-multiplets are generally small.

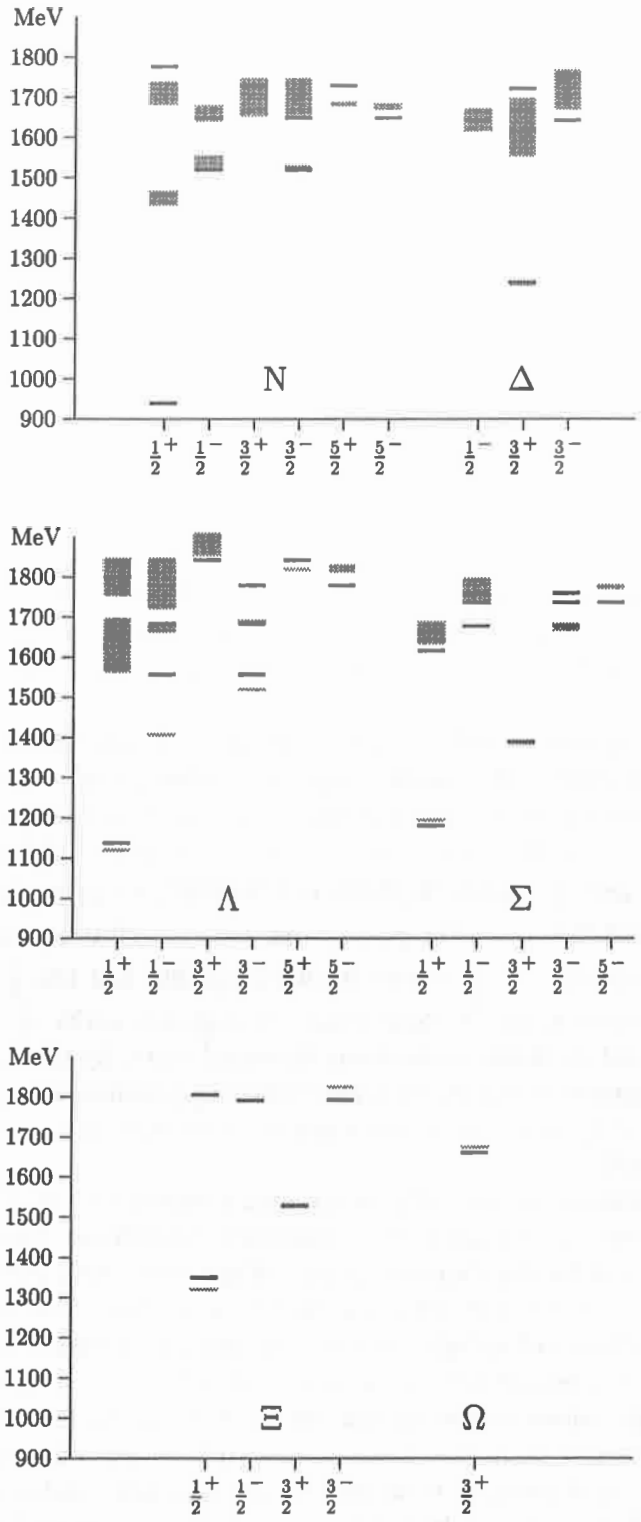

Figure 1. Energy levels of the lowest light- and strange-baryon states with total angular momentum and parity J^P. The nucleon ground state is 939 MeV. The shadowed boxes represent the experimental values with their uncertainties. The Δ, Σ^*, and Ξ^* ground-state levels practically fall into their rather tight experimental boxes.

THREE-QUARK WAVE FUNCTIONS

Once the spectra are described in a reasonable manner, it is interesting to examine the baryon wave functions. They constitute the essential ingredients for describing further baryon properties like magnetic moments, electromagnetic form factors, hadronic decays and other dynamical observables.

After projecting on the center-of-momentum frame $\vec{P} = \vec{p}_1 + \vec{p}_2 + \vec{p}_3 = 0$ the 3-Q wave function for a certain baryon state B ($B = N, \Delta, \Lambda, \Sigma, \Xi, \Omega$) can be expressed in configuration space as

$$B_{E_N}^{JM_J,P}(\vec{x},\vec{y}) = \sum_{\beta=1}^{3} \left[\psi_{E_N}^{L,P}(\vec{x}_\beta,\vec{y}_\beta)\chi_\beta^S \phi_\beta^B\right]_{JM_J}. \tag{8}$$

Here, the sum runs over the three different partitions β, with the Jacobi coordinates $\vec{x}_\beta$ and $\vec{y}_\beta$ defined in the usual way [11], see Fig. 2. $\psi_{E_N}^{L,P}(\vec{x}_\beta,\vec{y}_\beta)$ represents the spatial part of the wave-function component of partition β, for some eigenenergy E_N, total orbital angular momentum L and parity P. It is coupled with the spin wave function χ_β^S of total spin S to yield total angular momentum J, with z-component M_J. ϕ_β^B is the flavor wave function characterizing the baryon B. The six variables $(\vec{x},\vec{y})$ in Eq. (8) can be chosen as the Jacobi coordinates of either one of the specific partitions $\beta = 1, 2, 3$. The baryon wave function (8) is symmetric under the exchange of any two quarks. After angular-momentum decomposition we may view the angle-integrated 3-Q probability densities as functions of the magnitudes of the coordinate vectors, x and y. In Fig. 3 we present a few examples for the N and Δ ground states and their first two $L = 0$ excitations. It is quite instructive to observe the most probable sites for finding the three quarks at relative distances x and y.

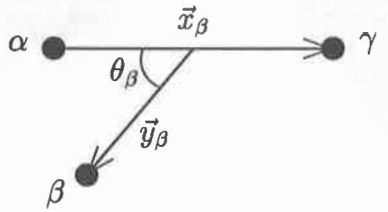

Figure 2. Jacobi coordinates for a certain three-body partition β ($\alpha, \beta, \gamma = 1, 2, 3$).

From the pictures in Fig. 3 one can already get an idea about the root-mean-square radii, and likewise the overlap of different wave functions. In Table 2 we give the results for the root-mean-square radii of the octet and decuplet ground states for point-like constituent quarks. They are computed according to the formula

$$< r^2 >= \frac{1}{3}\sum_{i=1}^{3} \int d^3x d^3y r_i^2(\vec{x},\vec{y}) \left|B_{E_N}^{JM_J,P}(\vec{x},\vec{y})\right|^2, \tag{9}$$

where $\vec{r}_i$ is the coordinate of the quark i relative to the 3-Q center of mass. Though the values are not realistic, it is satisfying to find them in reasonable relations among each other. It is quite conceivable that the phenomenological sizes of the baryons can be reproduced, once the finite extensions of the constituent quarks are taken into account.

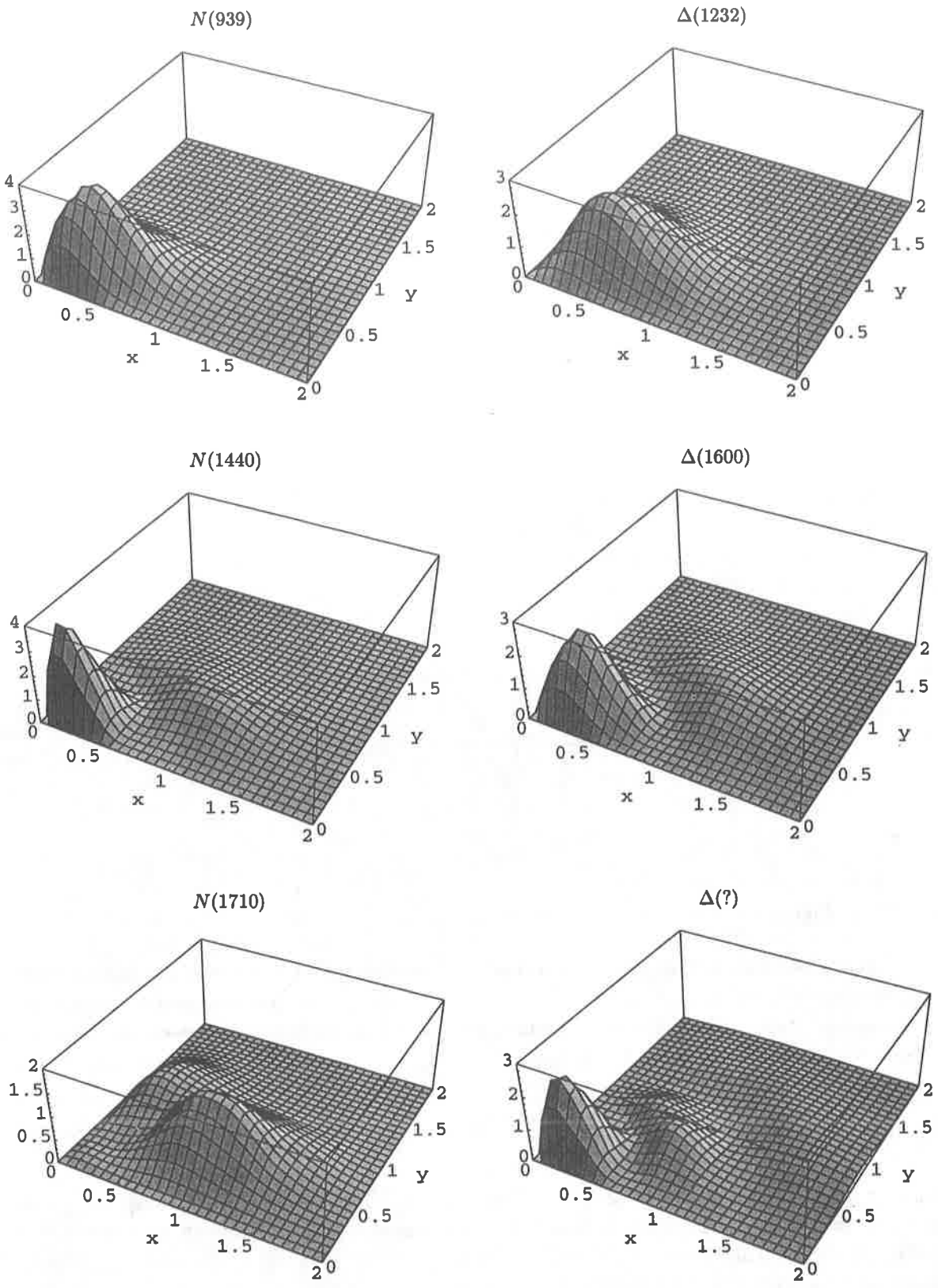

Figure 3. Angle-integrated 3-Q probability densities as functions of the magnitudes of Jacobi coordinates x and y (see Fig. 2 and the text) for the N and Δ ground states and the first two $L = 0$ (positive-parity) excitations.

Table 2. Root-mean-square radii of the octet and decuplet ground states as defined by Eq. (9) for point-like constituent quarks.

	N	Δ	Λ	Σ	Σ^*	Ξ	Ξ^*	Ω
$\sqrt{< r^2 >}$ [fm]	0.304	0.390	0.317	0.298	0.398	0.320	0.399	0.395

HADRONIC DECAYS OF N AND Δ RESONANCES

One of the simplest applications of the 3-Q wave functions consists in the calculation of strong decays in the elementary emission model (EEM). This model was invented a long time ago [12–17] and assumes the emission of a meson from a point-like constituent quark; for details see ref. [18]. We take the corresponding decay operator with recoil corrections, i.e. in the form

$$\hat{O} = -\frac{ig_8}{2m_i}\lambda_i^F e^{-i\vec{q}\cdot\vec{r}_i}\left[\left(1+\frac{\omega}{2m_i}\right)\vec{\sigma}_i\cdot\vec{q} - \frac{\omega}{m_i}\vec{\sigma}_i\cdot\vec{p}_i\right], \tag{10}$$

where $F = 1, 2, 3$ for pion and $F = 8$ for η decays. In Eq. (10) ω and $\vec{q}$ are the meson energy and momentum and $\vec{r}_i$ and $\vec{p}_i$ the coordinate and momentum of the constituent quark i, respectively.

The results for the partial π- and η-decay widths of the 13 lowest-lying N and Δ resonances are given in Tables 3 and 4. There we have also provided a comparison to a similar recent work by Cano et al. [19], where a one-gluon-exchange Q-Q interaction was used; the results of their model have been recalculated with the 3-Q wave functions from our stochastic variational method. Note that, contrary to some other works in the literature, we always use the theoretical resonance energies of the specific quark model rather than the experimental ones. Also we do not introduce any further phenomenological parametrization for the description of the decay widths, in contrast to previous papers, e.g., Refs. [20,21].

As we cannot discuss here all the results in detail, we give just a global characterization. Only a few theoretical decay widths compare well with experiment*; for the GBE model, e.g., $N(1535) \to \Delta\pi$, $N(1650) \to \Delta\pi$, $N(1680) \to \Delta\pi$, $N(1710) \to N\pi$, or $N(1720) \to \Delta\pi$. Others are close to experiment or correct by the order of magnitude, for example, $N(1650) \to N\pi$, $N(1700) \to N\pi$, $\Delta(1600) \to N\pi$, and also $N(1520) \to N\pi$, $\Delta(1232) \to N\pi$, $\Delta(1620) \to N\pi$, or $\Delta(1620) \to \Delta\pi$. On the other hand, there are a number of severe shortcomings. For instance, the decays of the radial excitations into their respective ground states, $N(1440) \to N\pi$ or $\Delta(1600) \to \Delta\pi$, cannot be described at all.

The η-decays are usually suppressed. It is remarkable that especially in the GBE model the two η-decays that have considerable widths experimentally (in the 1996 compilation of the PDG [10]) are also just the (only) ones with the largest theoretical widths – though the magnitudes are not really in agreement with the experimental values. With respect to the $N(1535) \to N\eta$ decay the GBE model shows an important improvement over the OGE model: due to the correct reproduction of the resonance energy this decay is possible with a

*The experimental data in Tables 3 and 4 represent the central values and ranges of partial decay widths calculated from the mean values of the respective total resonance widths according to the estimates given by the PDG in Ref. [10]

Table 3. Predictions for N and Δ π-decay widths of the EEM in comparison to experiment [10]. The columns labeled GBE contain the results of the GBE constituent quark model [5,6]. The columns labeled OGE provide a comparison to a model by Cano et al., potential V_I in ref. [19], based on one-gluon-exchange dynamics (recalculated results). In all cases the theoretical values of the resonance energies given in the first columns have been used (instead of the experimental ones). All numbers in MeV.

Resonance		Theoretical Energy		$N\pi$ Decay			$\Delta\pi$ Decay		
N^*, Δ^*	J^P	GBE	OGE	Exp.	GBE	OGE	Exp.	GBE	OGE
$N(1440)$	$\frac{1}{2}^+$	1459	1701	228 ± 18	8	0.4	88 ± 18	15	68
$N(1520)$	$\frac{3}{2}^-$	1520	1457	66 ± 6	38	51	24 ± 6	160	36
$N(1535)$	$\frac{1}{2}^-$	1520	1457	67 ± 15	566	139	< 2	3	1
$N(1650)$	$\frac{1}{2}^-$	1648	1647	109 ± 26	156	26	6 ± 5	6	10
$N(1675)$	$\frac{5}{2}^-$	1648	1647	68 ± 8	13	27	83 ± 8	27	43
$N(1680)$	$\frac{5}{2}^+$	1729	1789	85 ± 7	19	86	13 ± 7	22	11
$N(1700)$	$\frac{3}{2}^-$	1648	1647	10 ± 5	2	4	75 ± 20	813	320
$N(1710)$	$\frac{1}{2}^+$	1777	1855	15 ± 5	9	31	28 ± 13	114	110
$N(1720)$	$\frac{3}{2}^+$	1729	1789	23 ± 8	349	234	11 ± 8	4	4
$\Delta(1232)$	$\frac{3}{2}^+$	1240	1248	120 ± 5	88	100			
$\Delta(1600)$	$\frac{3}{2}^+$	1721	1945	61 ± 26	95	107	193 ± 53	0.3	0.01
$\Delta(1620)$	$\frac{1}{2}^-$	1642	1571	38 ± 8	76	17	68 ± 23	30	17
$\Delta(1700)$	$\frac{3}{2}^-$	1642	1571	45 ± 15	10	0.1	135 ± 45	398	2

considerable width whereas in the OGE model the resonance energy falls below the η-decay threshold (see Fig. 1 in ref. [19] or Fig. 1 in ref. [22]), and the decay is thus forbidden.

We should, however, beware of attributing too much relevance to the present results for hadronic decays. We must bear in mind that the applied EEM decay model is rather unrealistic. Also the constituent quark models need to be improved to produce broad (rather than sharp) resonance levels.

SUMMARY

In the present stage, the achievements of the semirelativistic quark model with GBE hyperfine interactions lie in the description of the light- and strange-baryon spectra. The GBE constituent quark model has thus cured some notorious difficulties of baryon spectroscopy. However, it also needs a number of further improvements, e.g., with respect to incorporating further components from meson-exchange forces (tensor interactions, ...) or including additional Fock states ($QQQ\pi$, $QQQ\eta$, $QQQK$, ...) into the wave functions. The coupling to decay channels will affect especially those states lying close to continuum thresholds. One may expect, in particular, that thereby the $\Lambda(1405)$ level will be shifted down since it lies close to $\bar{K}N$ threshold [23]. Furthermore such a refinement, leading to a unitary model, will especially influence also the higher-lying resonances. Evidently it would also make the 3-Q

Table 4. Predictions for N η-decay widths of the EEM in comparison to experiment [10]. Same description as in Table 3.

Resonance		Theoretical Energy		$N\eta$ Decay		
N^*	J^P	GBE	OGE	Exp.	GBE	OGE
$N(1440)$	$\frac{1}{2}^+$	1459	1701		0	2
$N(1520)$	$\frac{3}{2}^-$	1520	1457		0.04	0
$N(1535)$	$\frac{1}{2}^-$	1520	1457	64 ± 19	129	0
$N(1650)$	$\frac{1}{2}^-$	1648	1647	10 ± 5	284	158
$N(1675)$	$\frac{5}{2}^-$	1648	1647		1	2.4
$N(1680)$	$\frac{5}{2}^+$	1729	1789		0.2	2
$N(1700)$	$\frac{3}{2}^-$	1648	1647		0.2	0.4
$N(1710)$	$\frac{1}{2}^+$	1777	1855		2.9	1.6
$N(1720)$	$\frac{3}{2}^+$	1729	1789		17	25

wave functions more appropriate for calculations of resonance decays.

REFERENCES

[1] A. Manohar and H. Georgi, Nucl. Phys. **B234**, 189 (1984).
[2] D. I. Diakonov and V. Yu. Petrov, Nucl. Phys. **B272**, 457 (1986).
[3] L. Ya. Glozman and D. O. Riska, Phys. Rep. **268**, 263 (1996).
[4] L. Ya. Glozman, in: H. Latal and W. Schweiger (eds.), *Perturbative and Nonperturbative Aspects of Quantum Field Theory*, Lecture Notes in Physics, vol. 479 (Springer, Berlin, 1997).
[5] L. Ya. Glozman, W. Plessas, K. Varga, and R. F. Wagenbrunn, Preprint hep-ph/9706507.
[6] L. Ya. Glozman, Z. Papp, W. Plessas, K. Varga, and R. F. Wagenbrunn, Preprint nucl-th/9705011.
[7] K. Varga and Y. Suzuki, Phys. Rev. C **52**, 2885 (1995); K. Varga, Y. Ohbayasi, and Y. Suzuki, Phys. Lett. **B396**, 1 (1997).
[8] L. Ya. Glozman, Z. Papp, W. Plessas, K. Varga, and R. F. Wagenbrunn, Nucl. Phys. **A623**, 90c (1997).
[9] L. Ya. Glozman, Z. Papp, and W. Plessas, Phys. Lett. **B381**, 311 (1996).
[10] Particle Data Group, Phys. Rev. D **54**, 1 (1996).
[11] E. W. Schmid and H. Ziegelmann, *The Quantum-Mechanical Three-Body Problem* (Vieweg, Braunschweig, 1974).
[12] C. Becchi and G. Morpurgo, Phys. Rev. **149**, 1284 (1966).
[13] A. Mitra and M. Ross, Phys. Rev. **158**, 1630 (1967).
[14] R. van Royen and V. F. Weisskopf, Nuovo Cim. **50A**, 617 (1967).

[15] H. J. Lipkin, H. R. Rubinstein, and H. Stern, Phys. Rev. **161**, 1502 (1967).
[16] D. Faiman and A. W. Hendry, Phys. Rev. **173**, 1720 (1968); ibid. **180**, 1572 (1969).
[17] D.R. Divgi, Phys. Rev. **175**, 2027 (1968)
[18] A. Le Yaouanc, L. Oliver, O. Pène, and J.-C. Raynal, *Hadron Transitions in the Quark Model* (Gordon and Breach, New York, 1988).
[19] F. Cano, P. González, S. Noguera, and B. Desplanques, Nucl. Phys. **A603**, 257 (1996).
[20] R. Koniuk and N. Isgur, Phys. Rev. D **21**, 1868 (1980).
[21] R. Bijker, F. Iachello, and A. Leviatan, Phys. Rev. D **55**, 2862 (1997).
[22] L. Ya. Glozman, Z. Papp, W. Plessas, K. Varga, and R. F. Wagenbrunn, in *Proceedings of the International Conference on Perspectives in Hadronic Physics, Trieste, 1997* (World Scientific, Singapore, to appear).
[23] M. Arima, S. Matsui, and K. Shimizu, Phys. Rev. C **49**, 2831(1994).

Conformal Mapping Methods for Evaluating Dispersion Integrals

A. Donnachie
Department of Physics and Astronomy, University of Manchester,
Manchester M13 9PL, UK

Abstract

Conformal mapping techniques were used to evaluate dispersion relations to allow analyticity constraints to be imposed on amplitude analysis of pion-nucleon scattering. The procedure used is outlined and modifications suggested for application to pion photoproduction and electroproduction.

Amplitude analysis of pion-nucleon scattering and pion photoproduction and electroproduction data requires the imposition, *inter alia*, of unitarity and analyticity. The latter is most readily applied via a fixed-t partial wave dispersion relation, which can be written generically as:

$$Ref_l(s) = f_l^{Born} + \frac{P}{\pi}\int_{(m+\mu)^2}^{\infty} ds' \frac{Imf_l(s')}{s'-s} + \frac{1}{\pi}\int_{(m+\mu)^2}^{\infty} ds' \sum_{l'} K_{l,l'}(s,s') Imf_{l'}(s') \qquad (1)$$

where m is the nucleon mass, μ the pion mass and $K_{l,l'}(s,s')$ is a non-singular kernel. The Born terms are given and the non-singular integral presents no difficulty other than deciding where to terminate the sum. This is a problem of physics, not mathematics. The reverse is true of the singular s'-integral, the rescattering contribution, which does pose a problem of evaluation. Conformal mapping provides an analytic solution and avoids numerical instabilities.

The advantage of of dispersion-relation constraints was amply demonstrated in the early energy-independent analyses of pion-nucleon scattering (for example [1]) and we will use that to illustrate the technique.

First change the variable from s to ν where

$$\nu = s - (m+\mu)^2 \qquad (2)$$

so that the principal value integral is from 0 to ∞ and not from $(m+\mu)^2$ to ∞. Then make the further change to

$$x = cos\zeta = \frac{\nu_0 - \nu}{\nu_0 + \nu} \qquad (3)$$

which maps the cut 0 to ∞ in the ν-plane on to the cut -1 to 1 in the x-plane. ν_0 is an arbitrary constant and for obvious reasons is called the "conformal zero". From eqn.(2) we have that

$$(1-x^2)^{\frac{1}{2}} = sin\zeta = \frac{2(\nu\nu_0)^{\frac{1}{2}}}{\nu+\nu_0} \qquad (4)$$

From this we see that $(1-x^2)^{\frac{1}{2}} \sim q$ as $\nu \to 0$ and $\sim q^{-1}$ as $\nu \to \infty$.

By unitarity, $Imf_l \sim q^{2l+1}$ as $\nu \to 0$ and $\sim q^{-2l-1}$ as $\nu \to \infty$, and hence the approximation

$$Imf_l = \sum_{n=1}^{N} a_n (1-x^2)^{l+\frac{1}{2}} C_{n-1}^{l+1}(x) \qquad (5)$$

where $C_{n-1}^{l+1}(x)$ is a Gegenbauer polynomial [2], will have the correct behaviour both at threshold and infinity.

The integral required is of the form

$$\int_0^\infty d'nu' \frac{A(\nu')}{\nu' - \nu} = -\int_{-1}^{1} dx' \Big[\frac{1}{x' - x} - \frac{1}{1 + x'}\Big] A(x') \tag{6}$$

and so the contribution to the real part of the partial wave amplitude from rescattering will be

$$[Ref_l]_{Rescattering} = \sum_{n=1}^{N} a_n [g_n^l(x) - g_n^l(-1)] \tag{7}$$

where

$$g_n^l(x) = -\frac{P}{\pi} \int_{-1}^{1} dx' \frac{(1 - x'^2)^{l+\frac{1}{2}} C_{n-1}^{l+1}(x')}{x' - x} \tag{8}$$

and the subtraction at -1, which arises naturally, ensures that the real part vanishes at infinity.

It can be shown that [3]

$$C_{n-1}^{l+1}(x) = \frac{\Gamma(2l + n + 1)\Gamma(l + \frac{3}{2})}{\Gamma(2l + 2)\Gamma(l + n + \frac{1}{2})} P_{n-1}^{(l+\frac{1}{2}, l+\frac{1}{2})}(x). \tag{9}$$

and we can write the integral in eqn.(8) as [4]

$$-\int_{-1}^{1} dx' \frac{(1 - x'^2)^{l+\frac{1}{2}} P_{n-1}^{(l+\frac{1}{2}, 1+\frac{1}{2})}(x')}{x' - x - i\epsilon} = 2(x^2 - 1)^{l+\frac{1}{2}} Q_{n-1}^{(l+\frac{1}{2}, l+\frac{1}{2})}(x) \tag{10}$$

where $Q_{n-1}^{(l+\frac{1}{2}, l+\frac{1}{2})}(x)$ is a Jacobi polynomial of the second kind.

Thus we have

$$g_n^l(x) = \frac{1}{\pi} \frac{\Gamma(2l + n + 1)\Gamma(l + \frac{3}{2})}{\Gamma(l + n + \frac{1}{2})\Gamma(2l + 2)} 2Re\Big\{(x^2 - 1)^{l+\frac{1}{2}} Q_{n-1}^{(l+\frac{1}{2}, l+\frac{1}{2})}(x)\Big\} \tag{11}$$

For $-1 \leq x \leq 1$ [4], $(x^2 - 1)^{l+\frac{1}{2}} Q_{n-1}^{(l+\frac{1}{2}, l+\frac{1}{2})}(x) =$

$$\frac{2^{2l}\Gamma(l + \frac{1}{2})\Gamma(l + n + \frac{1}{2})}{\Gamma(n + 2l + 1)} F(n, -n - 2l, \frac{1}{2} - l; \frac{1}{2} - \frac{1}{2}x) - \frac{\pi(x^2 - 1)^{l+\frac{1}{2}}}{2sin(\pi[l + \frac{1}{2}])} P_{n-1}^{(l+\frac{1}{2}, l+\frac{1}{2})}(x) \tag{12}$$

The region $\nu \geq 0$ corresponds to $x^2 \leq 1$, for which the second term in eqn.(12) is purely imaginary. Hence we have finally

$$g_n^l(x) = \frac{1}{\pi} \frac{\Gamma(l + \frac{1}{2})\Gamma(l + \frac{3}{2})}{\Gamma(2l + 2)} 2^{2l+1} F(n, -n - 2l; \frac{1}{2} - l; \frac{1}{2} - \frac{1}{2}x) \tag{13}$$

$$= \frac{1}{\sqrt{\pi}} \frac{\Gamma(l + \frac{1}{2})}{l!} F(n, -n - 2l; \frac{1}{2} - l; \frac{1}{2} - \frac{1}{2}x) \tag{14}$$

Since the second argument of the hypergeometric function is a negative integer the function reduces to a polynomial. Convenient transformations to make are [6]

$$F(n, -n - 2l; \frac{1}{2} - l; \frac{1}{2} - \frac{1}{2}x) = F(\frac{n}{2}, -\frac{n}{2} - l; \frac{1}{2} - l; 1 - x^2) \tag{15}$$

and

$$F(n,-n-2l;\frac{1}{2}-l;\frac{1}{2}-\frac{1}{2}x)=xF(\frac{n+1}{2},-\frac{n-1}{2}-l;\frac{1}{2}-l;1-x^2) \tag{16}$$

The hypergeomtric function on the right-hand side of eqn.(14) terminates for n even, and that in eqn.(15) for n odd. Thus we have

$$g^l_{2m}(x) = \frac{1}{\sqrt{\pi}}\frac{\Gamma(l+\frac{1}{2})}{l!}F(m,-m-l;\frac{1}{2}-l;1-x^2) \tag{17}$$

$$g^l_{2m+1}(x) = \frac{1}{\sqrt{\pi}}\frac{\Gamma(1+\frac{1}{2})}{l!}xF(m+1,-m-l;\frac{1}{2}-l;1-x^2) \tag{18}$$

Thus given Imf_l by eqn.(5), then eqns.(7),(16),(17) and (18) together determine the rescattering integral. The expressions in eqns.(16) and (17) terminate more quickly than the more general expression in eqn.(13), which may be beneficial if this procedure is being used in a minimisation routine.

The choice of Gegenbauer polynomials for pion-nucleon scattering was driven by the unitarity conditions on the partial-wave amplitudes. For pion photoproduction or electroproduction the kinematical factors in the multipoles have to take account of two thresholds so that their low-energy behaviour is of the form $k^m q^{l+\frac{1}{2}}$. The required q-dependence at threshold can still be obtained, replacing eqn.(5) with

$$ImM_l = \sum_{n=1}^{N} a_n(1-x^2)^{\frac{1}{2}}C^1_{n-1} \tag{19}$$

where M_l is a multipole divided by the appropriate $k^m q^l$ factor. The same procedure then applies, but with $l=0$ in all equations.

An alternative for pion photoproduction or electroproduction is to make use of the simpler Chebychev polynomials [7], $T_n(x)$ and $U_n(x)$. The starting procedure is the same, namely to map, the physical cut from $(m+\mu)^2$ to infinity in the ν-plane on to the cut -1 to 1 in the x-plane.

The Chebychev polynomials have a particularly simple representation [7]:

$$T_n(cos\theta) = cosn\theta \tag{20}$$

$$U_n(cos\theta) = \frac{sin(n+1)\theta}{sin\theta} \tag{21}$$

The relevant integral in this case is:

$$\frac{P}{\pi}\int_{-1}^{1} dx' \frac{(1-x'^2)^{\frac{1}{2}}}{x'-x}U_{n-1}(x') = -T_n(x) \tag{22}$$

so that eqn.(19) is replaced with

$$ImM_l = \sum_{n=0}^{N} a_n(1-x^2)^{\frac{1}{2}}U_n(x) \tag{23}$$

from which we obtain immediately that

$$[ReM_l]_{Rescattering} = -\sum_{n=1}^{N+1} a_{n-1}T_n(x) \tag{24}$$

REFERENCES

[1] A Donnachie, R G Kirsopp and C Lovelace: Phys.Lett.B26(1968)161
[2] *Higher Transcendental Functions* vol.II, Ed. A Erdelyi (McGraw-Hill 1953)
[3] ibid., p.174
[4] ibid., p.171
[5] ibid., p.112
[6] *Higher Transcedental Functions* vol.I, Ed A Erdelyi (McGraw-Hill 1953) p.112
[7] *Higher Transcedental Functions* vol.II, Ed A Erdelyi (McGraw-Hill 1953) p.184

Covariant Quark Models for the Baryon Spectra and Form Factors

D. O. Riska*
Department of Physics, POB 9,
00014 University of Helsinki,Finland

Abstract

The possibility of constructing simple Poincaré covariant constituent models for the baryons, which provide satisfactory spectral predictions in all flavor generations along with form factor predictions is outlined. It is argued that instant form kinematics provides the most obvious framework for construction of the current operators. The models incorporate the standard quark model phenomenology for magnetic moments and axial coupling constants.

INTRODUCTION

A natural requirement of a constituent quark model for the baryons is that it build in Poincaré invariance from the beginning, as the velocities of the confined quarks within the the baryons are close to c. The requirements of Poincaré invariance for the mass operator actually coincide with those of Galilean invariance, as the groups of Poincaré and Galilean transformations have the same little group [1,2]. Explicitly this implies that the mass operator has to commute with the total velocity and angular momentum of the system. Any rotationally invariant mass operator, which only depends only on the Jacobi coordinates of the 3 quark system in addition to spin and flavor operators meets this requirement.

Here a class of such confining mass operators is described, which with optimal parameter choices provide very satisfactory descriptions of the baryon spectrum in all flavor generations. The mass operators considered are sums of a confining term, which depends only on the Jacobi coordinates of the 3-quark system, and a flavor and spin dependent hyperfine correction. The former provides the basic shell structure of the spectrum and is readily diagonalized by means of hyperspherical harmonics [3]. The latter is built on the observation that a superior description of the baryon spectrum in all flavor generations may be achieved by assuming that the main hyperfine correction should have the flavor-spin structure which is suggested by the short range part of the Goldstone boson exchange interaction between the constituent quarks [4,5].

The quark currents that are consistent with these mass operators, and the covariance conditions, lead to values for the magnetic moments and axial coupling constants of the ground state baryons, which are similar to those obtained by conventional quark models.

THE MASS OPERATOR

The 3-Quark States

The baryon states are described by vectors in the little Hilbert space $\mathcal{H}_\ell$, which is the representation space of the direct product of the little group, $SU(2)$, with flavor and color $SU(3)$. These are functions, of the quark positions, and spin and flavor variables, which are symmetric under permutations and invariant under translations.

The representations of the Poincaré group are constructed on the tensor product of the little Hilbert space $\mathcal{H}_\ell$ with the Hilbert space $\mathcal{H}_c$ of functions of the four-velocity v, which

*E-mail: riska@pcu.helsinki.fi

is specified by 3 independent components. Translations are generated the four-momentum operator $P = \mathcal{M}v$.

The Poincaré invariant inner product of the functions representing baryon states is defined as

$$(\Psi, \Psi) = \int d^4v 2\delta(v^2 + 1)\,\theta(v^0) \int d^3\kappa \int d^3k |\Psi(v, \vec{\kappa}, \vec{k})|^2, \tag{1}$$

where $\vec{\kappa}$ and $\vec{k}$ are the momenta conjugate to the Jacobi coordinates $\vec{r} = (\vec{r}_1 - \vec{r}_2)$ and $\vec{\rho} = (2\vec{r}_3 - (\vec{r}_1 - \vec{r}_2))/\sqrt{6}$.

For the construction of quark currents currents it is convenient to define internal four-momenta p and q by

$$p := B(v)\{0, \vec{\kappa}\}, \quad q := B(v)\{0, \vec{k}\}, \tag{2}$$

so that $p^2 = |\vec{\kappa}|^2$ and $q^2 = |\vec{k}|^2$. Here $B(v)$ is a canonical boost.

This construction of unitary representations of the Poincaré group leads to point-form kinematics. Once the eigenfunctions of the mass operator are known, unitary transformations to other forms of kinematics become possible [2]. Let $\Psi_n(v, \vec{\kappa}, \vec{k})$ be eigenfunctions of $\mathcal{M}$, with eigenvalues M_n. Any state $\Psi = \sum_n \Psi_n c_n$ can be represented by functions $\Psi(\vec{P}, \vec{p}, \vec{q})$, where the unitary transformation $\Psi(v, \vec{\kappa}, \vec{k}) \to \Psi(\vec{P}, \vec{p}, \vec{q})$ is specified by the variable transformation $\{v, \vec{\kappa}, \vec{k}, n\} \to \{\vec{P}, \vec{p}, \vec{q}, n\}$ where $\vec{p} = \vec{p}(v, \vec{\kappa})$ and $\vec{q} = \vec{q}(v, \vec{k})$ are specified by eq. (2) and $\vec{P} = M_n\vec{v}$ in each term of the sum over n.

The Confining Mass Operator

We shall consider the confining part of the mass operator to have the form

$$\mathcal{M}_0 = \sqrt{3\{\vec{k}^2 + \vec{\kappa}^2 + f(R)\} + n_S\Delta_S^2}, \tag{3}$$

where the "hyperradius" R is defined as $R = \sqrt{2(\vec{r}^2 + \vec{\rho}^2)}$. In (3) the integer n_S indicates the number of strange and the parameters Δ_S is related to the flavor dependence of constituent quark masses. It is convenient to define an auxiliary variable z such that

$$r = \frac{R}{2}\sqrt{1+z}, \quad \rho = \frac{R}{2}\sqrt{1-z}\,. \tag{4}$$

The eigenfunctions of the mass operator (3) will then be products of the form

$$\phi(\vec{r}, \vec{\rho}) = \mathcal{Y}_K u_{nK}(R), \tag{5}$$

where $\mathcal{Y}_K$ is a hyperspherical harmonic of grand orbital angular momentum K:

$$\mathcal{Y}_K = [Y_{\ell_1}(\hat{r}) \otimes Y_{\ell_2}(\hat{\rho})]_{\ell m}(1+z)^{\ell_1/2}(1-z)^{\ell_2/2}P_\nu^{\ell_1+\frac{1}{2},\ell_2+\frac{1}{2}}(z). \tag{6}$$

Here $K = 2\nu + \ell_1 + \ell_2$ and P_ν is a Jacobi polynomial. The functions $u_{nK}(R)$ are solutions to the hyperradial equation

$$\left[2\left\{-\frac{1}{R^{5/2}}\frac{d^2}{dR^2}R^{5/2} + \frac{\mathcal{L}(\mathcal{L}+1)}{R^2}\right\} + f(R)\right]u_{nK}(R) = \epsilon_K^2 u_{nK}(R), \tag{7}$$

where $\mathcal{L} = K + \frac{3}{2}$. Here n is the number of nodes in the hyperradial wave function and $\mathcal{L}$ the orbital angular momentum.

The eigenvalues of the mass operator $\mathcal{M}_0$ are then

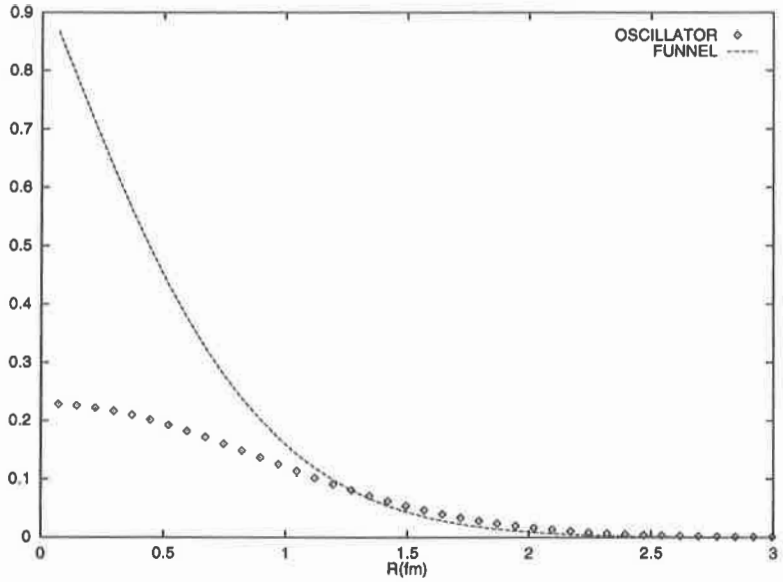

Figure 1. The ground state wave functions $u_{00}(R)$ for the confining models (9(a)) (oscillator) and (9(b)) (funnel) as functions of the hyperradius.

$$\mathcal{E}_0 = \sqrt{\epsilon_{nK}^2 + n_S \Delta_S}. \tag{8}$$

We shall here consider the following two models for the function f in (3):

$$(a): \quad f_1(R) = \frac{\omega^4}{2} R^2; \quad (b): \quad f_2(R) = -\frac{a}{R} + bR. \tag{9}$$

The former yields wave functions, which are Gaussian in the hyperradius, with the lowest three eigenvalues $\epsilon_{00} = \sqrt{18}\omega$, $\epsilon_{01} = \sqrt{24}\omega$ and $\epsilon_{10} = \epsilon_{02} = \sqrt{30}\omega$. The confining model (9(b)) yields wave functions, which are more sharply peaked at small R and flatter than Gaussians at large R. It yields a far better spectrum since it splits the SD shell in the baryon spectrum, which is degenerate in the case of the oscillator model. The ground state wave functions for these two models for the function $f(R)$ as obtained with the parameter choices described below are shown in Fig.1.

The Hyperfine Mass Splitting

The baryon spectrum in the light flavor sectors is complicated by the fact that the hyperfine interaction is sufficiently strong to mix up the shell structure of the confining well. The clearest manifestation of this is the fact that the lowest excited states of the nucleon and the $\Delta(1232)$ are positive and not negative parity states.

We consider the following phenomenological model for the hyperfine interaction:

$$\mathcal{M}' = -\{1 - \alpha[(\vec{r} \times \vec{k})^2 + (\vec{\rho} \times \vec{\kappa})^2]\} \sum_{i<j} \left\{ \sum_{a=1}^{3} C \lambda_i^a \lambda_j^a + \sum_{a=4}^{8} C_S \lambda_i^a \lambda_j^a \right\} \vec{\sigma}_i \cdot \vec{\sigma}_j. \tag{10}$$

The parameters C and C_S are to be determined from the empirical spectrum. The angular momentum dependent term in (10) is motivated by the substantial empirical splitting of the SD-shell (cf. the splitting between the $N(1440)$ and the $N(1720) - N(1680)$ multiplet).

The hyperfine interaction model (10) is suggested by the successful phenomenology achieved by the perturbative model in refs. [4,5]. The flavor-spin structure of the interaction (10) corresponds to that of the short range part of the Goldstone boson exchange mechanism in the light flavor sectors. If the hyperfine term is viewed as an effective representation of pseudoscalar exchange mechanisms between quarks, the matrix elements C represent π, and the matrix elements C_S, K and η meson exchange. The flavor-spin dependent form of the hyperfine interaction (10) is crucial for achieving the experimentally required reversal of the normal ordering of the lowest $1/2^+$ and $1/2^-$ states in the spectra of the nucleon and the Δ resonances [4].

Since the contributions $\mathcal{M}_0$ and $\mathcal{M}'$ commute, the eigenvalues of the combined mass operator $\mathcal{M}_0 + \mathcal{M}'$ take the form

$$\mathcal{E} = \mathcal{E}_0 + c, \tag{11}$$

where c is an eigenvalue of $\mathcal{M}'$. The hyperfine correction c depends on the orbital angular momentum of the 3 quark state and on the symmetry character of the spin-flavor part of the wave function.

The Current Operator

Covariance Conditions

The quark current density operators $I^\mu(x)$ have to satisfy the covariance conditions

$$U^\dagger(\Lambda) I^\mu(x) U(\Lambda) = \Lambda^\mu{}_\nu I^\nu(\Lambda^{-1}x), \quad e^{iP\cdot a} I^\mu(x) e^{-P\cdot a} = I^\mu(x+a)\,. \tag{12}$$

for arbitrary Lorentz transformations Λ and space time translations respectively. Current conservation requires that

$$[P_\nu, I^\nu(0)] = 0\,. \tag{13}$$

If $|M, \vec{P}, j, \sigma, \tau, \zeta >$ are eigenstates of the four momentum operator $P = \{\sqrt{\vec{P}^2 + M^2}, \vec{P}\}$ and the canonical spin, where σ is an eigenvalue of j_z and $\zeta = \pm 1$ is the intrinsic parity, the Lorentz invariant form factors are matrix elements of the form

$$< \kappa', \tau', \sigma', j', \vec{P}\,', M' | I^\mu(0) | M, \vec{P}, j, \sigma, \tau, \kappa >\,. \tag{14}$$

Because of the covariance of the current operator and the basis states only matrix elements with $\vec{P}\,' = -\vec{P} \equiv \vec{Q}/2$ are required, and thus the initial and final states are related kinematically. We may assume, without loss of generality, that the z-axis is in the direction of $\vec{Q}$.

Single Quark Currents

Single quark currents may be defined by kernels of the charge and transverse currents,

$$(\vec{p}_1\,', \vec{p}_2\,', \vec{p}_3\,' | \rho | \vec{p}_3, \vec{p}_2, \vec{p}_1) = 3(\vec{p}_3\,' | \rho_3 | \vec{p}_3) \delta^{(3)}(\vec{p}_1\,' - \vec{p}_1) \delta^{(3)}(\vec{p}_2\,' - \vec{p}_2). \tag{15}$$

$$(\vec{p}_1\,', \vec{p}_2\,', \vec{p}_3\,' | I_\perp | \vec{p}_3, \vec{p}_2, \vec{p}_1) = 3(\vec{p}_3\,' | I_{\perp,3} | \vec{p}_3) \delta^{(3)}(\vec{p}_1\,' - \vec{p}_1) \delta^{(3)}(\vec{p}_2\,' - \vec{p}_2). \tag{16}$$

Because of the complete antisymmetry of the baryon wave functions it is sufficient to consider the current matrix elements of only one constituent, e.g. $i = 3$.

The simplest model for the electromagnetic current density for the light and strange baryons, which matches the features of conventional quark models, is specified by kernels

$(\vec{p}_i\,'|\vec{\mathcal{I}}|\vec{p}_i)$ that depend on the momentum transfer $\vec{p}_i\,' - \vec{p}_i = \vec{Q}$, the spin and flavor variables, but do not depend on $\vec{p}_i\,' + \vec{p}_i$. That is

$$(\vec{p}_i\,'|\rho_i|\vec{p}_i) = \left[\frac{1}{2}\lambda_3^{(i)} f_3(\vec{Q}^2) + \frac{1}{2\sqrt{3}}\lambda_8^{(i)} f_8(\vec{Q}^2)\right] \otimes 1\,. \tag{17}$$

$$(\vec{p}_i\,'|I_{\perp i}|\vec{p}_i) = i\frac{\vec{\sigma}_i \times \vec{Q}}{2m_i}\left[\frac{1}{2}\lambda_3^{(i)} f_3(\vec{Q}^2) + \frac{1}{2\sqrt{3}}\lambda_8^{(i)} f_8(\vec{Q}^2)\right] \otimes 1\,. \tag{18}$$

The functions $f_3(\vec{Q}^2)$ and $f_8(\vec{Q}^2)$ represent charge form factors of the constituent quarks and the scale factor m_i represents the mass of the ith quark.

The Charge Form Factors of the Nucleons

The charge density operator (17) leads to the following expressions for the electromagnetic form factors of the nucleons:

$$G_E^p(\vec{Q}^2) = \frac{1}{2}[f_8(\vec{Q}^2) + f_3(\vec{Q}^2)]F_0(\vec{Q}^2), \quad G_E^n(\vec{Q}^2) = \frac{1}{2}[f_8(\vec{Q}^2) - f_3(\vec{Q}^2)]F_0(\vec{Q}^2). \tag{19}$$

Here the function $F_0(\vec{Q}^2)$ is defined as

$$F_0(\vec{Q}^2) = \frac{3\pi}{16\tilde{Q}^2}\int_0^\infty dR R^3 J_2(\tilde{Q}R)u_{00}^2(R), \tag{20}$$

where $u_{00}(R)$ is the ground state wave function and the variable $\tilde{Q}$ is defined as $\tilde{Q} := \sqrt{\vec{Q}^2/(1+\vec{Q}^2/4m_p^2)}$.

With point quarks, $f_3 = f_8 = 1$, the wave function for either model (2.17) or (2.18) yields a proton charge radius smaller than the empirical value, and form factors larger than the experimental values for all values of the momentum transfer. This discrepancy is reduced by assuming a spatially extended structure of the constituent quarks (an alternative would be to invoke exchange currents [6,7]). If this structure is parameterized by a common quark form factor:

$$f_3(\vec{Q}^2) = f_8(\vec{Q}^2) = \frac{1}{1+\frac{\vec{Q}^2}{\Lambda^2}}, \tag{21}$$

the calculated form factors can be brought into fair agreement with the empirical form factors. In the case of the funnel potential model (9(b)) the value $\Lambda = 707$ MeV leads to a good representation of the empirical charge form factor of the proton, as shown in Fig. 2.

The quark form factor (21) implies a mean square radius of the constituent quarks $r_q^2 \simeq 0.47$ fm^2. In Fig. 2 we compare calculated proton form factors with a parameterization of the empirical values [8]. We show form factors calculated with point quarks, $f_3 = f_8 = 1$, and with the wave functions of the models (9(a)) ("oscillator") and (9(b)) ("funnel"), together with the effect of the quark form factors (21). The potential parameters are determined by the mass spectra below.

The Magnetic Moments and Axial Couplings

The magnetic moments that are obtained from the current operator (18) are the usual linear combinations of proton to quark mass ratios of the static quark model, and are in fair

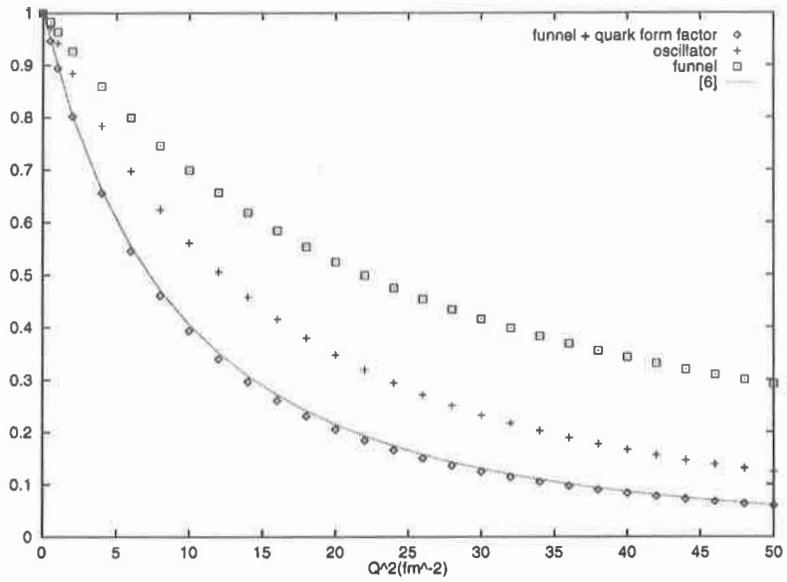

Figure 2. The proton charge form factor $G_E^p(\vec{Q}^2)$ calculated with the wave functions that correspond to the confining models (9(a)) (oscillator) and (9(b)) (funnel). The effect of inlcuding the quark form factor (21) is also shown. The curve GEPH is the phenomelological parametrization of the empirical values given in ref. [8].

agreement with the empirical values [9] for the nucleons and the strange hyperons. These expressions obtain with the assumption $f_3(0) = f_8(0) = 1$. The constituent masses of the u, d and s quarks may then be determined by the empirical magnetic moments of the proton and the Ω^- to be $m_u = m_d = 336$ MeV and $m_s = 465$ MeV.

A model for the axial current density, which corresponds to that of the vector current (18) is

$$\vec{\mathcal{A}}_i(\vec{Q}) = g_A^q \frac{\lambda_a^{(i)}}{2} \vec{\sigma}_i \, . \tag{22}$$

Here g_A^q represents the axial coupling constant for a single constituent quark. This model for the axial current leads to the same results as the conventional quark model for the g_A/g_V ratios of the nucleons and the strange hyperons. Agreement with the empirical value for the axial vector coupling for neutron decay would require that g_A^q have the value 0.76.

THE SPECTRA OF THE NUCLEON AND THE Δ RESONANCES

The spectra of the nucleon and the Δ resonances depend on the choice of the parameters C, C_S and α in the hyperfine interaction (10). The expressions for these hyperfine shifts of the states in the S, P, and SD shells of these spectra are listed in Table 1, where we have employed the symmetry assignments of ref. [4]. The real values of the empirical pole positions of the known resonances given in ref. [9] have also been listed in Table 1.

Table 1

The nucleon and Δ-states in for $L \leq 2$. The empirical energies are written above the bracketed model values, which correspond to the confining well (9(b)).

$nKL[f]_{FS}[f]_F[f]_S$	LS Multiplet	EXP (model value)	ϵ
$000[3]_{FS}[21]_F[21]_S$	$\frac{1}{2}^+, N$	939 (939)	$\epsilon_{00} - 15C + C_S$
$000[3]_{FS}[3]_F[3]_S$	$\frac{3}{2}^+, \Delta$	1209-1211 (1237)	$\epsilon_{00} - 3C - C_S$
$100[3]_{FS}[21]_F[21]_S$	$\frac{1}{2}^+, N(1440)$	1346-1385 (1376)	$\epsilon_{10} - 15C + C_S$
$011[21]_{FS}[21]_F[21]_S$	$\frac{1}{2}^-; N(1535), \frac{3}{2}^- N(1520)$	1496-1527 (1527)	$\epsilon_{01} - 3C + C_S$ $-\alpha(9C + C_S)$
$100[3]_{FS}[3]_F[3]_S$	$\frac{3}{2}^+, \Delta(1600)$	1541-1675 (1674)	$\epsilon_{10} - 3C - C_S$
$011[21]_{FS}[3]_F[21]_S$	$\frac{1}{2}^-, \Delta(1620); \frac{3}{2}^-, \Delta(1700)$	1575-1700 (1687)	$\epsilon_{01} + 3C + C_S$ $-\alpha(9C + 3C_S)$
$011[21]_{FS}[21]_F[3]_S$	$\frac{1}{2}^-, N(1650); \frac{3}{2}^-, N(1700)$ $\frac{5}{2}^-, N(1675)$	1648-1710 (1666)	$\epsilon_{01} + 3C - C_S$ $-\alpha(9C - C_S)$
$022[3]_{FS}[3]_F[3]_S$	$\frac{1}{2}^+; \Delta(1750), \frac{3}{2}^+, \Delta(1754?)$ $\frac{5}{2}^+, \Delta(1754), \frac{7}{2}^+, \Delta(?)$	1710-1780 (1832)	$\epsilon_{02} - 3C - C_S$ $+3\alpha(3C + C_S)$
$022[3]_{FS}[21]_F[21]_S$	$\frac{3}{2}^+, N(1720); \frac{5}{2}^+, N(1680)$	1656-1748 (1731)	$\epsilon_{02} - 15C + C_S$ $+3\alpha(15C - C_S)$
$020[21]_{FS}[21]_F[21]_S$	$\frac{1}{2}^+, N(1710)$	1636-1770 (1742)	$\epsilon_{02} - 3C + C_S$ $-\alpha(9C + C_S)$
$020[21]_{FS}[21]_F[3]_S$	$\frac{3}{2}^+, N(1879?)$	? (1881)	$\epsilon_{02} + 3C - C_S$ $-\alpha(9C - C_S)$
$022[21]_{FS}[21]_F[21]_S$	$\frac{3}{2}^+, N(1900); \frac{5}{2}^+, N(2000)$	1879-2175 (1875)	$\epsilon_{02} - 3C + C_S$ $+\frac{\alpha}{2}(27C - 5C_S)$
$022[21]_{FS}[21]_F[3]_S$	$\frac{1}{2}^+, N(?); \frac{3}{2}^+, N(?)$ $\frac{5}{2}^+ N(?); \frac{7}{2}^+, N(1990)$	1920-2114 (1915)	$\epsilon_{02} + 3C - C_S$ $-\frac{\alpha}{2}(9C - 5C_S)$
$020[21]_{FS}[3]_F[21]_S$	$\frac{1}{2}^+, \Delta(1910)$	1792-1950 (1902)	$\epsilon_{02} + 3C + C_S$ $-\alpha(9C + 3C_S)$
$022[21]_{FS}[3]_F[21]_S$	$\frac{3}{2}^+, \Delta(1920); \frac{5}{2}^+, \Delta(1905)$	1794-1870 (1936)	$\epsilon_{02} + 3C + C_S$ $-\frac{\alpha}{2}(9C + 3C_S)$

With the parameter values $a = 5.66$ fm^{-1} and $b = 6.09$ fm^{-3} in the mass operator model (9(b)) and with the parameter values $C = 28$ MeV, $C_S = 19$ MeV and $\alpha = 0.22$ in the hyperfine term (10) we obtain very satisfactory energies for all the known states. The eigenvalues ϵ_{nK} determined by the first two of these values are

$$\epsilon_{00} = 1340\text{MeV}, \epsilon_{01} = 1652\text{MeV}, \epsilon_{10} = 1777\text{MeV}, \epsilon_{02} = 1867\text{MeV}. \tag{23}$$

The same value for ϵ_{00} obtains for the oscillator model (9(a) with $\omega = 316$ MeV. been calculated with these parameter values.

The value for C_S is directly determined by the empirical mass splitting between the Σ and and $\Sigma(1385)$ hyperons:

$$m[\Sigma(1385)] - m[\Sigma] = 10C_S, \tag{24}$$

The value for the parameter C is then chosen so as to obtain agreement with the empirical $N\Delta$ splitting (Table 1):

$$m[\Delta(1232)] - m[N] = 12C - 2C_S. \tag{25}$$

Finally the value for the parameter α is chosen so as to obtain agreement with the splitting between the SD shell multiplets $N(1440)$ and $N(1720) - N(1680)$ multiplets.

The calculated resonance energies in Table 1 agree with the empirical pole positions of the known states to within 2 % in most cases. A number of the still missing states have been identified in recent phase shift analyses. The $\frac{3}{2}^+$ member of the $L = 2$ Δ multiplet near 1750 MeV has been located in ref. [10] at 1754 MeV. In that analysis a P_{13} state has also been located at 1879 MeV: this corresponds well to the $L = 0$ nucleon resonance predicted at 1881 MeV. The additional P_{11} resonance predicted at 1916 MeV may be related to the additional, if somewhat lower lying P_{11} resonance found in the phase shift analysis [11].

THE STRANGE HYPERONS

The parameter values above may be employed directly to the spectrum of the strange $S = -1$ hyperons. The only additional parameter required is the mass parameter Δ_S in (3). With $\Delta_S = 587$ MeV and the confining potential (9(b)) the spectrum of the Λ -hyperon is obtained satisfactorily. The one missing feature is the large spin-orbit splitting of the $\Lambda(1405) - \Lambda(1520)$ multiplet, which is expected to have an anomalously large $\bar{K}N$ -admixture [12]. The peculiar aspect of this flavor singlet multiplet is brought out by the fact that it is the only P-shell baryon multiplet for which the empirical spin-orbit splitting is not consistent with zero.

The quality of the Λ spectrum given by the model (Table 2) is similar to that of ref. [4]. One $3/2^-$ state in the P shell of the Λ spectrum near 1800 MeV remains to be found experimentally. This state would correspond to the $N(1700)$ resonance in the nucleon spectrum.

The still uncertain quantum number assignments in the empirical Σ hyperon spectrum rules out a definite assessment of the quality of the predicted Σ spectrum, which is obtained with the same parameter values. The energies of low lying well established positive parity Σ resonances $\Sigma(1385)$ and $\Sigma(1660)$ and the negative parity $\Sigma(1775)$ and $\Sigma(1915)$ resonances are however in satisfactory agreement with the empirical energies.

DISCUSSION

The present formulation of Poincaré covariant quark models illustrates the possibility of satisfying all the requirements of relativistic covariance, while reproducing the good phenomenological results of conventional constituent quark models for the magnetic moments and axial couplings along with a good description of the known baryon spectrum. The emphasis in the present work is consistency with general principles and simplicity, at the price of abandoning the notion of constituent quarks as a system of free particles that "incidentally" are confined in an infinite potential well. The key to the satisfactory description of the spectrum here is the addition of a simple spin- and flavor dependent hyperfine term to the confining mass operator [4,5].

Table 2

The S, P and SD shell states in the Λ hyperon spectrum. The column ϵ contains the eigenvalues of the mass operator. The averages over the multiplets of of the empirically extracted mass values are denoted EXP. The model values obtained with the confining well (9(b)) and the hyperfine interaction (10) are listed below the empirical ones.

$nKL[f]_{FS}[f]_F[f]_S$	LS Multiplet	EXP (model value)	ϵ $\sqrt{\epsilon_{nK}^2+\Delta_S^2}-c$
$000[3]_{FS}[21]_F[21]_S$	$\frac{1}{2}^+,\Lambda$	1116 (1116)	$\hat{\epsilon}_{00}-9C-5C_S$
$011[21]_{FS}[111]_F[21]_S$	$\frac{1}{2}^-,\Lambda(1405)$ $\frac{3}{2}^-,\Lambda(1520)$	1405-1520 (1535)	$\hat{\epsilon}_{01}-3C-5C_S$ $-\alpha(3C+5C_S)$
$100[3]_{FS}[21]_F[21]_S$	$\frac{1}{2}^+,\Lambda(1600)$	1560-1700 (1524)	$\hat{\epsilon}_{10}-9C-5C_S$
$011[21]_{FS}[21]_F[21]_S$	$\frac{1}{2}^-,\Lambda(1670)$ $\frac{3}{2}^-\Lambda(1690)$	1660-1695 (1640)	$\hat{\epsilon}_{01}-3C+C_S$ $-\alpha(3C+7C_S)$
$011[21]_{FS}[21]_F[3]_S$	$\frac{1}{2}^-,\Lambda(1800);\frac{3}{2}^-,\Lambda(?)$ $\frac{5}{2}^-,\Lambda(1830)$	1720-1830 (1773)	$\hat{\epsilon}_{01}+3C-C_S$ $-2\alpha(3C+C_S)$
$020[21]_{FS}[111]_F[21]_S$	$\frac{1}{2}^+,\Lambda(1810)$	1750-1850 (1739)	$\hat{\epsilon}_{02}-3C-5C_S$ $-\alpha(3C+5C_S)$
$022[3]_{FS}[21]_F[21]_S$	$\frac{3}{2}^+,\Lambda(1890)$ $\frac{5}{2}^+,\Lambda(1820)$	1815-1910 (1839)	$\hat{\epsilon}_{02}-9C-5C_S$ $+3\alpha(9C+5C_S)$
$020[21]_{FS}[21]_F[21]_S$	$\frac{1}{2}^+,\Lambda(?)$	? (1844)	$\hat{\epsilon}_{02}-3C+C_S$ $-\alpha(3C+7C_S)$
$020[21]_{FS}[21]_F[3]_S$	$\frac{3}{2}^+,\Lambda(?)$	? (1977)	$\hat{\epsilon}_{02}+3C-C_S$ $-2\alpha(3C+C_S)$
$022[21]_{FS}[21]_F[3]_S$	$\frac{1}{2}^+,\Lambda(?);\frac{3}{2}^+,\Lambda(?)$ $\frac{5}{2}^+\Lambda(?);\frac{7}{2}^+,\Lambda(2020)$	2020? (2001)	$\hat{\epsilon}_{02}+3C-C_S$ $-2\alpha(3C-2C_S)$
$022[21]_{FS}[111]_F[21]_S$	$\frac{3}{2}^+,\Lambda(?);\frac{5}{2}^+,\Lambda(2110?)$	2090-2140 (1916)	$\hat{\epsilon}_{02}-3C-5C_S$ $+\frac{\alpha}{2}(21C+35C_S)$
$022[21]_{FS}[21]_F[21]_S$	$\frac{3}{2}^+,\Lambda(?);\frac{5}{2}^+,\Lambda(2110?)$	2090-2140 (1959)	$\hat{\epsilon}_{02}-3C+C_S$ $+\frac{\alpha}{2}(21C+C_S)$

The choice of instant form kinematics is motivated by the fact that the obvious alternative of point form kinematics would require a current operator that depends on the velocities rather than the momentum transfer $\vec{Q}$. Replacement of the the transverse current operator $\vec{\sigma}\times\vec{Q}$ (18), by an operator of the form $\vec{\sigma}\times(\vec{v}'-\vec{v})$ would imply magnetic baryon magnetic moments that are inversely proportional to the baryon mass rather than to the constituent quark mass. The empirical magnetic moments of e.g the proton and the Ω^- definitely require scaling with the inverse quark mass.

The covariant quark models described here may be applied to the calculation of the electromagnetic form factors and transition amplitudes of the baryons for all the states in the S, P and D shells of the baryons. The requirements of Poincaré invariance are built in ab initio. The models can be extended to incorporate configuration mixing through tensor components in the hyperfine term, if experimental results for the transition form factors suggest the need for it.

ACKNOWLEDGMENTS

This material represents a preview of a more comprehensive report coauthored with F. Coester [13], whose influence throughout the text will be apparent. The work is supported in part by grant #34081 of the Academy of Finland.

REFERENCES

[1] R. Haag, *Local Quantum Physics* Sec. I.3.2 Springer Verlag (1992)
[2] F.Coester and D.O.Riska, "Poincaré Covariant Quark Models of Baryon Form Factors", hep-ph/9707388 (1997)
[3] M.Fabre de la Ripelle, Few Body Systems, Supp.2, 489 (1987)
[4] L.Ya. Glozman and D.O.Riska, Phys.Rept. **268**, 268 (1996)
[5] L.Ya. Glozman and D.O.Riska, Nucl.Phys. **A603**, 326 (1996)
[6] K. Dannbom et al., Nucl. Phys. **A616**, 555 (1997)
[7] C. Helminen, hep-ph/9711252
[8] G. Höhler et al., Nucl. Phys. **B114**, 505 (1976)
[9] Particle Data Tables Phys. Rev. **D 54**, 601 (1996)
[10] D. M. Manley and E. M. Saleski, Phys. Rev. D45, 4002 (1992)
[11] M. Batinic et al., Phys. Rev. **C51**, 2310 (1995)
[12] R. H. Dalitz et al., Proc. Int. Conf. Hypernuclear and Kaon Physics, Max Planck Inst. f. Kernphysik, Heidelberg, 201 (1982)
[13] F. Coester, K. Dannbom and D. O. Riska, hep-ph/9711458

Recent Progress in the Photo- and Electroproduction of Kaons on the Nucleon

T. Mart
Jurusan Fisika, FMIPA, Universitas Indonesia, Depok 16424, Indonesia
C. Bennhold and H. Haberzettl
Center for Nuclear Studies, Department of Physics,
The George Washington University, Washington, D.C. 20052, U.S.A.

Abstract

Several recent models in kaon electromagnetic production on the nucleon are reviewed. The use of different prescriptions to remedy the violation of gauge invariance after inclusion of hadronic form factors is presented. The application of the corresponding elementary operator in the investigation of strange hadron form factors is briefly discussed.

INTRODUCTION

Among the impressive characteristics of the new results from TJNAF is the data quality which had not been achieved in previous experiments [1]. These new results will clarify some ambiguities in old data and will severely limit the number of degrees of freedom that theorists and phenomenologists can exploit and, therefore, drastically constrain the number of theoretical models which try to explain the reactions. On the theoretical side, the interest in strangeness electromagnetic production has been revived more than ten years ago, due to the construction of new accelerators which have sufficient energy and intensity for exploring the regions beyond the experimental ability of the past.

It is the aim of this note to review recent theoretical models of kaon electromagnetic production, especially the isobaric one, and to discuss a number of achievements that has been attained in the elementary operator as well as in the application of this operator. We feel that further improvement of theoretical models is inevitable with the start of data flows from TJNAF, ELSA, GRAAL, and other accelerator facilities.

RECENT MODELS AND OPEN PROBLEMS

In an attempt to recover a low energy theorem, which is based on chiral symmetry, a chiral quark model for kaon photoproduction on the nucleon has been introduced by Li [2]. The model is parameterized by a set of parameters which includes the constituent quark masses and coupling constants between the Goldstone bosons and quarks. For both $p(\gamma,K^+)\Lambda$ and $p(\gamma,K^+)\Sigma^0$ channels the model gives satisfactory results. An extension to all $K\Sigma$ channels has also been done [3], where the calculation is in good agreement with experimental data, although we will comment on the $K^0\Sigma^+$ differential cross section in the next subsection.

Steininger and Meißner calculated the $p(\gamma,K^+)\Lambda$, $p(\gamma,K^+)\Sigma^0$, and $p(\gamma,K^0)\Sigma^+$ reactions using one loop heavy baryon chiral perturbation theory [4]. They reproduced the few total cross section data in the (γ,K^+) channels up to 100 MeV above thresholds, especially in the $K^0\Sigma^+$ channel their prediction is in good agreement with the new SAPHIR data [5]. The predicted recoil polarization fits experimental data well, however the experimental data for the recoil polarization are averaged between threshold and 1.5 GeV, whereas the theoretical comparison is made at $E_\gamma^{\rm lab} = 1.21$ GeV. Such an energy range is clearly too large for a calculation which is supposed to be valid near threshold. Future experimental data should be able to resolve this issue.

A coupled-channels model from Kaiser *et al.* has also calculated those three channels [6]. Using s-waves amplitudes of the SU(3) chiral meson-baryon Lagrangian they are able to reproduce the total cross sections up to 200 MeV above threshold, whereas for higher energies the predictions are poor.

Nevertheless, this approach provides progress in phenomenological analyses of kaon electromagnetic production since it includes 16 different channels in one calculation, thus providing a better consistency check for all channels. In view of unitarity, a coupled channel approach is almost inevitable, since neglecting the final meson-baryon interaction in the full (γ, K) T-matrix automatically leads to a violation of unitarity. Physically, this means the flux that can "leak out" into inelastic channels has not been properly accounted for.

The most recent coupled-channels approach by employing the K-matrix approximation within an effective Lagrangian framework has been performed by Feuster and Mosel [7]. The model is an extension from the hadronic sector where only the on-shell part of the intermediate propagator G in the Bethe-Salpeter equation is taken into account. The model works moderately well for the $K^+\Lambda$ photoproduction. An extension to the $p(\gamma, K^+)\Sigma^0$ process as well as to electroproduction is in progress.

For the production at higher energies Regge analysis is usually more satisfactory than other approaches. Previous analyses were performed by making use of the t-channel trajectories, such as K^+, $K^*(892)$, and $K^{**}(1420)$ [8]. In both leading channels the model reproduces the differential cross section data very well. A recent improvement has been suggested in Ref. [9], where the electric term of the s-channel Born terms is included in the amplitude in order to preserve gauge invariance.

Isobaric Models

The isobaric model provides a simple tool to analyze kaon photoproduction off the nucleon because it is relatively easy to calculate and to use for production on nuclei. It is based on suitable Feynman diagrams shown in Fig. 1 for s-, u-, and t-channel, with some unknown coupling parameters to be adjusted in order to reproduce the experimental data. Using standard procedures one can construct the invariant amplitude

$$\mathcal{M}_{\mathrm{fi}}(s,t,k^2) \;=\; \bar{u}(p_Y) \sum_{j=1}^{6} A_j(s,t,k^2)\, M_j\, u(p_N)\,, \tag{1}$$

and calculate the differential cross section for an experiment without polarization

$$\frac{d\sigma_v}{d\Omega_K} \;=\; \frac{d\sigma_T}{d\Omega_K} + \varepsilon\,\frac{d\sigma_L}{d\Omega_K} + [2\varepsilon(1+\varepsilon)]^{\frac{1}{2}}\,\frac{d\sigma_{TL}}{d\Omega_K}\cos\phi_K + \varepsilon\,\frac{d\sigma_{TT}}{d\Omega_K}\cos 2\phi_K\,. \tag{2}$$

Experimental data for photoproduction are only available for the first term, whereas in electroproduction ϕ_K has been averaged in most cases. Allowing for the polarization in electron, target, and recoil, the cross sections may be written in terms of response functions as

$$\begin{aligned}\frac{d\sigma_v}{d\Omega_K} \;=\; & \frac{|\,\vec{q}_K\,|}{k_\gamma^{\mathrm{cm}}} P_\alpha P_\beta \Big\{ R_T^{\beta\alpha} + \varepsilon_L R_L^{\beta\alpha} + [2\varepsilon_L(1+\varepsilon)]^{\frac{1}{2}}\,({}^cR_{TL}^{\beta\alpha}\cos\phi_K + {}^sR_{TL}^{\beta\alpha}\sin\phi_K) \\ & + \varepsilon({}^cR_{TT}^{\beta\alpha}\cos 2\phi_K + {}^sR_{TT}^{\beta\alpha}\sin 2\phi_K) + h[2\varepsilon_L(1-\varepsilon)]^{\frac{1}{2}}\,({}^cR_{TL'}^{\beta\alpha}\cos\phi_K + {}^sR_{TL'}^{\beta\alpha}\sin\phi_K) \\ & + h(1-\varepsilon^2)^{\frac{1}{2}} R_{TT'}^{\beta\alpha} \Big\}, \end{aligned} \tag{3}$$

where $P_\alpha = (1, P_x, P_y, P_z)$ and $P_\beta = (1, P_{x'}, P_{y'}, P_{z'})$ indicate the target and the recoil polarization vectors, respectively. A complete list of those response functions can be found in Ref. [10].

Previous isobaric models were mostly developed to fit experimental photoproduction data below 1.5 GeV. Up to now, only the models of Refs. [11–13] include photo- and electroproduction data up to 2.2 GeV. The recent analysis of Ref. [11] gives a very comprehensive description of the elementary

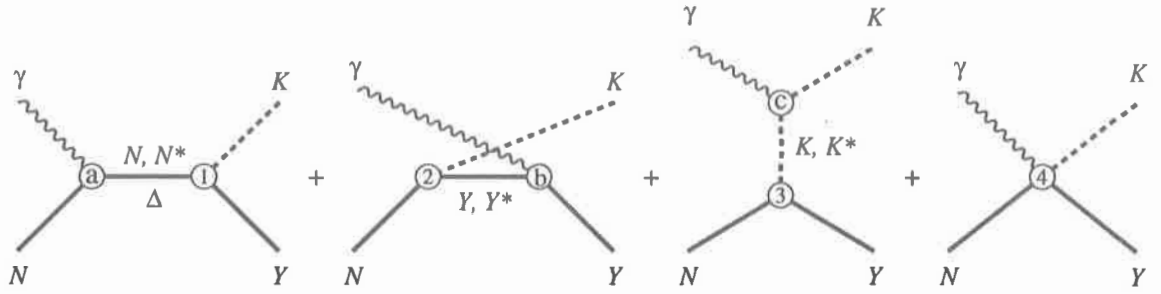

Figure 1. Feynman diagrams for the electromagnetic production of kaons on the nucleon. Contributions from the Δ are only possible in Σ production. Electromagnetic vertices are denoted by (a), (b), and (c), hadronic vertices by (1), (2), and (3). The contact diagram (4) is required in both PS and PV couplings in order to restore gauge invariance after introducing hadronic form factors. The Born terms contain the N, Y, K intermediate states and the contact term.

process. However, since this model incorporates spin 5/2 resonances, the corresponding elementary operator is rather cumbersome for nuclear applications. The elementary model developed in Ref. [13] incorporates the intermediate K^*-exchange, the N^* resonances $S_{11}(1650)$ and $P_{11}(1710)$ and, in addition, the s-channel Δ resonances $S_{31}(1900)$ and $P_{31}(1910)$ for the $K\Sigma$ production. To achieve a reasonable χ^2 for the experimental data in all six isospin channels, Ref. [13] introduced for the first time a hadronic form factor, which provides suppression at higher energies and increases the leading coupling constants to values closer to the SU(3) prediction.

Hadronic Form Factors and Gauge Invariance

It has been well known that the existence of hadronic form factors at hadronic vertices in Fig. 1 can destroy gauge invariance in the Born amplitude. Furthermore, most isobaric models show a divergence at higher energies, which clearly demonstrates the need for a cut-off. The use of point like particles disregards the fact that nucleons and mesons are composite objects, thus losing the full complexity of a strongly interacting hadronic system. Recent calculations [11,14] moreover proved that models which are able to describe (γ, K^+) experimental data tend to unrealistically overpredict the (γ, K^0) channel.

In the model of Ref. [13] a hadronic form factor is introduced by multiplying the whole amplitude in Eq. (1) with an overall monopole form factor

$$F(\Lambda, t) = \frac{\Lambda^2 - m_K^2}{\Lambda^2 - t}, \tag{4}$$

where the cut-off mass Λ was treated as a free parameter. In spite of successfully minimizing the χ^2 and producing leading coupling constants which are consistent with those extracted in hadronic sectors, no microscopic explanation supports this procedure.*

One prescription to handle the inclusion of such form factors has been proposed by Ohta [15]. By making use of minimal substitution Ohta has derived an additional amplitude which eliminates the form factors in the electric terms of the Born amplitude. Recently, Haberzettl [16,17] has proposed another prescription which is more general than that of Ohta. In contrast to Ohta's recipe, Haberzettl allows for a multiplication of the electric terms with a form factor.

To be more precise, in the following we give an example for the case of photoproduction, where A_5 and A_6 in Eq. (1) do not exist. In general, the inclusion of form factors in hadronic vertices of Born

*Since the whole amplitude is multiplied with a form factor, no question of gauge invariance can be raised.

terms in Fig. 1 is equivalent to the modification of the first four amplitudes by form factors[†]

$$A_1^{\text{Born}} = \frac{eg_{KYN}}{s-m_N^2}(Q_N+\kappa_N)\ F_1(\Lambda,s)+\frac{eg_{KYN}}{u-m_Y^2}(Q_Y+\kappa_Y)F_2(\Lambda,u) + \frac{eg_{KY'N}}{u-m_{Y'}^2}\kappa_T\ (1-|Q_Y|)\,F_2(\Lambda,u), \tag{5}$$

$$A_2^{\text{Born}} = \frac{2eg_{KYN}}{t-m_K^2}\left(\frac{Q_N}{s-m_N^2}+\frac{Q_Y}{u-m_Y^2}\right)\tilde{F}\ , \tag{6}$$

$$A_3^{\text{Born}} = \frac{eg_{KYN}}{s-m_N^2}\frac{\kappa_N}{m_N}\,F_1(\Lambda,s)\ , \tag{7}$$

$$A_4^{\text{Born}} = \frac{eg_{KYN}}{u-m_Y^2}\frac{\kappa_Y}{m_Y}\,F_2(\Lambda,u)+\frac{2eg_{KY'N}}{u-m_{Y'}^2}\frac{\kappa_T}{m_{Y'}+m_Y}(1-|Q_Y|)\,F_2(\Lambda,u)\ , \tag{8}$$

where Q_N and Q_Y denote the charge of the nucleon and the hyperon in $+e$ unit, while κ_N, κ_Y, and κ_T indicate the anomalous magnetic moments of the nucleon, hyperon, and the transition of $\Sigma^0\Lambda$. It is understood that $Y'=\Sigma^0$ [Λ] for $K\Lambda$ [$K\Sigma^0$] production. The difference between the three recipes can be summarized as follows:

$$\tilde{F}_{\text{overall}} \quad \text{replaces} \quad F_1,\ F_2,\ F_3,\ \text{and}\ \tilde{F} \quad [\text{e.g., } \tilde{F}_{\text{overall}}=F_3(\Lambda,t)]\ , \tag{9}$$

$$\tilde{F}_{\text{Ohta}} = 1\ , \tag{10}$$

$$\tilde{F}_{\text{Haberzettl}} = a_1F_1(\Lambda,s)+a_2F_2(\Lambda,u)+a_3F_3(\Lambda,t), \quad \text{with}\ a_1+a_2+a_3=1\ . \tag{11}$$

Results

Results of our previous model that employs an overall form factor have been partially reported in Ref. [13]. The use of Ohta's method in comparison to the previous model is briefly discussed in Ref. [5]. Here we will compare those models with the calculation which uses Haberzettl's method [17].

In using the last method we employ covariant vertex parameterizations without any singularities on the real axis, i.e. [cf. Eq. (11)]

$$F_i(\Lambda,r_i) = \frac{\Lambda^2}{\sqrt{\Lambda^4+\left(r_i-m_i^2\right)^2}}\ , \quad i=1,2,3, \tag{12}$$

with $r_1=s, r_2=u, r_3=t$ and $m_1=m_N, m_2=m_\Lambda, m_3=m_K$.

In this study our attention is mainly focussed on the magnitude of the leading Born coupling constants $g_{K\Lambda N}$ and $g_{K\Sigma N}$ extracted from the photoproduction data of $K^+\Lambda$ and $K^+\Sigma^0$. In contrast to the well-known πNN coupling constant, there are serious discrepancies between values for the KYN coupling constants extracted from electromagnetic reactions and those from hadronic processes which tend to be closer to accepted SU(3) values.

The numerical results for different methods are summarized in Table 1 in comparison with the prediction of SU(3). If the leading coupling constants $g_{K\Lambda N}/\sqrt{4\pi}$ and $g_{K\Sigma N}/\sqrt{4\pi}$ are not allowed to vary freely and are fixed at reasonable SU(3) values of -3.80 and 1.20 (close to what is obtained from hadronic reactions [18]), respectively, the χ^2 obtained in our model *without* hadronic form factors comes out to be 55.8. On the other hand, if the two couplings are allowed to vary freely, one obtains $g_{K\Lambda N}/\sqrt{4\pi}=-1.90$ and $g_{K\Sigma N}/\sqrt{4\pi}=-0.37$ with $\chi^2/N=3.3$. In spite of the small χ^2/N in the latter case, this result obviously indicates that either there is a very large amount of SU(3) symmetry

[†]The amplitude for each resonance is separately gauge invariant, by construction.

Table 1. The extracted leading coupling constants $g_{K\Lambda N}$ and $g_{K\Sigma N}$, the hadronic form factor cut-off Λ, and χ^2/N from fitting to photoproduction data by means of different prescriptions.

form factor method	no	no	overall	Ohta	Haberzettl	
coupling constants	fixed	free	fixed	fixed	fixed	SU(3)
$g_{K\Lambda N}/\sqrt{4\pi}$	-3.80	-1.90	-3.80	-3.80	-3.80	-3.70 ± 0.70
$g_{K\Sigma N}/\sqrt{4\pi}$	1.20	-0.37	1.20	1.20	1.20	1.10 ± 0.20
Λ (GeV)	-	-	0.213	1.422	1.128	-
χ^2/N	55.76	3.33	2.84	14.21	4.63	-

breaking or that important physics has been left out in the extraction of coupling constants from the (γ, K) processes. In this study, we advocate the second position and demonstrate that the inclusion of structure at the hadronic vertex permits an adequate description of kaon photoproduction with couplings close to the SU(3) values, provided one uses the gauge procedure of Ref. [17].

As shown in Table 1, a better χ^2 is obtained by the overall form factor method using $F_3(\Lambda, t)$ of Eq. (12). This reveals the fact that the data tend to prefer $1/t$ dependence of the hadronic form factor. A further investigation of this issue will certainly be important to clarify the dependency of form factors on the momentum of the off-shell particles.

We also investigate the sensitivity of the χ^2/N and the cut-off parameter Λ to the leading coupling constants. The results are summarized in Fig. 2. The upper-left panel shows the χ^2 per data point as a function of $g_{K\Lambda N}/\sqrt{4\pi}$ for the two different gauge prescriptions by Ohta and Haberzettl. At a value of $g_{K\Lambda N}/\sqrt{4\pi} = -3.4$, the χ^2 obtained with Ohta's method is almost a factor of two larger compared to using the method by Haberzettl. With increasing coupling constant the Ohta result rises sharply, leading to an unacceptably large χ^2 of 29.3 for $g_{K\Lambda N}/\sqrt{4\pi} = -4.2$. On the other hand, using the procedure of Ref. [17] keeps the χ^2 more or less constant. This dramatic difference between the two gauge prescriptions can easily be understood from Eq. (6). Ohta's method provides no possibility to suppress electric contributions since the form factor for this term is unity [cf. Eqs. (10) and (11)]. In contrast, the method by Haberzettl allows for a hadronic form factor in this term as well.

The lower-left panel of Fig. 2 explains the suppression mechanism. In the fits we performed the cut-off Λ of the form factor was allowed to vary freely. In the case of Haberzettl's method, the cut-off decreases with increasing $K\Lambda N$ coupling constant, leaving the magnitude of the *effective* coupling, i.e., coupling constant times form factor, roughly constant. Again, since Ohta's method does not involve form factors for electric contributions no such compensation is possible there, and as a consequence the cut-off remains insensitive to the coupling constant.

The variation of $K\Sigma N$ coupling constant is shown in both upper-right and lower-right panels of Fig. 2. In contrast to the previous case, varying this coupling between 1.0 and 1.4 leads only to very small changes. This can be understood since the main contribution of the χ^2 in this model comes from the $K^+\Lambda$ channel, which is driven by the $K\Lambda N$ coupling constant.

Figure 3 shows differential cross sections for the $p(\gamma, K^0)\Sigma^+$ channel. As shown in Fig. 3, the ChPT calculation predicts the smallest cross section at $E_\gamma^{\rm lab} = 1.075$ GeV which is within the experimental uncertainties. However, due to its range of validity the ChPT calculation is not comparable to the other data. The calculation of the chiral quark model [3] that has far fewer free parameters compared to isobaric descriptions underestimates the data and shows a backward peaking behavior. Although

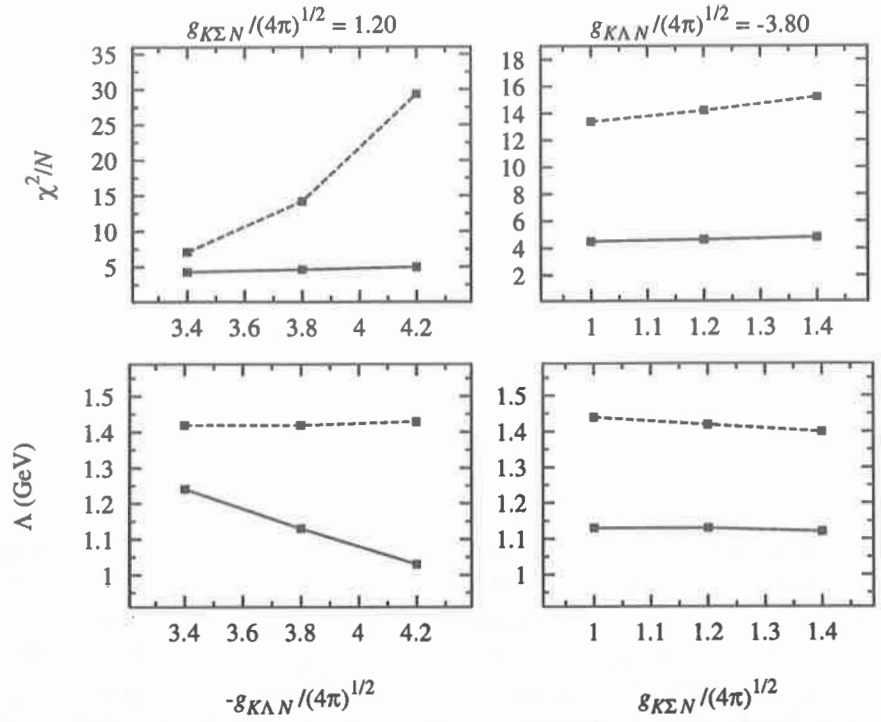

Figure 2. Values of χ^2/N and cut-off parameter Λ as a function of the coupling constants $g_{K\Lambda N}$ and $g_{K\Sigma N}$. Solid lines connect the result obtained by using Haberzettl's gauge method and the dotted lines refer to Ohta's prescription.

the experimental data are not sufficiently precise for making a quantitative judgement, the data for higher energies show, however, a forward peaking pattern. The three isobaric models are able to predict this pattern, albeit they mostly tend to overestimate experimental data. A better description can be produced by the isobaric model using Haberzettl prescription at $E_\gamma = 1.275$ GeV. A systematic study to improve the model is clearly needed in this case.

Total cross sections for the three isospin channels are shown in Fig. 4. Note that, the three curves in $K^0\Sigma^+$ channel are pure predictions. In this isospin channel the same pattern as in the differential cross section is found. For the $K^+\Lambda$ and $K^+\Sigma^0$ channels, the overall form factor prescription is able to explain the data beyond 1.5 GeV, where other recipes start to diverge. This can be explained by Table 1, where it is shown that this method has the smallest χ^2.

In the electroproduction sector the separation of longitudinal and transverse cross sections [see Eq. (2)] is necessary to allow K^+ form factor measurements which is the subject of a completed experiment at TJNAF [20]. An extrapolation of the longitudinal cross section to the kaon pole enables the extraction of this form factor. Such a separation was formerly attempted by the Harvard-Cornell collaboration in the late seventies [19] with much larger error bars. Figure 5 displays a comparison between our previous model [13], using an overall form factor with a cut-off about 850 MeV, and the preliminary results of the TJNAF experiment [20], where the improvement in the data quality is obvious. We note that the predicted partial cross sections underestimate experimental data, but their ratio reproduces the previous measurement and lower momentum transfer TJNAF data. Given the quality of the new data, we suspect that the discrepancy could originate from the electromagnetic form factors used in the model. Figure 5 advocates a stronger cut-off to be necessary in order to explain the new data for $-k^2 > 1$ GeV^2, since the longitudinal cross section will be more sensitive to the form factor rather than the transverse one.

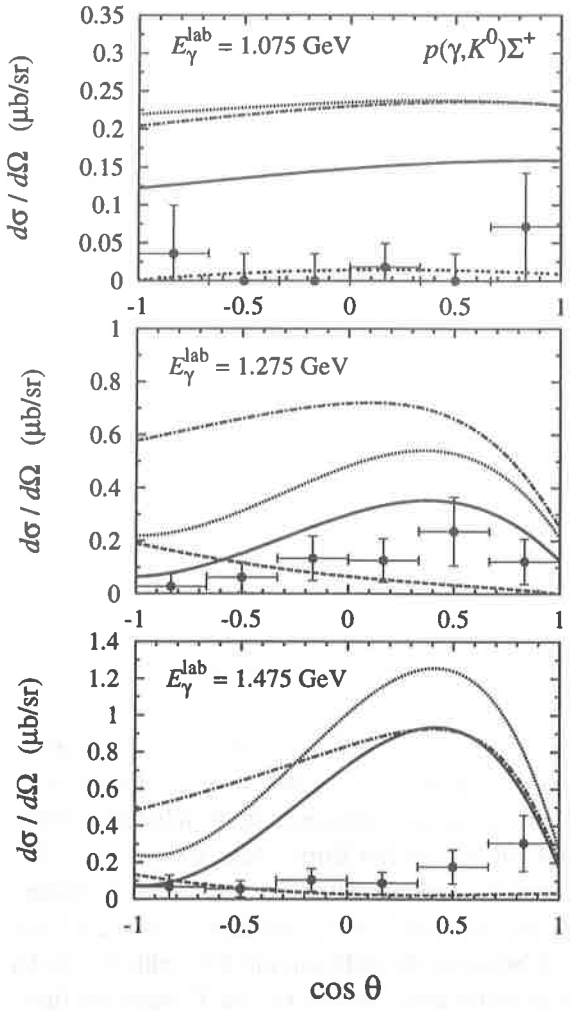

Figure 3. Differential cross sections for $p(\gamma,K^0)\Sigma^+$. The dashed curve shows the prediction from the chiral quark model [3], whereas the ChPT calculation [4] is given by the triple-dotted line. The dash-dotted curve displays the prediction of the isobaric model with an overall hadronic form factor, while the dotted curve includes the hadronic form factor according to Ohta [15]. The solid curve denotes the use of Haberzettl's method. Experimental data are from SAPHIR [5].

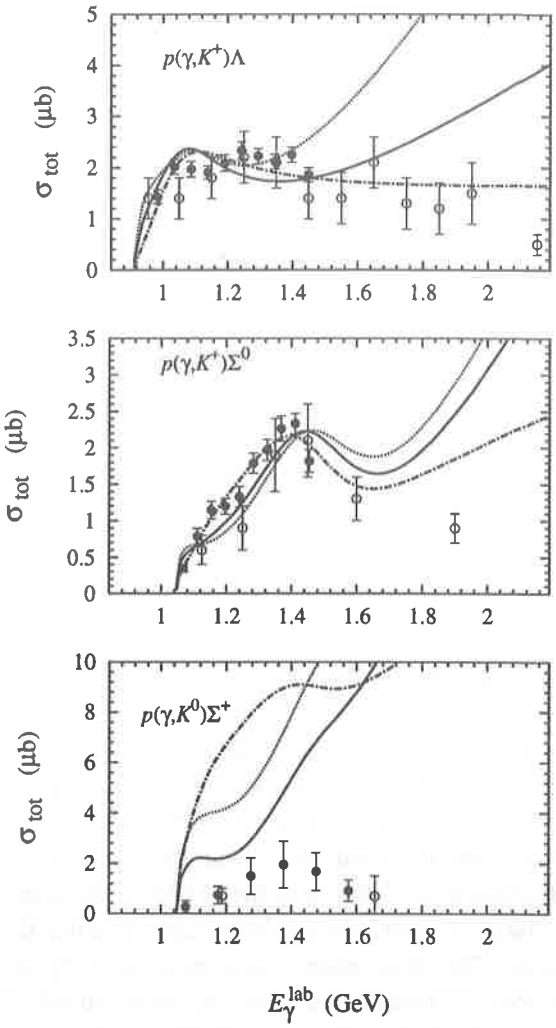

Figure 4. Total cross section for three different isospin channels. Open circles denote the old data, while solid circles are the new SAPHIR data. The dash-dotted curve shows the model with an overall hadronic form factor, the dotted curve displays the isobaric model with a hadronic form factor which assumes Ohta's method. The solid curve shows the model using Haberzettl's prescription.

INVESTIGATIONS OF STRANGE HADRON FORM FACTORS

During the last several years there has been considerable effort to develop models for not only the nucleon, but also hyperon and meson form factors. Nevertheless, a significant issue is the lack of experimental verification of these models due to the lack of stable targets in the case of strange hadrons. Unlike the case of the proton, where both electric and magnetic form factors can be extracted directly, the measurement of strange hadron form factors requires an indirect technique. One possible way is through kaon electroproduction. A systematic study of the sensitivity of response functions in Eq. (3) to the kaon and hyperon form factors is given in Ref. [21]. Here we will only briefly discuss the case of transition $K^+K^{*+}\gamma$ and Λ form factors where the sensitivity can be found in $p(e,e'K^+)\Sigma^0$

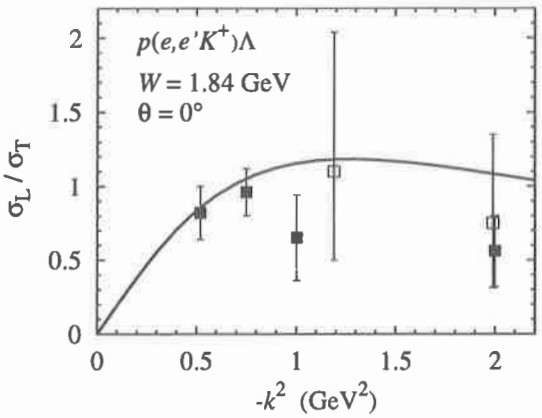

Figure 5. The ratio σ_L/σ_T in $K^+\Lambda$ electroproduction according to the elementary operator given in Ref. [13]. The experimental data are from Ref. [19] (open squares) and Ref. [20] (solid squares).

and $p(e,e'K^+)\Lambda$ channels, in which the data quality is expected to be better than in other isospin channels.

Figures 6 shows the sensitivity of T and TT' response functions to different models of the charged KK^* transition form factor of Ref. [12] which uses vector meson dominance and the calculation of Ref. [22] which solves a covariant Salpeter equation for a confining plus instanton-induced interaction. Since the small size of the $g_{K\Sigma N}$ coupling constant suppresses the Born terms, the $p(e,e'K^+)\Sigma^0$ reaction is used to study the $K^+K^{*+}\gamma$ form factor. Questions remain regarding additional t-channel resonance contributions from states like the $K_1(1270)$ which would have a different transition form factor. The observables displayed can clearly distinguish between the different models, with the model of Ref. [22] leading to a much faster fall-off. The large differences shown by the T response function indicate that the unpolarized experiment would be able to distinguish the models once we had a reliable elementary production model.

In Fig. 7 we show the sensitivity of double polarization response functions to different Λ form factors as predicted by a hybrid vector meson dominance (HVMD) calculation [24] and the chiral quark-soliton (CQS) model [25]. Since the Λ form factor is multiplied by the large hadronic coupling constant $g_{K\Lambda N}$, the $p(e,e'K^+)\Lambda$ channel is well suited to extract this form factor. The TT' and TL' observables were subject of a recent TJNAF proposal [23]. As shown in Fig. 7, both TT' and TL' structure functions display large sensitivities for most of the momentum transfer range. Measuring these response functions could be accomplished with CLAS in TJNAF's Hall B.

FUTURE OUTLOOK

The study of kaon photo- and electroproduction on the nucleon has paved the way for investigating strange hadron structures. High quality experimental data are beginning to come from new accelerators and, therefore, significant improvements in theoretical analyses are urgently needed. We have shown that one of the possible ways to achieve this goal is by including the hadronic form factor. Although qualitatively showing a better result, the model strongly requires quantitative improvements.

In view of several ongoing experimental activities that will be finished almost simultaneously, we feel that a coupled-channels analysis which incorporates unitarity and couples all relevant elementary reactions, is an important issue to be included in future studies.

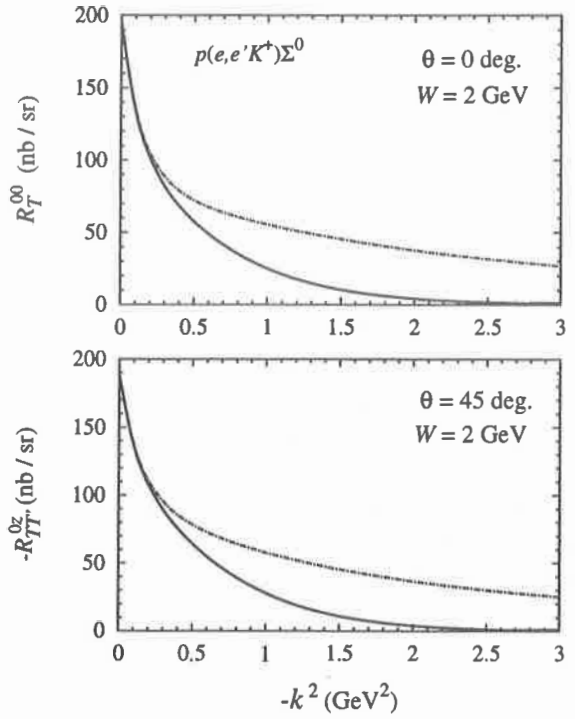

Figure 6. The sensitivity of response functions to different $K^+K^{*+}\gamma$ form factors. The solid (dash-dotted) line is obtained using the model of Ref. [22] ([12]). The elementary model is from Ref. [12].

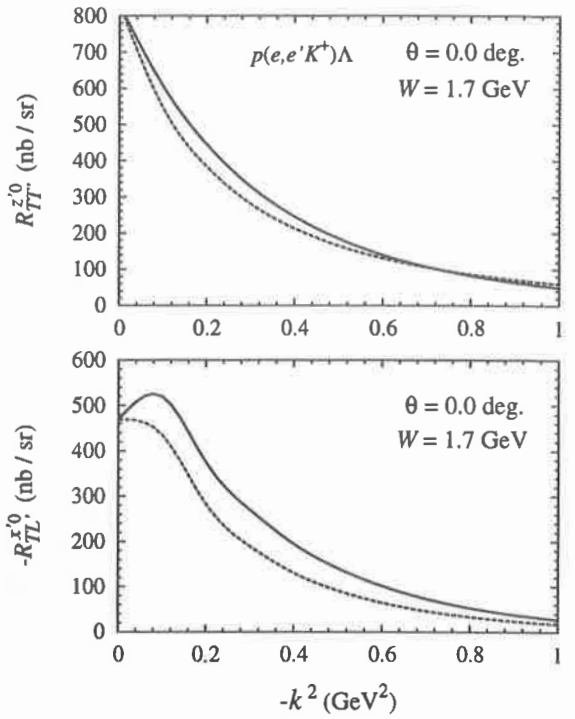

Figure 7. The sensitivity of response functions to different Λ form factors, the HVMD model (solid lines) [24] and the CQS model (dashed lines) [25].

Acknowledgments

TM acknowledges the support from University Research for Graduate Education (URGE) grant. CB and HH are supported in part by US DOE under contract no. DE-FG02-95ER-40907.

REFERENCES

[1] See e.g.: R. M. Mohring, *New* $(e,e'K^+)$ *Results from Jefferson Lab*, these Proceedings.
[2] Zhenping Li, Phys. Rev. C **52**, 1648 (1995).
[3] Zhenping Li, M. Wei-Hsing, and Z. Lin, Phys. Rev. C **54**, R2171 (1996).
[4] S. Steininger and U. G. Meißner, Phys. Lett. B **391**, 446 (1997).
[5] C. Bennhold *et al.*, *Proceedings of the International Conference on Hypernuclear and Strange Particle Physics*, Brookhaven, USA, Oct. 1997 (to appear in Nucl. Phys. A).
[6] N. Kaiser, T. Waas, and W. Weise, Nucl. Phys. A **612**, 297 (1997).
[7] T. Feuster and U. Mosel, *Photon and Meson Scattering on the Nucleon*, these Proceedings; nucl-th/9803057 (1998).
[8] N. Levy, W. Majerotto, and B. J. Read, Nucl. Phys. B **55**, 493 (1973).
[9] M. Guidal, J.-M. Laget, M. Vanderhaeghen, Nucl. Phys. A **627**, 645 (1997).
[10] G. Knöchlein, D. Drechsel, and L. Tiator, Z. Phys. A **352**, 327 (1995).
[11] J. C. David, C. Fayard, G. H. Lamot, and B. Saghai, Phys. Rev. C **53**, 2613 (1996).
[12] R. A. Williams, C. -R. Ji, and S. R. Cotanch, Phys. Rev. C **46**, 1617 (1992).

[13] C. Bennhold, T. Mart, and D. Kusno, *Proceedings of the CEBAF/INT Workshop on N* Physics*, Seattle, USA, 1996 (World Scientific, Singapore, 1997, T.-S. H. Lee and W. Roberts, editors), p.166.
[14] T. Mart, C. Bennhold, and C. E. Hyde-Wright, Phys. Rev. C **51**, R1074 (1995).
[15] K. Ohta, Phys. Rev. C **40**, 1335 (1989).
[16] H. Haberzettl, Phys. Rev. C **56**, 2041 (1997).
[17] H. Haberzettl, C. Bennhold, T. Mart, and T. Feuster, Phys. Rev. C **58**, R40 (1998).
[18] R. G. E. Timmermans *et al.*, Nucl. Phys. A **585**, 143c (1995).
[19] C. J. Bebek *et al.*, Phys. Rev. D **15**, 3082 (1977).
[20] G. Niculescu *et al.*, *Proceedings of the International Conference on Hypernuclear and Strange Particle Physics*, Brookhaven, USA, Oct. 1997 (to appear in Nucl. Phys. A); *ibid.*, Phys. Rev. Lett. 1998 (in press).
[21] T. Mart and C. Bennhold, *Proceedings of the International Conference on Hypernuclear and Strange Particle Physics*, Brookhaven, USA, Oct. 1997 (to appear in Nucl. Phys. A).
[22] C. R. Münz, J. Resag, B. C. Metsch, and H. R. Petry, Phys. Rev. C **52**, 2110 (1995).
[23] *Polarization Transfer in Kaon Electroproduction*, TJNAF Proposal, O. K. Baker (spokesperson).
[24] R. A. Williams and T. M. Small, Phys. Rev. C **55**, 882 (1997).
[25] H. C. Kim, A. Blotz, M. Polyakov, K. Goeke, Phys. Rev. D **53**, 4013 (1996).

New (e,e'K^+) Results from Jefferson Lab

R. M. Mohring*
University of Maryland, College Park, MD 20742
For the E93-018† and E91-016‡ Collaborations

Abstract

Measurements of kaon electroproduction from various targets were made in Hall C at the Thomas Jefferson National Accelerator Facility (Jefferson Lab, formerly CEBAF) during experiments E93-018 and E91-016. A general overview of the data taken, experimental setup, and a survey of preliminary results from these experiments are presented.

INTRODUCTION

There is currently a great level of interest within the intermediate energy nuclear physics community regarding the electroproduction of strangeness. Recently, data on this subject have been collected by experiments E93-018 [1] and E91-016 [2], which ran in Hall C at Jefferson Lab from August-November 1996. These two experiments performed an extensive study of the (e,e'K^+) reaction by taking electroproduction data on liquid hydrogen, liquid deuterium, and solid carbon targets. The high-intensity continuous-wave (100% duty factor) medium-energy (up to 4 GeV) electron beam available at the CEBAF accelerator is particularly well suited for carrying out such a program.

Data taken on the hydrogen target are being used to study the elementary processes p(e,e'K^+)Λ and p(e,e'K^+)Σ°. For both reactions, data were taken at four different values of the squared virtual photon four-momentum transfer, i.e., $Q^2 = 0.52, 0.75, 1.00, 2.00$ (GeV/c)^2. Within each Q^2 setting, the virtual photon polarization, ϵ, was varied between three values. These data allow for a Rosenbluth separation of the longitudinal and transverse contributions to the cross section in both the Λ and Σ° channels, which in turn allows for an investigation of the relative strengths of these two channels. Studies of the separated cross sections (both individually and their ratio) will help to further understand the electroproduction mechanism and the coupling constants needed in various theoretical models. Additional data were collected at $Q^2 = 0.75$, 1.00, and 1.25 (GeV/c)^2 for different values of the Mandelstam variable, t (the squared four-momentum transferred to the kaon by the virtual photon.) The t-dependence will be combined with the Rosenbluth separation results and an attempt will be made to extract the kaon electromagnetic form factor via the Chew-Low extrapolation technique. Of course, a thorough exploration of these elementary reactions is also necessary as a baseline for understanding measurements of kaon electroproduction on $A > 1$ nuclei.

The simplest choice of target to enable investigation of production on an $A > 1$ nucleus is deuterium. Studies of production on a deuterium target allow a first test of the concept of quasifree production off a proton that is embedded in a nuclear medium [3]. Once again, it is important to thoroughly understand this simplest case of in-medium production as a baseline for production off of larger nuclei. Data were taken on both hydrogen and deuterium targets at two Q^2 settings, viz $Q^2 = 0.38$, 0.50 (GeV/c)^2. By considering data from both targets, information regarding the elementary process on the neutron, n_{bound}(e,e'K^+)Σ^- can be extracted. Furthermore, angular distributions of the kaons relative to the virtual photon

*E-mail: mohring@physics.umd.edu
†O. K. Baker, spokesman
‡B. Zeidman, spokesman

direction were taken at each Q^2 setting over the ranges (in the lab frame): $\theta_{\gamma K}$ = 0° - 11° for Q^2 = 0.38 (GeV/c)^2, and $\theta_{\gamma K}$ = 0° - 13° for Q^2 = 0.50 (GeV/c)^2. The study of these distributions has the potential for providing information on the elementary hyperon-nucleon interaction and may also give some hints about the controversial issue of strange di-baryonic states postulated to occur in the vicinity of the Σ^-n threshold [3]. Further measurements are planned on ^{3}He and ^{4}He targets in order to explore these questions further, and to examine the A-dependence of quasifree kaon electroproduction (because the density of the nuclear medium varies dramatically in these light nuclei.)

Additionally, approximately 31 hours of beam time during the running period were utilized to perform a feasibility study of the measurement of both quasifree (e,e'K$^+$) and the production of $^{11}_{\Lambda}$B hypernuclear states from a ^{12}C target. These data were taken at both Q^2 = 0.357 and 0.397 (GeV/c)^2. This test run was intended mainly to provide knowledge to help optimize future high-resolution hypernuclear spectroscopy experiments in Hall C, the first of which is scheduled to run in Fall 1999 [4]. Also, the carbon data can be combined with the deuterium data as a preliminary study of the A-dependence of quasifree kaon electroproduction.

EXPERIMENTAL DETAILS

Experiments E93-018 and E91-016 were both performed in Hall C at Jefferson Lab. Electron beams with intensities up to 30 μA were focussed onto a liquid hydrogen (4.36 ± 0.01 cm), liquid deuterium (4.20 ± 0.01 cm), solid carbon target, or an aluminum dummy target (used to subtract the contributions from the walls of the liquid targets). Scattered electrons were detected using the High Momentum Spectrometer (HMS), and the electroproduced kaons were detected in coincidence using the Short Orbit Spectrometer (SOS). The nominal acceptances of the HMS(SOS) were $\Delta\Omega$ = 6.7 msr (7.7 msr) in solid angle, and $\Delta p/p_0$ = ±10% (±20%) in momentum.

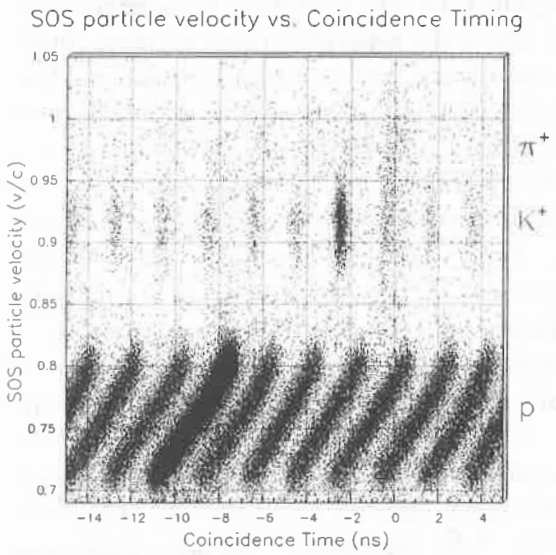

Figure 1. Hadron arm particle velocity vs. coincidence timing ($p_{central}$ = 1.126 GeV/c).

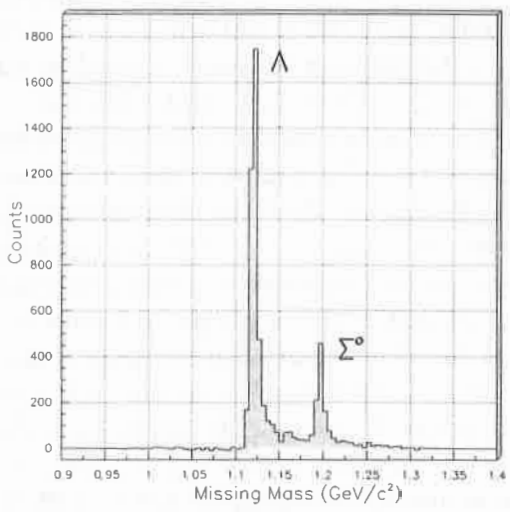

Figure 2. Missing mass spectrum for p(e,e'K$^+$)Λ/Σ° at Q^2 = 0.52 (GeV/c)^2, W = 1.84 GeV/c^2.

Both spectrometers were outfitted with two multiwire drift chambers for tracking, four planes of segmented hodoscopes for time-of-flight measurement and triggering, plus a gas

Čerenkov and lead-glass calorimeter for π^-/e^- separation. The SOS was also equipped with an aerogel Čerenkov (n=1.034) detector for K^+/π^+ discrimination, and with a lucite Čerenkov detector for K^+/p discrimination. Both of these Čerenkov counters were sufficiently fast enough to be incorporated at the trigger level when needed. Typical resolutions in the system were 0.2% in momentum, $\sigma \approx$ 2-3 mr in angular reconstruction, and $\sigma \approx$ 120 ps for the individual hodoscope planes. A spectrum of particle velocity in the SOS (π^+, K^+, and p) versus coincidence timing between the HMS and SOS is shown in Fig 1. In this figure, a cut has already been placed on the aerogel Čerenkov to eliminate a substantial portion of the pion background. One can see that the true in-time kaon peak (and the randomly occuring kaon peaks) are very well-defined; the timing structure of the peaks corresponds to the 499 MHz RF structure of the CEBAF beam. The real/random ratio is typically better than 10:1.

After the coincident kaons and electrons are identified (and the appropriate background and target wall contributions are subtracted), the missing mass can be calculated. A missing mass spectrum for $p(e,e'K^+)\Lambda/\Sigma^\circ$ is shown in Fig 2. The two peaks represent the Λ (1115) and Σ° (1192) channels. The tails on both peaks projecting towards higher missing mass are due to radiative effects, and are taken into account in the analysis.

RESULTS

First, preliminary results for the unseparated center-of-mass cross section for $p(e,e'K^+)\Lambda$ are shown in Fig 3 compared to the world data set on this reaction [5]. The errors assigned to this cross section measurement range from (5.0 - 7.0)% systematic error, and from (1.0 - 2.5)% statistical error (depending on the Q^2 in question). Our data are in agreement with the previous results and have equal or better precision. A longitudinal/transverse separation of the cross section for $p(e,e'K^+)\Lambda$ is nearing completion at the time of this writing, and will be presented in a forthcoming paper [6].

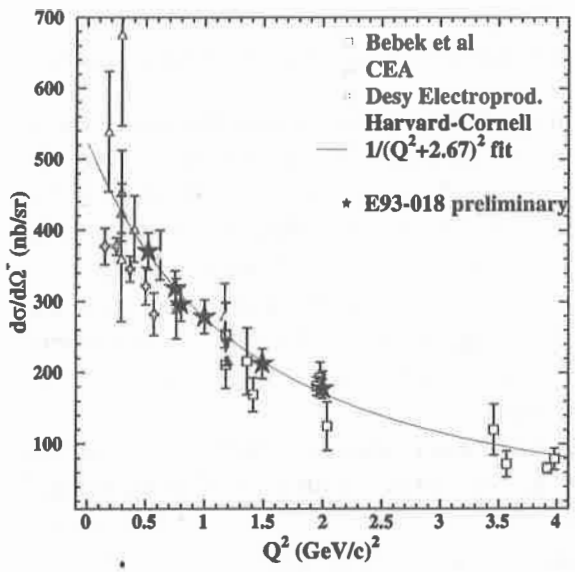

Figure 3. E93-018 preliminary results for the unseparated $p(e,e'K^+)\Lambda$ cross section, scaled to $W = 2.15$ GeV and plotted against the world data set [7].

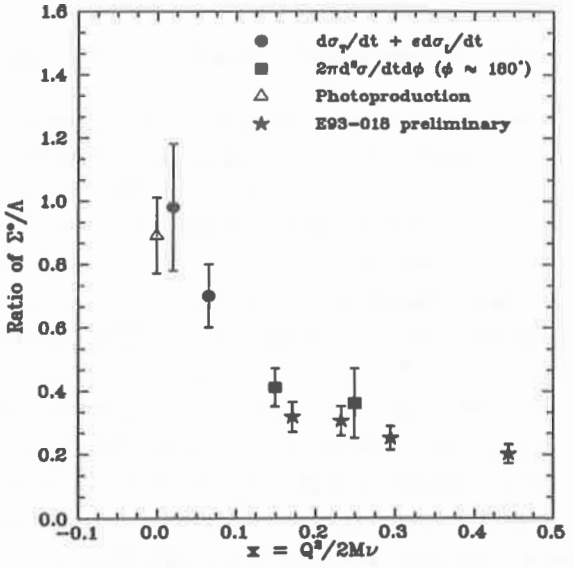

Figure 4. E93-018 preliminary results for the ratio of unseparated $p(e,e'K^+)\Sigma^\circ/p(e,e'K^+)\Lambda$ yields plotted against the world data set [8].

Next, preliminary results on the ratio of unseparated yields between the Λ and Σ° channels

are shown in Fig 4 compared to the world data set as a function of Björken x. The statistical error on these points is at the 5% level (this represents only about 60% of the total statistics taken), while the systematic error is at the 15% level. In the final analysis, the statistical error in the Σ° channel is expected to be about (3 - 4)%, with systematic errors of approximately (7 - 10)%.

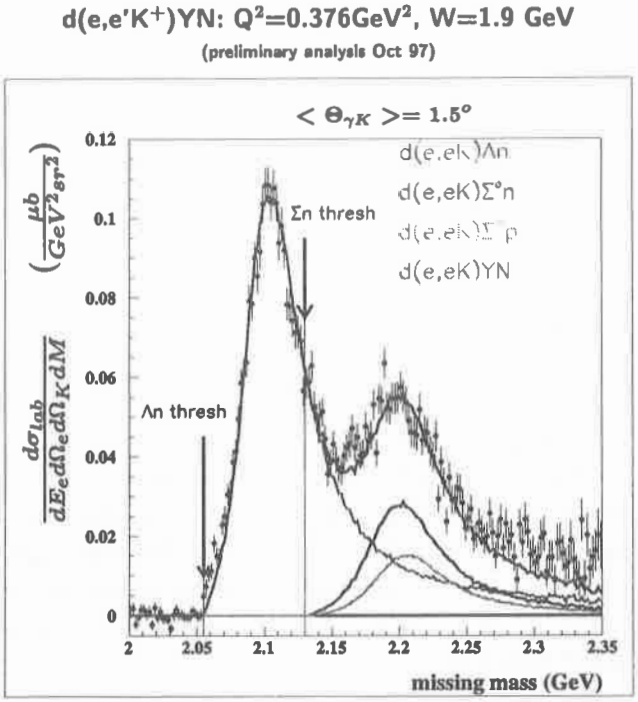

Figure 5. Missing mass for d(e,e'K$^+$)YN with Monte Carlo distributions for the contributing processes.

Third, a missing mass spectrum is presented in Fig 5 for the electroproduction of kaons from a deuterium target, along with curves representing Monte Carlo simulations of the various contributing reactions [3]. Note that the Λ and Σ peaks are now broadened due to Fermi motion. In this analysis, the simulation for d(e,e'K$^+$)Λn is first normalized to fit the data. Then, the simulation for d(e,e'K$^+$)Σ°n is scaled by the Λ/Σ° ratio measured on a hydrogen target at the same kinematic setting. Finally, the counts left above what the simulation predicts for the Λn and Σ°n channels are assigned to the d(e,e'K$^+$)Σ^-p channel. From these data, a ratio of about 0.5 is determined for the relative strengths of Σ^- to Σ° production, consistent with simple quasifree production.

Finally, two spectra representing the total yield from kaon electroproduction on a carbon target are shown in Fig 6, one for each Q^2 setting [9]. The regions with a "Λ binding energy" of greater than zero represent quasifree production of kaons. The triangular hatched regions indicate random coincidences, implying a real/random ratio on the order of 1:1. Although only a few counts were gathered for a Λ binding energy of less than zero, the number of such counts was consistent with expectations [9].

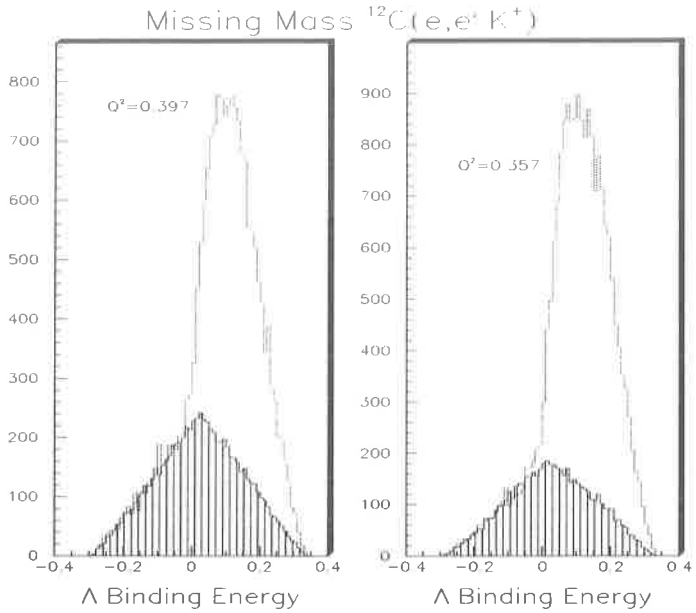

Figure 6. Missing mass for ^{12}C(e,e'K$^+$)X at two different values of Q^2.

CONCLUSIONS

A survey of preliminary results from both Jefferson Lab kaon electroproduction experiments E93-018 and E91-016 has been presented. These data represent the highest quality (e,e'K$^+$) data taken to date, and upon completion of the analysis, promise to yield important contributions to the study of hadron structure and the production of strangeness.

The author would like to acknowledge that this work was supported in part by the U. S. Department of Energy, Nuclear Physics Division, and by the National Science Foundation.

REFERENCES

[1] O. K. Baker, *et al.*, CEBAF proposal for experiment E93-018, and references therein.
[2] B. Zeidman, *et al.*, CEBAF proposal for experiment E91-016.
[3] J. Reinhold, proc. of the Hyperon '97 conference, Brookhaven National Lab, Oct 1997.
[4] E. Hungerford, *et al.*, CEBAF proposal for experiment E89-009.
[5] G. Niculescu, proc. of the Hyperon '97 conference, Brookhaven National Lab, Oct 1997.
[6] G. Niculescu, *et al.*, to be submitted to Phys Rev Lett.
[7] C. J. Bebek, *et al.*, Phys. Rev. C **48**, 3082 (1977).
[8] P. Brauel, *et al.*, Z. Phys. C **3**, 101 (1979).
[9] W. Hinton, proc. of the Hyperon '97 conference, Brookhaven National Lab, Oct 1997.

Overview of $(\gamma, \pi\pi)$

H.Ströher*
Institut für Kernphysik,
Johannes Gutenberg Universität Mainz, D-55099 Mainz, Germany

Abstract

In recent years, a number of new experiments on the photoproduction of two pions in elementary reactions on the nucleon have yielded data with significantly increased precision for channels which had been investigated before (like e.g. $\pi^+\pi^-$) as well as for previously not measured channels (like $\pi^0\pi^0$). Simultaneously theoretical investigations have been used to shed light on the production mechanisms involved. In my talk, I have tried to give a status report of the experimental and theoretical situation as of the time of the workshop (October 1997). Copies of the transparencies can be obtained on request from the author.

INTRODUCTION

Since the talk has essentially summarized published experimental results and theoretical investigations, in the following I will only quote these references:

a) Experiments:

- A. Braghieri et al. [1]:
  Total cross sections for $p(\gamma, \pi^+\pi^-)$, $p(\gamma, \pi^+\pi^0)$ and $p(\gamma, \pi^0\pi^0)$ between about 400 and 800 MeV. Experiment at MAMI using DAPHNE–detector.
- F. Härter et al. [2]:
  Total cross section for $p(\gamma, \pi^0\pi^0)$ between threshold (309 MeV) and 800 MeV. Dalitz–plot of $m^2_{\pi^0\pi^0}$ versus $m^2_{p\pi^0}$. Experiment at MAMI using TAPS–detector.
- A. Zabrodin et al. [3]:
  Total cross section for $n(\gamma, \pi^-\pi^0)$ for the energy range 450 – 800 MeV. Results have been obtained with a deuteron–target; test of the procedure by also analyzing $p(\gamma, \pi^+\pi^0)n$ p_s. Experiment with DAPHNE–detector at MAMI.

b) Theory:

- J. A. Gomez-Tejedor, E.Oset [4]:
  Model for the $\gamma p \to \pi^+\pi^-$ reaction, which includes N, Δ, $P_{11}(1440)$, and $D_{13}(1520)$ baryonic states and the ρ–meson and is applicable up to energies of about 800 MeV. Interference between the D_{13}–resonance and the $\Delta\pi$ Kroll–Ruderman term produces a structure in the total crosss section around 750 MeV.
- V. Bernard, N. Kaiser, U.-G. Meissner, A. Schmidt [5]:
  Study of 2 pion–photoproduction (and electroproduction) on the nucleon in heavy baryon chiral perturbation theory, i.e. close to threshold. Due to pion loops the cross section for two neutral pions is expected to be considerably enhanced but still very small (less than a few nb).

*E-mail: stroeher@kph.uni-mainz.de

- M. Benmerrouche, E.Tomusiak [6]:
  Low energy expansion for double–pion photoproduction, using an effective chiral Lagrangian.

- J. A. Gomez-Tejedor, F. Cano, E. Oset [7]:
  Investigation of the $\gamma p \to \pi^+\pi^- p$ reaction between threshold and 800 MeV. Extraction of $N^*(1520) \to \Delta\pi$ amplitudes.

- V. Bernard, N. Kaiser, U.-G. Meissner [8]:
  Investigation of $\gamma p \to \pi^0\pi^0 p$ within heavy baryon chiral perturbation theory. An estimate for the total cross section close to threshold is given.

- L. Y. Murphy, J. P. Laget [9]:
  Calculation of total cross sections and invariant mass distributions for all isospin channels on the proton within an effective Lagrangian model. Born-terms, Δ–Born-terms and formation of additional baryonic resonances are included. The model reproduces the $\pi^+\pi^-$ and the $\pi^0\pi^0$ cross sections but fails to account for half of the cross section for $\pi^+\pi^0$. It is claimed that the 2 neutral pion cross section indicates the excitation of the Roper–resonance by real photons.

- J. A. Gomez-Tejedor, E. Oset [10]:
  Extension of the previously developed model [4] to all isospin channels. One finding is that the reaction chain $\gamma N \to N^*(1520) \to \Delta\pi$ affects all channels. Discrepancies for the $\pi^+\pi^0$–channel: predictions are too small by a factor of two.

- M. Hirata, K. Ochi, T. Takaki [11]:
  Calculation of total cross sections and invariant mass distributions for three channels: $\pi^+\pi^-, \pi^+\pi^0, \pi^-\pi^0$ between threshold and about 850 MeV. They claim that the ρN channel plays an important role in two pion photoproduction.

RESULTS

The results of the measurements and the calculations can be summarized as follows:

- The experimental cross sections are small between threshold and about 450 MeV; they rise to a maximum of about 80 μb ($\pi^+\pi^-$), 55 μb ($\pi^+\pi^0$), and 12 μb ($\pi^0\pi^0$) at around 1 GeV, from there they start to decrease again. This rise of the cross section for two pion photoproduction accounts for most of the structure seen in the total photoabsorption cross section for nucleons, which is usually ascribed to the socalled second resonance region.

- Dalitz-plots show the importance of the Δ–resonance for all channels. For double neutral pion production on the proton, it is observed that the decay chain includes the Δ–resonance as an intermediate state.

- The total cross sections for charged channels are dominated by the $\Delta\pi$ Born–terms.

- Interference between these and the $N^*(1520)$–resonance is important to understand the structure in the total cross section around 750 MeV for the $\pi^+\pi^-$ channel.

- The theoretical models are inconsistent among themselves except for the $\Delta\pi$ Born–terms.

- None of the models is able to reproduce all isospin channels quantitatively. In particular the large cross sections for channels with one charged and one neutral pion in the final state are difficult to understand. If one assigns the observed large cross sections in these reactions to an increased contribution of the ρ–meson, then the cross section for double neutral pion photoproduction is badly underestimated (since there is no ρ–contribution in this case).

OUTLOOK

New experimental data have already been taken at MAMI (using TAPS), which will yield new precision data for $p(\gamma,\pi^0\pi^0)p$ between threshold and 800 MeV. Also data for the channel $p(\gamma,\pi^+\pi^0)n$ will be obtained from this measurement. They are currently being analyzed. New results can also be expected from GRAAL, which will add the polarization degree of freedom and extend the measurements to higher energies (see contribution of E. Hourany to this Workshop). Preliminary cross sections at higher energies for the $\pi^+\pi^-$-channel from ELSA (SAPHIR) are available and final results will be published in the near future. Certainly results at higher energies from CEBAF/TJNAF will add to the data–base soon. It is important to stress that in order to cover a large fraction of the available phase space for the multi–particle final states, large acceptance detector systems are required.
On the theoretical side, additional efforts seem to be necessary to understand the reaction mechanism quantitatively.

REFERENCES

[1] A. Braghieri et al., Phys. Lett. B **363** (1995) 46
[2] F. Härter at al., Phys. Lett. B **401** (1997) 229
[3] A. Zabrodin et al., Phys. Rev. C **55** (1997) R1
[4] J. A. Gomez-Tejedor, E. Oset, Nucl. Phys A **571** (1994) 667
[5] V. Bernard, N. Kaiser, U.-G. Meißner, A.Schmidt, Nucl. Phys. A **580** (1994) 475
[6] M. Benmerrouche, E. Tomusiak, Phys. Rev. Lett. **73** (1994) 400
see also Comment/Reply:
V. Bernard, N. Kaiser, U.-G. Meißner, Phys. Rev. Lett. **74** (1995) 1036
M. Benmerrouche, E. Tomusiak, Phys. Rev. Lett. **74** (1995) 1037
[7] J. A. Gomez-Tejedor, F. Cano, E. Oset, Phys. Lett. B **382** (1996) 39
[8] V. Bernard, N. Kaiser, U.-G. Meißner, Phys. Lett. B **382** 19
[9] L. Y. Murphy, J. P. Laget, DAPHNIA/SPhN-96-10 (1996)
[10] J. A. Gomez-Tejedor, E. Oset, Nucl. Phys. A **600** (1996) 413
[11] M.Hirata, K.Ochi, T. Takaki, nucl-th/9711031 (1997)

Overview of Vector Meson Photoproduction

F. J. Klein
Thomas Jefferson National Accelerator Facility,
Jefferson Ave. 12000, Newport News, VA 23606, U.S.A.

SAPHIR Collaboration
Physikalisches Institut der Universität Bonn, Germany;
Institut für Strahlen- und Kernphysik, Universität Bonn, Germany;
II. Physikalisches Institut der Universität Göttingen, Germany;
Center for Nuclear Studies, The George Washington University, U.S.A.;
Jagellionian University, Cracow, Poland

Abstract

Almost all existing data on vector meson photoproduction at low energies date from experiments in the 1960's and 1970's. The only new data (from SAPHIR, Bonn, Germany) confirm the main results of previous experiments, deviations are observed in the midrange momentum transfer $t_{pp'}$.

INTRODUCTION

Photo- and electroproduction of neutral vector mesons allow an insight into the coupling of virtual and real photons to matter. The self energy of the photon is defined by its dissociation in hadrons ($\gamma^{(*)} \to \bar{q}q$) and in leptons ($\gamma^{(*)} \to \bar{l}l$); the vector mesons $\rho, \omega, \Phi, J/\Psi$, as well as their radial excitations, represent the quark/anti-quark bound states ($J^\pi = 1^-$) corresponding to the generational hierarchy in the Standard Model.

Extensive studies on vector meson leptoproduction beginning in the 1960's, as accelerators achieved the energies necessary to exceed the production energy thresholds, led to a wide knowledge of their properties, production, and decay dynamics. With progressively increasing accelerator energies most impact was given to the study of high energy phenomena. Photon-hadron interactions at high energies are dominated by the purely hadronic interaction of dissociated $\bar{q}q$ pairs with matter (Vector Meson Dominance). According to this description photoproduction of vector mesons is dominated by diffractive scattering of $\bar{q}q$ pairs on matter, assuming the $\bar{q}q$ pairs almost on the mass shell of the corresponding vector meson.

Nevertheless, open questions remain on the production mechanisms of light vector mesons near threshold, i.e. in the center-of-mass energy range of a few GeV.

First, on meson spectroscopy: are the approximations for high energies still valid in the low energy range?
Diffractive processes dominate obviously the leptoproduction of vector mesons at low $t_{pp'}$, Q^2 respectively. The enhancement of the cross section of ω (in its decay channel $\omega \to \pi^+\pi^-\pi^0$) in the low energy range can roughly be described by a large contribution of π^0 exchange in the t-channel but there are still deviations with respect to the data recently measured at SAPHIR. The determination of the ρ cross section suffers from the broad width of the ρ, esp. in the low energy range where the meson can only be described within models used to disentangle ρ, Δ, and other background distributions in the $N\pi\pi$ channel. Therefore the contributions to ρ production at low energy are still uncertain.

Secondly, is it possible to obtain information on baryon spectrocopy via photoproduction of light vector mesons?
An important motivation for studying the spectrum of baryon resonances with photons is

to determine the photoproduction amplitudes of the individual resonances. At c.m. energies above 1.7 GeV the multiple pion decay channels become dominant, and in this energy range the masses and partial widths of the resonances are poorly determined. An outstanding problem in our current day understanding of baryon spectroscopy is that of missing resonances. Probably these resonances tend to couple weakly to the largely analyzed πN channel and strongly to $\Delta\pi$, ρN, or ωN and γN [1]. Esp. the ωN decay channel can be comparatively well identified because of the narrow width of ω and the restriction of its coupling to N^* (I=$\frac{1}{2}$).

RECENT RESULTS FROM SAPHIR

The SAPHIR detector [2] is a magnetic spectrometer covering a large solid angle. The experiment is performed at the high duty cycle electron accelerator ELSA at Bonn University. The tagging system covers a photon energy range of 55% to 94% of the primary electron energy. By means of a cylindrical driftchamber a momentum resolution of 6.5% at 1.0 GeV/c is achieved. The time-of-flight information of the scintillator hodoscopes provides a particle separation (π–N for $|\vec{p}| < 1.5$ GeV/c; π–K for $|\vec{p}| < 0.8$ GeV/c). During data taking runs from Oct. 1993 to May 1994 about 6 mill. trigger were taken using electron beams of 1.7 GeV and 2.2 GeV to produce bremsstrahlung photons. The photon flux was determined via scalers on the tagging scintillators and corrected on beam quality.
The errors of the presented preliminary data were calculated as quadratic sum of statistical and (estimated) systematical errors. They mainly reflect the systematical uncertainty in the adjustment of the magnetic field, in the efficiency and time resolution of the scintillation counters, in the momentum resolution of the drift chambers, in the efficiency of the track reconstruction, and in the determination of the photon flux.

The event topologies were determined via several cuts on vertex position, probability of the vertex fit, identification of at least one positive charged particle, missing mass, missing momentum, and a kinematical fit. The cuts were determined by Monte-Carlo simulations of the dominant processes known for the reaction channels keeping contaminations below 3 % for the pionic channels and below 0.1 % for the K^+K^- channel [3].

The vector mesons were identified via their dominant decay channels:
$\rho^0 \to \pi^+\pi^-$ ($\approx 100\%$), $\omega \to \pi^+\pi^-\pi^0$ ($88.8 \pm 0.7\%$), $\Phi \to K^+K^-$ ($49.1 \pm 0.9\%$).

Reaction $\gamma p \to \rho^0 p \to \pi^+\pi^- p$

The determination of the ρ^0 cross section depends on assumptions concerning the separation procedures as well as the accuracy of the measured total cross section of $\pi^+\pi^-$ photoproduction [3,4] (fig. 1).

The fractions of ρ^0, Δ^{++}, and Δ^0 production were determined via the fitting procedures described in the appendix. Due to the moderate statistics each 6 tagger channels are grouped to one energy interval.

For the data from ρ threshold ($E_\gamma \approx 1.07$ GeV) up to 1.2 GeV photon energy an interference of ρ^0 and Δ^{++} production is taken into consideration. An interference between ρ^0 and ω seems to contribute scarcely at these low energies, the contribution is less than 0.5 % in all energy intervals. Δ^0 contributes up to a few percent at low energies but scarcely above 1.5 GeV. Above 1.5 GeV photon energy the $\pi^+\pi^-$ mass distribution shows a shift of the ρ mass and a very asymmetrical shape (fig. 2) that can be described by an interference of ρ^0 production and nonresonant $\pi^+\pi^-$ background [5].

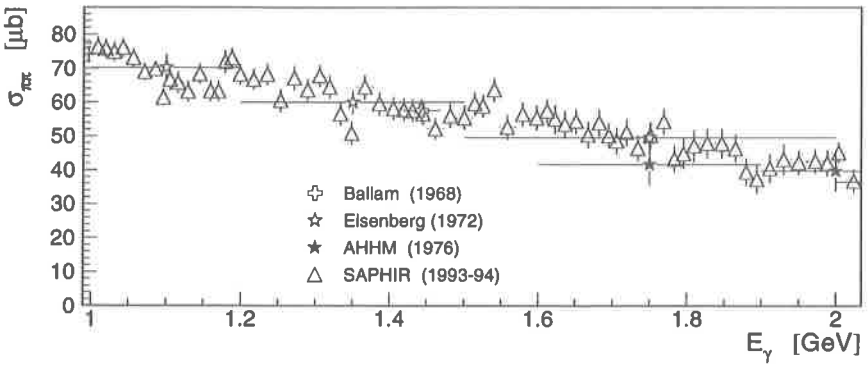

Figure 1. Total cross section of $\gamma p \to \pi^+\pi^- p$ at $1.0 < E_\gamma < 2.03$ GeV. For SAPHIR data: the widths of the energy bins reflect the energy resolution of the tagger.

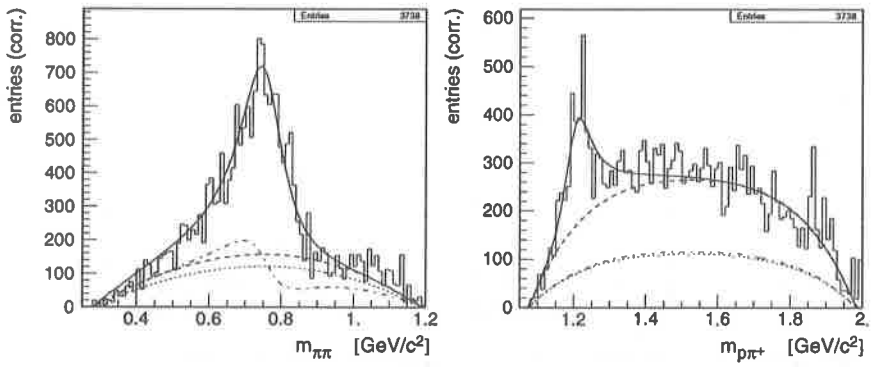

Figure 2. Influence of Δ^{++} reflection and interference with non resonant $\pi\pi$ background on the ρ^0 shape at $1.92 < E_\gamma < 2.03$ GeV. The *dotted* line shows the phase space contribution, the *dash-dotted* line the interference with non resonant $\pi\pi$, the *dashed* line in the $m_{\pi\pi}$ plot the Δ^{++} reflection, in the $m_{p\pi+}$ plot the ρ^0 reflection.

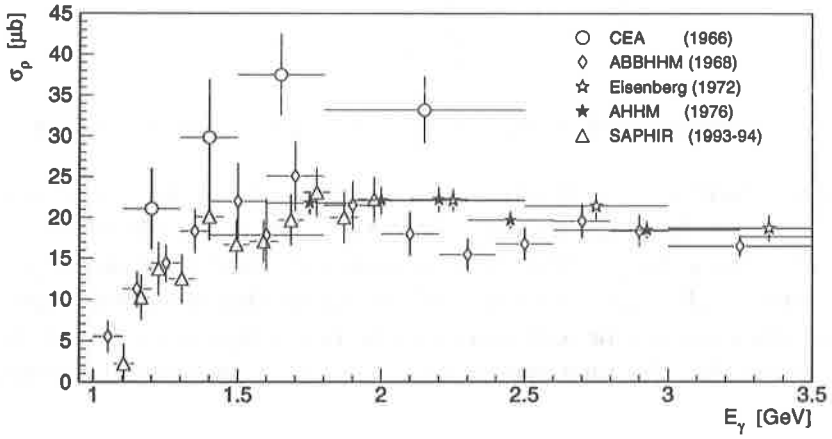

Figure 3. Comparison of cross section data for $\gamma p \to \rho^0 p$. The deviation of CEA data is due to their fitting solely within the $\pi^+\pi^-$ mass distribution regarding ρ^0 contribution and uncorrelated $\pi^+\pi^-$ (phase space).

The determination of the ρ^0 proportion to the channel $\gamma p \to \pi^+\pi^- p$ leads to the total cross section which is compared with all previous experiments [6] in fig. 3.

The differential cross section $d\sigma/dt(\gamma p \to \rho^0 p)$ is calculated by applying the fitting procedure for incoherent production of ρ^0 and Δ^{++} in intervals of the squared four-momentum transfer $t_{pp'}$, i.e. via disentangling the contributions of ρ^0, Δ^{++}, and phase space within intervalls of width $\Delta t_{pp'} = 0.1$ GeV^2/c^2.

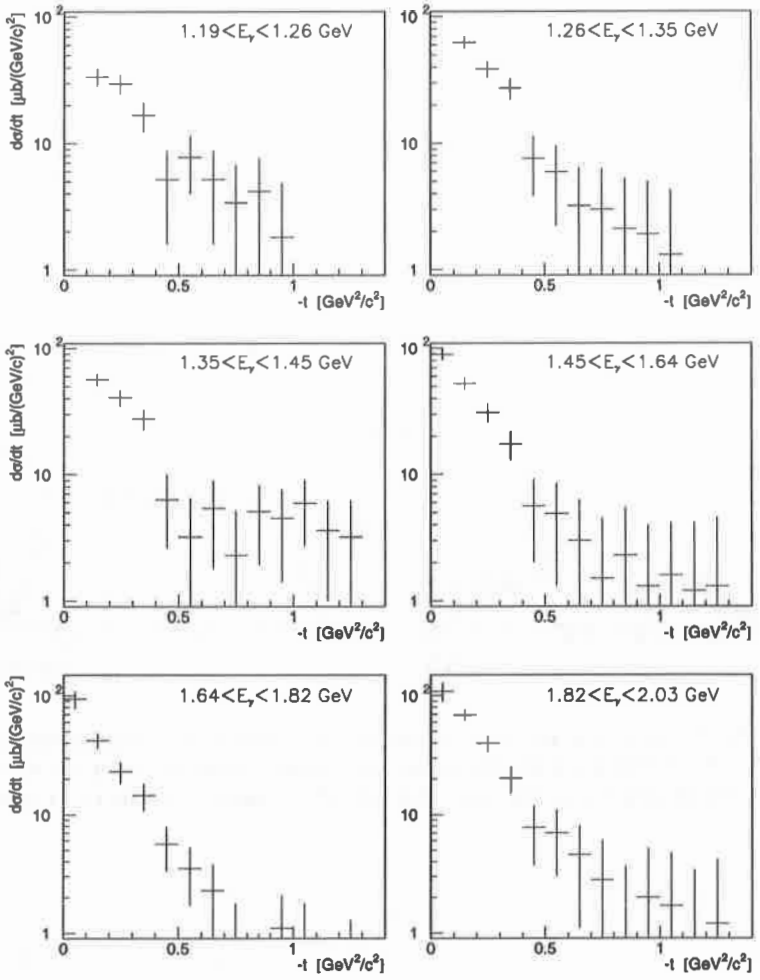

Figure 4. Differential cross section of $\gamma p \to \rho^0 p$ when the searation procedure is applied in intervals of $t_{pp'}$

The ρ^0 decay distribution is determined via weighting the transition amplitude T_ρ by $W(\cos\theta_{hel}, \phi_{hel})$ where θ_{hel}, ϕ_{hel} are the polar and azimutal angle of the decay π^+ with repect to the ρ^0 helicity frame. The fitted spin density matrix elements ρ_{00}, ρ_{1-1}, Re ρ_{10} are consistent with zero for $t_{pp'} < 0.4$ GeV^2/c^2 indicating that the decay angular distribution of ρ^0 in forward direction can be well described by $W(\cos\theta_{hel}, \phi_{hel}) = \frac{3}{2}\sin^2\theta_{hel}$ as expected for diffractive production. For photon energies above 1.65 GeV such a behaviour is also found for higher $t_{pp'}$.

Reaction $\gamma p \to \omega p \to \pi^+\pi^-\pi^0 p$

Unlike the broad ρ resonance, the ω meson can accurately be extracted in the $\pi\pi\pi$ mass distribution. Nevertheless, there are some uncertainties in separating the ω signal in kinematical regions where the data is rather poor. Without detecting the π^0 of the ω decay at SAPHIR the measured data is restricted on $|t_{pp'}| > 0.12$ GeV^2/c^2 because all three charged particles must be reconstructed to identify the triple pion channel.

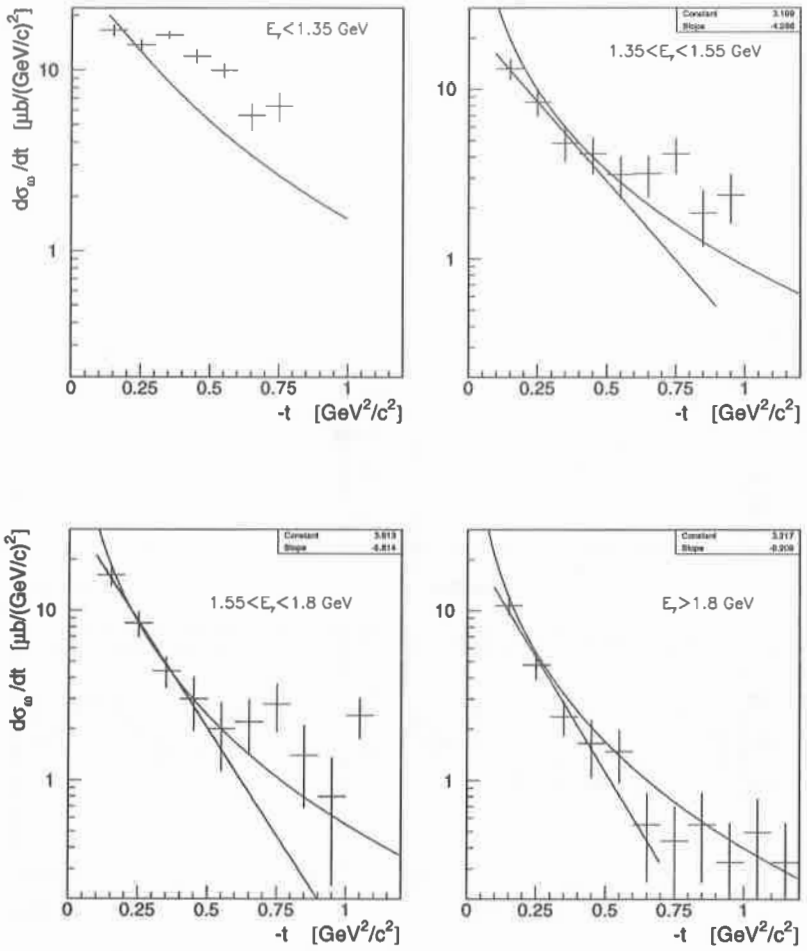

Figure 5. Differential cross section $\gamma p \to \omega p \to \pi^+\pi^-\pi^0 p$. SAPHIR data in comparison with predictions of the model of Friman and Soyeur (*curve*) and an exponential fit to SAPHIR data (*straight line*).

Fig. 5 shows the differential cross section. The curves represent the predictions of pure diffractive production ($d\sigma/dt \propto e^{-b|t|}$) and one-pion-exchange according to the model of Friman and Soyeur [7]. In the low energy range ($E_\gamma < 1.2$ GeV) the diff. cross section is almost flat with respect to the four-momentum transfer. With increasing center-of-mass energy the exponential falloff with $t_{pp'}$, as predicted by diffractive models, becomes more obvious – at least in the low $t_{pp'}$ range whereas in the mid $t_{pp'}$ range departures from the predicted values are obvious [3,8].

Extrapolation to $\frac{d\sigma}{dt}|_{t=0}$ and integration lead to the total cross section (fig. 6, cf. [9]). The steep increase at the ω photoproduction threshold ($E_\gamma = 1.1$ GeV) can't be solely explained within the framework of the model of Friman-Soyeur nor vector meson dominance.

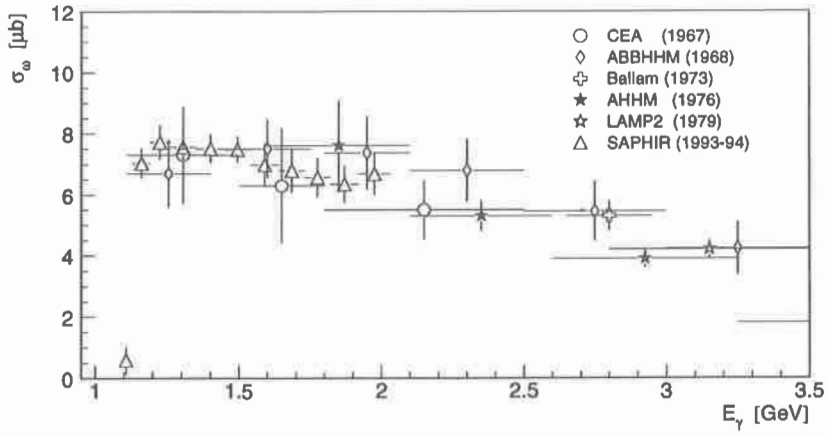

Figure 6. Total cross section $\gamma p \to \omega p \to \pi^+\pi^-\pi^0 p$

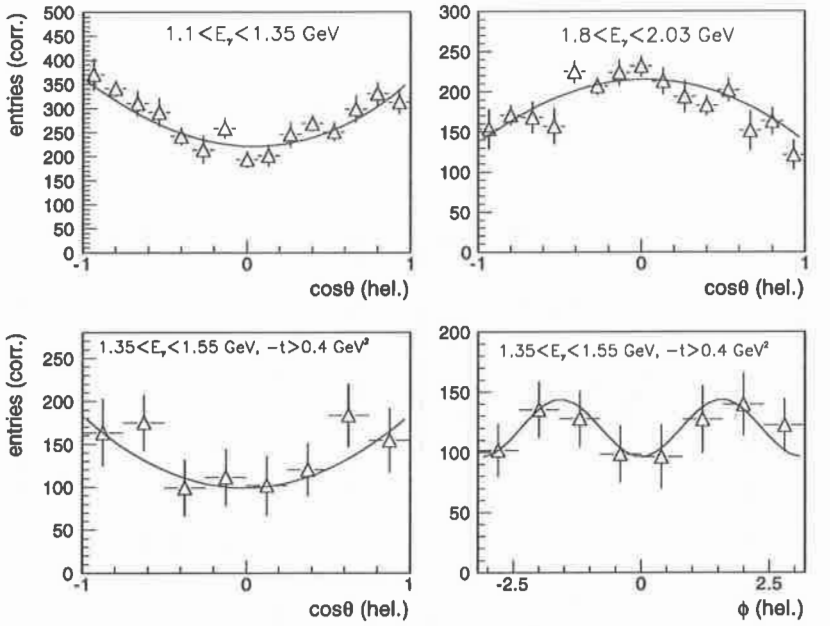

Figure 7. Decay distribution of ω (helicity frame) in selected energy ranges. The *curves* represent the fit on $W(\cos\theta_{hel},\phi_{hel})$ according to eq. (6).

This is confirmed by the decay angular distribution (in the ω helicity frame). Fig. 7 shows for the low energy range a more $\cos^2\theta_{hel}$ behaviour whereas at higher energy the decay angular distribution looks more diffractionlike ($\propto \sin^2\theta_{hel}$).

At photon energies between 1.35 and 1.55 GeV the differential cross section has large deviations from the predicted values for $0^{\pm}$ transfers in the mid $t_{pp'}$ range; this is confirmed by the decay distribution reflecting non diffractive behaviour and large interference effects (cf. fig. 7).

Reaction $\gamma p \to \Phi p \to K^+K^- p$

Tighter cuts for the Φ analysis – taking into consideration the low Φ cross section and the moderate particle identification of $K^\pm$ – lead to a clear resonance signal in the invariant mass distribution $m_{K^+K^-}$ but low statistics (ca. 180 events) [3]. The favoured forward direction and the exponential falloff in the differential cross section (fig. 8a) as well as the distribution of the decay angle θ_{hel} in the Φ helicity frame (fig. 8b) indicate dominantly diffractive production of this vector meson even near threshold ($E_\gamma^{thr} = 1.57$ GeV). The integrated cross section between threshold and $E_\gamma = 2.03$ GeV totals $0.25 \pm 0.06 \mu$b. Nevertheless, a more precise investigation of Φ photoproduction can only be carried out with higher statistics and accurate data samples.

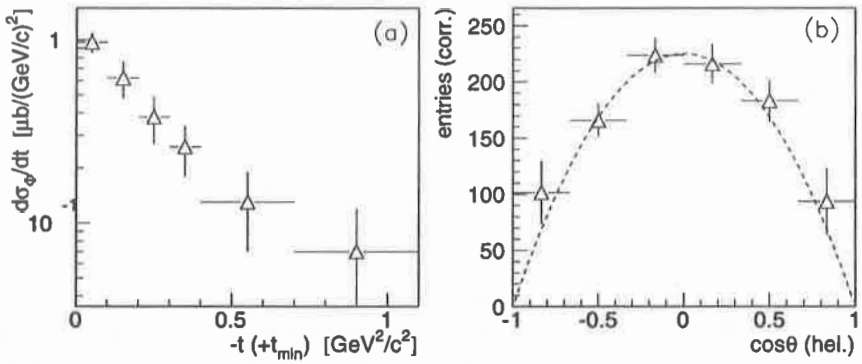

Figure 8. (a) Differential cross section of $\gamma p \to \Phi p \to K^+K^- p$ as function of $(|t| - |t_{min}|)$. (b) Decay angular distribution of Φ in its helicity frame; the *dashed* curve indicates the prediction for s-channel helicitiy conservation.

OUTLOOK

In 1997, SAPHIR has taken larger data samples that are supposed to be more homogeneous than the previous ones. The analysis of this data (with about 20 times higher statistics than the here reported) is in progress, results will soon be available.

Several experimental proposals at TJNAF deal with vector meson photo- and electroproduction. We want to emphasize those proposals that will use a coherent bremsstrahlung facility to produce linear polarized photons allowing to separate natural and unnatural parity exchange [10] (cf. [11]). Nevertheless, it is not certain whether such an experimental approach will be sufficient to disentangle N^* and Δ^* contributions in the $p\pi\pi$ channel. The variations in the spin density matrix elements that are crucial to settle the question are supposed to be very small. In the case of ω photoproduction polarisation data will help to extract contributions of baryon resonances; due to the isospin selectivity of this channel the search for 'missing resonances' is supposed to be more successful, a proper candidate will be the resonance $F_{15}(2000)$ [12].

Φ Photoproduction is of special interest as deviations from diffractive production may allow an insight into the strange quark content of the nucleon ('$s\bar{s}$–knockout') due to OZI suppression of meson exchange. It also allows to study the transition from 'soft pomeron exchange' to 'hard pomeron exchange' and other hard processes at high $t_{pp'}$ [13].

ACKNOWLEDGEMENTS

The authors want to point out that the presented vector meson data from SAPHIR are preliminary. Thanks to all members of the SAPHIR collaboration who contributed to these remarkable results. Author (FJK) would like to thank the organizers of the N^* Workshop to give the opportunity to present this overview.

APPENDIX: MULTIDIMENSIONAL FITTING PROCEDURES

Via multidimensional fitting procedures one tries to disentangle the contributions of different scattering processes with statistical methods. The procedures used in the analysis of the SAPHIR data are mainly based on the assumption that ρ production and concurring processes (such as baryon resonances or uncorrelated $\pi\pi$ production) show different dependences on the invariant masses $m_{\pi^+\pi^-}$, $m_{p\pi^+}$, and $m_{p\pi^-}$ [14,3].

The cross section for γN–scattering with final state particles p, π^+, π^- is given by

$$d\sigma \propto \sum_{spins} |T_1 + T_2 + \ldots + T_n|^2 \frac{1}{flux} dLIPS \tag{1}$$

if the reaction can be described by n transition amplitudes $(T_1, \ldots, T_n)$.

In the analysis of the SAPHIR data the processes $\gamma p \to \pi^- \Delta^{++}$, $\gamma p \to \pi^+ \Delta^0$, $\gamma p \to \rho^0 p$, and a background (phase-space distribution) are taken into account. For ρ^0 and Δ production the transition amplitudes are parametrized by relativistic Breit-Wigner terms:

$$T_k(m_{ij}) = \frac{1}{\sqrt{N_k}} \sqrt{\frac{m_{ij}\Gamma(m_{ij})}{q(m_{ij})}} \frac{1}{m_k^2 - m_{ij}^2 - i m_k \Gamma(m_{ij})} \tag{2}$$

where m_k is the mass of the resonance $k = (\rho^0, \Delta^{++}, \Delta^0)$, m_{ij} the invariant mass of the decay particles i, j, $q(m_{ij})$ the three-momentum of i, j in the joint rest frame, $N_k = \int |T_k|^2 dLIPS$ the normalisation integral, and $\Gamma(m_{ij})$ an energy dependent width [15]:

$$\Gamma(m_{ij}) = \Gamma_k \left(\frac{q(m_{ij})}{q(m_k)} \right)^{(2l+1)} \frac{\rho(m_{ij})}{\rho(m_k)} \tag{3}$$

The factors $\rho(m)$ are empirical correction terms reflecting the large widths of ρ and Δ:

$$\begin{array}{lll} \Delta: & \rho(m_{N\pi}) = & (2.2 m_\pi^2 + q^2(m_{N\pi}))^{-1} \\ \rho^0: & \rho(m_{\pi\pi}) = & (q^2(m_{\pi\pi}) + q^2(m_\rho))^{-1} \end{array} \tag{4}$$

The density distribution of events in the Daltiz plot $m^2_{p\pi^+}$ vs. $m^2_{\pi^+\pi^-}$ is then described via the expression:

$$dW = (a_\rho |T_\rho|^2 + a_\Delta |T_\Delta|^2 + 2\alpha \sqrt{a_\rho a_\Delta} \mathrm{Re}|T_\Delta T_\rho^*| + a_0 |T_0|^2 + a_{ps} |T_{ps}|^2) dLIPS(E_{cm}, m^2_{p\pi^+}, m^2_{\pi\pi}) \tag{5}$$

Here $a_\rho, a_\Delta, a_0, a_{ps}$ are the fraction of ρ^0, Δ^{++}, Δ^0 production, and background, resp., to the channel $\gamma p \to \pi^+\pi^- p$. The interference of Δ^0 with other processes is not taken into account because of the small Δ^0 contribution compared with the other processes. For $E_\gamma > 1.5$ GeV it is reasonable to assume incoherent production, i.e. the cross section is set proportional

to the sum of the squared amplitudes, because ρ^0, Δ^{++}, and Δ^0 are then mainly produced in kinematically separated regions in the Dalitz plot of $m^2_{p\pi^+}$ vs. $m^2_{\pi\pi}$.

When the strengths of the contributions are roughly determined via this fitting procedure, the transition amplitudes are weighted by terms describing the production $G(s,t)$ and decay dynamics $W(\cos\theta,\phi,s,t)$: $T_i \longrightarrow T_i \times \sqrt{G(s,t)} \times \sqrt{W(\cos\theta,\phi,s,t)}$,
e. g. for diffractive production: $G(s,t) = A(s)e^{-B(s)|t|}$.
For vector mesons decaying into spinless particles the decay distribution reads [11]:

$$W(\cos\theta,\phi) = \begin{array}{l} \frac{3}{4\pi}(\frac{1}{2}(1-\rho_{00}) + \frac{1}{2}(3\rho_{00}-1)\cos^2\theta \\ -\sqrt{2}\mathrm{Re}\rho_{10}\sin 2\theta\cos\phi - \rho_{1-1}\sin^2\theta\cos 2\phi), \end{array} \quad (6)$$

if photon beam and target are both unpolarized. ρ_{ik} are the density matrix elements in the spin space; the polar and azimuthal angles (θ, ϕ) describe the direction of the positive charged decay particle (in three-particle decays the direction of the normal to the decay plane) in the rest frame of the vector meson with respect to a quantization axis z in the production plane.

REFERENCES

[1] R. Koniuk and N. Isgur, Phys.Rev. D**21**, 1898 (1980); S. Capstick and N. Isgur, Phys.Rev. D**34**, 2809 (1986); S. Capstick and W. Roberts, Phys.Rev. D**47**, 1994 (1993).

[2] W. Schwille et al. (SAPHIR coll.), Nucl.Instr.Meth. A**344**, 470 (1994).

[3] F. J. Klein, Ph.D. thesis, Bonn IR-96-08 (1996).

[4] Y. Eisenberg et al., Phys.Rev. D**5**, 15 (1972); J. Ballam et al., Phys.Rev. D**5**, 545 (1972); P. Struczinski et al. (AHHM coll.), Nucl.Phys. B**108**, 45 (1976).

[5] P. Soeding, Phys. Lett. **19**, 702 (1965).

[6] Crouch et al. (CEA coll.), Phys.Rev. **146**, 994 (1966); ABBHHM collaboration, Phys.Rev. **175**, 1669 (1968); Y. Eisenberg et al., Nucl.Phys. B**42**, 349 (1972); P. Struczinski et al. (AHHM coll.), Nucl.Phys. B**108**, 45 (1976).

[7] B. Friman and M. Soyeur, Nucl.Phys. A**600**, 477 (1996).

[8] J. Hannappel, Ph.D. thesis, Bonn IR-96-04 (1996).

[9] Crouch et al. (CEA coll.), Phys.Rev. **155**, 1468 (1967); ABBHHM collaboration, Phys.Rev. **175**, 1669 (1968); J. Ballam et al., Phys.Rev. D**7**, 3150 (1973); P. Struczinski et al. (AHHM coll.), Nucl.Phys. B**108**, 45 (1976); D. P. Barber et al. (LAMP2 coll.), Z.Phys. C**2**, 1 (1979).

[10] CEBAF experimental proposals: E94-109 (P. L. Cole, J. P. Connelly, R. R. Whitney), E97-005 (D. J. Tedeschi, P. L. Cole, J. A. Mueller), LOI97-002 (F. J. Klein, P. L. Cole).

[11] K. Schilling, P. Seyboth, and G. Wolf, Nucl.Phys. B**15**, 397 (1970).

[12] CEBAF experimental proposals: E91-024 (H. Funsten, V. Burkert, D. M. Manley, B. Mecking), LOI97-002 (F. J. Klein, P. L. Cole).

[13] CEBAF experimental proposals: E93-022 (E. Smith, H. Funsten, P. Rubin), E93-031 (C. Marchand, M. Anghinolfi, J. M. Laget), E97-005 (D. J. Tedeschi, P. L. Cole, J. A. Mueller).

[14] H. Spitzer, Ph.D. thesis, Hamburg, DESY F1/4 (1967); ABBHHM Collaboration, Phys.Rev. 175 (1968) 1669.

[15] J. D. Jackson, Nuovo Cim. **34**, 1644 (1964).

The Crystal Ball Baryon-Resonance Program

B. M. K. Nefkens
Department of Physics and Astronomy
UCLA, Los Angeles, CA 90095, U.S.A.

Abstract

The Crystal Ball multiphoton spectrometer is the principal detector used in a comprehensive program of baryon spectroscopy of the N^*, Δ^*, Λ^*, and Σ^* resonances. The objectives of the program are the determination of the characteristics of the resonances, the pole values, width, and chief decay rates, furthermore, to make a massive search for the "hidden" resonances of flavor $SU(3)$ and the simple quark model. The data can be used for a thorough investigation of possible hidden symmetries of Strong QCD by an extensive study of spectroscopic regularities that are apparent in the pole-spin/parity plots of the N^*, Δ^*, Λ^*, and Σ^* families such as Höhler baryon clusters and parity doublets. Special attention will be given to measurements of the radiative decay of hyperons which are almost unknown. This is done by measuring the reaction $K^-p \to \Lambda\gamma$ or $\Sigma^0\gamma$. Presently, the CB is set up in the C-line of the AGS which furnishes separated π and K beams to 760 MeV/c. The measurements cover all neutral final states produced in π^- or K^- interactions on protons. Plans for the future are to move to the D-line of the AGS which goes to 1.8 GeV/c, this will allow us to investigate the resonances with masses to 2.1 GeV/c^2. The CB is particularly suited for measuring multi-meson final states such as $2\pi^0$, $\pi^0\gamma$, $\pi^0\eta$, $\pi^0\omega$, $\pi^0\eta'$, etc. This will facilitate the search for hidden resonances.

INTRODUCTION

The credentials of QCD include excellent agreement with all high energy data and a good theoretical framework. A major unfulfilled goal of QCD is to provide the theory of *quark confinement*. Over one hundred baryonic resonances have been discovered and their features are consistent with the assumption that all baryon resonances are three-quark systems. There is no impeccable evidence at low energy for the gluon degree of freedom, which is expected from QCD. There is no evidence for bona fide hybrids, pentaquarks, molecular states and other "exotica" of QCD.

An interesting controversy of baryon spectroscopy concerns "missing" resonances. Constituent quark-model calculations predict the existence of 64 N^* and 32 Δ^* states with $m \lesssim 3$ GeV/c^2 [1], only 22 of each have been found. Flavor $SU(3)$, which is a pillar of QCD, requires the ratio of N^* to Δ^* states to be two [2]; experimentally it is one [3]. Two very different reasons for this have been proposed:

a) the "missing" states are missing because of the severe limitations in the available experimental data. The crucial information on the existence of the known N^* and Δ^* states comes from the Partial Wave Analyses of the πN scattering data. If for one reason or another certain N^* and Δ^* states would have a small πN coupling, such resonances could have been missed by the PWA.

b) the "missing" states are not missing. They are non-existent. The number of baryonic states is smaller than flavor-$SU(3)$ or quark models predict because of the operation of new, "hidden" symmetries of Strong QCD. An obvious candidate for such a hidden symmetry is chiral symmetry. Another possibility is a diquark baryon substructure. Such "hidden" symmetries may show up as subtle regularities in baryon spectroscopy. They could be looked for in the pole-spin/parity plots of the various resonance families.

Some possibilities are Höhler clusters and parity doublets. Other evidence may be found in the occurrence of unorthodox decay modes and large decay rates, for instance the extraordinarily large η decay rate of several s-wave resonances.

Major new experimental data on baryon spectroscopy will be needed to solve the mystery of the "missing" states. The prospects for new data in the near future appear to be good.

a) A focussed, direct attack is under way at the AGS using the Crystal Ball detector. The plan is to measure all neutral decay channels of all resonances that are produced by π and K interactions on protons. Resonances may be produced directly such as in $\pi^- p \to N^*$ or $K^- p \to \Lambda^*$ or indirectly such as in $\pi p \to N^*(A) \to N^*(X) + \pi^0/\eta/\omega/\eta'$, where $N^*(A)$ is an established state and $N^*(X)$ a missing state.

b) At Jefferson Lab the CLAS collaboration has embarked on a large program in photo- and electroproduction of baryonic states. This effort is expected to measure all radiative couplings and electromagnetic form factors of the baryon resonances.

c) Much new data is expected from CELSIUS and COSY on resonance production in pp and pd interactions. LEAR has data on $\overline{p}p \to N^*\overline{N^*}$. Finally, the 4 LEP detectors have interesting baryon resonance data in jet events.

In the following we discuss the Crystal Ball program at BNL.

The Crystal Ball is a multiphoton spectrometer, it has a solid-angle coverage of 94% of 4π. The energy resolution is typically 5%. The angular resolution is 2-3%. Brad Tippens has presented an informative description of the CB in a separate talk at this conference [4].

Baryonic Resonances

The three light quarks can be arranged in 6 baryonic families, the N^*, Δ^*, Λ^*, Σ^*, Ξ^*, and Ω^*. The number of family members that can exist is not arbitrary. Rather, the following proportionality is expected when the $SU(3)$-flavor symmetry of QCD is the controlling symmetry [2]:

$$2N^* : 1\Delta^* : 3\Lambda^* : 3\Sigma^* : 3\Xi^* : 1\Omega^*. \quad (1)$$

The number of experimentally identified resonances of each baryon family is [3]

$$22N^*,\ 22\Delta^*,\ 18\Lambda^*,\ 26\Sigma^*,\ 11\Xi^*, \text{ and } 4\Omega^*. \quad (2)$$

Constituent quark models predict the existence of no less than 64 N^* and 22 Δ^* states with mass < 3 GeV/c^2. The seriousness of the "missing-states" problem is obvious from these numbers. Recently, the hypothesis of a very small πN coupling of missing states has received support from a new quark-model calculation [2]. However, conclusions on missing states should await the results of more realistic, coupled-channel calculations in which rescattering of other mesons, the η, ω, and ρ, is considered. For instance, the reaction $\omega N \to \pi N$ is strongly exothermic and much favored by phase space. At the ω-threshold the reaction $\omega N \to \pi N$ has a singularity favoring the πN final state.

There are two types of hidden symmetries: the unbroken and broken ones. The classic example of an unbroken, hidden symmetry is color $SU(3)$. It is required that all observable states are colorless. This has an interesting consequence: it reduces the number of allowed Λ states because the Λ singlet ground state is forbidden by Fermi statistics. A good example

of a broken, hidden symmetry is chiral symmetry, χS. It is based on the spin-momentum alignment of massless quarks. χS is broken because physical quarks have mass. χS shows up in many low energy reactions that involve a pion. The ramifications of χS for baryon spectroscopy are being explored.

An interesting hidden symmetry would be a diquark substructure of baryons. It would reduce the number of expected states and could eliminate the problem of the missing states.

Another type of symmetry may play a role in baryon spectroscopy, namely, dynamic symmetry. It has had some spectacular successes in nuclear physics such as in the Interacting Boson Model. Dynamic symmetries may be handled conveniently by group theoretic techniques. This is being applied to baryon physics by Bijker et al. [5]

The available data on the properties of the various baryon resonances show some interesting regularities. They can be readily observed with the help of the pole-spin/parity plots of the 6 different families. Figure 1 shows such a plot for the N^* family and Fig. 2 for the Δ^*, specifically, each plot gives the real part of the pole position as well as spin and parity. Each state of each family is uniquely given by its pole values and spin/parity. There are other important resonance parameters such as the rates for different decay channels but they are not unique. Some regularities seen in the available data on the N^*, Δ^*, Λ^*, and Σ^* families are:

a) Höhler clusters. These are groups of states that have the same value for the real part of the complex pole but different spin and parity. For instance, in Fig. 1 one can see 6 N^* states that all have the same pole value of 1680 ± 20 MeV. In Fig. 2 one sees a cluster of 7 Δ^* states with a pole value 1870 ± 40 MeV. About half of the known baryons appear to belong to a Höhler cluster. More and better data are needed to show the extent and quality of the cluster phenomenon.

b) Parity doublets. This is the occurrence of pairs of states having the same spin and pole value but different parity. An example of a nice N^* parity doublet is the $H_{19}(2220)$ and $G_{19}(2250)$. Over half the baryon resonances come in parity doublets. Better data are needed to study the extent of this phenomenon.

c) Regge trajectories. They occur in each family and provide a simple relation between the value of the spin and the mass squared. They have been known for a long time.

The experimental information on different baryons is not of uniform quality. A system with a number of stars is used to indicate the confidence level in the quality of a state. The four-star resonances are well established, the three star ones are good, but two star states are questionable and the one star ones are not reliable. In Figs. 1 and 2 we have used shades of grey to mark the quality; dark grey corresponds to a 4-star status down to very light grey for the 1-star ones.

The N^* states can only belong to an octet of flavor $SU(3)$ and the Δ^* only to a decuplet. However, the Σ^* and Ξ^* can belong either to an octet or to a decuplet while the Λ^* must belong to an octet or be a singlet. The latter are rather interesting states. Only two singlets are well established, the $\Lambda(1405)$ and the $\Lambda(1520)$. The mass of the $\Lambda(1405)$ is much below quark model expectations. This has prompted the suggestion by Dalitz and others that the $\Lambda(1405)$ is actually a $\overline{K}N$ bound state rather than a 3-quark state. The $\Lambda(1520)$ is the one hyperon for which a radiative decay has been observed.

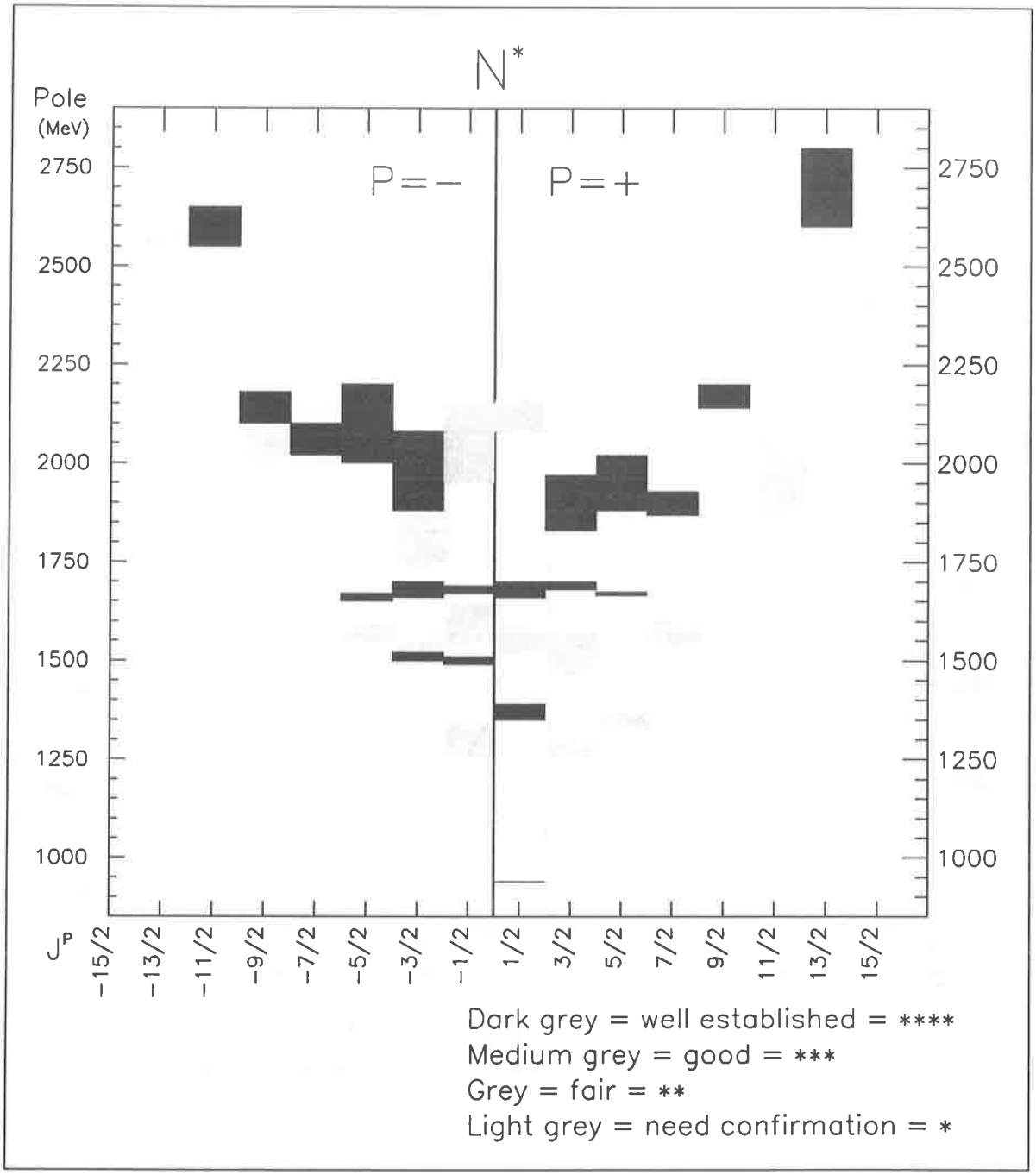

Figure 1. Pole-spin/parity plot of the 22 known N^* states. The experimental confidence level usually expressed in the number of stars, is indicated here by different shades of grey.

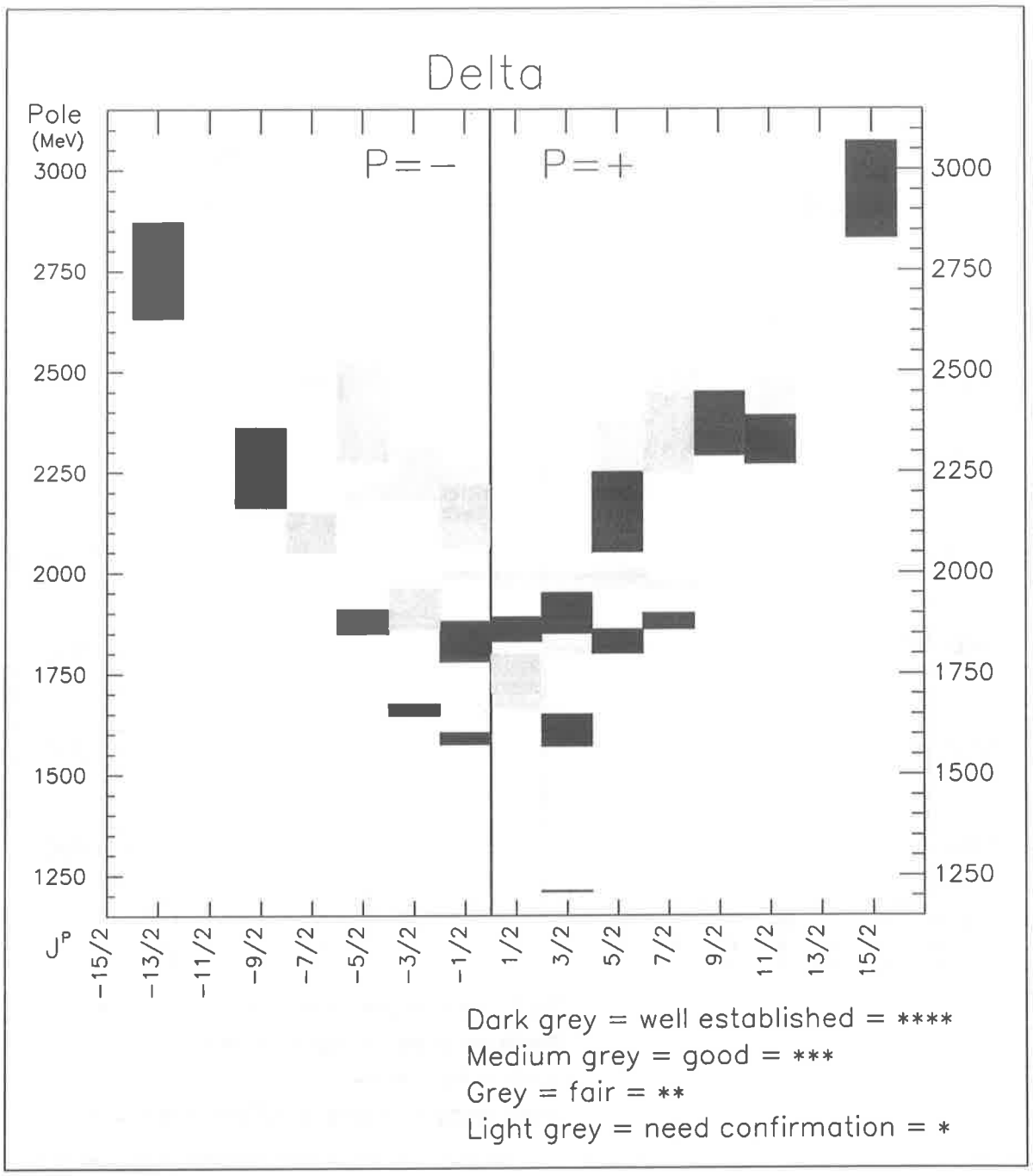

Figure 2. Same as Fig. 1 for the 22 known Δ^* states.

The Crystal Ball Baryon-Resonance Program at BNL

The Crystal Ball, CB, multiphoton detector is presently at BNL. It is installed at the AGS in the C-6 line which is a separated π and K beam, the maximum momentum is 760 MeV/c. Two experiments are under way to measure the many different neutral decay modes of the baryon resonances simultaneously, this is a very efficient approach. AGS Exp E913 is designed for measuring N^* and Δ^* states in $\pi^- p \rightarrow$neutrals, while AGS E914 is aimed at the Λ^* and Σ^* states, not only the known ones but also the many missing resonances possibly produced in $K^- p \rightarrow$neutrals.

The chief objectives of these two experiments are the following:

1. The primary goal is the determination of the characteristics, which are the pole values, width, and major decay rates of the various N^*, Δ^*, Λ^*, and Σ^* states with $m \lesssim 2.1$ GeV/c^2. The main technique employed in the case of the N^* and Δ^* states is the Partial Wave Analysis of the πN, ηN, $\pi^0\pi^0 N$, ωN, and $\eta' N$ decay channels. The Λ^* and Σ^* states are studied via their different neutral decay modes including, 1, 2, and 3 π^0, and/or η, ω, and η' mesons. Also much data will be collected automatically on K^- charge exchange, $K^- p \rightarrow K^0 n \rightarrow 2\pi^0 n$.

2. A thorough search will be made for unorthodox baryonic matter, such as hybrids, pentaquarks, bound states, and so forth. The technique employed is based on observing some of the unorthodox decay modes that have been predicted and on measuring certain "anomalously" large decay rates of exotic states. If time permits we would like to investigate the possible occurrence of eta-mesonic hypernuclei and nuclei, as well as other cases of nuclear exotica.

3. A special effort is devoted to measuring the radiative decays of the Λ^* and Σ^* states by inverse kaon photoproduction, $K^- p \rightarrow \Lambda^*/\Sigma^* \rightarrow \Lambda\gamma$ or $\Sigma^0\gamma$. Radiative hyperon decays have never been measured with the exception of $\Lambda(1520) \rightarrow \Lambda\gamma$. Because the Λ and Σ^0 are highly unstable particles, the direct kaon photo- and electroproduction processes are not accessible. There is fortunately a link, admittedly a minor one, between the reaction $\gamma p \rightarrow \Sigma^0 K^+$ which is readily accessible at Jefferson Lab and the $K^- p \rightarrow \Sigma^0\gamma$ part of the CB program, it goes via the crossing relation.

The only radiative hyperon decay that has been seen is a big one, $\sigma_t(K^- p \rightarrow \Lambda^*(1520) \rightarrow \Lambda\gamma) = 0.3$ mb. Based on $SU(3)$ flavor symmetry one can readily predict that $\sigma_t(K^- p \rightarrow \Lambda^*(1520) \rightarrow \Sigma^0\gamma) \approx 0.8$ mb. This is a surprisingly large value since the strong decays are only a factor of 10 larger e.g. $K^- p \rightarrow \Lambda^*(1520) \rightarrow \Sigma^0\pi^0 \approx 7$ mb. It is of interest to verify this prediction experimentally.

In 1997 the CB had a two week run which was used to measure $\pi^- p \rightarrow$neutrals from 300-760 MeV/c^2. The angular distributions of the $n\gamma$, $n\pi^0$, $n2\pi^0$, and $n\eta$ final states are measured at the same time. Preliminary results of these have been discussed by Tippens [4].

In 1998 the major effort is going to be on measuring the neutral final state reactions in $K^- p$ interactions from 450 to 760 MeV/c, specifically the $\Lambda\gamma$, $\Lambda\pi^0$, $\Lambda 2\pi^0$, and $\Lambda\eta$, as well as $\Sigma^0\gamma$, $\Sigma^0\pi^0$, $\Sigma^0 2\pi^0$, and $K^0 n$ $(= 2\pi^0 n)$ states. It is very helpful in an amplitude or partial wave analysis that all final states that include the π^0, η, ω, or η' are isospin unique. For example, the $\Lambda 2\pi^0$, $\Lambda\eta$, $\Lambda\omega$, $\Lambda\eta'$, and $\Sigma^0\pi^0$ states have $I = 0$, while $\Lambda\pi^0$, $\Lambda 3\pi^0$, $\Sigma^0 2\pi^0$, $\Sigma^0\eta$, $\Sigma^0\omega$, and $\Sigma^0\eta'$ are exclusively $I = 1$ states.

An important feature of reactions that have a final state containing a Λ or Σ^0 is that the polarization of the hyperon can be determined from its decay distribution. Such information

greatly facilitates the making of a unique partial wave analysis of the reaction. Thus, it will not be necessary to do also a separate experiment on a polarized target to investigate the hyperon resonances. However, the study of the 2 body decays of the N^* are Δ^* is in need of separate polarization data.

The maximum available beam momentum of 760 MeV/c in the AGS C-6 line still affords the investigation of 6 Λ^* and 10 Σ^* states and candidates. Of special interest is the confirmation of the two star $\Sigma^*(1560)$ candidate of undetermined spin and parity. If this turns out to be a full fledged resonance there will be serious difficulty for the viability of constituent quark models.

A radiative decay which is especially interesting is that of the $\Lambda^*(1405)$. This state is an enigma to constituent quark models because its mass is much too low compared to its companion, the $\Lambda^*(1520)$. This difficulty has led Dalitz and coworkers to suggest that the $\Lambda(1405)$ may be a special pentaquark, namely, a $\overline{K}N$ bound state with $Q = -30$ MeV. An important test of this idea can be made by measuring the ratio of radiative decays

$$R = \frac{\Gamma[\Lambda(1405) \to \Lambda\gamma]}{\Gamma[\Lambda(1405) \to \Sigma^0\gamma]}$$

as function a of the value for Q. We plan to do this using the following sequential production process:

$$K^-p \to \Sigma(1660) \to \Lambda(1405) + \pi^0,$$

followed by the decay of the $\Lambda(1405)$ to $\Lambda\gamma$ and $\Sigma^0\gamma$.

After the completion of the measurements in the C-6 line we would like to move the Crystal Ball to the D-line of the AGS. This is a nice "clean" separated π and K beam up to 1.8 GeV/c. This will enable us to investigate the different baryon resonances up to masses of 2.1 GeV/c^2 by their neutral decays. We would like to search for "missing" resonances that have a small πN coupling via the method of sequential reactions, e.g. $\pi^-p \to N^*(A) \hookrightarrow N^*(X) + \pi^0$ and $N^*(X) \to n + \omega$ or $n + \eta$ etc. Here $N^*(A)$ is one of the known N^* resonances that has a strong coupling to the πN channel.

The potential of the sequential-reaction method may be illustrated for the case of missing Δ^* states. We have found some fabulous old bubble chamber data on the reaction $\pi p \to \pi p\eta$ and $\pi p \to \pi p\omega$ which we have discussed at the recent MENU '97 conference [2]. It is found that $\sigma_t(\pi^+p \to \pi^+p\eta) \approx$ (6-9)$\sigma_t(\pi^-p \to \pi^-p\eta)$, similarly, that $\sigma_t(\pi^+p \to \pi^+p\omega) \approx$ (6-9)$\sigma_t(\pi^-p \to \pi^-p\omega)$ from threshold to 3.5 GeV. The ratios imply that the intermediate state for both η and ω production by π^- are Δ^* states and not N^* resonances. The sequential decay reactions which are possible here include $\pi^+p \to \Delta^*$(known) $\to \eta\Delta^*$("missing") and $\pi^+p \to \Delta^*$("missing") $\to \eta\Delta^*(1232)$ etc. The magnitude of these reactions is large $\sigma_t(\pi^+p \to \pi^+p\eta) \approx 1$ mb and $\sigma_t(\pi^+p \to \pi^+p\omega) \approx 2$ mb which makes the production of η or ω in these 3 body final state reaction integrated up to 3 GeV larger than in the two body reaction $\pi^-p \to \eta n$ and $\pi^-p \to \omega n$! We note in passing that a new η decay has been established [2], namely, $D_{33}^{++}(1700) \to \Delta^{++}(1232) + \eta$ from the analysis of the $\pi p \to \pi p\eta$ data.

This work was supported in part by US DOE. It is a pleasure to acknowledge the assistance of Matt Pulver in preparing the manuscript and of Edo Berger in making the figures.

REFERENCES

[1] S. Capstick and W. Roberts, Phys. Rev. **D49**, 4570 (1994).
[2] B. Ncfkcns, Proc. MENU '97. πN Newsletter No. 13, p. 270 (1997).

[3] Review of Particle Physics, Phys. Rev. **D54**, 575 (1996).
[4] B. Tippens, this workshop.
[5] R. Bijker, F. Iachello, and A. Leviatan, Ann. Phys. **236**, 69 (1994).

The Need for New Experiments with Both Electromagnetic and Hadronic Probes

D. M. Manley*
Department of Physics and Center for Nuclear Research,
Kent State University, Kent, OH 44242, U.S.A.

Abstract

A discussion is presented of the connections between meson photoproduction and purely hadronic reactions, as regarding the decays of N* resonances. It is argued that new N* experiments with hadronic probes are necessary to optimize the physics that can be learned from the new generation of experiments with electromagnetic probes at Jefferson Lab and elsewhere.

INTRODUCTION

One of the goals of studying N* resonances is to be able to distinguish between various models of baryon structure and of baryon decay mechanisms. In addition to identifying the spin, parity, mass, and width of a resonance, it is therefore desirable to learn as much as possible about the different decay modes of a given resonance. Certain experiments are capable of yielding unique information about particular resonance decay properties. For example, meson photoproduction measurements provide essentially the only direct way of determining the helicity couplings, $A_{1/2}$ and $A_{3/2}$, for the γp and γn decays of N* resonances. (In principle, Compton scattering measurements provide similar information, but the analysis is more complicated.) The helicity photocouplings may then be considered as the most important resonance parameters that can be extracted uniquely from meson photoproduction experiments. Before one can determine these photocouplings, however, it is usually necessary to determine the full multipole or helicity amplitudes as functions of the c.m. energy W. (For meson electroproduction experiments, one wants to determine the transition multipole amplitudes as functions of both W and Q^2, the squared momentum transfer.) For meson photoproduction, essentially the only detailed partial-wave analyses (PWAs) to extract multipole amplitudes have been for pion photoproduction experiments[1,2]. Most attempts to extract helicity photocouplings from PWAs of pion photoproduction take the existence, masses, and widths of resonances from analyses of πN elastic scattering.

Here, I will attempt to summarize how the extraction of helicity photocouplings from analyses of meson photoproduction is connected with the analyses of data from purely hadronic reactions. I will also discuss the quality of existing PWAs for certain hadronic reactions. Finally, I will make suggestions on how to improve our knowledge of the hadronic and photodecay couplings.

MULTIPOLE AND HELICITY AMPLITUDES FOR $\gamma N \to \pi N$

In this section, we consider a simplified description of pion photoproduction to show how the helicity couplings, $A_{1/2}$ and $A_{3/2}$, may be determined from the corresponding energy-dependent electric and magnetic multipole amplitudes. As will be apparent, the determination of these γN helicity couplings relies on information most easily obtained from a PWA of $\pi N \to \pi N$ data.

*E-mail: manley@zeus.kent.edu

Let $E_{\ell\pm}$ and $M_{\ell\pm}$ denote the energy-dependent multipole amplitudes, according to the conventions adopted by the Virginia Tech group[1,2]. For the purpose of carrying out a multichannel analysis for a given partial wave, it is convenient to convert these amplitudes into *dimensionless* Argand multipole amplitudes according to the prescription:

$$\bar{E}_{\ell+} = C_I \sqrt{kq(\ell+1)(\ell+2)}\, E_{\ell+} \tag{1}$$

$$\bar{M}_{(\ell+1)-} = C_I \sqrt{kq(\ell+1)(\ell+2)}\, M_{(\ell+1)-} \tag{2}$$

$$\bar{E}_{(\ell+1)-} = C_I \sqrt{kq\ell(\ell+1)}\, E_{(\ell+1)-} \tag{3}$$

$$\bar{M}_{\ell+} = C_I \sqrt{kq\ell(\ell+1)}\, M_{\ell+} \tag{4}$$

where C_I is an isospin factor ($C_I = -\sqrt{3}$ for $I = \frac{1}{2}$, and $C_I = \sqrt{2/3}$ for $I = \frac{3}{2}$), k is the relative momentum in the c.m. frame of the photon and initial nucleon, and q is the relative momentum in the c.m. frame of the pion and final nucleon. We may then define the corresponding dimensionless Argand helicity amplitudes, according to

$$\begin{bmatrix} \bar{A}_{\ell\pm} \\ \bar{B}_{\ell\pm} \end{bmatrix} = \begin{bmatrix} -C_{\ell\pm} & -S_{\ell\pm} \\ -S_{\ell\pm} & C_{\ell\pm} \end{bmatrix} \begin{bmatrix} \bar{M}_{\ell\pm} \\ \bar{E}_{\ell\pm} \end{bmatrix} \tag{5}$$

where $\bar{A}_{\ell\pm}$ and $\bar{B}_{\ell\pm}$ are the helicity $\frac{1}{2}$ and $\frac{3}{2}$ amplitudes, respectively, and

$$C_{\ell+} = S_{(\ell+1)-} = \left[\frac{\ell}{2(\ell+1)}\right]^{1/2}, \tag{6}$$

$$S_{\ell+} = -C_{(\ell+1)-} = \left[\frac{\ell+2}{2(\ell+1)}\right]^{1/2}. \tag{7}$$

For simplicity, let us assume the following Breit-Wigner form for the amplitudes:

$$\bar{A}_{\ell\pm} = \frac{\frac{1}{2}\, g_{1/2}\, g_{\pi N}}{M - W - i\Gamma/2}, \tag{8}$$

$$\bar{B}_{\ell\pm} = \frac{\frac{1}{2}\, g_{3/2}\, g_{\pi N}}{M - W - i\Gamma/2}, \tag{9}$$

where M is the mass of the resonance, Γ is its total width, W is the c.m. energy, $\Gamma_{\pi N} = (g_{\pi N})^2$ is the πN partial width, $\Gamma_{1/2} = (g_{1/2})^2$ is the γN partial width for helicity $\frac{1}{2}$, and $\Gamma_{3/2} = (g_{3/2})^2$ is the γN partial width for helicity $\frac{3}{2}$. (The Argand multipole amplitudes $E_{\ell\pm}$ and $M_{\ell\pm}$ would have a similar form, but with $g_{1/2}$ and $g_{3/2}$ replaced by g_E and g_M, respectively.) We shall refer to $g_{\pi N}$, $g_{1/2}$, and $g_{3/2}$ as "decay amplitudes". These decay amplitudes have a sign that can be measured relative to the unmeasureable sign of the πN production amplitude. Consequently, both the magnitude and sign of a decay amplitude may be used to test quark-model predictions[3]. The *conventional* γN helicity couplings are given in terms of $g_{1/2}$ and $g_{3/2}$ evaluated at $W = M$:

$$A_{1/2} = \left[\frac{\pi M(2J+1)}{2k^2 m}\right]^{1/2} g_{1/2}, \qquad A_{3/2} = \left[\frac{\pi M(2J+1)}{2k^2 m}\right]^{1/2} g_{3/2}, \tag{10}$$

where M and k are defined as before, J is the spin of the resonance, and m is the nucleon mass. To determine $A_{1/2}$ and $A_{3/2}$, we therefore need to know $g_{1/2}$ and $g_{3/2}$. Equivalently, we need to know the electric and magnetic decay amplitudes g_E and g_M, where

$$\begin{bmatrix} g_{1/2} \\ g_{3/2} \end{bmatrix} = \begin{bmatrix} -C_{\ell\pm} & -S_{\ell\pm} \\ -S_{\ell\pm} & C_{\ell\pm} \end{bmatrix} \begin{bmatrix} g_M \\ g_E \end{bmatrix} . \tag{11}$$

Note that

$$(g_{1/2})^2 + (g_{3/2})^2 = (g_M)^2 + (g_E)^2 , \tag{12}$$

or equivalently,

$$\Gamma_{1/2} + \Gamma_{3/2} = \Gamma_M + \Gamma_E \equiv \Gamma_{\gamma N} . \tag{13}$$

It is important to note that measurements of $\gamma N \to \pi N$ determine *only* the products $g_E\, g_{\pi N}$ and $g_M\, g_{\pi N}$, and *not* g_E and g_M separately. For that, we need to know $g_{\pi N}$, the pion-nucleon decay amplitude. This quantity is determined from PWAs of $\pi N \to \pi N$.

THE $S_{11}(1535)$ RESONANCE

One nearly model-independent quantity characterizing the $S_{11}(1535)$ resonance is given by[4]

$$\xi = \left(\frac{m\ k\ x_{\eta N}}{q\ M\ \Gamma} \right)^{1/2} A_{1/2} , \tag{14}$$

where $x_{\eta N} = (g_{\eta N})^2/\Gamma$ is the ηN branching ratio of the resonance, with $g_{\eta N}$ the ηN decay amplitude evaluated at $W = M$. Since $J = \frac{1}{2}$ for the $S_{11}(1535)$ resonance, it follows from Eq. (10) that we may write

$$\xi = \left[\frac{\pi}{kq} \right]^{1/2} \frac{g_{\eta N}\ g_{1/2}}{\Gamma} , \tag{15}$$

where the first factor is mainly kinematical. Note that if we can write the S_{11} amplitude for $\gamma N \to \eta N$ in the simple Breit-Wigner form,

$$T_{\gamma N \to \eta N} = \frac{\frac{1}{2}\ g_{\eta N}\ g_{1/2}}{M - W - i\Gamma/2} , \tag{16}$$

then at $W = M$, we have

$$T_{\gamma N \to \eta N} = i\, \frac{g_{\eta N}\ g_{1/2}}{\Gamma} . \tag{17}$$

Thus, ξ is basically a kinematic factor times the S_{11} amplitude for $\gamma N \to \eta N$, evaluated at the resonance energy.

It is possible to determine ξ by making near-threshold measurements of the $\gamma N \to \eta N$ cross section. One may then solve for $A_{1/2}$ by inverting Eq. (14):

$$A_{1/2} = \xi \left(\frac{q}{m\ k} \right)^{1/2} \left(\frac{M\Gamma}{x_{\eta N}} \right)^{1/2} \tag{18}$$

Table 1. Helicity amplitudes (in units of 10^{-3} GeV$^{-1/2}$) for γN decays of the $S_{11}(1535)$ resonance.

$A^p_{1/2}$	$A^n_{1/2}$	Method	Reference
61 ± 3	-46 ± 5	$\gamma N \to \pi N$	VPI93[6]
125 ± 25	-100 ± 30	$\gamma N \to \eta N$	Mainz95[5]
60 ± 15	-20 ± 35	$\gamma N \to \pi N$	VPI96[1]
87 ± 21	-52 ± 24	multichannel fit	Pitt97[7]

Here, the last factor must be determined independently from hadronic reactions. For example, we may determine $x_{\eta N}$ by either a PWA of both $\pi N \to \pi N$ and $\pi N \to \eta N$, or by a PWA of both $\pi N \to \pi N$ and $\pi N \to \pi\pi N$. In the latter case, unitarity may be used to deduce the ηN branching ratio. It follows that we need high-quality PWAs of the hadronic reactions $\pi N \to \eta N$ and/or $\pi N \to \pi\pi N$ if we wish to obtain a precise determination of $A_{1/2}$. It is further necessary that a high-quality, varied data base be available for those reactions before one can carry-out such partial-wave analyses. As I discuss below, the quality of the data for these hadronic reactions is currently rather limited.

Before high-precision measurements of $\gamma N \to \eta N$ at Mainz in 1995[5], the best values for $A^p_{1/2}$ and $A^n_{1/2}$ were obtained from multipole analyses of $\gamma N \to \pi N$. Table 1 gives the values (in units of 10^{-3} GeV$^{-1/2}$) of these helicity couplings in 1993, based on the work of the Virginia Tech group (VPI93)[6]. It should be noted that the text of Ref. [6] contains a caution that "the true errors could be larger than those ... quoted." Two years later, the $\gamma N \to \eta N$ measurements at Mainz[5] resulted in helicity couplings about twice as large as those obtained from the $\gamma N \to \pi N$ analysis. Then in 1996, the Virginia Tech group updated their $\gamma N \to \pi N$ analysis[1], giving new values consistent with their earlier ones, but with error bars five times larger for $A^p_{1/2}$ and seven times larger for $A^n_{1/2}$. Even with these dramatically increased error bars, the values from $\gamma N \to \pi N$ still disagreed with the Mainz results from $\gamma N \to \eta N$. More recently, Tom Vrana and Steve Dytman at the University of Pittsburgh, working with Harry Lee from ANL, have carried out a multichannel fit of the S_{11} amplitudes for several reactions, including $\pi N \to \pi N$, $\gamma N \to \pi N$, and $\pi N \to \pi\pi N$. In addition, they required their results to reproduce the near-threshold cross-section measurements of $\gamma N \to \eta N$ from Mainz. Their values for the helicity amplitudes, as presented at this Workshop, are also listed in Table 1 (Pitt97). Perhaps it is not surprising that their values lie intermediate between those of the Mainz group and the Virginia Tech group.

How are we to understand these contradictory results? From Eq. (18), we see that the method used to determine $A_{1/2}$ from $\gamma N \to \eta N$ depends on three factors: (i) ξ, which is determined by the magnitude of the $\gamma N \to \eta N$ cross section near threshold; (ii) $\sqrt{q/mk}$, which is mainly a kinematic factor that depends only weakly on the resonance mass M; and (iii) $\sqrt{M\Gamma/x_{\eta N}}$, which must be determined, for example, from $\pi N \to \pi N$ and $\pi N \to \eta N$. We require that the value of $A_{1/2}$ be fixed and independent of the reaction used to determine it. Let us assume that $\sqrt{M\Gamma/x_{\eta N}} = 715$ MeV, and then let us explore the reasonable range of permitted values for M, Γ, and $x_{\eta N}$. Table 2 shows three possible cases. Values given in the first row correspond to choosing the Pitt97 values, $M = 1545$ MeV and $\Gamma = 126$ MeV[7]. We see that a large range in the width is permitted, corresponding to a narrow resonance with $\Gamma = 126$ MeV, to a broad resonance with $\Gamma = 200$ MeV. The latter value is consistent with that obtained in the fits of the Mainz data by Krusche *et al.*[5]. One might hope that cross-section

Table 2. Allowed range of parameters for the $S_{11}(1535)$ resonance, given a fixed ratio, $A_{1/2}/\xi$ (see text).

M (MeV)	Γ (MeV)	$x_{\eta N}$	$\sqrt{x_{\pi N} x_{\eta N}}$
1545	126	0.38	0.465
1545	165	0.50	0.474
1535	200	0.60	0.458

data for $\pi N \to \eta N$ near threshold could resolve this ambiguity, but the currently available data are probably too imprecise. We note that at $W = M$, the cross section for $\pi N \to \eta N$ is dominated by the magnitude of the S_{11} amplitude, which can be written as $\sqrt{x_{\pi N} x_{\eta N}}$. Here $x_{\pi N}$ is the πN branching ratio for the S_{11} resonance. To a very good approximation, we can write $x_{\pi N} + x_{\eta N} + x_{\pi\pi N} = 1$, where $x_{\pi\pi N} \sim 0.05$ is the $\pi\pi N$ branching ratio for the $S_{11}(1535)$ resonance. From this value of $x_{\pi\pi N}$ and the values of $x_{\eta N}$ in Table 2, we obtain the corresponding values of $\sqrt{x_{\pi N} x_{\eta N}}$, which are listed in the fourth column of Table 2. As can be seen, there is very little sensitivity to different parameter choices.

We have seen that a determination of $A_{1/2}$ for the $S_{11}(1535)$ resonance using the $\gamma N \to \pi N$ reaction requires separate measurements involving πN elastic scattering to determine $g_{\pi N}$. Similarly, a determination of $A_{1/2}$ using the $\gamma N \to \eta N$ reaction requires separate measurements involving purely hadronic reactions to determine $g_{\eta N}$. This is most easily accomplished if there are sufficient data to perform a PWA of $\pi N \to \eta N$, from which we can determine the product, $g_{\pi N} g_{\eta N}$. Once $g_{\pi N}$ is determined from πN elastic scattering, we may then determine $g_{\eta N}$.

STATUS OF PARTIAL-WAVE ANALYSES OF HADRONIC DATA

The ideas in the previous section are easily generalized to other reactions. For example, suppose that we want to determine the various helicity couplings, $A_{1/2}$ and $A_{3/2}$, from $\gamma N \to \pi\Delta$ data. In this case, as for $\gamma N \to \pi N$, we must have at least three charge reactions to perform an isospin decomposition. A reasonable choice would be to use the CLAS detector in Hall B at Jefferson Lab to measure the reactions $\gamma p \to \pi^+\pi^- p$ and $\gamma d \to \pi^\circ\pi^- pp$. From these measurements and appropriate energy cuts on the πN invariant mass, we may obtain data for four $\gamma N \to \pi\Delta$ reactions, namely, $\gamma p \to \pi^+\Delta^\circ$, $\gamma p \to \pi^-\Delta^{++}$, $\gamma n \to \pi^-\Delta^+$, and $\gamma n \to \pi^\circ\Delta^\circ$. A multipole analysis of these data could in principle be performed to determine the products of decay amplitudes, $g_{\gamma N} g_{\pi\Delta}$. Then, if we knew $g_{\pi\Delta}$, we could find $g_{\gamma N}$ and determine the γN helicity couplings. To determine $g_{\pi\Delta}$, it is necessary to perform a PWA of $\pi N \to \pi\Delta$ (an important intermediate state in $\pi N \to \pi\pi N$ at c.m. energies below 2 GeV), and then to carry out a coupled-channel analysis involving $\pi N \to \pi N$ amplitudes. This raises the question: How well do we know the partial-wave amplitudes for $\pi N \to \pi\Delta$? The answer is, not as well as we know the amplitudes for πN elastic scattering, but better than we know those for $\pi N \to \rho N$. In particular, the amplitudes for $\pi N \to \pi\Delta$ are poorly determined above a c.m. energy of $W = 1.7$ GeV. This can be seen in Figs. 1 and 2, which show Argand diagrams for two $\pi N \to \pi\Delta$ partial-wave amplitudes, as determined from an isobar-model PWA of $\pi N \to \pi\pi N$ events[8]. The curves in these figures are based on a recent unitary, multichannel fit by M. Niboh[9]. The isobar-model analysis was performed by fitting 241,000 bubble-chamber events, separated into 22 energy bins having widths between 20 and 40 MeV. Six partial-wave amplitudes were included at the lowest energy of 1.34 GeV, but 36 amplitudes were found to be important at 1.70 GeV. There were not enough data to

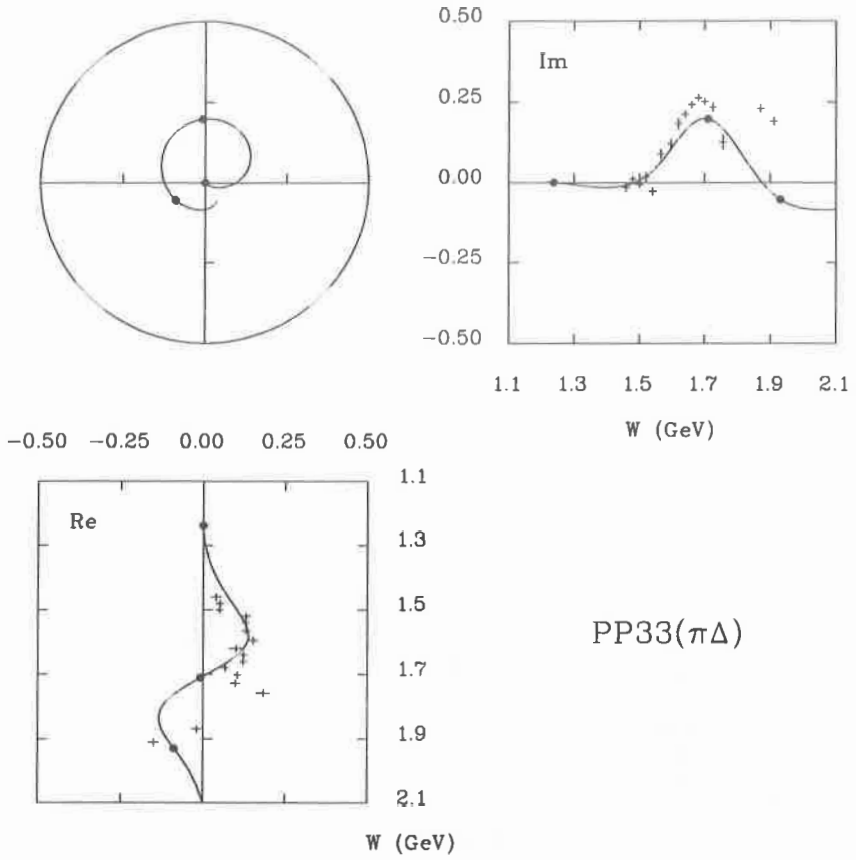

Figure 1. Argand diagram for the P_{33} $\pi N \rightarrow \pi\Delta$ partial-wave amplitude, where the $\pi\Delta$ pair is in a relative P-wave. The data are from Ref. [8] and the curve is from a recent multichannel fit[9].

determine all of these amplitudes reliably at higher energies. This can be seen in Figs. 1 and 2 by the noticeable increase in scatter that occurs above 1.7 GeV. Thus, our knowledge of the $\pi N \rightarrow \pi\Delta$ amplitudes is poor above 1.7 GeV because of the sparsity of data at those energies and because of the relatively large number of partial-wave amplitudes that need to be determined at those energies. It should be noted that some $\pi N \rightarrow \pi\Delta$ amplitudes are better determined, and some are worse determined, than those described here.

To appreciate the relative complexity of performing a PWA for any given reaction, it is instructive to compare the number of partial-wave amplitudes that could be important in a particular energy range. Below a c.m. energy of about 2 GeV, for example, the important partial waves are expected to be those with $J \leq \frac{7}{2}$. Table 3 compares the number of amplitudes that may contribute to various reactions, subject to this criterion. In the table, γ^* represents a virtual photon, and four intermediate channels ($\pi\Delta$, ρN, ϵN, and πN^*) are assumed to contribute for $\pi N \rightarrow \pi\pi N$[8]. The number of amplitudes is large when a γN channel is involved (with real or virtual photons) due to the many different spin couplings, and due to the fact that the photon is a mixture of isospin 0 and 1. The number of amplitudes is similarly large when ρN or ωN channels are involved due to the many different spin couplings. A small number of amplitudes is needed for reactions involving the ηN and $K\Lambda$ channels because only terms with total isospin $I = \frac{1}{2}$ and total intrinsic spin $S = \frac{1}{2}$ contribute. It is encouraging to note that the present state of PWAs for pion photoproduction is rather good[1,2], even

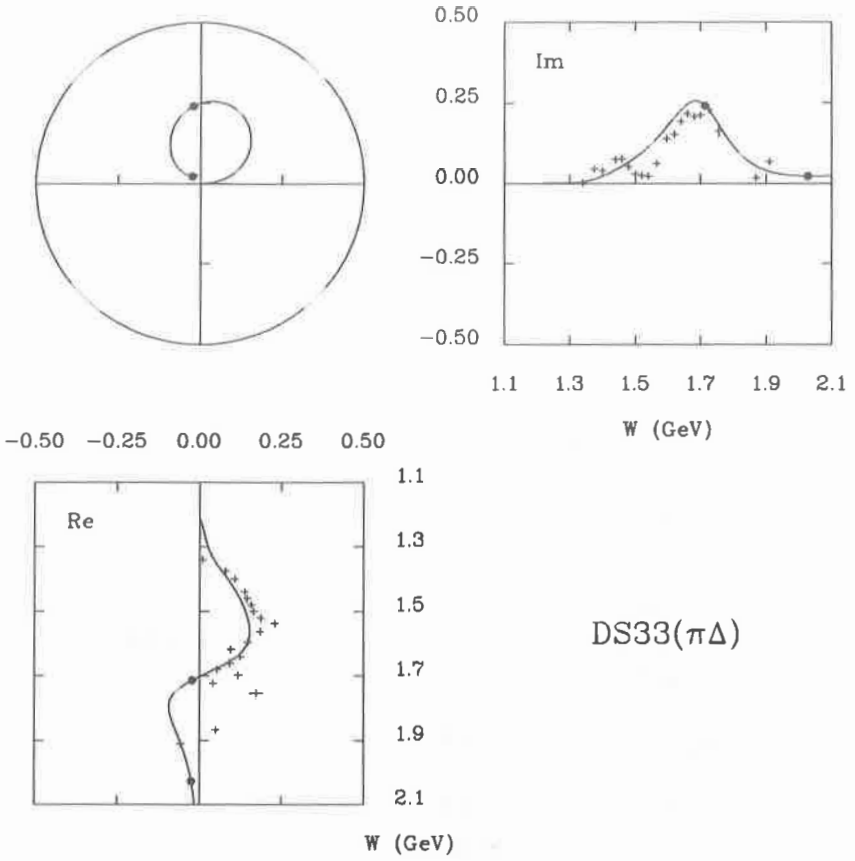

Figure 2. Argand diagram for the D_{33} $\pi N \to \pi\Delta$ partial-wave amplitude, where the $\pi\Delta$ pair is in a relative S-wave. The data are from Ref. [8] and the curve is from a recent multichannel fit[9].

though a relatively large number of partial waves contribute to the process.

Table 4 summarizes the important resonance reactions that may be studied using complementary hadronic and electromagnetic probes. The effective threshold listed in the third column takes into account the width of unstable particles such as the Δ resonance and the ρ meson. The partial-wave amplitudes are best known for $\pi N \to \pi N$[10], although single-energy PWAs have also been performed for $\pi N \to \pi\pi N$[8] [which includes the intermediate reactions $\pi N \to \pi\Delta$, $\pi N \to \rho N$, and $\pi N \to \pi N^*(1440)$], and for $\gamma N \to \pi N$[1,2]. Energy-dependent PWAs have also been performed for $\pi N \to \eta N$[11], $\pi N \to K\Lambda$[12], and for $\pi N \to K\Sigma$[13,14]. Although not well known, an energy-dependent PWA of $\pi N \to \omega N$ has also been performed in the threshold region[15]. (Various indications suggest that P_{13} resonances make important contributions to $\pi N \to \omega N$ near threshold.) I know of no PWAs for the other reactions listed in Table 4.

SUMMARY

One program to study baryon resonances using purely hadronic reactions was initiated at the Brookhaven National Laboratory AGS in May, 1997 using the Crystal Ball Spectrometer[16]. AGS experiment E913 is a study of neutral baryon resonances through the simultaneous measurement of reactions such as $\pi^- p \to \gamma n$, $\pi^0 n$, ηn, and $\pi^0\pi^0 n$. Measurements have been performed already at 12 c.m. energies ranging from $W = 1.22$ GeV to $W = 1.53$ GeV.

Table 3. The number of partial-wave amplitudes with $J \leq \frac{7}{2}$ that may contribute to various reactions. The contributions are sorted into columns labeled (S, I), where I is the total isospin and, for the two-body and quasi-two-body hadronic (electromagnetic) reactions, S is the total intrinsic spin of the exit (entrance) channel. Here ϵ denotes the S-wave isoscalar $\pi\pi$ interaction, N^* refers to the $P_{11}(1440)$ resonance, and γ^* denotes a virtual photon (for electroproduction processes). The entries for $\pi N \to \pi\pi N$ are the sums of the entries for $\pi N \to \pi\Delta$, ρN, ϵN, and πN^*.

Reaction	$(\frac{1}{2}, \frac{1}{2})$	$(\frac{3}{2}, \frac{1}{2})$	$(\frac{1}{2}, \frac{3}{2})$	$(\frac{3}{2}, \frac{3}{2})$	Total
$\pi N \to \pi N$	8	0	8	0	16
$\pi N \to \eta N$	8	0	0	0	8
$\gamma N \to \pi N$	0	28	0	14	42
$\gamma N \to \eta N$	0	28	0	0	28
$\gamma^* N \to \pi N$	16	28	8	14	66
$\gamma^* N \to \eta N$	16	28	0	0	44
$\pi N \to \pi\Delta$	0	14	0	14	28
$\pi N \to \rho N$	8	14	8	14	44
$\pi N \to \epsilon N$	8	0	0	0	8
$\pi N \to \pi N^*$	8	0	8	0	16
$\pi N \to \pi\pi N$	24	28	16	28	96
$\pi N \to K\Lambda$	8	0	0	0	8
$\pi N \to \omega N$	8	14	0	0	22
$\pi N \to \eta\Delta$	0	0	0	14	14

Table 4. Some important resonance reactions. Entries labeled N^* refer to the $P_{11}(1440)$ resonance. $W^{\rm eff}_{\rm thresh}$ is the effective c.m. threshold energy for a reaction, taking into account hadronic widths.

Hadronic Reaction	Photoproduction Reaction	$W^{\rm eff}_{\rm thresh}$ (GeV)
$\pi N \to \pi N$	$\gamma N \to \pi N$	1.08
$\pi N \to \pi\pi N$	$\gamma N \to \pi\pi N$	1.22
$\pi N \to \pi\Delta$	$\gamma N \to \pi\Delta$	1.31
$\pi N \to \pi N^*$	$\gamma N \to \pi N^*$	1.41
$\pi N \to \eta N$	$\gamma N \to \eta N$	1.49
$\pi N \to K\Lambda$	$\gamma N \to K\Lambda$	1.61
$\pi N \to \rho N$	$\gamma N \to \rho N$	1.63
$\pi N \to K\Sigma$	$\gamma N \to K\Sigma$	1.69
$\pi N \to \omega N$	$\gamma N \to \omega N$	1.72
$\pi N \to \eta\Delta$	$\gamma N \to \eta\Delta$	1.72
$\pi N \to \eta N^*$	$\gamma N \to \eta N^*$	1.82
$\pi N \to \rho\Delta$	$\gamma N \to \rho\Delta$	1.87
$\pi N \to \omega\Delta$	$\gamma N \to \omega\Delta$	1.95

The $\pi^- p$ measurements will be completed in 1998, and AGS experiment E914 will begin a new study of neutral hyperon resonances using the reactions $K^- p \rightarrow$ neutrals.

A summary of the differential cross-section data available for $\pi^- p \rightarrow \eta n$ before the new Crystal Ball measurements is shown in Fig. 3 of Ref.[11]. It is apparent from that figure that the differential cross section is not isotropic even at 1535 MeV, where the $S_{11}(1535)$ resonance is dominant. Thus, the new measurements of $\pi^- p \rightarrow \eta n$ using the Crystal Ball will not only provide much needed hadronic data to constrain the properties of the $S_{11}(1535)$ resonance, but should also allow precise determinations of the non-S-wave $\pi N \rightarrow \eta N$ partial waves. Currently, little $\pi N \rightarrow \eta N$ data are available above $W = 1.58$ GeV (again, see Fig. 3 of Ref.[11]), so new measurements at higher energies are necessary to investigate the ηN decays of the higher N* resonances. It should be noted that the Crystal Ball is now located in the C6 line of the AGS, with a maximum c.m. energy of 1.53 GeV possible using pion beams. In order to make measurements at higher energies, it will be necessary to move to the D-line.

Another important two-body reaction that can, in principle, be studied with the Crystal Ball is $\pi^- p \rightarrow K^\circ \Lambda$, where the K° is detected via the decay, $K^\circ_S \rightarrow \pi^\circ \pi^\circ \rightarrow 4\gamma$, and the Λ is detected via $\Lambda \rightarrow \pi^\circ n \rightarrow \gamma\gamma n$. This reaction presumably has a strong contribution from the $S_{11}(1650)$ resonance. This hadronic reaction provides necessary and complementary information for carrying out a multipole analysis of $\gamma p \rightarrow K^+ \Lambda$. The best PWA of data for $\pi^- p \rightarrow K^\circ \Lambda$ is arguably the energy-dependent analysis performed by Saxon *et al.* in 1980[12]. Polarization data were included (see Fig. 7 of Ref.[12]) in the PWA, although the data have rather large error bars. Since the threshold for this reaction is at $W = 1.61$ GeV, the Crystal Ball detector would need to be moved to the higher-energy D-line at the AGS before measurements are possible there.

While the properties of several resonances are known rather well (primarily those with large πN decay amplitudes), we actually know very little about several "established" resonances, including $D_{13}(1700)$, $P_{11}(1710)$, $P_{13}(1720)$, $F_{37}(1950)$, and $D_{35}(1930)$. For several of these resonances, the total widths are not well determined, and their major inelastic decay modes are essentially unknown. New N* experiments at Jefferson Lab and elsewhere should attempt to learn more about these states, as well as search for the more glamourous "missing" and "exotic" baryon resonances. To make full use of the new photoproduction and electroproduction data that will be forthcoming, we need new experiments for various hadronic reactions with the goal of being able to carry-out single-energy PWAs. The possibility exists to enhance our current data base for several hadronic reactions, including $\pi^- p \rightarrow \eta n$, $\pi^- p \rightarrow K^\circ \Lambda$, $\pi^- p \rightarrow K^\circ \Sigma^\circ$, and $\pi^- p \rightarrow \omega n$, by using the Crystal Ball detector at the AGS. As noted above, it would be necessary to move this detector to the D-line to carry out measurements at c.m. energies $W > 1.53$ GeV. The urgent need for new purely hadronic data cannot be overemphasized. The lack of agreement in values of the $A_{1/2}$ helicity amplitude for the $S_{11}(1535)$ resonance, as determined from $\gamma N \rightarrow \pi N$ and $\gamma N \rightarrow \eta N$ measurements, is due in large part to the poor quality of existing data for $\pi N \rightarrow \eta N$. It is also important to explore resonance decays previously not investigated, including $\eta\Delta$, $\omega\Delta$, and η'N.

ACKNOWLEDGMENTS

I wish to thank the organizers of the GW/TJNAF Workshop on N* Physics for their invitation and their hospitality. This work was supported in part by the National Science Foundation.

REFERENCES

[1] R. A. Arndt, I. I. Strakovsky, and R. L. Workman, Phys. Rev. C**53**, 430 (1996).
[2] R. A. Arndt, I. I. Strakovsky, and R. L. Workman, Phys. Rev. C**56**, 577 (1997).
[3] S. Capstick and W. Roberts, Phys. Rev. D**49**, 4570 (1994).
[4] M. Benmerrouche and N. C. Mukhopadhyay, Phys. Rev. Lett. **67**, 1070 (1991).
[5] B. Krusche *et al.*, Phys. Rev. Lett. **74**, 3736 (1995); Phys. Lett. B**358**, 40 (1995).
[6] Z. Li, R. A. Arndt, D. Roper, and R. L. Workman, Phys. Rev. C**47**, 2759 (1993).
[7] T. Vrana, S. Dytman, and T.-S. H. Lee, Proceedings of the GW/TJNAF Workshop on N* Physics, *πN Newsletter* (to be published).
[8] D. M. Manley, R. A. Arndt, Y. Goradia, and V. L. Teplitz, Phys. Rev. D**30**, 904 (1984).
[9] M. M. Niboh, Kent State University, Ph.D. Thesis (1997).
[10] R. A. Arndt, I. I. Strakovsky, R. L. Workman, and M. M. Pavan, Phys. Rev. C**52**, 2120 (1995).
[11] M. Batinić, I. Šlaus, A. Švarc, and B. M. K. Nefkens, Phys. Rev. C**51**, 2310 (1995).
[12] D. H. Saxon *et al.*, Nucl. Phys. **B162**, 522 (1980).
[13] D. J. Candlin *et al.*, Nucl. Phys. **B238**, 477 (1984).
[14] S. R. Deans, R. W. Mitchell, D. L. Montgomery, G. C. Wood, and J. E. Rush, Nucl. Phys. **B96**, 90 (1975).
[15] H. Karami *et al.*, Nucl. Phys. **B154**, 503 (1979).
[16] B. M. K. Nefkens, in *N* Physics: Proceedings of the Fourth CEBAF/INT Workshop*, edited by T.-S. H. Lee and W. Roberts (World Scientific, 1997), p. 186.

Status of the Nucleon Resonances S11(1535) and S11(1650)†

G. Höhler*
Institut für Theoretische Teilchenphysik, Universität Karlsruhe,
Postfach 6980, D-76128 Karlsruhe, Germany

Abstract

In many recent papers πN scattering and the photoproduction of η and π are treated in the neighborhood of the η-production threshold. All analyses include the effect of the nucleon resonance S11(1535) and use the *conventional resonance parameters* which are based on generalized Breit-Wigner parametrizations, for which each group has its own prescription. It is the purpose of this paper to call attention to the fact that a definition of the mass parameter of an excited state of the nucleon which has a theoretical justification starts from the *time-delay in the scattering process* which leads to peaks in *speed plots.* These peaks are related to *resonance poles* in the complex energy-plane. The *location of the pole must be the same if a resonance is an intermediate state in different reactions*, e.g. in πN scattering and in photoproduction of π or η. Furthermore, a greater effort is required than applied in recent analyses if a resonance pole is located close to a threshold cusp for the production of a long-living particle (η), because shadow poles in other Riemann sheets can give contributions. – Some remarks on isospin breaking and on the resonance S11(1650) are added.

1 INTRODUCTION

Evidence for a nucleon resonance in the S11 πN partial wave at about $1500 - 1520\,MeV$ with a fairly strong isotropic decay into $n + \eta$ was reported already in the sixties (see e.g. Ref. [31]). This resonance was found in the partial wave analyses of the CERN and Saclay groups (Table 5.1 in Ref. [20]) and in all more recent analyses.

Theoretical predictions for a S11-resonance in this mass region followed from nonrelativistic constituent quark-shell models (Reviews: Refs. [45,51]). Recent calculations of resonance decays in a relativized quark model [22] led to the result that the decay into $N + \eta$ is by far the strongest inelastic channel and has a branching ratio comparable to that for elastic $N + \pi$ scattering. In Ref. [58] the resonance S11(1535) is discussed within the framework of a chiral quark model. The large $n\eta$ branching ratio has not been fully understood.

In the "Baryon Summary Table" of the "Review of Particle Properties" (RPP1996) [76] one finds for N(1535)S11 the statement: "Mass m=1520 to 1555 ($\approx$ 1535) MeV". It will be seen that authors who relied on this statement did not notice the serious complications following from the fact that the resonance pole lies near to the branch point of the $n + \eta$-channel.

On p.57 of the RPP96 and in the "Baryon Particle Listings" which contain more details, one can see that the mass m given in the Summary Table is a parameter of a generalized Breit-Wigner parametrization. It is an old tradition to use formulas of this type for fits to resonances. But the ansatz for the generalization is not uniquely determined from theoretical arguments, in particular in the inelastic region and for the separation between resonance and background. As a consequence, each group made its own choice. Discrepancies between the results for the parameters are mainly due to this model-dependence, which leads to uncertainties larger than the errors of the fits. Only Cutkosky et al. [25] made an attempt to estimate this effect and enlarged their errors.

---

†Considerably extended version of my talk at the 7th Int'l Symposium at Vancouver (July 28–August 1, 1997).

*E-mail: gerhard.hoehler@physik.uni-karlsruhe.de

One of the parameters is usually denoted by m and called the mass of the resonance, but I have not seen a good theoretical argument why this parameter is closely related to the total c.m. energy W of the unstable excited nucleon. A second parameter is the value of the energy-dependent full width $\Gamma(W)$, taken at $W = m$. An important information on the resonance is included in the strong energy dependence of Γ, but it can of course not be given in the RPP. I doubt that the users of the Tables in the RPP spend much time in order to get this information from a study of the original papers. Instead they probably use m and $\Gamma(m)$ in the calculations.

The "Baryon Particle Listings" also give tables of the parameters of the resonance poles. But I have not seen a paper, in which these parameters have been used in analyses of data near the η-production threshold.

Since a good understanding of the notion of a resonance is important for authors of papers on reactions which have excited states of the nucleon as intermediate states, some points will be discussed in the following. This is useful also because the chapters on resonances in textbooks are not always satisfactory (An excellent and detailed treatment can be found in the recent book *Quantum Mechanics* by A. Bohm [18]).

At a discussion meeting in London in 1970, R.H. Dalitz gave a talk with the title "What is resonance?" [30]. He said "in order to clarify the notion of resonance ... it still seems worthwhile to take a few moments to draw attention to a number of points about the description of resonance, which deserve to be more widely known".

In my opinion, this statement is still valid in 1997!

1.1 Time-delay, speed plots and resonance poles

The papers and monographs on resonance scattering in quantum mechanics (e.g. Refs. [72,70,28,40,36,69,30,64,82,18]) start either from resonance poles as generalizations of particle poles or from the *time-delay in a scattering process* in the case of a short-range interaction. Following ideas of E. Wigner [86], Goldberger and Watson [40] calculated the time-delay between the arrival of the incident wave packet and its departure from the collision region. The crucial point is that this could be done using asymptotic wave-functions, so the time-delay can be calculated from the S-matrix.

A good description which omits the complicated mathematical formalism can be found in the book by Bransden and Moorhouse [20]. It is of course similar to Ref. [30]. A quite different approach [80] led to the same result. For elastic scattering, the S-matrix element is $S = exp(2i\delta)$ where δ is the real scattering phase shift. The time-delay is then

$$Q = 2\frac{d\delta(W)}{dW}, \tag{1}$$

where W is the total energy in the c.m. system. It is useful to write this relation in terms of the dimensionless partial wave $T(W)$ (the quantum numbers are omitted). The absorption parameter $\eta = 1$ for elastic scattering; the use of the same letter as for the η-meson should not lead to confusion

$$T(W) = \frac{1}{2i}(\eta e^{2i\delta} - 1); \qquad Q = 2\,Sp(W); \qquad Sp(W) = \left|\frac{dT}{dW}\right|. \tag{2}$$

The energy dependence of the partial wave T(W) is usually described by a plot of the complex vector $T(W)$ in the *Argand diagram*. Sp(W) is the speed with which this vector traverses the diagram.

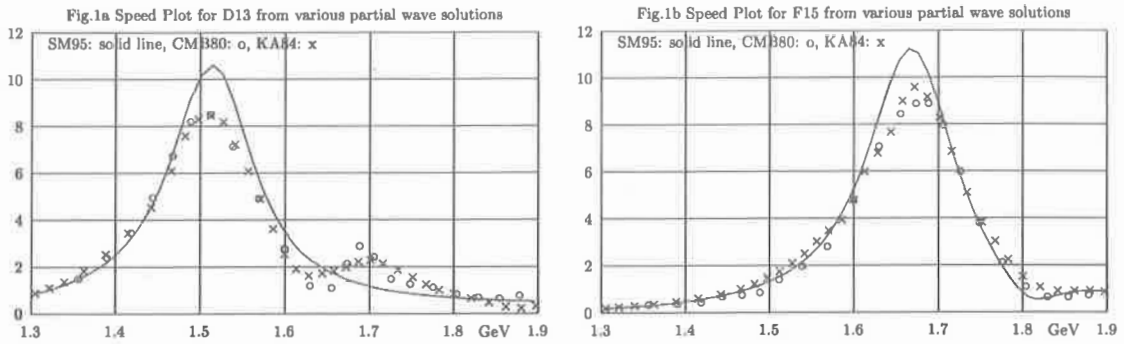

Figure 1. Examples for speed plots: (a) D13 and (b) F15. Ordinate: Speed in GeV^{-1}. Solid lines: SM95, x: KA84, o: CMB80. For D13, the KA and CMB solutions lead to a structure near 1700 MeV which was not seen in SM95.

In the speed plots Sp(W) for πN partial waves one finds pronounced peaks of which two are shown as examples in Fig. 1. There are narrow energy intervals in which the time-delay is large. The tables in RPP96 list 17 4-star resonances. 16 of them show similar peaks, but the shapes are in some cases distorted by a rapid energy dependence of the background. **A peak for S11(1535) is not seen.**

At $W = 1487\,MeV$ there is a large peak which has a qualitatively different shape (Fig. 2). It lies at the threshold for η-production. The time-delay is caused by the production of the long-living particle η in an S-wave.

In all other cases, the peak of the time-delay indicates the *formation of unstable excited states of the nucleon* (the woolly cusps should find more attention, see e.g. Refs. [68,38]).

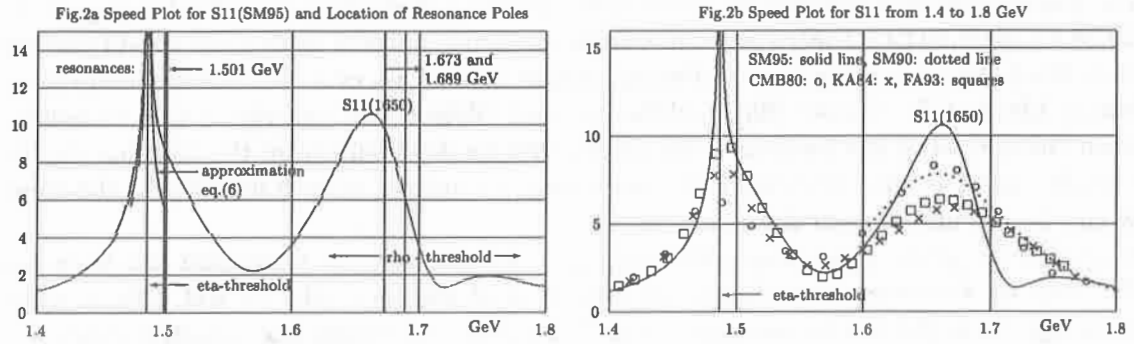

Figure 2. Speed plots for S11 in the range of S11(1535) and S11(1650). (a) This shows the speed plot and the resonance poles as calculated from the VPI solution SM95. The upper part of the high peak at $W = W_\eta = 1487\,MeV$ belongs to the threshold cusp for η-production. The solid line which is shown only above $6\,GeV^{-1}$ is the approximation Eq. (6) in sect. 2.1. The bump near $W = 1660\,MeV$ belongs to S11(1650). SM95 has a pole at 1501 MeV. It leads to a broadening of the lower part of the right wing of the peak at 1487 MeV. S11(1650) is described by two poles which lie *in the same Riemann sheet*, in contrast to the two poles found for P11(1440) which lie in different Riemann sheets (one of them is a shadow pole). Part (b) shows in addition speed plots calculated from other partial wave solutions. Arndt et al. had already shown the difference between the results from SM95 and their earlier solution SM90 (dotted line above 1.6 GeV). Squares show the speed plot from the first VPI solution FA93 which took into account dispersion constraints. (For KA84 the S11-wave below W_η was replaced by results of single-energy fits to the LAMPF data. In this range, old data had led to bad results in KH80 and KA84 (see Fig. 2.2.f in Ref. [50]). One should estimate the effect of the woolly cusps at the thresholds for ρ and ω-production. A contribution from a second pole in a *different Riemann sheet* could exist, because the branch points due to the thresholds for $N\omega$ and $N\rho$ final states lie at $1720 - 4\,i\,MeV$ and $1706 - 75\,i\,MeV$, respectively.

The value $M = W$ at the peak of the speed is *the only definition of the mass of an excited state which has a direct physical interpretation.* The peak is related to a resonance pole in the second sheet and the value of M gives the real part of the pole position. The energy dependence of the background can modify the shape of $Sp(W)$, but its influence on a high peak is in general small.

If the background in the same partial wave has a slow energy dependence, it can be neglected in the upper half of the peak of the speed plot. Then one can determine from a fit three resonance parameters *in an almost model-independent way*: the location of the pole: $M - i\,\Gamma/2$ and the height H of the peak. Γ is the full width at half height(see Refs. [47–49,76] for applications to partial wave analyses published since 1979). From H and Γ one can derive the modulus r of the complex-valued residue of the pole. The pole contribution is described by a simple Breit-Wigner formula *with constant* Γ, since Γ is given by the location of the pole in the complex plane.

The neglection of the background in the upper half of the peak in the speed plot is justified for about half of the 4-star resonances.

In order to determine the phase ϕ of the residue, I have introduced *Argand plots of the complex-valued vector* dT/dW which also give a useful check for the magnitude of the background [48]. The phase is not a property of the resonance alone. It also depends on the background and is needed to satisfy unitarity.

Non-symmetrical shapes of a resonance curve for ImT are due to the phase of the residue, which is e.g. about $-50°$ for $\Delta(1232)$. In conventional parametrizations by a generalized Breit-Wigner formula, this shape is described by the energy-dependence of the width in the denominator.

Other methods for the determination of pole parameters have been developed by R.E. Cutkosky et al. [25] and by R. Arndt et al. [7–9]. A comparison of results from the speed plot method applied to the CMB80 solution with Cutkosky's table in cases where the background contribution is negligible can be found in Ref. [47]. If the background has a fast variation, model-dependent assumptions are necessary in all methods (e.g. for P33(1600) where the resonance signal is comparable with the magnitude of the tail of P33(1232) and an assumption on the energy-dependence of this tail is needed).

Unstable excited state of the nucleon, resonance in πN scattering or "isobar" are different names for the same phenomenon, which is a generalization of the notion of a particle. In suitable models, one can start with a stable particle which has a pole of the partial wave amplitude on the real axis at an energy below the branch point of the cut. By a change of a parameter, the pole can go to the branch point and enter the lower part of the complex W-plane. If the real part is not near to the location of a branch point and the distance of the pole from the real axis is not too large, the pole is a typical resonance pole [46,32]. If the imaginary part of the pole position becomes large, the width of the resonance increases and a separation from the background becomes more and more model-dependent.

The case that the real part of the pole position is near to the location of a branch point is well known from the deuteron and the ^1S neutron-proton state at low energies. The deuteron has its pole on the physical real axis (first sheet) below threshold, whereas the ^1np-state has its pole on the real axis in the second sheet (virtual state pole, see e.g. Ref. [38]).

Some authors used K-matrix poles for the resonances. In his detailed discussion of resonances, including poles in complex conjugate positions in the 2nd sheet, R. Oehme [70] concluded that this pair of poles of partial waves are the actual representation of unstable particles and not the K-matrix poles. R.E. Cutkosky explained in the 2nd paper in Ref. [25]

why he preferred the T-matrix poles.

1.2 One excited state in different reactions

An important point which is not sufficiently emphasized in some introductions to the notion of a resonance is that *the location of a resonance pole is the same for all reactions to which the resonance couples*, e.g. in πN scattering and photoproduction of π or η. This property should be applied in calculations of $N\gamma$ couplings. Arndt et al. [6] circumvented the separation of resonance and background contributions by using resonance pole parameters for the evaluation of the photon decay widths (at that time their pole position was somewhat too low).

In his thesis, O. Hanstein [43] determined the resonance pole position from speed plots for the photoproduction multipoles $M_{1+}^{3/2}$ and $E_{1+}^{3/2}$. He found $M = 1211\,MeV$, $\Gamma = 100\,MeV$ in good agreement with the resonance parameters from πN scattering. As expected, the mass parameter $m = 1232\,MeV$ of the Breit-Wigner formula does not play a role.

1.3 Shadow poles

In the inelastic region, one resonance has in general poles in several Riemann sheets [37,35,29,53,36]. If the real parts of the pole positions are not lying near a branch point, it is sufficient to consider the pole which has the shortest distance from the physical real axis. The other poles are called *shadow poles* (see sect.4.9 in Ref. [36]).

Considerable complications arise if the real part of the pole position lies near a branch point. In πN physics, this problem was well known to R.E. Cutkosky [25]. But he calculated further poles for P11(1440) only after R.A. Arndt et al. [7] had reported two poles in different Riemann sheets for this resonance [26,27]. The branch point belongs to the decay to $\Delta(1232)+\pi$ and lies in the lower half plane at $W = 1338 - i\,50\,MeV$. The location of the poles is $W_p = 1346 - 88i$ and $1383 - 105i\,MeV$ (SM95). In the speed plot, the pole in the sheet which is nearest to the physical real axis ($ReW_p = 1346\,MeV$) is strongly dominant, except that the peak is shifted to about $1360\,MeV$.

Observable effects of poles and shadow poles in coupled-channel systems were studied by B.C. Pierce and B.F. Gibson [71] using separable potentials. A possible application to the P11-wave in πN scattering is mentioned but not treated in detail.

Other cases where shadow poles are physically significant were discussed for S-wave $\pi\pi$-scattering by D. Morgan and M.R. Pennington [66] and recently by M.P. Locher et al. [59], where further references are given. The resonance $f_0(980)$ is located very near to the threshold for the final state $K\bar{K}$. The investigations are based on the resonance poles of the S-matrix. I think that further work on πN scattering near the η-threshold should be done in a similar way.

In nuclear physics shadow poles assume physical relevance in a two-pole description of a well-known resonance in ^5He. The channels are $n - \alpha$ and $d - t$. [41,65].

1.4 A problem of the conventional Breit-Wigner parameters

The ansatz for the energy-dependent width in the conventional Breit-Wigner parametrization for $\Delta(1232)$ was chosen such that the P33 partial wave could be fitted from threshold to an energy somewhat below the resonance $\Delta(1600)P33$. It is well known since the mid-fifties, when Chew and Low published their famous plot, that the nucleon Born term gives an important contribution to this partial wave. From this plot one could even determine an

approximate value for the πNN coupling constant. The study of the partial wave dispersion relation for P33 by J. Hamilton et al. [42,34] and more recently by Koch and Hutt [54] confirmed the important contribution of the nucleon Born term and showed that contributions from t-channel exchanges are not negligible (see also sect. 3 and Fig. 3a in Ref. [50]).

It is also known for a long time that the real part of the $\Delta(1232)$ resonance pole position is about $M = 1210\,MeV$, where the P33 phase amounts to about 67°, i.e. the background is so large that the phase is shifted from the pole term contribution (90°) by −23°. The width from the resonance location is about $100\,MeV$, whereas the strongly energy-dependent conventional width at $W = 1232\,MeV$ is about $120\,MeV$.

If $\Delta(1232)$ is calculated in a model, e.g. a quark model, the aim is to treat the resonance alone and not together with the background in πN scattering, which is different from the background if the excited state is created in another reaction. Therefore, I think that predictions for the masses and widths of excited states of the nucleon should be compared with the parameters of the resonance pole.

2 THE SPEED PLOT FOR THE S11 PARTIAL WAVE

Fig. 2a shows the speed plot as calculated from the VPI solution SM95 and Fig. 2b includes in addition points from other partial wave solutions. There is no doubt that these figures show *only two pronounced peaks.* The peak around $W = 1670\,MeV$ belongs to S11(1650) and the other peak occurs at the η-production threshold. A threshold is known to produce a peak of this shape, if it belongs to the production of a *long-living particle in an S-wave.* It is surprising that one does not see a signal from the 4-star resonance S11(1535). In my talk at the Conference in Jülich [49] I suggested that the pole or poles of S11(1535) are so close to the η-threshold that S11(1535) has to be treated in a different way than all other nucleon resonances. It is a *combined threshold + resonance phenomenon.*

2.1 The speed plot near the η-threshold

The kinematical parameters of the threshold are:

$W_\eta = 1487.0 \pm 0.2\,MeV$: total c.m. energy, $\quad p_{Lab} = 684.7\,MeV/c$: pion lab. momentum
$T_\pi = 559.2\,MeV$: pion kinetic lab. energy, $\quad T_\gamma = 709.2\,MeV$: photon lab. energy

$$q_{th} = 432.0\,MeV/c : \text{ c.m. momentum of the incoming pion}$$

The effect of the very small width of η is negligible ($\Gamma_\eta = 1.2\,keV$), i.e. the threshold lies practically on the real axis. The angular distribution shows that the η-production starts with a strong S-wave. The real part of the pole position of D13(1520) is near to threshold: $1515\,MeV$ (SM95). In their accurate measurements, Krusche et al. [56] found in photoproduction a significant D13-contribution of about 10% to the η-production.

Since some authors mentioned a possible contribution from P11(1440), we give the energy of the peak in the speed plot $\approx 1360\,MeV$. If we add half of the total width of the dominant pole, we arrive at $1450\,MeV$, well below the η-threshold ($1487\,MeV$). In η-production [56] a significant contribution from P11(1440) was not seen.

In a close neighborhood of the η-threshold, the speed can be calculated from Eq. (2) and an approximation for the partial wave, which takes into account only the two dominant channels and a correction linear in the c.m. η-momentum q_η. This is the zero-range approximation [15]

$$T = T_{th} + i q_{th} q_\eta b^2 + \cdots; \qquad b^2 = |b|^2\, e^{2i\phi}. \tag{3}$$

We use the kinematical relation

$$q_\eta^2 = (s - s_\eta)[s - (m_n - m_\eta)^2]/(4s). \tag{4}$$

m_n denotes the neutron mass and $s = W^2$. An approximation valid near threshold reads

$$q_\eta \approx \left[\frac{2m_n m_\eta}{m_n + m_\eta}\right]^{1/2} \sqrt{W - W_\eta} = \beta\sqrt{W - W_\eta}; \qquad \beta = 0.8317\, GeV^{1/2}. \tag{5}$$

If one considers the dependence on s, the increase starts with a factor $\sqrt{s - s_\eta}$.

Since T_{th} in Eq. (3) is a constant, the speed follows from the second term in Eq. (3) and Eq. (5)

$$Sp(W) \approx q_{th}|b|^2 \left|\frac{dq_\eta}{dW}\right| = q_{th}|b|^2\beta \left|\frac{1}{2\sqrt{W - W_\eta}}\right|. \tag{6}$$

It is seen that the upper part of the peak is symmetric to a vertical line at $W = W_\eta$. It looks like a needle which becomes thinner as the height increases and ends at a height which depends on the width of the η-meson.

In order to get a numerical value for $|b|^2$ we use the expression for the increase of the cross section for η-production near threshold in the zero-range approximation [15]

$$\sigma(\pi^- p \to n\eta) = \frac{2}{3}\frac{4\pi}{q_{th}}|b|^2 q_\eta. \tag{7}$$

The factor 2/3 comes from the isospin coefficients.

At present the most accurate result $|b|^2$ follows from the fit of Clajus and Nefkens to a carefully selected set of η-production data [23]. The linear approximation is valid up to about $W \approx 1500\, MeV$ ($p_{Lab} = 706\, MeV/c$, $q_\eta = 0.095 GeV/c$, $E_\gamma = 730\, MeV/c$).

$$|b|^2 = 0.11\, fm^2 = 2.8\, GeV^{-2}; \qquad \frac{\sigma_\eta}{q_\eta} = 21\, mb/GeV/c. \tag{8}$$

The result for the ratio agrees with the value reported by Binnie et al. [16]: 21.2 ± 1.8.

Another determination of $|b|^2$ follows from the expression for the total cross section for η-meson production in terms of the absorption parameter η, which should agree with Eq. (7) if the isospin factor is omitted.

$$\sigma_\eta = \frac{\pi}{q_{th}^2}(1 - \eta^2) = 4\pi\frac{q_\eta}{q_{th}}|b|^2. \tag{9}$$

We solve for $|b|^2$ and and determine the absorption parameter from the VPI partial wave solution SM95 in the range $q_\eta = 0.05 \ldots 0.1\, GeV/c$, because at smaller values of q_η the small contribution of $N\pi\pi$ final states cannot be neglected. The ratio σ_η/q_η is now about 30% larger than the result of Binnie et al. [16].

$$|b|^2 = \frac{1 - \eta^2}{4q_{th}q_\eta}; \qquad |b|^2 \approx 0.14\, fm^2. \tag{10}$$

The discrepancy is mainly due to the fact that Arndt et al. [9] *have not used a fit to the η-production data.* Another reason is our neglection of the $N\pi\pi$ final states.

In comparison with KH80, the VPI solution has the advantage that an additional channel has been introduced for $n + \eta$. Furthermore, the partial waves are given as continuous functions, whereas the first mentioned solutions are the result of an iteration of fits to the data and fits to dispersion constraints. The iteration ended with fits to the data. Therefore, the tables give partial waves only at the centers of the chosen energy bins.

Cutkosky et al. [25] developed a rather complicated multichannel analysis in order to be able to include data for inelastic final states. However, it turned out that the compatibility of their absorption parameters with the data for inelastic final states was so poor that they had to enlarge the errors considerably (see the remarks on p.2844 in the 2nd paper of Ref. [25]). They had constructed partial waves with a smooth energy dependence (see the second paper in Ref. [25]), but unfortunately, the files were lost in the early eighties, when their computer was replaced by an new model.

In Fig. 2a the value $|b|^2 = 0.14\, fm^2$ was chosen, since we show in addition to the approximation Eq. (6) the result calculated from SM95.

The upper part of the speed plot agrees with our approximation Eq. (6). Below a height of about $10\, GeV^{-1}$ one can see a broadening, which is not only due to our approximation Eq. (6). The terms neglected in Eq. (6) include the effect of a pole which, according to SM95, has the location $W = 1501 - i\,62\ MeV$.

Since the real part of the pole position lies only $14\, MeV$ above threshold, this pole does not produce a peak similar to that of the other resonances but only an enhancement on the lower part of the right wing of the peak which belongs to the threshold. It is disappointing that the signal of this 4-star resonance is hardly visible in contrast to that of all other 4-star resonances.

The enhancement is smaller for other solutions (Fig. 2b). SM90 has the pole almost at the same location, but the modulus of the residue is smaller than for SM95. It is clear that KH80 and CMB80 cannot reproduce details of the threshold peak, because they have only a few points in its range.

Table 1 gives a list of the published resonance parameters. An average of the real parts of the pole positions calculated from various Breit-Wigner formulas [63] lies at $1502 \pm 12\, MeV$.

The existence of S11(1535) is favored by the fact that it would be difficult to find another mechanism for the strength of the η-production. Furthermore, a second S11 resonance in addition to S11(1650) is predicted in nonrelativistic constituent quark models for nucleon resonances. In a recent paper [22] the authors developed a semirelativistic version starting from the work of Isgur and Karl [51]. Their S11-resonance with the lowest mass (1460 MeV in

Table 1. Resonance pole parameters for S11(1535) and S11(1560). The table gives ReW_p, $-2 \cdot ImW_p$ and the modulus r of the residue in MeV units.

	$S11(1535)$			$S11(1650)$		
	ReW_p	$-2 \cdot ImW_p$	r	ReW_p	$-2 \cdot ImW_p$	r
$SM95$	1501	124	31	1673	82	22
$SM95$				1689	192	72
$SM90$	1499	110	23	1657	160	54
$KH80$				1670	163	39
$CMB80$	1510 ± 50	260 ± 80	120 ± 40	1640 ± 20	150 ± 30	60 ± 10

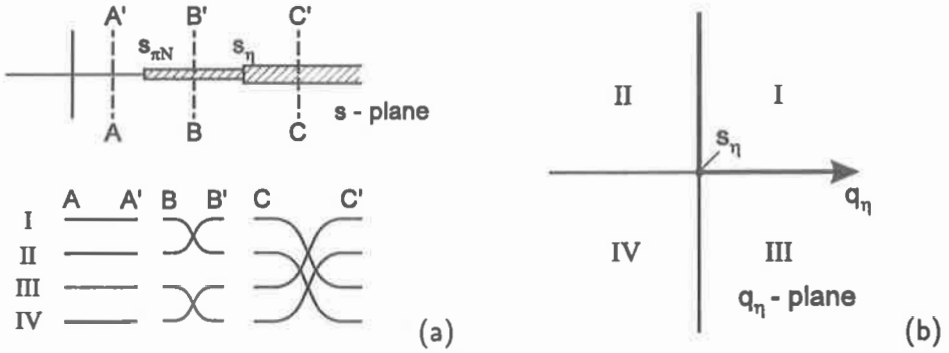

Figure 3. Topology of the Riemann surface of $T(S11)$: (a) shows the connection between different sheets in the s-plane [38]. In (b), we have carried out a local uniformization by using the c.m. momentum q_η as the new variable. The thick lines belong to the physical energy axis. It is seen that sheet IV touches this line only at the branch point. The location of a pole in this sheet determines the magnitude of the threshold cusp.

their model, some corrections to this mass have not yet been calculated) has a strong decay to $N + \eta$. It is considered to belong to S11(1535). The location of the resonance pole found from SM95 near threshold shows that the shadow poles mentioned in sect.1.3 have a good chance play a role for S11(1535). It will be of interest to search for these poles as soon as the experimental information has been improved [78].

We show the connection between the different Riemann sheets near the η-threshold for simplicity only in the simplified case of the two-channel problem, ignoring the weak $N\pi\pi$ channel. Figs. 3a and 3b are discussed e.g. in Ref. [38], Ref. [20], p.183, Ref. [53] and Ref. [69], p.524. Fig. 3a shows the connection between the 4 sheets. Sheet I is the physical sheet, where singularities cannot occur. Fig. 3b belongs to a *local uniformization*, i.e. to the introduction of a new variable in which the S-matrix element is single-valued. The square root cut is opened up. In our case, the new variable is q_η. The mappings in Refs. [53,69] also includes the πN threshold (see also Ref. [65]).

A pole in sheet II for $s < s_\eta$ would be an (unstable) bound state of n and η. There is no evidence in our reaction, but an unstable $N\bar{K}$ bound state was discussed for $\Lambda(1405)$. A pole in sheet III for $s > s_\eta$ belongs to a resonance in both channels. *A pole in sheet IV leads to the threshold cusp* [39,38,83]. In the inelastic region, one resonance has in general poles in different Riemann sheets (Refs. [35,28]. In the vicinity of a threshold, it happens that several poles can have a comparable distance to the physical real axis.

In πN scattering, new information in our range of interest since 1979 follows from the data at the highest momenta measured at LAMPF [77,81] and at the PNPI [1,55]. Furthermore, $\pi^- p$-scattering and the analyzing power have been measured at the ITEP accelerator by Abramov et al. and Alekseev et al. [3,4]. Unfortunately, the charge-exchange data measured at Rutherford Lab [23] as well as the unpublished charge-exchange data measured at LAMPF [19] have problems.

2.2 The speed plot near S11(1650)

Fig. 2b shows that the speed plots calculated from different partial waves have considerably different heights. In GeV^{-1} units the height is 10.5 for SM95, about 8 for SM90 and CMB80 and about 6 for FA93 and KA84. The above mentioned ITEP data were available since 1989 and the first VPI solution with dispersion constraints was FA93. (these constraints were

imposed only up to $T_\pi = 600\,MeV$ [8]. This is about $W = 1520$ MeV, i.e. below the resonance S11(1650). So one has to assume that the discrepancies are mainly due to a different treatment of contradictory data.

The dip near 1720 MeV in the speed plot for VPI95, which was not seen in the earlier solutions, occured when an additional term was introduced in the empirical ansatz in a search for further resonances [9]. I think the introduction of *two poles with strongly overlapping widths in the same Riemann sheet* (see Table 1) is not a convincing solution. The list of "missing states" in the table of Capstick and Roberts [22] does *not* include a third S11-resonance.

It is interesting to note that the threshold for ω-production lies at $1721.5 \pm 4.2\,MeV$ if one uses the mass and the half-width. This threshold leads to a "woolly" cusp [68,38] whose shape differs considerably from the η-cusp because of the much larger width of the ω-meson (it is almost 5000 times larger than the width of the η). The differential ω-production cross section is close to isotropic [52] and the ratio σ_ω/q_ω is of the same order as the ratio of the corresponding quantity for η-production. The branch point for $n\omega$ final states lies in the lower half plane at $1721.5 - i\,4.2\,MeV$.

The threshold for $K\Lambda$-production at $1613.4\,MeV$ is located on the left wing of S11(1650). Although long-living particles are produced in an S-wave and data exist [62], one does not see a signal in our plots.

The threshold for ω-production could also modify the signal for the resonance P11(1710) in the speed plot, which in earlier work has been assumed to belong to P11(1710) alone. Another difference in comparison with papers written before 1993 is that Clajus and Nefkens [23] gave reasons to eliminate the data of Brown et al. [21] and Baker et al.[10] from the data base. As a consequence, *the large branching fraction of about* 25% *for the decay of P11(1710) to* $n\eta$ was omitted in recent issues of the RPP.

According to Manley et al. [61], the elasticity of S11(1650) amounts to 0.89(7). This is higher than the values from KH80 (0.61) and and CMB80 (0.65). The most recent VPI solution SM95 gives 0.99 and 0.21 for the two states with poles at 1673 and 1689 MeV, respectively. The ratio of the elastic cross section to the total cross section is 0.76.

The discrepancy is related to differences between data sets which also led to the discrepancies in Fig. 4a for $ImT(S11)$ and in Fig. 2 of Ref. [9]. Fig. 4b shows in addition to the total $ImT(S11)$ the decomposition into the elastic and inelastic parts.

The prediction of Capstick and Roberts [22] for the magnitude of η-production from S11(1650) is too large. Fig. 6 shows that at and beyond the resonance peak the absorption parameter η determined from πN partial wave analyses is saturated already by the $N\pi\pi$-channel [60,61]. Furthermore, Fig. 5 shows that in this case the notion of a branching ratio is doubtful, since *along the left wing of S11(1650)* the $N\pi\pi$ final state has a *very rapid increase* from a small value to a saturation of the absorption parameter. This is probably related to the opening of the $N\rho$-channel. The branch point for this channel lies near $1707 - i\,75\,MeV$. The shape for this combination of a woolly cusp with a resonance has not yet been calculated. Due to the poor experimental information, it is probably at present not possible to check if a second pole in a different Riemann sheet exists at a comparable distance to the physical real axis in analogy to the case of P11(1440).

In a paper based on a constituent quark model, Arima et al. [5] concluded that a mixing of S11(1535) and S11(1650) is reponsible for the strong coupling of η to S11(1535) and the weak coupling to S11(1650). In their Fig. 2 they used mainly the data rejected by Clajus and Nefkens [23]. The good data of Binnie et al. [16] had not come to their attention.

In Ref. [48] figures for ImT_{in} have been shown for many partial waves. In some cases, one

Fig.4a ImT(S11) from various partial wave solutions

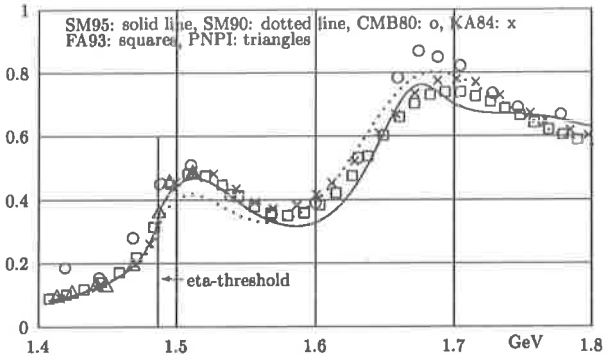

Fig.4b ImT(S11) from SM95, total, elastic and inelastic part

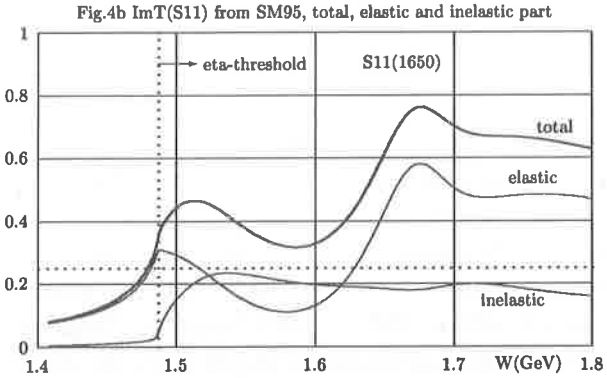

Fig.4c S11(SM95): Sigma(tot), elastic and inelastic part in mb

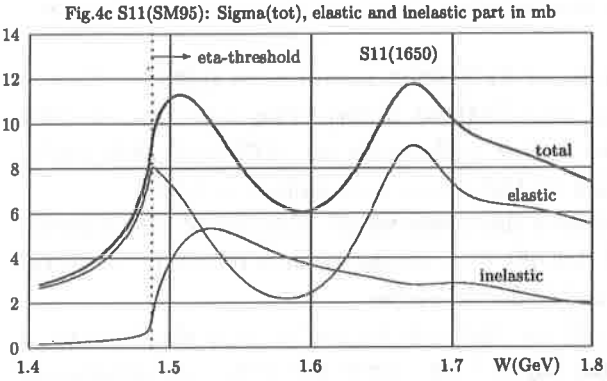

Figure 4. The imaginary part of $T(S11)$. (a) $ImT(S11)$ as determined from different partial wave analyses. The notation is the same as in Fig. 2b except that we have added below 1.5 GeV some triangles, which belong to the PNPI analysis [1]. The largest discrepancies occur in the range of S11(1650). (b) The decomposition of ImT into its elastic and inelastic parts, using SM95. One can see the threshold cusp of the elastic part and the peak of the inelastic part near 1540 MeV. In contrast to several other resonances, there is no peak of the inelastic part near 1670 MeV. In this plot the unitarity limit is the dotted horizontal line at the ordinate 0.25. (c) The contribution of S11 to the total cross section differs from (b) only by a factor $4\pi/q^2$, whose denominator enhances the decrease on the right wings of the peaks. The peak of the total S11 cross section at 1510 MeV looks like a resonance peak. But it is the sum of the elastic part, which has a pronounced cusp, and the rapidly rising inelastic part. It is of interest to compare the height of the peaks with the total isospin 1/2 cross section at threshold: 53.8 mb. The resonance D13(1520) contributes about 30 mb to the total cross section and about 10 mb to its inelastic part.

Fig.5 ImTin(S11) from various partial wave solutions and data

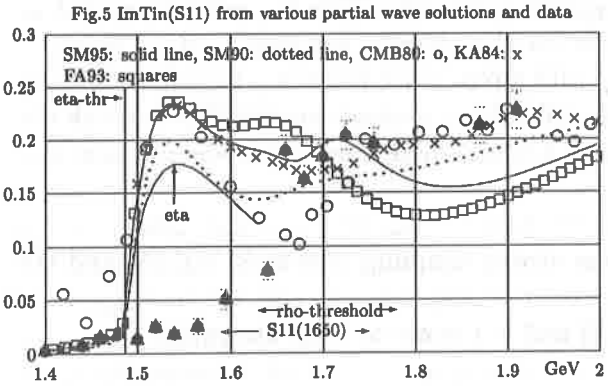

Figure 5. Plot of $ImT_{in}(W)$ for $S11$. We show $ImT_{in}(W) = (1-\eta^2)/4$ as determined from various partial wave solutions. The notation is the same as in Fig. 2b. In addition, we have plotted below 1640 MeV the contributions from η-production [23] (vertical arrow) and from $N\pi\pi$ final states (filled circles) [60,61]. There are large discrepancies between the different partial wave solutions, even between the VPI solutions. The sum of the η-production and the $N\pi\pi$ final states around 1.54 GeV is not in agreement with the values derived from the absorption parameter of partial wave analyses. Since five points of Manley et al. practically saturate the absorption parameter found in partial wave analyses near the top of S11(1650), one can expect that S-wave η-production in this range is very small. There is a very strong increase of the $N\pi\pi$ final states on the left wing of S11(1650). The fact that two points of Manley et al. near 1.9 MeV are *much higher* than the curves from SM95 and FA93 shows that either these points or the curves are not correct.

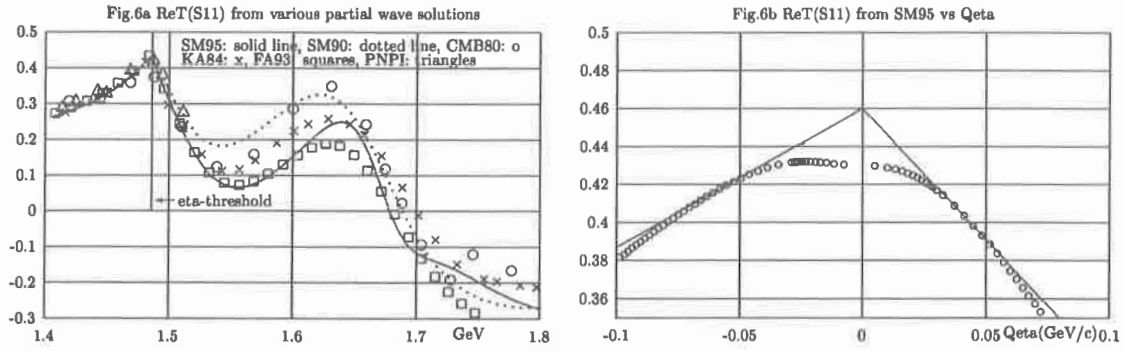

Figure 6. The real part of $T(S11)$. (a) Here the existence of the threshold cusp is visible in all analyses. Again, the energy dependence is not well determined from the data. The new experiment of the Crystal Ball group [78] will improve the information on the πN charge-exchange cross sections. (b) In the neighborhood of the threshold it is preferable to use for the abscissa $q_\eta^2/|q_\eta|$ which agrees with q_η above threshold [15]. In a two-channel model, one expects two straight lines, but near threshold the η-production is small in comparison with the production of $N\pi\pi$ final states which is neglected in the two-channel model. Furthermore, the corrections to the zero-range approximation become larger as the distance to threshold increases. So we have only a range of about 0.05 in the units of our abscissa on both sides in which the linear approximation is valid. This is sufficient for an estimate of the phase ϕ from Eq. (11).

can see a pronounced peak (e.g. D13(1520), D15(1675), F15(1680), S31(1900)), but others (e.g. P11(1440), P13(1720)) *do not even show a structure at the resonance position.* It will be of interest to find out if this is related to effects of woolly cusps.

One should notice that these figures differ from the inelastic total cross sections shown in Fig. 4c and in Figs. 2 of Ref. [61] by a factor $4\pi/q^2$, which leads to a more rapid decrease of the right wings due to unitarity.

At high energies, there are in some cases (e.g. S31) large differences between ImT_{in} as calculated from KH80 and CMB80 on the one hand and SM95 and SM90 on the other hand. Some points of Manley [60,61] for S31 even lie almost at the unitarity limit (Fig. 7.7 in Ref. [48]). It is necessary to check if this is due to the relatively small number of data published after 1979, the choice of the empirical energy-dependent parametrization or to the missing dispersion constraints of the VPI solutions in this energy range.

3 THE THIRD ZERO-RANGE PARAMETER AT THRESHOLD

The effect of a threshold on scattering amplitudes has been studied by many authors, starting with Wigner [85] and Baz [13]. Ross and Shaw [73] and Dalitz [28] developed a multichannel effective-range formalism. In the mid-sixties, this formalism was used for the study of S-matrix poles close to a threshold in several papers [74,38,53,83,84,44,33]. An excellent treatment and further references can be found in Newton's book [69]. Davies and Moorhouse [31] gave a detailed review and supported the existence of a S11 resonance near threshold, but at that time the data were still rather poor.

An interesting different approach based on dispersion relations was proposed by Ball and Frazer [11]. It was discussed by Kato [53].

Of the more recent papers I mention the work of Bhandari and Chao [15], since I want to use some of their formulas and some papers published in 1995, where further references can be found [12,1].

If one neglects the small contribution of the channel leading to $N\pi\pi$ final states and as-

sumes isospin invariance, one has a 2×2 T-matrix, whose elements belong to the reaction $\pi N \to \pi N$ in the S11 partial wave, the reactions $\pi N \to N\eta$ and ηn S-wave elastic scattering. In the zero range approximation, the matrix can be described by three constant real parameters [73]. We choose the S11 πN phase shift and a complex-valued constant $b = |b|\, exp(i\phi)$ introduced in Eq. (3). Most of the other authors used the complex-valued scattering length a for elastic ηn-scattering. Within the two-channel formalism, the $n\eta$ scattering length a can be calculated from our parameters [73].

The modulus $|b|$ has been determined from Eq. (7) from data for η-production in $\pi^- p$-scattering. Following Wigner [85], Baz [13] showed that the phase angle ϕ of b can be determined from the singularity at threshold in plots of $d\sigma/d\Omega$ as a function of energy. Bhandari and Chao [15], who were working in Cutkosky's group, demonstrated that it was better to plot the differential cross section at fixed angle as a function of $q_\eta^2/|q_\eta|$ and that elastic $\pi^- p$ scattering data at 180° showed a large kink at threshold. However, the phase ϕ could only be derived if the phase of the elastic πN amplitude was known. Sarma et al. [79] made a improved experiment on elastic $\pi^- p$-scattering at Rutherford Lab., but they did not peform a detailed analysis.

Therefore, we determine the phase ϕ from the VPI partial wave analysis, which had these data as part of their input. Instead of using differential cross sections, it is sufficient to study the singularity in the energy dependence of $ReT(S11)$ (Fig. 6a).

It follows from analyticity that the vicinity of the threshold for η-production makes itself felt already at energies *below* $W = W_\eta$. This can be considered to be due to "virtual" transitions (see e.g. p.533 in Ref. [69]). The cross sections for $\pi^- p$ elastic scattering have infinite slopes in plots of the energy dependence, if the η-threshold is approached from *both sides* (threshold cusp).

Below threshold, q_η is purely imaginary. One has to take $q_\eta = +i|q_\eta|$ (see e.g.Refs. [13,15]). This gives from Eq. (8)

$$\begin{aligned} ReT &= ReT_{th} - q_{th} q_\eta |b|^2 \sin(2\phi) \qquad q_\eta^2/|q_\eta| > 0 \\ ReT &= ReT_{th} - q_{th} |q_\eta| |b|^2 \cos(\phi) \qquad q_\eta^2/|q_\eta| < 0 \end{aligned} \tag{11}$$

and similar equations for ImT.

Fig. 6b shows a plot of ReT(S11) vs. $q_\eta^2/|q_\eta|$. Near threshold, the curve is flat instead of the expected linear behavior. In this range, the η-production is smaller than the production of $N\pi\pi$ states, which has been ignored in our discussion. The amplitude for this channel also has a singularity at threshold, but its shape has not been calculated. The linear behavior is seen in a range outside the interval $q_\eta^2/|q_\eta| = -0.04 \ldots 0.03$. The dashed lines are a crude estimate. Using $|b|^2 = 0.11\, fm^2$ we find the phase angle $\phi = 31°$. The fit fulfils the condition that the same value for the angle is found on both sides. Fig. 6a shows that the existence of the singularity W_η is seen also if results of other analyses are included in the plot. Since in the second plot the abscissa is W, a two-channel model gives an upwards directed cusp.

The present result

$$|b|^2 \approx 0.11\, fm^2; \phi \approx 30° \tag{12}$$

will be considerably improved by the data of the Brookhaven experiment 909 (Ref. [78]) which uses the SLAC Crystal Ball. Since only neutral final states are measured, the cusp which is needed for the determination of the phase ϕ has to be studied in the πN charge-exchange reaction. A calculation based on the solution SM95 shows that a pronounced effect

is expected near 45° c.m. in contrast to elastic $\pi^- p$ scattering, where the largest effect occurs near backward angles.

The most important correction comes from the channel with $N\pi\pi$ final states. Results for the production in this channel have been given by Manley et al. [60,61]. At the peak for η-production near 1530 MeV, the sum of these two channels is somewhat smaller than expected from the absorption parameter of partial wave analyses (Fig. 5).

RPP96 omits the decay of P11(1440) into $N + \eta$ in the Summary Table but mentions two results (not used) in the Baryon Particle Listings. These are probably related to the large values for the width of this resonance found by some authors from Breit-Wigner fits. The published values for M and Γ derived from the $\alpha - p$ scattering experiment at Saturne lie near to our results [67]. I am at present in discussion with H.P. Morsch, who is working on a continuation of the experiment.

4 BUMPS AND CUSPS IN VARIOUS CROSS SECTIONS

In $\pi^- p \to \eta n$ the data show a bump near 1530 MeV. Clajus and Nefkens [23] used a Breit-Wigner formula for a fit and found the mass parameter $m = 1483 \pm 16\, MeV$. As noticed by Manley [63] the reason is that they used a *constant* Γ, so they found approximately the pole position.

A similar peak occurs in the reaction $\gamma + p \to n + \eta$, where much more accurate data were measured by Krusche et al. [56] at the MAMI accelerator in Mainz from threshold to 790 MeV which corresponds to W=1537 MeV. They used a generalized Breit-Wigner formula with a special choice for an energy-dependent width $\Gamma(W)$ and found the parameters

$$m = 1544 \pm 13\, MeV; \Gamma(M) = 200 \pm 40\, MeV. \tag{13}$$

This fit is based on data, which lie essentially only on the left wing of the peak. In both cases, the location of the peak does not give a direct information on the resonance pole.

η-production starts with zero at threshold. Since it is produced in an S-wave, it is increasing proportional to q_η. But this increase cannot continue because this would violate unitarity(Fig. 5). So the curve must have a peak and turn downwards. A curvature would follow already if the zero range ansatz is replaced by an effective range approximation. The location of the peak also depends on the increase of transitions to other final states. Fig. 5 shows that near the threshold for ρ-production, the $N\pi\pi$ final states give a contribution which is *rapidly increasing on the left wing of the resonance S11(1650).* They saturate the absorption parameter at the peak of this resonance, so η-production in the S-wave must be very small. It follows that a bump must exist between 1487 and 1650 MeV. Its location is also related to the decrease of the right wing of the S11(1535) resonance. The parameters derived from SM95 give $M + \Gamma/2 \approx 1560\, MeV$.

Furthermore, it was pointed out in the Introduction that the only mass parameters of excited states of the nucleon which have a theoretical justification are the real parts of the resonance pole positions which are related to the peaks of the speed plots. The location of the pole for a resonance must be *the same in all reactions to which this resonance is coupled.* The best reaction for the determination of the location of the pole is πN scattering. It follows that calculations of the photoproduction of η or a pion or production in $\pi^- p$ scattering have to use a resonance pole of S11(1535) near 1500 MeV (and possibly further poles in other Riemann sheets).

In a new paper, B. Krusche et al. [57] found the set of S11(1535) parameters suggested by the PDG to be *inconsistent* with their experimental results. Instead of studying exotic possibilities, I think it is better to consider the combined S11(1535)+threshold cusp phenomenon described in this paper.

In my opinion, the papers of Benmerrouche et al. [14] rely too much on the conventional parameters of the PDG although in the first paper a reference to the books of Goldberger-Watson and of Bransden-Moorhouse is given. It will be difficult to treat the shadow poles at the η-threshold with a Lagrangian formalism.

It is useful to remember a slogan mentioned in a talk on Light Hadron Spectroscopy by D. Morgan: *not all bumps are resonances and not all resonances produce a bump.*

5 ISOSPIN VIOLATION IN πN SCATTERING

In 1979, R.E. Cutkosky called attention to a special enhancement mechanism for isospin violation associated with the S11(1535) resonance due to $\eta - \pi^0$ mixing [24]. It would be of interest to update the estimates based on the data known in 1979. The largest effect is expected in the region where η-production is large, i.e. near W=1540 MeV. It could be of the order of 10%. Since the experiment of the Crystal Ball group [78] measures η-production together with π^0-production, the data are very well suited to look for the isospin violation.

6 CONCLUSIONS

i) The most important parameters of nucleon resonances are the locations of the resonance poles. S11(1535) differs from all other resonances insofar as its pole lies near the threshold for the production of a long-living particle which is strongly produced in an S-wave, so one has to study a combined resonance-threshold cusp phenomenon.

ii) The location of the resonance poles are the same for all reactions in which a resonance is excited. Therefore, the reactions πN scattering, photoproduction of η and of π should be studied together in determinations of the parameters S11(1535).

iii) At the η-production threshold all amplitudes of these reactions have a singularity. The existence of the threshold modifies the amplitudes and cross sections also below the energy W_η.

iv) As a first step, one can neglect the relatively small $N\pi\pi$ final states and consider the zero-range approximation of a two-channel problem. The next step should be to study the effective range approximation as it was done in the sixties with the old data.

v) Since the resonance pole lies near to the branch point for η-production, attention should be paid to contributions of shadow poles. One of these poles creates the threshold cusp.

ACKNOWLEDGMENTS

I wish to thank R.A. Arndt for our good collaboration in exchanging information and for many discussions. Until his early death it was a great pleasure to be in contact with R.E. Cutkosky, in particular when we worked together for the Review of Particle Properties in 1992. His critical comments were very helpful for the continuation of this work.

REFERENCES

[1] V.V. Abaev, S.P. Kruglov, *Z. Phys.* **A352**(1995)85
[2] V.V. Abaev, B.M.K. Nefkens, UCLA-10-P25-229

[3] B.M. Abramov et al., Phys. At. Nucl. (former Sov. J. Nucl. Phys. **54**(1991)332)
[4] I.G. Alekseev et al. Nucl. Phys. **B348**(1991)257
[5] M. Arima et al., *Nucl. Phys.* **A543**(1992)613
[6] R.A. Arndt et al., *Phys. Rev.* **C42**(1990)1853
[7] R.A. Arndt et al.,*Phys. Rev.* **D44**(1991)289
[8] R.A. Arndt et al.,*Phys. Rev.* **C49**(1994)2729
[9] R.A. Arndt et al.,*Phys. Rev.* **C52**(1995)2120
[10] R.D. Baker et al., *Nucl. Phys.* **B156**(1979)93
[11] J.S. Ball, W.R. Frazer, *Phys. Rev. Lett.* **7**(1961)204
[12] M. Batinić, I. Slaus, A. Svarc, *Phys. Rev* **C51**(1995)2310, **C52**(1995)2188
[13] A.I. Baz, *Sov. Physics JETP* **6**(1958)709
[14] M. Benmerrouche et al., *Phys. Rev.* **D51** (1995)3237; *Phys. Rev. Lett.* **77**(1996)4717
[15] R. Bhandari, Y. Chao, *Phys. Rev.* **D15**(1977)192
[16] D.M. Binnie et al., *Phys. Rev.* **D8**(1973)2789
[17] Proc. Sixth Int'l Symposium on Meson-Nucleon Physics and the Structure of the Nucleon, *πN Newsletter* **10,11**(1995)
[18] Arno Bohm, *Quantum Mechanics*, 3rd ed., Springer Verlag, 1993
[19] F.D. Borcherding, UCLA thesis, 1982, unpublished
[20] B.H. Bransden, R.G. Moorhouse, *The Pion-Nucleon System*, Princeton Univ. Press 1973
[21] R.M. Brown et al., *Nucl. Phys.* **B153**(1979)89
[22] S. Capstick, W. Roberts, *Phys. Rev.* **D49**(1994)4570
[23] M. Clajus, B.M.K. Nefkens, *πN Newsletter* **7**(1992)76 and private communication from M. Clajus
[24] R.E. Cutkosky, *Phys. Lett.* **B88**(1979)339
[25] R.E. Cutkosky et al., *Phys. Rev.* **D20**(1979)2804,2839; R.E. Cutkosky in Proc. *Baryon 80* , Proc. of the 4th Int'l Conference on Baryon Resonances in Toronto, ed. N. Isgur, p.19.University of Toronto, 1980
[26] R.E. Cutkosky, *Proc. 2nd Int'l Workshop on πN Physics* , eds. W.R. Gibbs, B.M.K. Nefkens, Los Alamos Report LA-11184-C (1987), p.167
[27] R.E. Cutkosky, S. Wang, *Phys. Rev.* **D42**(1990)235
[28] R.H. Dalitz, *Ann. Rev. Nucl. Sci.* **13**(1963)339
[29] R.H. Dalitz, G. Rajasekaran, *Phys. Lett.* **7**(1963)273
[30] R.H. Dalitz, R.G. Moorhouse: What is Resonance?, *Proc. Roy. Soc. London* **A.318**(1970)279
[31] A.T. Davies, R.G. Moorhouse, *Nuovo Cim.* **52A**(1967)1112
[32] J. Denschlag, *Diplomarbeit: Das Schwellenverhalten der Eta-Produktion am Proton, Univ. Mainz,* , KPH19/94 (1994)
[33] P.N. Dobson, *Phys. Rev.* **146**(1966)189
[34] A. Donnachie, *Pion-Nucleon Phase Shift Analysis* in Particle Interactions at High Energies, eds. T.W Preist, L.L.J. Vick, Oliver and Boyd, 1967
[35] R.J. Eden, J.R. Taylor, *Phys. Rev. Lett.* **11**(1963)516; *Phys. Rev.* **B133**(1964)1575
[36] R.J. Eden, P.V. Landshoff, D.I. Olive, J.C. Polkinghorne, *The Analytic S-Matrix*, Cambridge Univ. Press (1966)
[37] L. Fonda, R.G. Newton, *Ann. Phys. (N.Y.)* **10**(1960)490
[38] W.R. Frazer, A.W. Hendry, *Phys. Rev.* **B134**(1964)1307
[39] Y. Fujii, Uehara, *Prog. Theor. Phys.* **29**(1963)71
[40] M.L. Goldberger, K.M. Watson, *Collision Theory*, Wiley, 1964; M.L. Goldberger, K.M. Watson, *Phys. Rev.* **127** (1962); M. Froissart, M.L. Goldberger, K.M. Watson, *Phys. Rev.* **131**(1963)2820
[41] G.M. Hale et al., *Phys. Rev. Lett.* **59**(1987)763
[42] J. Hamilton, *Pion-Nucleon Scattering* in High Energy Physics, Vol.I, ed. E. Burhop, Academic Press 1967
[43] O. Hanstein, thesis, University of Mainz
[44] A.W. Hendry, R.G. Moorhouse, *Phys. Lett.* **18**(1965)171
[45] A.J.G. Hey, R.L. Kelly, *Physics Reports* **96**(1983)72
[46] G. Höhler, *Z. Phys.* **152**(1958)546
[47] G. Höhler, A. Schulte, *πN Newsletter* **7**(1992)76
[48] G. Höhler, *πN Newsletter* **9**(1993)1
[49] G. Höhler, *Physics with GeV Particle Beams* , Proc. Int'l Conference in Jülich August 1994, p.198, eds. H. Machner, K. Sistemich
[50] G. Höhler, H.M. Staudenmaier, *πN Newsletter* **11** (1995)194

[51] N. Isgur, *Int. Journal Mod. Phys.* **E1**(1992)465; G. Karl, p. 491
[52] H. Karami et al., Nucl. Phys. **B154**(1979)503
[53] M. Kato, *Ann. Phys. (N.Y.)* **31**(1965)130
[54] R. Koch, M. Hutt, *Z. Physik* **C19**(1983)119
[55] S.P. Kruglov, Talk at the 7th Symposium on Meson-Nucleon Physics at Vancouver, to be published in πN Newsletter 13
[56] B. Krusche, et al. *Phys. Rev. Lett.* **74**(1995)3736
[57] B. Krusche et al., *Phys. Lett.* **B397**(1997)171
[58] Zhenping Li, *Phys. Rev.* **D52**(1995)4961
[59] M.P. Locher et al., PSI preprint PR-97-13 (May 1997)
[60] D.M. Manley et al., *Phys. Rev.* **D30**(1984)904
[61] D.M. Manley, E.M. Saleski, *Phys. Rev.* **D45**(1992)4002
[62] D.M. Manley, *Baryon Resonances* in New Vistas in Physics with High Energy Pion Beams (1994)119
[63] D.M. Manley, *Phys. Rev.* **D51**(1995)4837
[64] A.D. Martin, T.D. Spearman *Elementary Particle Theory*, North Holland (1970)
[65] D. Morgan, M.R. Pennington, *Phys. Rev. Lett.* **24** (1987)2818
[66] D. Morgan, M.R. Pennington, *Phys. Rev.* **D48**(1993)1185; D. Morgan, *Issues in Light Hadron Spectroscopy* **RAL-93-078**, invited talk at the Int'l Conf. Hadron 93 in Como, 1993
[67] H.P. Morsch et al. *Phys. Rev. Lett.* **69**(1992)1336
[68] M. Nauenberg, A.Pais, *Phys. Rev.* **126**(1962)360
[69] R.G. Newton, *Scattering Theory of Waves and Particles*, McGraw-Hill, 1966
[70] R. Oehme, *Phys. Rev.* **121**(1961)1840; *Nuovo Cim.* **20**(1961)334; Lectures on High Energy Physics, Hercegnovi 1961, Vol.II, ed. B.Jaksic, Gordon and Breach, 1965
[71] B.C. Pearce, B.F. Gibson, *Phys. Rev.* **C40**(1989)902
[72] R.E.Peierls, Proc. *Glasgow Conf. on Nuclear and Meson Physics*, Pergamon Press, 1954, p.296
[73] M.H. Ross, G.L. Shaw, *Ann. Phys. N.Y.* **9**(1960)391, **13**(1961)147
[74] M. Ross, *Phys. Rev. Lett.* **11**(1963)450
[75] Particle Data Group, *Phys. Rev.* **D50**, 1 August 1994
[76] Particle Data Group, *Phys. Rev.* **D54**, 1 July 1996
[77] M.E. Sadler, *Proc. Third Int'l Symposium on Pion-Nucleon and Nucleon-Nucleon Physics* , Vol.I, p. 124, Gatchina, April 1989
[78] AGS experiment E913: Baryon Spectroscopy with the Crystal Ball, spokespersons M.E. Sadler, H. Spinka, W.B. Tippens
[79] H.N.K. Sarma et al., *Nucl. Phys.* **B161**(1979)1
[80] F.T. Smith, *Phys. Rev.* **118**(1960)349
[81] I. Supek et al., *Phys. Rev.* **D47**(1993)1762
[82] J.R. Taylor, *Scattering Theory* , John Wiley, 1972
[83] S.F. Tuan, *Phys. Rev.* **B139**(1965)1393
[84] F. Uchiyama-Campbell, *Phys. Lett.* **18**(1965)189
[85] E.P. Wigner, *Phys. Rev.* **73**(1948)1002
[86] E.P. Wigner, *Phys. Rev.* **98**(1955)145

Vector Meson Photoproductions off Nucleons in the Quark Model

Qiang Zhao[1], Zhenping Li[1] and C.Bennhold[2] *
[1]*Department of Physics, Peking University,*
Beijing, 100871, P.R.China
[2]*Department of Physics, Center for Nuclear Studies,*
The George Washington University, Washington, D.C., 20052, USA

Abstract

A unified approach for vector meson photoproduction is presented in the constituent quark model. The s- and u-channel resonance contributions are generated using an effective quark vector-meson Lagrangian. Taking into account π^0 and σ t-channel exchanges for diffractive production, the available total and differential cross section data for ω, ρ^0, ρ^+, and ρ^- photoproduction can be well described with the same quark model parameter set. Our results clearly indicate that polarization observables are essential to identify so-called "missing" resonances.

One of the main goals of vector meson photoproduction experiments is to search for so-called "missing" resonances, which have been predicted by theory but have not been established experimentally[1,2]. One possible explanation for this long-standing puzzle is that these states couple weakly to the πN channel, which has provided most information for N^* states until now, but decay strongly into channels like ρN and ωN. Encouraged by recent successful descriptions of pseudoscalar meson photoproduction[3] we propose a parallel approach to vector meson photoproduction starting with the effective Lagrangian

$$L_{eff} = -\bar{\psi}\gamma_\mu p^\mu \psi + \bar{\psi}\gamma_\mu e_q A^\mu \psi + \bar{\psi}\left(a\gamma_\mu + \frac{ib\sigma_{\mu\nu}q^\nu}{2m_q}\right)\phi_m^\mu \psi + \ldots \tag{1}$$

where e_q (m_q) denote the quark charge (mass), A^μ the photon field, and where the quark field ψ couples directly to the vector meson field

$$\phi_m = \begin{pmatrix} \frac{1}{\sqrt{2}}\rho^0 + \frac{1}{\sqrt{2}}\omega & \rho^+ & K^{*+} \\ \rho^- & -\frac{1}{\sqrt{2}}\rho^0 + \frac{1}{\sqrt{2}}\omega & K^{*0} \\ K^{*-} & \overline{K}^{*0} & \phi \end{pmatrix} \tag{2}$$

with momentum q^ν. The coupling constants a and b in Eq. 1 allow for the two possible couplings of the quarks to the vector mesons; they are free parameters to be determined by the data. Unlike the large mass difference between the π and η in the peudoscalar case, the ω and ρ states have nearly equal masses, thus isospin violations for the ω and ρ are relatively small. This encourages us to pursue an unified description of both ω and ρ photoproduction with a single set of parameters, where the vector mesons couple directly to the quarks inside the baryon.

We briefly outline our quark model approach to vector meson photoproduction below; a detailed derivation of the formalism is given in Ref. [4]. Based on the effective Lagrangian in Eq. 1, at tree-level there are s-, u- and t- channel contributions, thus the matrix element for the meson photoproduction can be written as

$$\mathcal{M}_{fi} = \mathcal{M}_t + \mathcal{M}_s + \mathcal{M}_u. \tag{3}$$

*E-mail: zhaoq@ibm320h.phy.pku.edu.cn

The derivation of the s- and u- channel contributions uses methods similar to previous calculations of pseudoscalar meson photoproduction[3]. We separate the s-channel contributions $\mathcal{M}_s$ in Eq. 3 into two parts; the s-channel resonances below 2 GeV and those above 2 GeV that are treated as continuum contributions. The electromagnetic transition amplitudes of s-channel baryon resonances and their mesonic decays have been investigated extensively in the quark model[2,5–7] in terms of helicity and the meson decay amplitudes. These transition amplitudes for s-channel resonances below 2 GeV have been translated into the standard helicity amplitudes[8] in Ref.[4] in the harmonic oscillator basis. The framework of vector meson photoproduction in terms of the helicity amplitudes has been thoroughly investigated[8], and the various observables can be easily evaluated in terms of these amplitudes. The resonances above 2 GeV are treated as degenerate, since little experimental information is available on those states. Qualitatively, we find that the resonances with higher partial waves have the largest contributions as the energy increases. Thus, we write the total contribution from all states belonging to the same harmonic oscillator shell in a compact form, using the mass and total width of the high spin states, such as $G_{17}(2190)$ for the $n = 3$ harmonic oscillator shell. While a separation at 2 GeV may appear as somewhat arbitrary we have performed a number of numerical tests and found the contributions of the resonances above 2 GeV to be neglegliable. It is the low-lying resonances with $n \leq 2$ that contribute dominantly to the s-channel.

The u-channel contributions $\mathcal{M}_u$ in Eq. 1 include the nucleon, the Δ resonance for ρ production, whose transition amplitudes are treated separately, and all other excited states. The excited states are treated as degenerate in this framework, allowing their total contribution to be written in compact form. This is again found to be a good approximation numerically since contributions from u-channel resonances are not sensitive to their precise mass positions.

The t-channel exchange, $\mathcal{M}_t$, is proportional to the charge of the outgoing meson and is needed to ensure gauge invariance of the total transition amplitude. Therefore, from the effective Lagrangian in Eq. 1, t-channel vector meson exchange term contributes to charged vector meson photoproduction while the s- and u-channel transitions produce the amplitudes for neutral vector meson photoproduction. However, we find that in the case of neutral vector meson photoproduction, the s- and u-channel amplitudes are not sufficient to account for the strong diffractive behavior, which, in the picture of Regge phenomenology, comes from contributions of the large background integral in the Regge trajectory expansion. As discussed in Ref.[9] and also in Ref.[10] and Ref.[11] the non-resonant imaginary background amplitude for neutral vector meson, such as ω and ρ^0, photoproduction leads to large differences between neutral and charged vector meson production cross sections. However, we would like to emphasize that the main focus of this study is the large-t region with potentially significant nucleon resonance contributions. We therefore do not require a sophisticated mechanism for diffractive production but rather use a simple phenomenological parametrization. Therefore, we add a t-channel π^0 exchange to the amplitude for ω photoproduction and a σ exchange term to the amplitude for ρ^0 photoproduction suggested by Friman and Soyeur[12] who showed that these two terms play the dominant role in diffractive ω and ρ^0 photoproduction, respectively, near the threshold in the Vector Meson Dominance (VMD) Model.

The introduction of the π^0 and σ exchanges for ω and ρ^0 production, respectively, leads to two additional parameters, α_{π^0} and α_σ, associated with the harmonic oscillator strength for the π^0 and σ contributions at the corresponding vertices. A detailed derivation of the π^0 exchange is given in Ref. [13]. It is worth noting that some experimental observations[14–16] have shown increased strength in the large t region of the differential cross sections, this

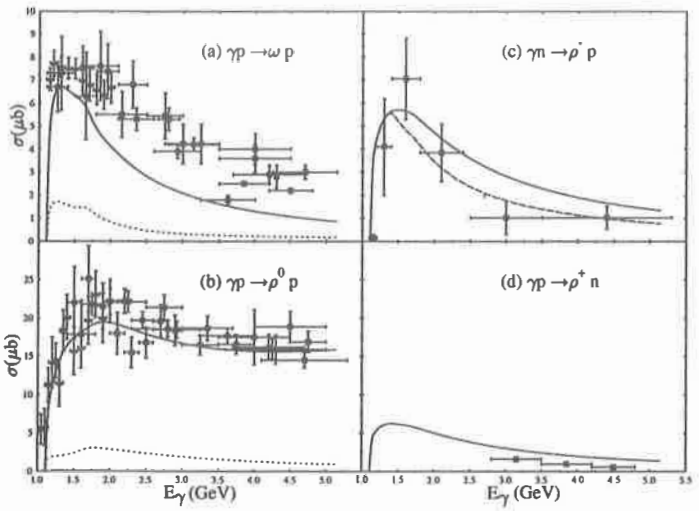

Figure 1. The total cross section for (a): $\gamma p \to \omega p$, (b): $\gamma p \to \rho^0 p$, (c): $\gamma n \to \rho^- p$, and (d): $\gamma p \to \rho^+ n$. The short-dashed line in (a) and (b) corresponds to the contributions from the transition matrix elements generated from the effective Lagrangian, while the dashed line in (c) represents to cross section for $t \leq 1.1$ GeV^2. The data in (a) and (b) come from Ref. [14](triangle) and Ref.[15](square). The data in (c) were taken with the restriction $t \leq 1.1$ GeV^2 given by Ref.[16], and the data in (d) come from Ref.[18].

behavior can not be explained by t-channel exchange alone and is most likely due to nucleon resonance contributions. As will be shown below, using the effective Lagrangian proposed in Eq.1, s- and u-channel resonance contributions are naturally generated which can explain this behavior at large t.

We assume that the relative strengths and phases of each s-, u- and t-channel term are determined by the quark model wavefunction in the exact $SU(6) \otimes O(3)$ limit. The masses and decay widths of the s-channel baryon resonances are obtained from the recent particle data group[17]. The quark masses m_q and the parameter α for the harmonic oscillator wavefunctions in the quark model are well determined in the quark model, they are

$$\begin{aligned} m_u = m_d &= 0.33 \quad \text{GeV} \\ \alpha &= 410 \quad \text{MeV}. \end{aligned} \tag{4}$$

The coupling constants for the π^0 and σ exchanges are taken from Ref. [12]. This leaves only the coupling constants a and b, and the parameters α_π and α_σ to be determined by the data. Qualitatively, we would expect that α_π (α_σ) to be smaller than the parameter $\alpha = 410$ MeV, since it represents the combined form factors for both πNN and $\omega\pi\gamma$ (σNN and $\rho\sigma\gamma$) vertices while the parameter α only corresponds to the form factor for the πNN or ωNN (ρNN) vertex alone.

In Fig. 1, we compare total cross section data for $\gamma p \to \omega p$ and the three channels in $\gamma N \to \rho N$ with our calculations. We did not perform a systematic fitting procedure due to the poor quality of the data. Our study suggests that

$$\begin{aligned} a &= -1.7 \\ b' &= b - a = 2.5 \\ \alpha_\pi &= 300 \quad \text{MeV} \\ \alpha_\sigma &= 250 \quad \text{MeV} \end{aligned} \tag{5}$$

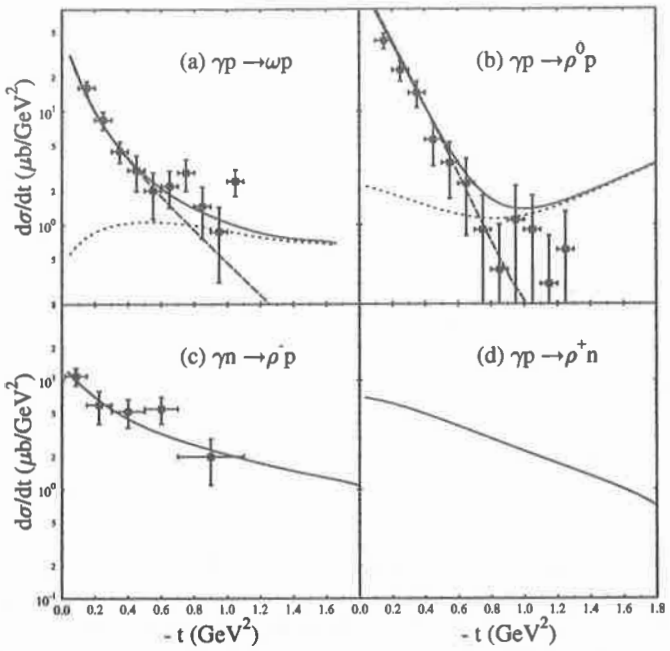

Figure 2. The differential cross section for (a): $\gamma p \to \omega p$ at $E_\gamma = 1.675$ GeV, (b): $\gamma p \to \rho^0 p$ at $E_\gamma = 1.730$ GeV, (c): $\gamma n \to \rho^- p$ at $E_\gamma = 1.850$ GeV, and (d): $\gamma p \to \rho^+ n$ at $E_\gamma = 1.850$. The short-dashed line in (a) and (b) denotes the contributions from the terms generated from the effective Lagrangian, while the dashed line denotes the contributions from the diffractive processes. The experimental data in (a) and (b) come from Ref. [14], and in (c) come from Ref.[16].

leads to good overall agreement with the available data. Our results for the s- and u- channel contributions alone are also shown for the reactions. In general, the contributions from the s- and u-channel resonances in ω and ρ^0 photoproduction account for only 20 to 40 percent of the total cross section, demonstrating the dominance of diffractive scattering in these processes. Nevertheless, in the case of ω photoproduction the quark model result exhibits some resonance structure around 1.7 GeV photon lab energy which comes from the $F_{15}(2000)$ state. A similar structure also appears in ρ^0 photoproduction, and additional contributions from the $F_{37}(1950)$, $F_{35}(1905)$, $P_{33}(1920)$ and $P_{31}(1910)$ resonances leads to a broader structure. Clearly, the presence of diffractive scattering complicates the extraction of the nucleon resonance contributions from the t-channel terms in the case of neutral vector meson photoproduction. Here, the photoproduction of charged vector mesons, ρ^- and ρ^+, presented in Fig. 1-c and 1-d, become very important. In these cases, the diffractive contributions are absent, and therefore, resonance contributions dominate the cross sections. Our numerical results for charged ρ production are in good agreement with the few available data, even though the poor quality of the data limit any conclusions that can be drawn. Note that the cross section for charged ρ production is smaller by about a factor of three compared to ρ^0 production, demonstrating that very different mechanisms come into play for charged and neutral ρ meson photoproduction, as analyzed in Ref.[10] and Ref.[11]. Once the t-channel terms are added as described above we obtain a good description of the more numerous ω and ρ^0 photoproduction data.

The results for the differential cross section for ω and ρ photoproduction are shown in Fig.

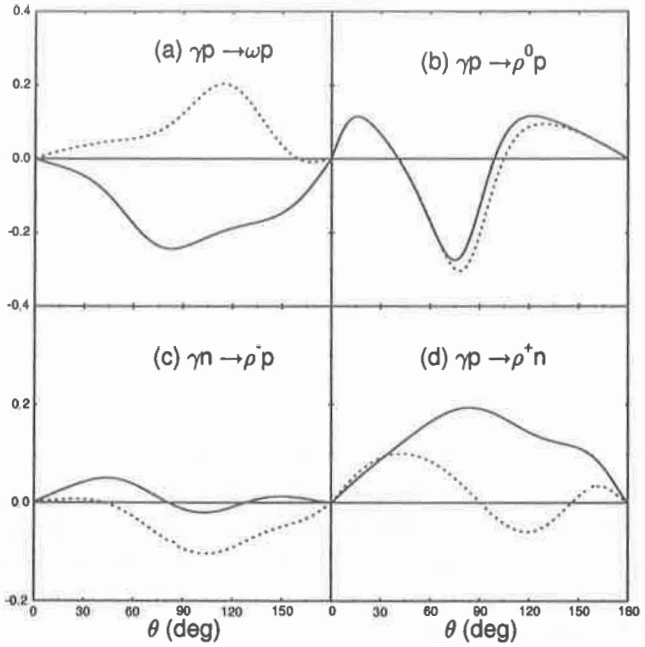

Figure 3. The target polarization for (a): $\gamma p \to \omega p$, (b): $\gamma p \to \rho^0 p$, (c): $\gamma n \to \rho^- p$, and (d): $\gamma p \to \rho^+ n$ at $E_\gamma = 1.7$GeV. The short-dashed lines show the result without the contribution from the $F_{15}(2000)$.

2. We find that the overall agreement with the available data for the differential cross sections is quite good as well. As expected, the π^0 and σ exchanges are responsible for the small-angle diffractive behavior, while the nucleon resonances dominate the large momentum transfer region. We point out that ρ^- and ρ^+ production also shows some the diffractive behavior, although the size of the effect is smaller compared to ω and ρ^0 production. This behavior can be explained by t-channel ρ^- or ρ^+ exhanges, which are naturally generated by the effective Lagrangian in Eq. 1. The data in the reaction $\gamma n \to \rho^- p$ are in very good agreement with the quark model predictions, indicating that the quark model wave functions appear to provide the correct relative strengths and phases among the terms in the s-, u- and t-channels.

While the shapes and magnitudes of the differential cross sections are well reproduced within our approach we find little sensitivity to individual resonances. For example, in the energy region of $E_\gamma \sim 1.7$ GeV, removing the $F_{15}(2000)$ state - one of the "missing" candidates - changes the cross section very little, indicating the differential cross section may not be the ideal experimental observable to study the structure of the baryon resonances. In contrast to the cross section, the polarization observables show a more dramatic dependence on the presence of the s-channel resonances. As shown in Ref. [19] these polarization observables are equivalent to the usually used density matrix elements. To illustrate their effects we show, as an example, the target polarization for the four channels in ω and ρ production with and without the contribution from the $F_{15}(2000)$ resonance. We do not expect the quark model in the $SU(6) \otimes O(3)$ limit to provide a good description of these observables. However, it demonstrates the sensitivity of these observables to the presence of s-channel resonances. Fig. 3 shows that the $F_{15}(2000)$ resonance has the most dramatic impact on the ω channel while the effects on the ρ channels are smaller due to the contributions from the isospin 3/2 resonances, $F_{37}(1950)$, $F_{35}(1905)$, $P_{33}(1920)$ and $P_{31}(1910)$, which reduce the significance of the $F_{15}(2000)$ state. This shows that polarization observables are essential in analyzing the role of s-channel

resonances.

In summary, this investigation presents the first attempt to describe ω and ρ meson photoproduction in a quark model plus diffractive scattering framework. With π^0 and σ exchange taken into account, a sizeable contribution of the Pomeron singularity in neutral vector meson photoproduction from high energies down to the threshold has been phenomenologically included, suggesting that the duality hypothesis constrains vector meson photoproduction as well. In this framework, the connection between the reaction mechanism and the underlying quark structure of the baryons resonances has been established. With the same set of parameters, we have obtained an overall description of the ω, ρ^0, ρ^+ and ρ^- photoproduction. It shows that the intermediate nucleon resonance contributions play important roles in the ω and ρ meson photoproduction, especially in the large-t region. The crucial role played by polarization observables in determining s-channel resonance properties is demonstrated. Data for these observables, expected from TJNAF in the near future, should therefore provide new insights into the structure of the resonance $F_{15}(2000)$ as well as other "missing" resonances.

One author (Z. Li) acknowledges the hospitality of the Center for Nuclear Studies at The George Washington University. Discussions with F.J. Klein regarding the data are also acknowledged. This work was supported in part by the Chinese Education Commission and the US-DOE grant DE-FG02-95-ER40907.

REFERENCES

[1] N. Isgur and G. Karl, Phys. Letts. **72B**, 109(1977); Phys. Rev. **D23**, 817(1981).
[2] R. Koniuk and N. Isgur, Phys. Rev. **D21**, 1868(1980).
[3] Zhenping Li, Ye Hongxing, and Lu Minghui, Phys. Rev. **C56** 1099(1997).
[4] Q. Zhao, Z. P. Li, and C. Bennhold, nucl-th/9711061, submitted to Phys. Rev. **C**.
[5] L. A. Copley, G. Karl and E. Obryk, Nucl. Phys. **B13**, 303(1969); R. P. Feynman, M. Kislinger and F. Ravndal, Phys. Rev. **D3**, 2706(1971).
[6] Le Yaouanc *et al*, Hadron Transitions in the Quark Model, (Gordon and Breach, New York, 1988); Phys. Rev. **D8**, 2223(1973); **D9**, 1415(1974).
[7] F. E. Close and Zhenping Li, Phys. Rev. **D42**, 2194(1990); *ibid.*, 2207(1990).
[8] M. Pichowsky, Ç. Şavklı, F. Tabakin, Phys. Rev. **C53**, 593 (1996).
[9] P.D.B.Collins, "An Introduction to Regge Theory and High-energy Physics", Cambridge University Press(1977).
[10] P.G.O. Freund, Phys. Rev. Lett., **20**, 235(1968).
[11] H. Harari, Phys. Rev. Lett., **20**, 1395(1968).
[12] B. Friman and M. Soyeur, Nucl. Phys. **A100**, 477(1996).
[13] Q. Zhao, Z. P. Li, and C. Bennhold, "Vector Meson Photoproduction with an Effective Lagrangian in the Quark Model II: ω Photoproduction", submitted to Phys. Rev. **C**.
[14] F. J. Klein, to appear on the Proceedings of the GW/TJNAF Workshop on N^* Physics, (Washington, D.C.) 1997, F.J. Klein, Ph.D. thesis, University of Bonn (1996).
[15] H. R. Crouch *et al*, Phys. Rev. **155**, 1468(1967); Y. Eisenberg *et al*, Phys. Rev. **D5**, 15(1972); Y. Eisenberg *et al*, Phys. Rev. Lett. **22**, 669(1969); D. P. Barber *et al*, Z. Phys. **C26**, 343(1984); J. Ballam *et al*, Phys. Rev. **D7**, 3150(1973); W. Struczinski *et al*, Nucl. Phys. **B108**, 45(1976).
[16] P. Benz *et al*, Nucl. Phys. **B79**, 10(1974).
[17] Particle Data Group, E. J. Weinberg, *et al*, Phys. Rev. **D54**, 1(1996).
[18] D. P. Barber *et al*, Z. Phys. **C2**, 1(1979).
[19] W. M. Kloet *et al.*, nucl-th/9803042.